10-1-1992

Residual Strength and Grout Repair of Dented Offshore Tubular Bracing

James Ricles

Troy Gillum

William Lamport
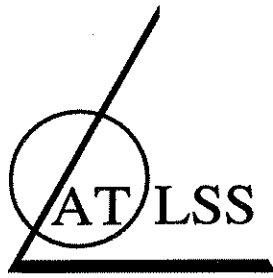
Follow this and additional works at: http://preserve.lehigh.edu/engr-civil-environmental-atlss-reports

Residual Strength and Grout Repair of Dented Offshore Tubular Bracing

Phase 1 Study

by

James Ricles
Associate Professor
Department of Civil Engineering

Troy Gillum
Civil Engineer
WGP Engineering, Inc
San Diego, California

William Lamport
Research Engineer
Unocal Corporation
Brea, California

ATLSS Report No. 92-14

October 1992

ABSTRACT

The first phase of a multi-phase research program involving the residual strength and repair of dented offshore tubular bracing is presented. Thirteen steel tubular braces of various diameter to thickness (D/t) ratio were tested to examine the effect of dent damage on their residual strength and to assess the effectiveness of internal grout and grouted steel clamp repair techniques. The braces were subjected to either concentric axial loading or combined axial and bending loads through an applied load with an end eccentricity of 20% of the specimen diameter. The thirteen specimens were tested in five series, which included: the testing of non-damaged specimens subjected to combined loads; dent damaged specimens subjected to concentric axial load; dent damaged specimens subjected to combined loads; internal grout repaired damaged specimens subjected to combined loads; and a grouted steel clamp repaired specimen subjected to combined loads. These tests allowed a direct evaluation by a comparison of the test results. The concentric axial load tests showed a pronounced loss of ultimate strength. The strength was further reduced for specimens subjected to the combined loading. The degradation of ultimate strength occurred due to a rapid growth of the dent, leading to a plastic hinging in the dented section. Both repair techniques reinstated each specimen's ultimate strength to the original non-damaged ultimate strength by arresting the growth in dent depth. Existing ultimate strength formulations for damaged and grout repaired members was evaluated. Modification of existing damage strength equations and development of new ones were found to reasonably assess the residual strength. Nonlinear finite element analysis also showed promising results in predicting specimen behavior.

This report is largely based on the Master of Science Thesis of Troy Gillum, under the supervision of Professor James Ricles while at the University of California, San Diego. Assessment of the results and writing of this report was completed at the Center for Advanced Technology for Large Structural Systems (ATLSS) located at Lehigh University. Subsequent research is continuing at ATLSS.

ACKNOWLEDGEMENTS

TABLE OF CONTENTS

LIST OF TABLES

LIST OF FIGURES

NOMENCLATURE

A	=	Original cross sectional area of non-damaged tube
A_d	=	Cross sectional area of dented section
C_d	=	empirical correction factor for lateral displacement of damaged members
C_m	=	Coefficient for buckling calculations
C_c	=	$\sqrt{\dfrac{2\pi^2 E}{F_y}}$
C_x	=	Local buckling coefficient
D	=	Outside Diameter of non-damaged tube
d_d	=	Dent depth
d_m	=	modified initial overall imperfection, Ellinas equation
E	=	Young's Modulus
F_a	=	Allowable axial compression buckling stress
F_b	=	Allowable bending stress
F_{bn}	=	Nominal bending stress capacity
F_{cn}	=	Nominal compressive stress capacity
F'_e	=	Euler buckling stress with factor of safety of 1.92
F_e	=	Euler buckling stress with no factor of safety
F_{pd}	=	Plastification force in dent saddle
F_y	=	Yield strength of steel
F_{xc}	=	Ultimate inelastic local buckling stress
F_{xe}	=	Elastic local buckling stress
e	=	End eccentricity of applied axial load
e_d	=	Centroidal shift for dented cross section
f_a	=	Applied axial stress
f_b	=	Applied bending stress
f_{bu}	=	Bond stress
f_c	=	Applied ultimate axial stress
f_{cu}	=	Unconfined grout compressive strength
f_y	=	Ellinas's squash stress
h	=	Shear key height
I	=	Cross sectional moment of inertia of nondamaged member
I_d	=	Cross sectional moment of inertia of dent section

K	=	Effective length factor
K_d	=	Effective length factor of dented member
K_o	=	Original effective length factor of non-damaged member
L	=	Total length of member
L_c	=	Length of grouted steel clamp
l_d	=	Dent length
l_1, l_2	=	Distances to dent centerline from end of member
M_e	=	Moment resisted by dent saddle, referenced with respect to centroid of dented cross section
M	=	Bending moment
M_p	=	Plastic moment capacity of non-damaged member
M_{pd}	=	ultimate bending moment developed in dent saddle
M_u	=	Ultimate moment capacity of non-damaged member
M_{ud}	=	Ultimate negative moment capacity of dent section of member
M^*	=	Neutral moment for dent section (dent in tension and compression)
M^-	=	Negative moment for dent section of member
P	=	Axial compressive force
P_a	=	AISC allowable axial load per ASD
P_E	=	$\dfrac{\pi^2 EI}{(KL)^2}$, Euler buckling Load
P_{Ed}	=	$\dfrac{\pi^2 EI_d}{(K_d L)^2}$, Euler buckling load for dented member
P_{crd}	=	Axial compression buckling capacity of dented member
P_{crdo}	=	Axial compression buckling capacity of dented member with no out-of-straightness
P_d	=	Design axial capacity based on allowable stresses
P_{max}	=	Specimen peak axial load.
P_p, P_y	=	Fully plastic axial squash load
P_{th}	=	Specimen predicted axial load capacity
P_u	=	Ultimate axial load capacity of non-damaged member
P_{ud}	=	Axial compression capacity (squash load) of short, dented member
r	=	$\sqrt{\dfrac{I}{A}}$, radius of gyration of nondamaged section
r_d	=	$\sqrt{\dfrac{I_d}{A_d}}$, radius of gyration of dent section
S	=	Section modulus of nondamaged section

S_d = Section modulus of dented section of member

s = Shear key spacing

t = Wall thickness

UC = Unity check value

Z = Plastic section modulus of nondamaged section

α = arccos(1 - 2d_d/D), Half angle subtended by the flat portion of the dented cross section

α_p = Imperfection parameter, Ellinas equation

δ_o = Initial out-of-straightness

Δ = Specimen out-of-straightness measured during test

δ_b = Out-of-straightness caused by dent eccentricity.

δ_d = Lateral displacement of damaged member.

δ_p = Out-of-straightness of damaged member.

ϕ = Knock down buckling factor

ϕ_b = resistance factor for flexural strength

ϕ_c = resistance factor for axial strength

γ = 2 - 3d_d/D

η = distance from centroid of damaged arc to midthickness of dent saddle

λ = $\dfrac{KL}{\pi r}\sqrt{\dfrac{F_y}{E}}$, slenderness parameter of non-damaged member

λ_d = $\dfrac{K_d L}{r_d} - 0.2\pi\sqrt{\dfrac{F_y}{E}}$, slenderness parameter of dented member for Ellinas equation

λ_d^{*} = $\dfrac{K_d L}{\pi r_d}\sqrt{\dfrac{F_y}{E}}$, slenderness parameter of dented member

σ_a = axial stress

σ_{ad} = average axial stress acting on dented section, Ellinas equation

σ_b = bending stress

σ_{bd} = bending stress near dent

σ_c = $\phi\sigma_y$, predicted inelastic buckling stress

σ_{cd} = additional uniform compressive stress over reduced effective section

σ_e = Euler buckling stress

σ_{pd} = plastification stress

σ_{ud} = ultimate axial capacity of dented member, Ellinas equation

σ_y = steel yield stress

ξt = depth to neutral axis of dent saddle

(This page intentionally blank)

(This page intentionally blank)

CHAPTER 1

INTRODUCTION

1.1. General

Damage to offshore drilling and production platforms is a topic of increasing concern in the U.S. and around the world due to the extraordinarily high stakes involved in terms of lost lives, environmental devastation, and wasted resources. There are presently over 6,000 platforms in U.S. waters, 25 of which lie off the coast of California [1]. A majority of these structures were designed for a 20 year life period, and are still in operation today after 30 and even 40 years. The cost to replace them is prohibitive and economic realities thus create strong incentives to develop ways to rehabilitate aging platforms and even to increase their capacity.

A large number of existing platforms are known to have suffered some form of damage. Damage records from a decade of recorded experiences worldwide indicate that a majority of accidents result from ship/platform collisions and impact with debris, including dropped objects from the deck. These accidents account for nearly 17% and 12% respectively of all recorded accidents [2]. In most cases the damage is less than severe, but an appreciable number (14%) result in severe damage or total loss of structure [2]. Typical bracing members susceptible to impact from a ship due to their location at the waterline are shown in Figures 1.1(a) and (b).

The steel jacket of an offshore platform is a complex system of cylindrical steel tubular members used to support large gravity loads while resisting large lateral loads, see Figure 1.2. Tubular members are important elements because of their minimization of hydrodynamic forces, high torsional rigidity, and small outer surface subject to corrosion. Most importantly, they provide the same global buckling strength in all directions. Under lateral impact, the circular cross section is susceptible to localized denting and ovalization. Such

deformations can drastically reduce the resistance of the members to axial and bending loads, affecting the overall integrity of the platform.

Offshore platforms are designed with a high level of structural redundancy and can typically tolerate the increased loads on remaining members even after the loss of numerous other members. However, a weakened platform inherently increases the probability of a catastrophic failure. Decisions regarding the safety of a damaged platform and the need for repair are derived from the assessment of the residual strength of the damaged members. Operators or certifying officials use the results to determine what type and magnitude of repair is required, if any at all.

Grout has been used extensively in offshore applications for its high strength, ease of placement, and low cost. Grout is presently used in the installation of most steel jackets to complete the connection between the foundation and the jacket itself. The connection involves the injecting of grout into the existing annulus between the concentric steel tubes (jacket leg and foundation pile). Grout has also been incorporated effectively into the repair and rehabilitation of damaged members. Traditional repair techniques available to operators have included the use of bolted sections, welded sections, and clamps. Grouted repair offers a viable alternative to these repair methods, for it does not involve underwater welding and the highly precise fabrication of repair components. Furthermore, it effectively utilizes the already well established knowledge of underwater grouting learned from pile-jacket connections. There are two types of grouted repairs used for repair of damaged members. These include internal grouting and grouted steel clamps. Both are relatively simple repair techniques that do not require extensive amounts of work offshore. Additional benefits that grouted repair techniques have over other methods include:

(1) Elimination of the need for an exact fit between adjacent steel components, and therefore avoiding the difficulty and cost of fabricating repair components to a high degree of accuracy

(2) Reinstatement of, and possibly increasing, the strength of the repaired member to a level greater than the original strength

(3)   Efficient and economic subsea repairs

(4)   Use of existing technology developed for other offshore applications

(5)   In the case of an internally grout repaired member, no increase in the outer diameter thus no increase in the hydrodynamic forces that develop from the member surface profile

Normally internal grouting involves injecting the entire damaged member with grout. Grouted clamp repairs involve the inclosure of the damaged section of the member with a steel clamp, formed from two sections bolted together. The annulus between the clamp and the member is then filled with grout. The load is transferred from the original member through the grout to the clamp itself. These types of repairs are simple, requiring no habitat to be constructed around the damaged member. Grout is injected into the member or annulus, depending on repair, displacing the trapped seawater by virtue of its higher specific gravity. A typical grouted clamp used to strengthen a fatigue damaged joint connection is shown in Figures 1.3(a) and (b). The grouted clamp was used to span a K-joint connection of a bracing member and jacket leg, relieving the fatigued joint by redistribution of the load path.

While internal grout and grouted clamp repairs are both well developed and widely used, the available information on the strength and performance of these repairs under ultimate load conditions is scarce. Repair design is typically based on full composite theory for the internal grouting, while extrapolated strengths from studies on pile-jacket connections are used to develop predictions for the grouted clamp.

4

1.2. Design Criteria

1.2.1. Allowable Stress Design (ASD)

The design of fixed offshore platforms in the U.S. has been customarily based on allowable stress design (ASD) as specified by the AISC (American Institute for Steel Construction) Specification for the Design, Fabrication and Erection of Structural Steel Buildings [3] and as recommended by the API (American Petroleum Institute) Recommended Practice for Planning, Designing and Constructing Fixed Offshore Platforms (API-RP-2A) [4]. The allowable stress design method applies a design safety factor to the ultimate stress of the member. A tubular member subjected to combined axial and bending loads, causing bending about one axis, is proportioned from computed stresses determined using the following interaction formulas

$$\frac{f_a}{F_a} + C_m \frac{f_b}{\left(1 - \frac{f_a}{F_e'}\right)F_b} \leq 1.0 \qquad (1.1)$$

and,

$$\frac{f_a}{0.6F_y} + \frac{f_b}{F_b} \leq 1.0 \qquad (1.2)$$

where f_a and f_b, respectively, are the applied (computed) axial and bending stress. The material yield stress is defined as F_y. The application of a moment at the ends of the member induces additional displacements (Δ) in the plane of bending along the member length. The resulting displacements lead to an additional secondary moment equal to the product of the resulting eccentricity and the applied axial load (P-Δ). This P-Δ effect is accounted for by amplifying f_b by the factor

$$\frac{C_m}{\left(1 - \frac{f_a}{F_e'}\right)} \qquad (1.3)$$

where F'_e is the Euler buckling stress with a factor of safety of 23/12, and C_m is a factor to used to account for the effect of a moment gradient on the secondary moment.

The allowable axial and flexural stresses, F_a and F_b, are dependent on the mode of failure of the tubular member. Members subject to axial compression fail either due to material yield, global column buckling, or local buckling. The design of short tubes with low diameter-to-thickness (D/t) ratios is controlled by material yield. Experimental test data shows a trend towards local buckling failure of axially compressed members when the D/t ratio exceeds 60. The appropriate inelastic local buckling stress is determined from

$$F_{xc} = F_y\left[1.64 - 0.23[D/t]^{0.25}\right] \leq 0.3Et/D \qquad \text{for D/t} > 60 \qquad (1.4)$$

$$F_{xc} = F_y \qquad \text{for D/t} \leq 60 \qquad (1.5)$$

where F_y is the material yield stress, E is the elastic modulus, D is the outer diameter of the member, and t is the wall thickness. The allowable axial compressive stress, F_a, based on global buckling is determined by

$$F_a = \frac{\left[1 - \frac{(Kl/r)^2}{2C_c^2}\right]F_y}{\frac{5}{3} + \frac{3(Kl/r)}{8C_c} - \frac{(Kl/r)^3}{8C_c^3}} \qquad \text{for Kl/r} < C_c \qquad (1.6)$$

$$F_a = \frac{12\pi^2 E}{23(Kl/r)^2} \qquad \text{for Kl/r} \geq C_c \qquad (1.7)$$

where K, l, and r, respectively, are the effective length factor, unbraced length of the member, and the radius of gyration. The slenderness parameter C_c is expressed in terms of F_{xc} where

$$C_c = \sqrt{\frac{2\pi^2 E}{F_{xc}}} \qquad \text{for D/t} > 60 \qquad (1.8)$$

When D/t is less than or equal to 60, the yield stress F_y should be used in Equation (1.8) in leu of F_{xc}.

6

The allowable bending stresses are based on a lower bound of test data for ultimate bending capacities, applying a factor of safety of 1.67. Trends in experimental data show that members with $F_y D/t$ ratios less than 1500 ksi have ultimate bending capacities which reach their plastic moment capacity and exhibit ductile modes of failure. When $F_y D/t$ is between 1500 and 3000 ksi the failure mode is more semi-ductile. Members with $F_y D/t$ ratios exceeding 3000 ksi develop a failure mode with very little ductile behavior. The test data was used in the determination of the allowable bending stress, F_b, resulting in

$$F_b = 0.75 F_y \qquad \text{for } D/t \leq \frac{1500}{F_y} \qquad (1.9)$$

$$F_b = \left[0.84 - 1.74 \frac{F_y D}{Et} \right] F_y \qquad \text{for } \frac{1500}{F_y} < D/t \leq \frac{3000}{F_y} \qquad (1.10)$$

$$F_b = \left[0.72 - 0.58 \frac{F_y D}{Et} \right] F_y \qquad \text{for } \frac{3000}{F_y} < D/t \leq 300 \qquad (1.11)$$

With the allowable axial compressive and bending stresses determined, the computed axial stress, f_a, to be applied in conjunction with the bending stress f_b is determined from the interaction formulas (Equations 1.1 and 1.2). The non-damaged allowable axial load of the steel tubular bracing member is thus

$$P_a = A f_a \qquad (1.12)$$

where A is the cross sectional area of the member.

1.2.2. Load and Resistance Factor Design (LRFD)

The traditional allowable stress design (ASD) described above will eventually be superseded in the U.S. by the load and resistance factor design (LRFD) method. The API recommended practice was redrafted in 1989 to include the LRFD method (API-RP-2A-LRFD) [5] and although it has not yet been recommended for use, it is a proven effective design practice. While the ASD method applies a safety factor to the extreme stress in a structure, the LRFD method amplifies the working loads by a load factor and reduces the resistance by a reduction factor to deal with uncertainties in member geometry and material properties. The load factors influence the margin of

safety factor in proportion to the significance of the load or resistance effect to which they relate.

As in allowable stress design of members subjected to combined axial and bending loads, the LRFD method incorporates interaction formulas in the determination of the computed stress, f_a, where for uniaxial bending

$$\frac{f_c}{\phi_c F_{cn}} + \frac{C_m f_b}{\left(1 - \frac{f_c}{\phi_c F_e}\right)\phi_b F_{bn}} \leq 1.0 \qquad (1.13)$$

and

$$1 - \cos\left(\frac{\pi}{2}\frac{f_c}{\phi_c F_{xc}}\right) + \frac{f_b}{\phi_b F_{bn}} \leq 1.0 \qquad (1.14)$$

where f_c and f_b, respectively, are the computed axial compression and bending stresses due to the applied loads. The resistance factors for the axial and bending strengths, ϕ_c and ϕ_b, are set equal to 0.85 and 0.95, respectively. The Euler buckling stress, F_e, is used without the safety factor. The nominal strength equations for the axial compression stress F_{cn} are a function of the column slenderness parameter, λ, which is in turn a function of the slenderness ratio, Kl/r:

$$F_{cn} = \left[1.0 - 0.25\lambda^2\right]F_y \qquad \text{for } \lambda < \sqrt{2} \qquad (1.15)$$

$$F_{cn} = \frac{1}{\lambda^2}F_y \qquad \text{for } \lambda \geq \sqrt{2} \qquad (1.16)$$

where the column slenderness parameter λ, is defined as

$$\lambda = \frac{Kl}{\pi r}\sqrt{\frac{F_y}{E}} \qquad (1.17)$$

To account for interaction between local and column buckling modes of failure that affect the range of D/t ratios commonly used in offshore structures, the local buckling strength F_{xc} or F_{xe}, whichever is smaller is substituted for F_y in Equations (1.15) and (1.16), where the elastic local buckling stress is

$$F_{xe} = 2C_x E\frac{t}{D} \qquad (1.18)$$

where $C_x = 0.3$, and $E = $ Young's Modulus. The inelastic local buckling stress

$$F_{xc} = F_y \quad \text{for } D/t \leq 60 \tag{1.19}$$

$$F_{xc} = \left[1.64 - 0.23(D/t)^{0.25}\right]F_y \quad \text{for } D/t > 60 \tag{1.20}$$

The nominal bending strength, F_{bn}, for tubular members is

$$F_{bn} = \frac{Z}{S}F_y \quad \text{for } D/t \leq \frac{1500}{F_y} \tag{1.21}$$

$$F_{bn} = \left[1.13 - 2.58\frac{F_y D}{Et}\right]\frac{Z}{S}F_y \quad \text{for } \frac{1500}{F_y} < D/t \leq \frac{3000}{F_y} \tag{1.22}$$

$$F_{bn} = \left[0.94 - 0.76\frac{F_y D}{Et}\right]\frac{Z}{S}F_y \quad \text{for } \frac{3000}{F_y} < D/t \leq 300 \tag{1.23}$$

where S and Z, respectively, are the elastic section modulus and the plastic section modulus for an undamaged member. With the nominal axial compressive and bending strengths F_{cn} and F_{bn} determined from above, the amount of axial stress, f_c, that can be applied in conjunction with the bending stress f_b of the member is determined by solving for f_c in Equations (1.13) and (1.14), taking the lowest value. The LRFD design strength of the steel tubular bracing member is then determined by the relationship

$$P_u = Af_c \tag{1.24}$$

1.3. Assessment of Residual Strength of Damaged Member

Decisions regarding safety of a damaged platform and the need for repair depend on the critical assessment of the residual strength of damaged members under combined axial and bending loads. Previous analytical and experimental investigations into this problem have shown that even minor damage levels in the form of denting can cause large member strength degradation.

1.3.1.   Previous Experimental Work

The effect of dent damage on the behavior of tubular members subjected to axial compression was first studied by Smith, Kirkwood and Swan [7]. For dent depths as small as 0.011D to 0.082D on small-scale tubes, axial compression tests indicated a substantial loss of strength. Full scale tests on tubular braces recovered from a North Sea platform were later conducted by Smith, Sommerville, and Swan [8]. These tests showed further evidence that damage significantly reduces the strength of tubular members.

A series of tests on small-scale manufactured tubes were undertaken by Taby to gain a better understanding of this problem [9,10]. Dent depths were varied from 0.02D to 0.10D. The results were later used in the development of a semi-empirical model, DENTA [10,11], to predict the load deflection behavior of simply supported dented ubular bracing members subjected to direct axial loading. DENTA was subsequently modified and calibrated to account for combined axial loading and bending, using tests performed by Yao, Taby and Moan [12] .

Axial compression tests on five small-scale dent damaged members were also carried out by Pacheco and Durkin [13], having dent depths of 0.053D and 0.086D. They observed a reduced ultimate axial strength due to the dent. Ueda and Rashed [14] conducted 21 tests with D/t = 34.55 and 64. Their specimens had nominal dent depths of 0.05D and 0.10D. They found that denting reduced the ultimate bending capacity of tubular members only when the dent was located on the compression face. Padula and Ostapenko [15] showed that large diameter dent damaged specimens subjected to axial compression lost very little ultimate strength. The authors concluded that the fixed-fixed end conditions and short member lengths involved in their tests influenced the insensitivity to the presence of damage.

Most recently, tests were performed by Landet and Lotsberg [16] on dent damaged small-scale manufactured tubes. A total of 35 ultimate load tests were performed on short columns and beam-columns subjected to direct axial load, pure bending, and combined loading. The dent depths included 0.0D (e.g. no dent), 0.10D and 0.20D. Their results produced moment-curvature-thrust

relationships of dented segments. The authors again showed that the ultimate capacity was significantly less than the capacity of non-damaged members.

There have been fewer experimental studies conducted which have been concerned with evaluating repair techniques for dent damaged tubular members. Parsanejad [17] tested small-scale grout filled damaged tubular members. The diameter of the test specimens ranged from 1.7 inch to 2.7 inch, with a D/t ratio from 29.4 to 48.7. Parsanejad concluded that full grouting of the members not only compensated for the loss of strength incurred as the result of the damage, but also provided an additional reserve of strength. He also showed that partial grouting of the dented region could improve the load carrying capacity of the members. Tests carried out at Wimpey Laboratories Limited on grouted steel clamps were the first to assess the effectiveness of applying current pile-jacket design rules (API-RP-2A, 1984) to the use of grouted clamps on pipe-to-pipe repair connections. Billington, et al. [19] showed that this approach provided a conservative design, with few restrictions. A total of 37 tests were conducted on complete grout-filled dented braces by Boswell et al. [35], which was part of a United Kingdom project addressing the technology of grout use for offshore platform construction and repair [36]. The test program of Boswell consisted of mostly small scale specimens (34 specimens had a 1.75 to 3.0 inch diameter), with concentric axial loading, and dent depths of less than 15% of the diameter.

Tebbet and Forsyth, of Wimpey Offshore Engineers & Constructors Ltd., presented test data on the capacity of non-damaged grout filled members [18]. They concluded that grouting of the tubes significantly increased their ultimate strength under combined loading, and produced design curves to estimate the increase in the capacity of a fully and partially grouted members.

1.3.2. Previous Analytical Work

Various analytical studies on dent damaged members have been conducted. In the case of global bending damage without denting; Smith, Kirkwood and Swan [7] found good correlation with test results by the use of an elasto-plastic beam-column analysis. Smith, Somerville and Swan [8] later modified the model to include the effect of local dent damage. Agreement with

experimental results were good, however the number of comparisons were small.

Investigations by MacIntyre [20] involved non-linear finite element analyses of dent damaged members. Duan, Loh, and Chen [21,22] developed a moment-curvature-thrust approach to predict non-linear beam-column behavior and ultimate strength. They implemented their approach into a computer program, named BCDENT, to analyze the behavior of dented (single or multiple) or undented tubular members. The algorithm incorporates closed-form expressions of moment-curvature-thrust $(M\text{-}\Phi\text{-}\Delta)$ for member cross sections and incrementally employs the Newmark numerical integration method to determine the deformed geometry of a member subjected to a prescribed axial and flexural loading. Padula and Ostapenko [15] had earlier developed an extensive data base of dented member behavior from experimental tests and nonlinear finite element analysis. Regression analysis was performed on the data base to generate expressions for the $M\text{-}P\text{-}\Phi$ relationships and axial load-shortening behavior.

As discussed previously the semi-empirical model DENTA [10,11,12] was developed to analyze the behavior of tubular members under combined loading. The tubes may have damage in the form of a dent and initial out-of-straightness. DENTA accounts for deformation of the cross section in the post ultimate range, based on a simplified characterization of the damaged tube length. The model was calibrated on a set of 107 experimental tests of dent damaged members. The dent geometry modeled by DENTA was based on a dent formed by knife-edge loading applied perpendicular to the longitudinal axis of the tubular member. The experimental work leading to the formulation of this model showed that there was very little increase in the dent depth until the ultimate axial load capacity of the tube was achieved. Therefore, the formulation of the model does not allow for a change in the dent depth until after the ultimate axial capacity is reached. The material behavior was assumed to be linear elastic-perfectly plastic. Strain hardening and residual stresses arising from the plastification of the tube wall during denting are not considered in the model. The analysis was divided into three stages: load and

12

displacement at first yield; post yield load and displacement leading to ultimate; and post ultimate load and displacement.

Simple design strength equations have also been developed to predict the behavior of dent damaged members. Ellinas [23] proposed a design oriented format based on a beam-column analysis with reduced section properties to predict the ultimate strength of a dented member. Failure is assumed to occur when the material adjacent to the dent saddle reaches yielding. Ellinas' formulation has been shown to provide a conservative lower bound for residual strength of past experimental findings, as shown in Figure 1.4. The dent was assumed to consist of two flat inclined planes which intersect at the maximum dent depth, d_d (see Figure 1.5 and 1.6). Ellinas' method used the simplifying assumption that once plastification occurs in the dented section of a member (see Figure 1.5), the damaged part of the section becomes ineffective, and additional load is subsequently supported only by the remaining non-affected section. Based on equilibrium of the damaged tube section under direct axial load and considering secondary effects, Ellinas concluded that the ultimate stress, σ_{ud}, corresponding to the residual strength of a dented member may be evaluated by solving the following quadratic equation

$$\frac{1}{\sigma_e}\sigma_{ud}^2 - \left[1 + \alpha_p\lambda_d + \frac{A_d e_d}{S_d} + \frac{f_y}{\sigma_e}\right]\sigma_{ud} + f_y + \sigma_{pd}\frac{A_d e_d}{S_d} = 0 \qquad (1.25)$$

where e_d is the eccentricity that exists in the dented region between the centroid of the dented and non-dented sections (see Figure 1.6(a)), f_y represents the average squash stress of the dented section, σ_e is the Euler buckling stress, and σ_{pd} is equal to the initial plastification stress in the saddle of the dent. Geometric parameters for the imperfection and the column slenderness, α_p and λ_d, respectively, are defined along with all other terms, in the nomenclature section of this report.

Parsanejad [30] studied the stability of internal grout repaired dented tubes, developing a quadratic expression for the ultimate strength of the member. This expression is written in terms of stress, considers transformed section properties, and assumes that failure occurs when the total stress σ_{ud} (axial

plus bending) in the dent saddle reaches the yield stress σ_y of the steel tube, where

$$\frac{1}{\sigma_{e,tr}}\sigma_{ud}^2 - \left[1 + \frac{A_{tr}e_t}{S_{tr}} + \frac{\sigma_y A_{tr}}{\sigma_{e,tr}A_{tr}^*}\right]\sigma_{ud} + \sigma_y\frac{A_{tr}}{A_{tr}^*} = 0 \tag{1.26}$$

Terms appearing in Equation (1.26) are defined in the nomenclature section. Mathematical expressions for the various terms appearing in Equation (1.26) are found in Reference 30. Parsanejad's formulation is compared with ten of his grout repaired specimens' capacities in Figure 1.7. The method is shown to provide a close agreement with his test data, having a maximum deviation of 11% and representing a lower bound solution.

1.3.3. Modification of Strength Equation

Although axial compression is the primary structural action in bracing members, bending moments are typically present as well. The need for an equation to assess the residual strength of a damaged member subject to combined axial and bending loads is therefore needed. Therefore, Ellinas' quadratic equation was modified to account for combined loading. By considering equilibrium of the damaged member, in his original formulation Ellinas expressed the bending stress, σ_{bd}, as

$$\sigma_{bd} = \frac{1}{S_d}\left[\sigma_{ad}A\frac{d_m + e_d}{1 - \frac{\sigma_{ad}}{\sigma_e}} - \sigma_{pd}A\frac{e_d}{1 - \frac{\sigma_{ad}}{\sigma_e}}\right] \tag{1.27}$$

where d_m represents a geometric imperfection parameter to account for the overall imperfection and built-in defects such as residual stress. To incorporate applied bending, the end eccentricity of the applied axial load is introduced into Equation (1.27). By summing moments about the centroid of the non-damaged section (see Figure 1.6(b)), the resulting bending stresses are

$$\sigma_{bd} = \frac{1}{S_d}\left[\sigma_{ad}A\frac{d_m + e_d + e}{1 - \frac{\sigma_{ad}}{\sigma_e}} - \sigma_{pd}A\frac{e_d}{1 - \frac{\sigma_{ad}}{\sigma_e}}\right] \tag{1.28}$$

14

where the second term in Equation (1.28) represents the resistance of the dent saddle in the damaged region of the cross section. A first yield collapse criterion requires that the ultimate stress that can be supported by the dented member, σ_{ud}, be attained when the maximum compressive stress adjacent to the dent reaches the yield stress of the material, σ_y. This, as seen from Figure 1.6(a), results in

$$\sigma_{pd} + \sigma_{cd} + \sigma_{bd} = \sigma_y \tag{1.29a}$$

where σ_{cd} is the uniform compressive stress developed in the cross section ouside the dented zone (πD-S), see Figure 1.6(a). The average stress σ_{ud} at failure over the complete section is

$$\sigma_{ud}A = \sigma_{cd}A_d + \sigma_{pd}A \tag{1.29b}$$

in which A and A_d, respectively, are the full and reduced cross-sectional areas of the tube in the dented zone. Substituting Equations (1.28) and (1.29b) into Equation (1.29a), setting the axial stress σ_{ad} equal to σ_{ud}, and noting that the average squash stress f_y of the damaged section is defined by

$$f_y = (\sigma_y - \sigma_{pd})\frac{A_d}{A} + \sigma_{pd} \tag{1.29c}$$

as well as

$$\frac{d_m A_d}{S_d} = \alpha_p \lambda_d \tag{1.29d}$$

one arrives at a modified form of Ellinas' original quadratic equation for the residual strength of an unrepaired dented tube, which accounts for end eccentricity:

$$\frac{1}{\sigma_e}\sigma_{ud}^2 - \left[1 + \alpha_p\lambda_d + \frac{A_d(e_d + e)}{S_d} + \frac{f_y}{\sigma_e}\right]\sigma_{ud} + f_y + \sigma_{pd}\frac{A_d e_d}{S_d} = 0 \tag{1.30}$$

1.3.4. Description of Computer Program, UC-DENT

In association with the experimental test program undertaken, a computer program entitled UC-DENT was developed to determine the residual strength of dent damaged members and to aid in the assessment of the experimental

results. The code was based on the equilibrium of the dented section at an ultimate stress state, and takes into account combined axial and bending loading through end eccentricity, initial plastification of the dented section, the effect of damaged section properties on Euler buckling, and initial out-of-straightness. The formulation uses a stress resultant approach, with results obtained from solution of an ensuing quadratic equation. The occurrence of a dent at any location along the member is accounted for in UC-DENT.

1.3.4.1. Development of the Dent Plastification Force

The ultimate strength of dent damaged tubular members is related to the plastification of the dented section. A portion of the axial load applied to the member is resisted by the damaged section. Force and moment relations in the idealized dent geometry require that the axial force F_{pd} and bending moment M_{pd} resisted by the saddle of the dent be equal to:

$$F_{pd} = \int_0^{2\alpha} \sigma_y dA \qquad (1.31)$$

$$M_{pd} = F_{pd}\eta = \int_0^{2\alpha} z\sigma_y dA \qquad (1.32)$$

where η is the distance from the flat part (saddle) of the dent to the centroid of the ineffective damaged section of Figure 1.5, z is the distance referenced from the centroid of the non-damaged cross section, and α is the half angle subtended by the flat portion of the dent to the center of the non-damaged section. It can be shown that

$$\eta = \frac{D}{2}\left(\frac{\sin \alpha}{\alpha} - \cos \alpha\right) \qquad (1.33)$$

Integrating the force and moment relationships, Equations (1.31) and (1.32), over the damaged section having a full plastic stress distribution in the saddle of the dent results in

$$F_{pd} = \alpha Dt\sigma_y[2\xi - 1] \qquad (1.34)$$

$$M_{pd} = \alpha Dt^2\sigma_y\xi[1 - \xi] \qquad (1.35)$$

16

where ξt is the depth to the neutral axis of the tube wall in the stress distribution through the dent saddle, as shown in Figure 1.5. Substituting Equations (1.34) and (1.35) into Equation (1.32) yields

$$t\xi^2 + \xi[2\eta - t] - \eta = 0 \qquad (1.36)$$

The solution for the depth of the stress block, ξt, can be found from Equation (1.36), and substituted back Equation (1.34) to obtain the expression for maximum load, F_{pd}, that the dent can sustain prior to plastification of the saddle of the dent, where

$$F_{pd} = \alpha D \sigma_y \left[\sqrt{4\eta^2 + t^2} - 2\eta \right]$$

$$= \alpha D \sigma_{pd} \qquad (1.37)$$

1.3.4.2. First Yield Criterion

First yield of an axially compressed member is reached when the sum of the axial (σ_a) and bending (σ_b) stresses reaches the yield stress (σ_y) of the material adjacent to the saddle of the dent:

$$\sigma_a + \sigma_b = \sigma_y \qquad (1.38)$$

For the idealized member shown in Figure 1.6(b), taking into account the resistance F_{pd} of the damaged section as well as initial out of straightness and second order effects, the first yield criteria can be stated as

$$\sigma_y = \frac{P}{A_d} - \frac{F_{pd}}{A_d} + \frac{P(e+\delta_d+e_d)}{S_d} - \frac{F_{pd}\left(\frac{D}{2}+\eta-d_d+e_d\right)}{S_d} \qquad (1.39)$$

where δ_d is the lateral displacement at the middle of the member with an initial damage of sinusoidal form [10]:

$$\delta_d = \frac{(\delta_b+\delta_o)[1+C_d]}{\left(1-\frac{P}{P_{Ed}}\right)} \qquad (1.40)$$

In Equation (1.40) C_d is an empirical correction factor used for the case where the dent is not located in the middle of the member, where:

$$C_d = \left[L \big/ (2l_1 - l_d) \right] \sin\left[\pi(l_2 + l_d/2) \big/ L \right] \qquad (1.41)$$

the lateral displacement caused by the eccentricity due to the dent is [10]:

$$\delta_b = \frac{l_d l_1 (Pe - M_e)}{EI_d(1 + l_1/l_2)} \qquad (1.42)$$

where δ_0 is the initial out-of-straightness at the dent location, l_1 and l_2 are the distances from each end of the dent to the corresponding end of the member and l_d the longitudinal length of the dent. Definitions for the reduced section properties, I_d, A_d, P_{Ed}, S_d, and e_d are listed in the nomenclature section. The moment resisted by the dented section, M_e, is obtained by summing moments about the neutral axis of the damaged section of the member, and represents the last term of Equation (1.39), where

$$M_e = F_{dp}\left(\frac{D}{2} + e_d - d_d + \eta \right) \qquad (1.43)$$

Upon substituting Equations (1.40) through (1.43) into Equation (1.39), a quadratic equation for the load P at first yield of the damaged member is obtained

$$
\begin{aligned}
& P^2 \left[\frac{1}{A_d} + \frac{e + e_d}{S_d} - \frac{l_1 l_d e}{EI_d(1 + l_1/l_2)} \frac{(1 + C_d)}{S_d} P_{Ed} \right] \frac{1}{P_{Ed}} \\
& - P \left[\frac{e + e_d}{S_d} + \left\{ \delta_0 - \frac{l_1 l_d M_e}{EI_d(1 + l_1/l_2)} \right\} \frac{(1 + C_d)}{S_d} + \frac{F_{pd} e^*}{P_{Ed} S_d} + \frac{1}{A_d} + \frac{F_{pd}}{A_d P_{Ed}} + \frac{\sigma_y}{P_{Ed}} \right] \\
& + \sigma_y + \frac{F_{pd}}{A_d}\left(1 + \frac{A_d e^*}{S_d} \right) = 0
\end{aligned}
\qquad (1.44a)
$$

where

$$e^* = D/2 + \eta - d_d + e_d \qquad (1.44b)$$

The load P corresponds to a lower bound collapse load of damaged members made of elastic-perfectly plastic material.

When the D/t ratio exceeds 60, the member is more susceptible to local buckling. In this case, the yield stress σ_y in Equation (1.44a) is replaced with the inelastic buckling stress σ_c. Others [10] have used a knock down factor ϕ to estimate σ_c, where

$$\sigma_c = \phi\sigma_y \qquad\qquad (1.45)$$

Expressions for ϕ can be found in Reference 10.

The source code for UC-DENT, an interactive program, is located in Appendix A. Analyses of the test specimens by UC-DENT are included in Chapter 4.

1.3.5. Parametric Study of Dent Damaged Members Using UC-DENT

The introduction of the additional eccentricity of the applied axial load in the above equation has enabled its use for a variety of end loading conditions. Parametric studies involving various values of end eccentricity have been undertaken here to illustrate the effect of dent depth on the ultimate capacity of damaged members subject to various degrees of combined loading. An initial out-of-straightness δ_0 of 0.001L was assumed, where L is the member's length. The slenderness ratio Kl/r for all cases was 60, with the dent placed at midspan. Analyses were performed with no end eccentricity, as well as an end eccentricity of e = 0.20D causing negative bending. The dent length l_d was assumed to be 6 inches. These curves are shown in Figures 1.8, 1.9, and 1.10. They indicate that the magnitude of dent depth has a pronounced effect on the residual strength, with greater depths resulting in decreasing strength. For a specific D/t ratio, the affect of eccentrically applied axial load on the reduction in the member's residual strength is apparent.

1.4. Unity Check Equations for Dent Damaged Members

It is common practice for design codes to present member strength calculations as a unity check. A unity check is related to the member load divided by the member's capacity. Design unity check values greater than a

value of 1.0 imply deficiencies in design. Ultimate load unity checks are written by substituting ultimate member capacities for allowable capacities, therefore eliminating all safety factors. Ultimate load unity check values greater than 1.0 imply possible member failure. An ultimate load unity check for a non-damaged member subject to combined axial and bending loads takes the following form

$$UC = \frac{P}{P_u} + \frac{M}{M_u} \tag{1.46}$$

where P_u represents the axial compression capacity (squash load) of a short, non-damaged member, M_u the ultimate moment capacity of a non-damaged member, P the applied axial load, and M the applied bending moment.

Unity checks can also be written for damaged members. Using the API-LRFD procedures for members subjected to combined axial compression and bending, unity checks for strength as well as stability have been developed using LRFD strength equations with reduced section properties of the damaged section [24].

1.4.1. Strength Check

A unity check for the local failure of a short dent section subjected to combined loading is referred to as a "strength check", and takes the form of Equation (1.46), considering uniaxial bending with damaged section ultimate axial (P_{ud}) and flexural (M_{ud}) capacities replacing non-damaged ultimate section capacities, where:

$$UC = \frac{P}{P_{ud}} + \left(\frac{M}{M_{ud}}\right)^{\gamma/2} \tag{1.47}$$

in which γ is an empirically derived constant

$$\gamma = 2 - 3\frac{d_d}{D} \tag{1.48}$$

and d_d is the initial dent depth. The damaged member's axial load and flexural capacities are determined by empirically relating the damaged and non-damaged section capacities, where

$$P_{ud} = P_u \exp\left[\frac{-0.08d_d}{t}\right] \geq 0.45 \qquad (1.49)$$

$$M_{ud} = M_u \exp\left[\frac{-0.06d_d}{t}\right] \geq 0.55 \qquad (1.50)$$

Non-damaged ultimate capacities P_u and M_u are determined as in Section 1.2.2 using the API-LRFD inelastic local buckling stress F_{xc}, and nominal bending strength, F_{bn}, where

$$P_u = AF_y \qquad \text{for D/t} \leq 60 \qquad (1.51a)$$

$$P_u = AF_y\left[1.64 - 0.23\left(\frac{D}{t}\right)^{0.25}\right] \qquad \text{for D/t} > 60 \qquad (1.51b)$$

and

$$M_u = M_p \qquad \text{for } 0 < \text{D/t} \leq \frac{1500}{F_y} \qquad (1.52a)$$

$$M_u = M_p\left[1.13 - 2.58\frac{F_y D}{Et}\right] \qquad \text{for } \frac{1500}{F_y} < \text{D/t} \leq \frac{3000}{F_y} \qquad (1.52b)$$

$$M_u = M_p\left[0.94 - 0.76\frac{F_y D}{Et}\right] \qquad \text{for } \frac{3000}{F_y} \leq \text{D/t} \leq 300 \qquad (1.52c)$$

in which

$$M_p = F_y t(D - t)^2 \qquad (1.53)$$

1.4.2. Stability Check

The unity check for the instability of a dented member under combined loading is referred to as the "stability check" and also takes the form of Equation (1.46). For stability calculations, the axial compression buckling capacity of a dented member, P_{crd}, takes the place of P_{ud}. The buckling capacity, P_{crdo}, of a dented member with no out-of-straightness is first computed by using a damaged slenderness parameter, λ^*_d, in Equations (1.15) and (1.16), representing API-LRFD guidelines for column buckling of tubular members, where

$$P_{crdo} = \left[1.0 - 0.25\lambda_d^{*2}\right]AF_y \qquad \text{for } \lambda_d^* < \sqrt{2} \qquad (1.54a)$$

$$P_{crdo} = \frac{1}{\lambda_d^{*2}}AF_y \qquad \text{for } \lambda_d^* \geq \sqrt{2} \qquad (1.54b)$$

The buckling capacity P_{crd} of the damaged member, considering out-of-straightness δ_p, is then determined by solving the following quadratic equation

$$\frac{P_{crd}}{P_{crdo}} + \frac{P_{crd}\delta_p}{\left(1 - \frac{P_{crd}}{P_{Ed}}\right)M_{ud}} = 1.0 \qquad (1.55)$$

where P_{Ed} is the Euler buckling load of the damaged member, respectively. All terms used, including λ^*_d, are defined in the nomenclature section. The moment $P_{crd}\delta_p$ is amplified in Equation (1.54c) to take into account second order effects. The "stability check" is then performed and is similar in format to the earlier unity checks, but incorporates the empirical constant γ (see Equation (1.48)) and amplification for second order effects, where

$$UC = \frac{P}{P_{crd}} + \sqrt{\left[\frac{C_mM}{\left(1 - \frac{P}{P_{Ed}}\right)M_{ud}}\right]^\gamma} \qquad (1.56)$$

1.5.   Objectives

There is currently a lack of information available on the strength and performance of grout repaired to damaged bracing members. Practicing engineers have been designing grouted repairs based on extrapolated data from applications other than that of the repair of damaged members. Experimental and analytical work would verify the amount of increased load carrying capacity produced by the grouted repair techniques. Therefore, a research study was conducted to enhance the knowledge base of the behavior of the residual strength of damaged bracing members and to assess the increased strength, if any, derived from grouted repair techniques.

The objectives of the research program were:

(1) Experimentally investigate the residual strength of dent damaged tubular steel bracing under direct axial loading and combined loading conditions through end eccentricity.

(2) Assess present strength equations and analytical methods, as well as newly formulated strength equations, for predicting the residual strength of dent damaged tubular steel bracing under direct axial loading and combined loading conditions.

(3) Experimentally investigate the use of internal grouted as well as external grouted steel clamps to repair and improve the residual strength of dent damaged tubular steel bracing under combined loading.

(4) Experimentally investigate the ultimate strength of non-damaged tubular steel bracing under combined loading to establish a baseline for assessing the strength of dent damaged bracing.

(5) Perform preliminary analytical investigations using nonlinear finite element techniques to assess applicability of the method in predicting damaged member strength.

1.6. Scope

Presented herein is a comprehensive report of the damaged tubular member study. Following the introduction given in Chapter 1 of this report, Chapter 2 is presented which describes the experimental program. The experimental behavior of the test specimens is discussed in Chapter 3. Chapter 4 presents analyses of the experimental results. Conclusions and recommendations are noted in Chapter 5. The appendices include various work associated with this project and are included here for completeness.

Figure 1.1 (a) and (b).   View of diagonal bracing members framing into platform jacket leg at waterline.
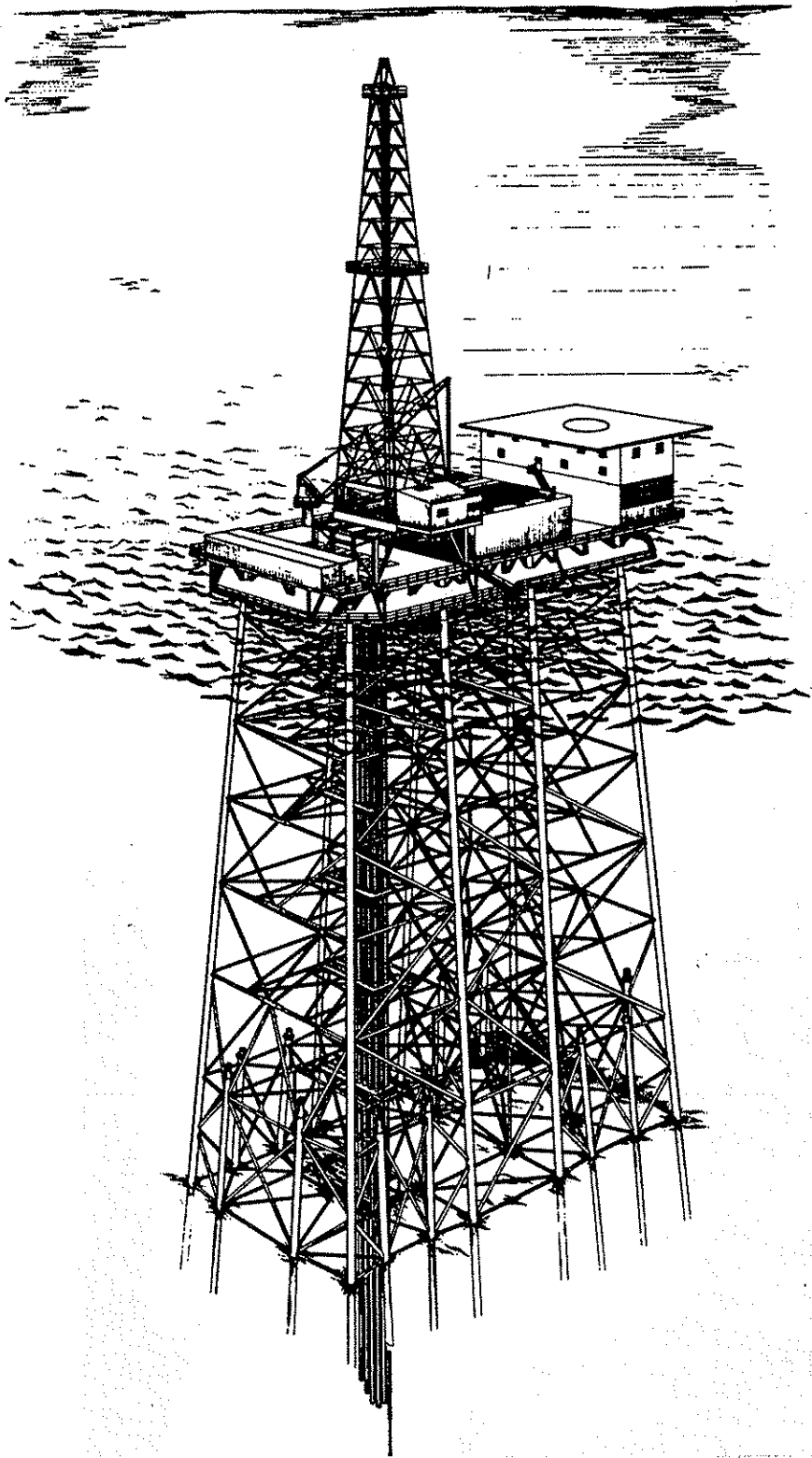
Figure 1.2. Sketch of a typical offshore platform steel jacket showing structural members above and below waterline.
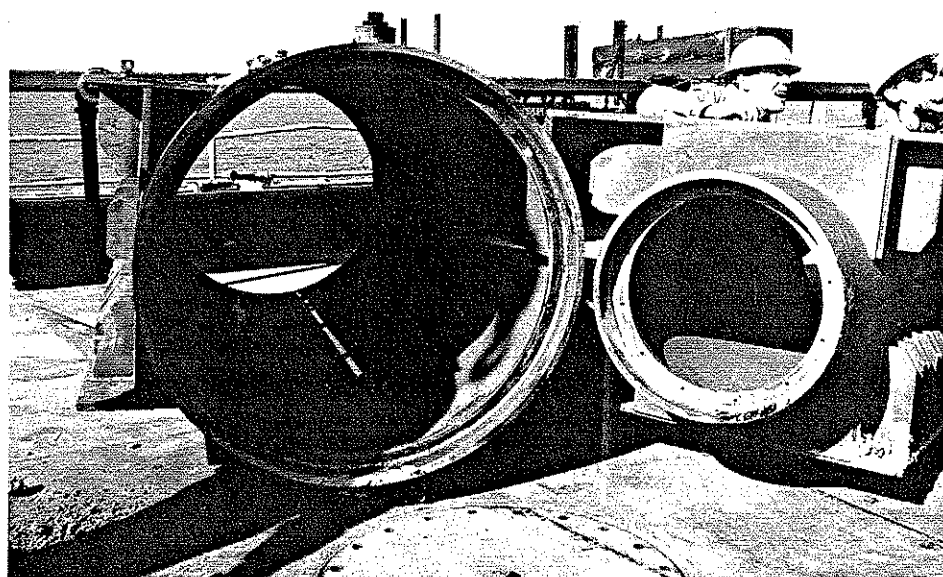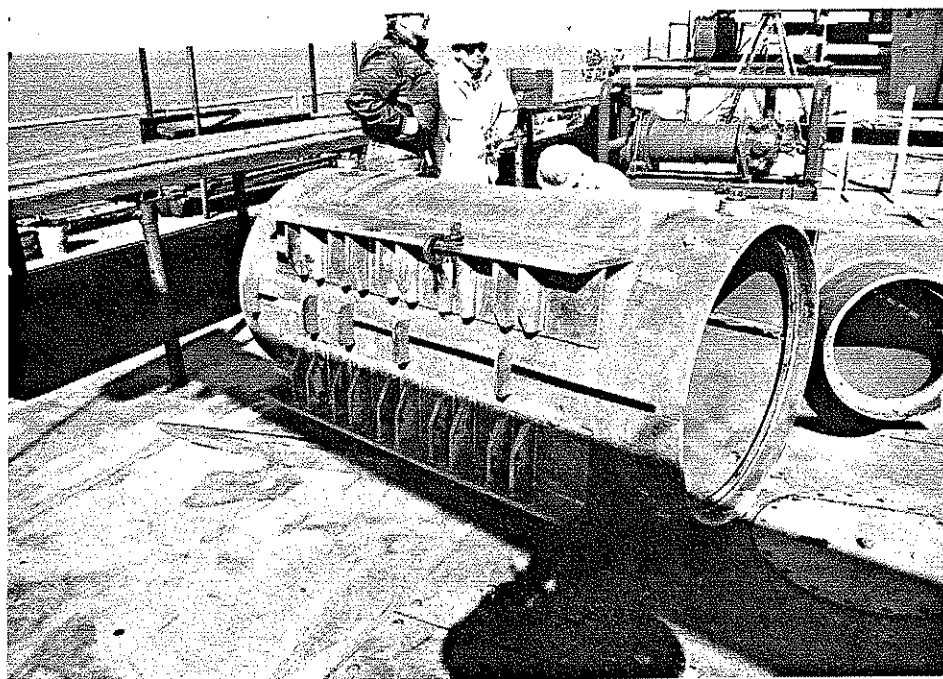
Figure 1.3 (a) and (b). A typical grouted clamp installed at Unocal operated offshore platform EVA to strengthen a fatigue damaged joint connection.
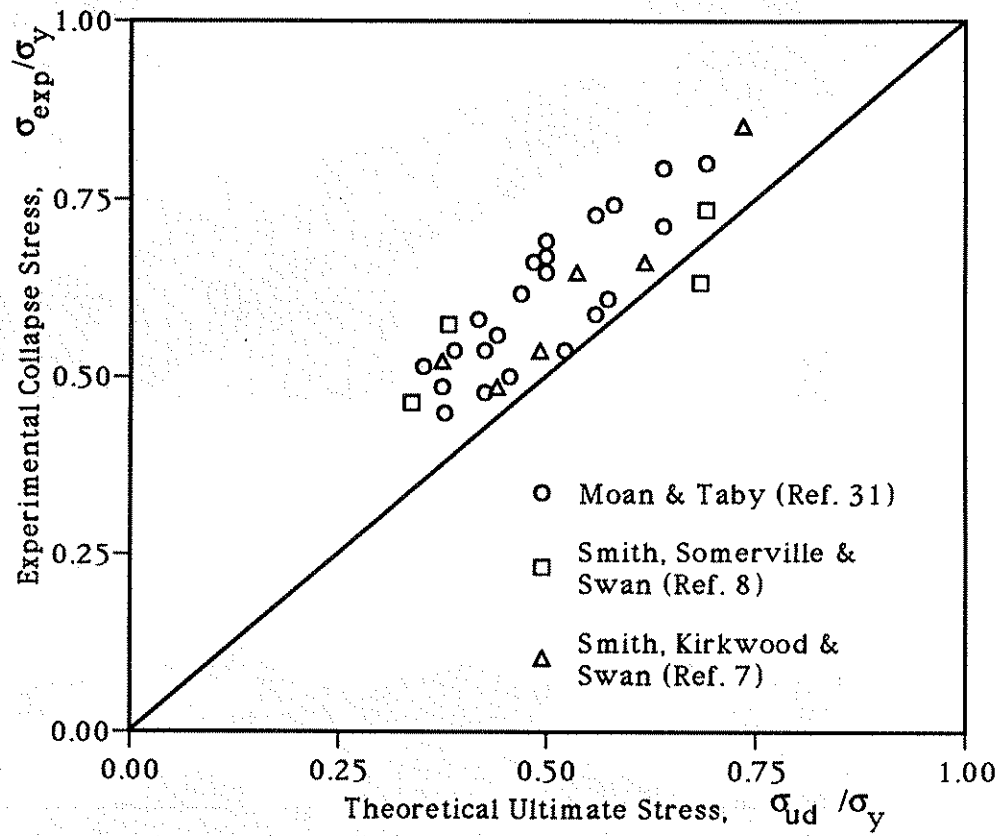
Figure 1.4 Comparison of Ellinas Strength Equation with Past Experimental Results, Showing Lower Bound.
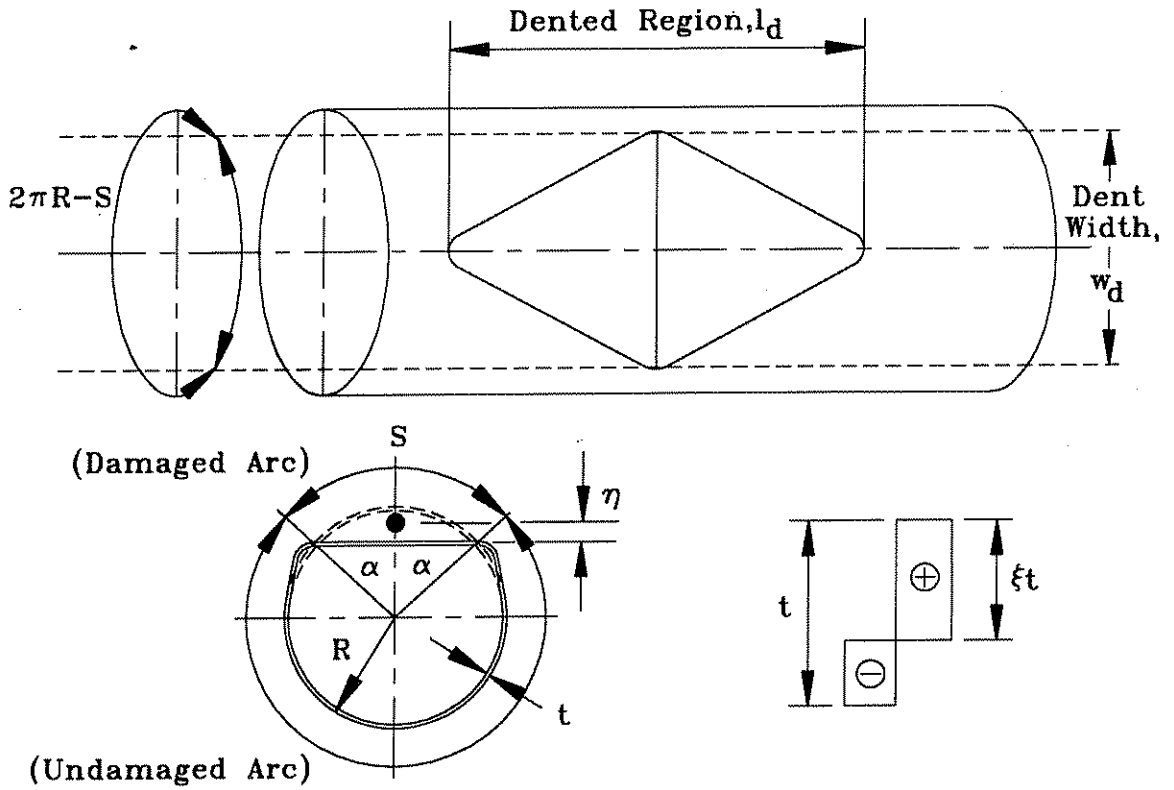
Figure 1.5. Idealization of Dent Geometry.

(a) Stress Distributions in
Dented Zone

(b) Equilibrium of
Damaged Member
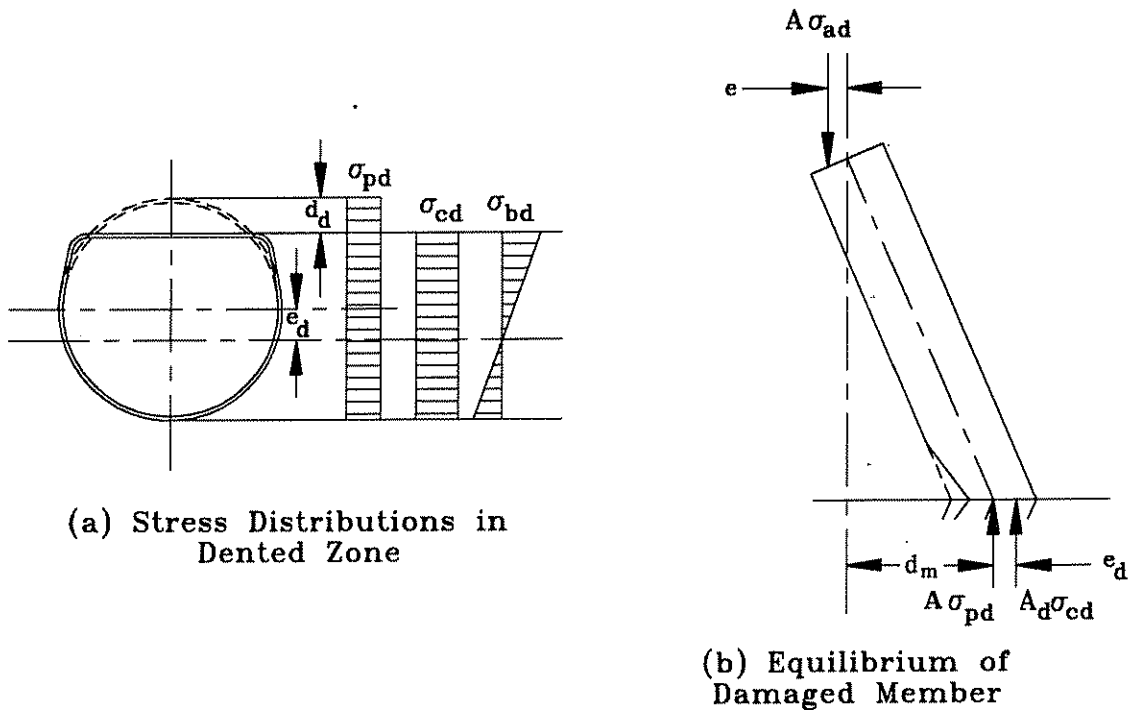
Figure 1.6 (a) and (b).
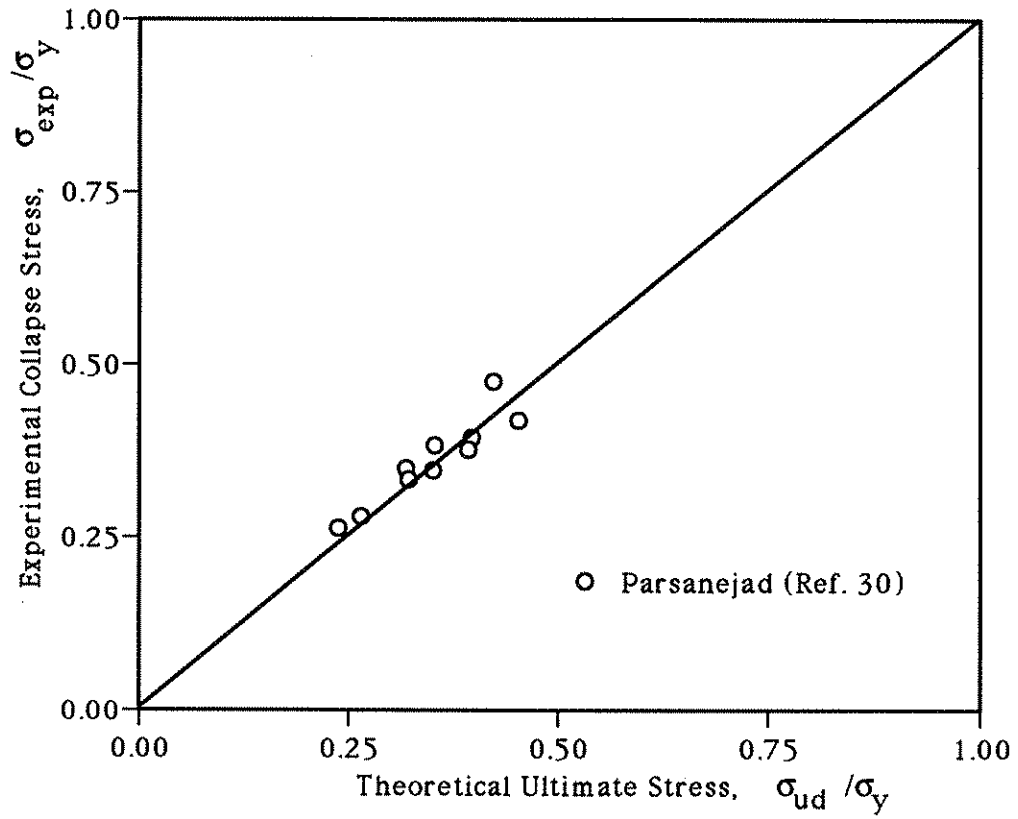
Figure 1.7 Comparison of Parsanejad's Strength Equation for Grout
.Repaired Tubulars with his Experimental Results
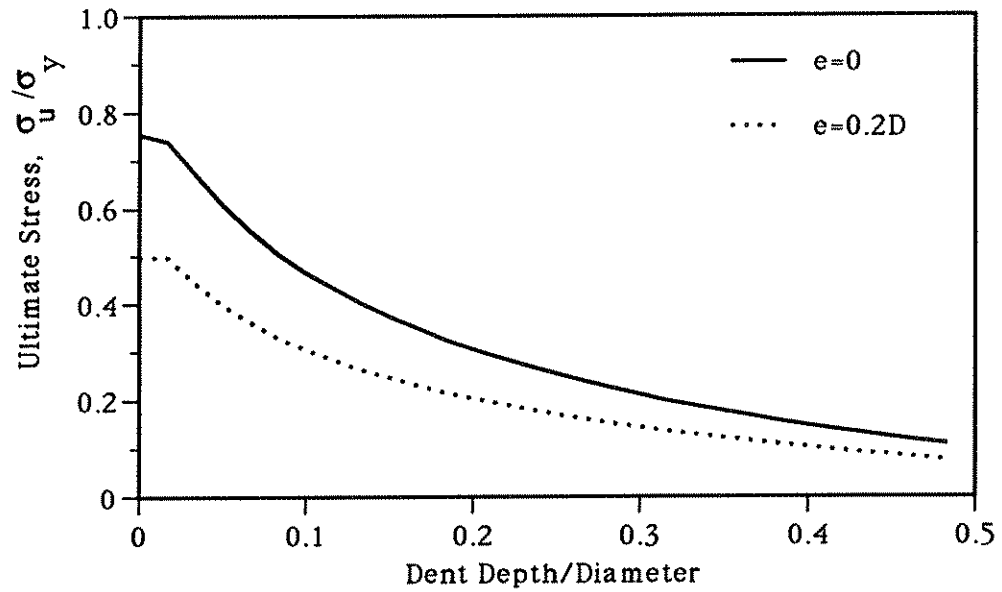
Figure 1.8   UC-DENT Normalized Residual Strength Curves for
Dented Tubular Members of D/t = 34.5.
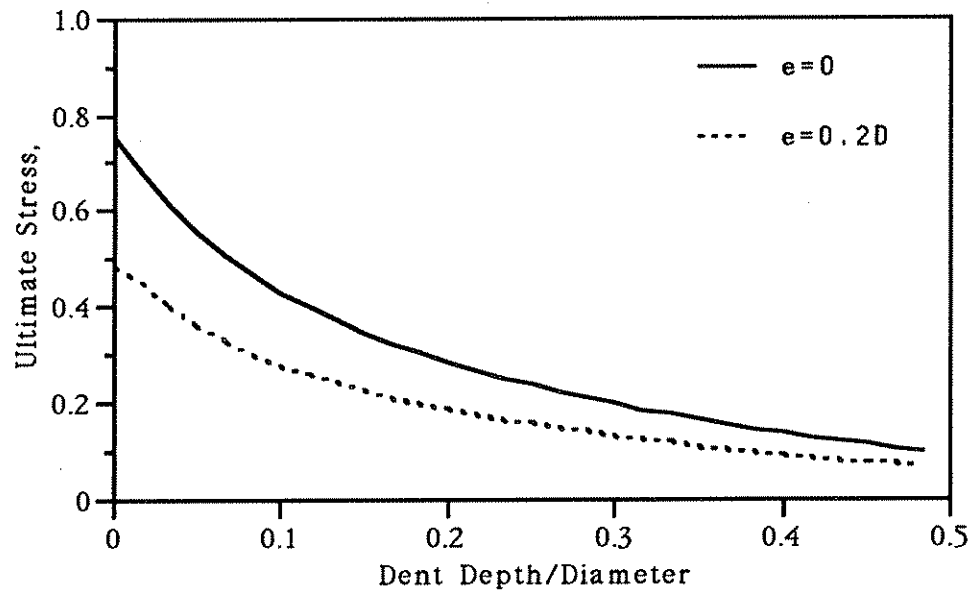
Figure 1.9   UC-DENT Normalized Residual Strength Curves for
Dented Tubular Members of D/t = 46.
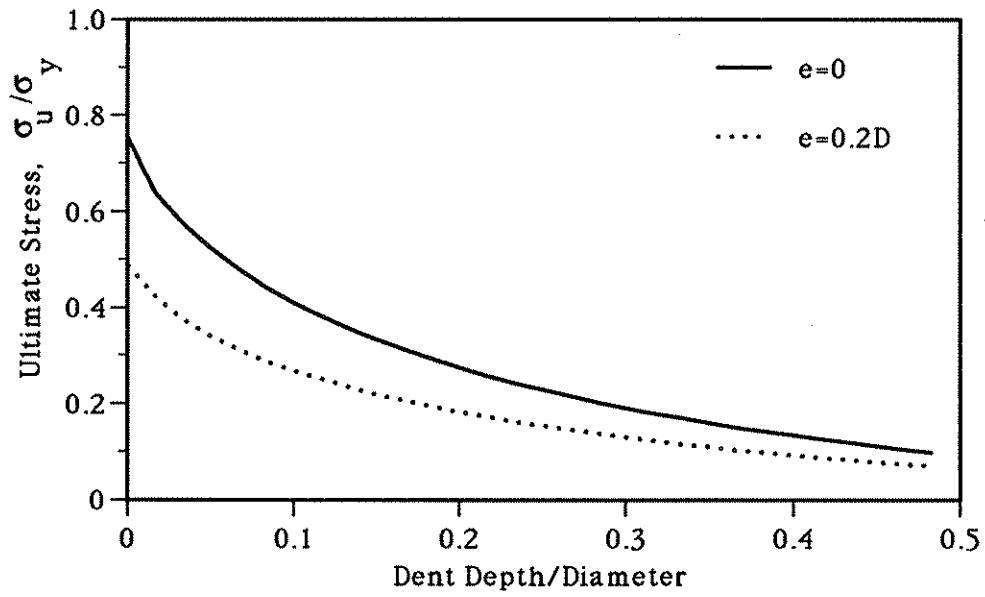
Figure 1.10 UC-DENT Normalized Residual Strength Curves for
Dented Tubular Members of D/t = 64.

CHAPTER 2

EXPERIMENTAL PROGRAM

2.1. General

The size of the test specimens was chosen to closely represent a large-scale model of a typical diagonal bracing member found in fixed platforms existing in U.S. waters. Values for the slenderness ratio (kL/r) and the column slenderness parameter (λ) were selected from typical design parameters and set at 60 and 0.75, respectively. Representative outer diameter D to wall thickness t ratios (D/t) of 30, 45 and 60 were tested. To facilitate the fabrication of the test frame connections for placement of a specimen, a nominal outside diameter of 8.625 inches was selected for all specimens. From this, wall thicknesses were determined which matched the targeted D/t ratios. Standard stock for steel tube resulted in actual D/t ratios of 34.5, 45 and 64 being tested. The specimens represent two-thirds to full-scale models of typical diagonal bracing, depending on platform geographic location and water depth. The length of the specimens for each D/t group was determined knowing the values for the outer diameter and slenderness ratio (kL/r), and found to be approximately 14 feet.

Structural analysis of platforms indicated that the ratio of member flexural force to axial force is equal to 0.2D. Therefore, for the combined loading tests, the axial load was applied through an end eccentricity of 0.20D from the centerline of the specimen. The specimen was loaded in single curvature to induce negative bending at the dented section, and was considered a worst case scenario.

To achieve the desired objectives, five series of tests were conducted in this study:

32

Series 1

Testing of dent damaged tubular bracing under direct axial load, one dented specimen from each D/t group, to assess unrepaired residual strength.

Series 2

Testing of dent damaged tubular bracing under combined loading, one dented specimen for each D/t group, in order to assess unrepaired residual strength under such conditions.

Series 3

Testing of internally grout repaired specimens. One from each D/t group was damaged, then repaired by internally grouting the full length of the member. The specimens were tested under combined loading.

Series 4

Testing of a grouted steel clamp specimen with D/t = 64 under combined loading. A specimen with D/t = 64 was selected because the member's susceptibility to fail under local buckling rather than column buckling. It was presumed that if this group could be strengthened by this means of repair, then the two lower D/t groups could be repaired by this means as well.

Series 5

Testing of a control set of non-damaged specimens, one from each D/t group under combined loading to provide baseline data for comparison with unrepaired and repaired specimen behavior.

A total of thirteen tests were conducted. The experimental test matrix is presented in Table 2.1. The measured geometry of each specimen is summarized in Table 2.2.

2.2. Test Specimens

2.2.1. General Description

The test specimens were fabricated and cut from hot rolled electric resistance welded (ERW) carbon steel pipe of ASTM A53 Grade B material. The weld was oriented longitudinally along the length of the pipes. Material certifications along with API recommended material properties for this material list a minimum yield strength of 35 ksi (API-RP-2A, Table 8.2.1-1 [4]).

2.2.2. Material Testing

A series of material tests were conducted to measure the mechanical properties of the tested specimens. The yield stress was obtained from tensile coupon tests. Stub-column tests aimed at determining the effect of local buckling and residual stresses on the strength of the fabricated tubes were also performed. To further identify the effect of residual stresses, the method of sectioning was used to determine the magnitude of longitudinal residual stress present in the tubes. Compression tests were conducted on all grout mixtures used in the two repair techniques initiated in this study to determine compressive strengths. Results from all tests are included in Table 2.3 and 2.4.

2.2.2.1. Tensile Coupon Tests

The tensile yield strength is a valuable property for analyzing and comparing test data. All data presented in this report is normalized with respect to the measured tensile yield stress. All analysis conducted also used the measured tensile yield stress.

Specimens with similar D/t ratios were taken from the same lot of material. Therefore, three tensile coupons were taken from the end regions of specimens, where a total of nine coupons were tested, three per D/t group. The coupons were machined in accordance with ASTM Specification E8-91 [25]. The coupons were cut in the longitudinal direction of the tube at an angle of 90 degrees from each other, originating at the weld but not including the weld, see Figure 2.1. Dimensions for each coupon are shown in Figure 2.1 as well.

A mechanical testing machine was used for testing the coupons, where each coupon was tested at a loading rate of 0.028 inch/minute of head travel. Static yield strengths were obtained for each coupon by loading the coupon

34

under displacement control and holding a prescribed displacement until the load had stabilized, approximately three minutes, before recording the load. Mechanical wedge grips were used in gripping the coupons. An extensometer incorporating two linear transducers, one on each side of the coupon, was used to average the strain reading across the gage length (6.4375 inches) and eliminate effects of longitudinal curvature in the coupons. A typical stress-strain curve is shown in Figure 2.2.

The yield stresses reported in Table 2.3 for each D/t ratio are the average of the three coupons tested. Young's Modulus was determined from the elastic slope of the stress-strain curves and reported as an average of coupons tested. Percent elongations of approximately 30% were determined for all D/t group coupons. A 30% elongation is typical for ASTM A53 Grade B material.

2.2.2.2 Stub-Column Tests

Stub-column tests were performed in accordance with CRC Technical Memorandum No. 3 [26] for each D/t group. Each stub-column was thirty inches in length, or approximately 3D, and was cold sawed from the end of the tube. One stub-column was sawed from a tube of each material lot, resulting in three column stubs. An eight inch gage length mechanical extensometer recorded the strains during the compressive testing at four locations around the circumference of the stub-column. The load was allowed to stabilize before readings were taken at each point along the curve.

The column stubs first yielded at 85% (D/t=34.5) and 87% (D/t=46 and 64) of the overall compressive yield capacity. This meant that the level of compressive residual stresses was 15% and 13% of the overall yield stress or less. After yielding developed in the entire section, a yield plateau became present which measured the overall compressive yield stress. Two of the three stub-columns tested (D/t ratios of 46 and 64) exhibited local buckling at the development of full yielding of the cross section, and failed abruptly. The stub-column for a D/t of 34.5 exhibited a plastic region of considerable extent, producing a well defined yield plateau. The stress-strain curve for this stub-column is presented in Figure 2.3 with the stress-strain curve for the stub-column of D/t=64 given in Figure 2.4 which had a local buckling failure after yielding. The compressive yield stress is summarized in Table 2.4, and is an average of 4% less than the tensile yield stress.

2.2.2.3.   Residual Stress

Residual stress tests were performed by the method of sectioning, in accordance with SSRC procedures [29].   Strains were measured before and after sectioning using the mechanical extensometer shown in Figure 2.5.   Strains were measured on the inside and outside of the sections.   Curvature of the coupons in the longitudinal direction, after sectioning, caused difficulty in accurately measuring the residual longitudinal strains.   The results for the sections tested from each D/t group are shown in Figures 2.6, 2.7, and 2.8. These results represent residual stresses at mid-thickness.   The recorded strains, however, were not considered reliable due to the measuring difficulties.

2.2.2.4.   Grout Compressive Strength

Grout mixes of API Class A portland cement combined with densified microsilica and high water/cement (w/c) ratios were used to achieve a targeted 28 day compressive strength of 5000 psi.   The densified microsilica flour provided good pumpability of the mix and replaced cement, increasing the w/c ratio.   The internally grouted specimens required approximately 5.5 cubic feet of grout. Restricted volume capabilities of the mixer and grout pump system required three batches of grout to be mixed, one per specimen during repair.   A fourth batch was mixed for the grouted steel clamp.   Typical w/c ratios for the various mixes ranged from 60 to 65% by weight.   Microsilica flour per weight of cement was set at 20%.

Grout was taken from each batch and used to mold two inch cube specimens in accordance with ASTM C109-87 [27] for determination of the compressive strength, f_{cu}.   All cubes were cured in a water bath at ambient temperature until testing.   Strengths given in Table 2.3 are based on the average of three cubes on the day of testing of the damaged member specimen.   The grout strengths for the internal grout repaired specimens were tracked over the 28- curing period and are shown in Figure 2.9(a).   The last data point for each curve coincides with age of the grout when testing the corresponding specimen.   Specimens C3 had a strength of 6894 psi, which was above the targeted strength.

36

Time demands required that the grouted clamp specimen be tested as soon possible after installation and grouting of the clamp. To obtain a grout strength similar to that used for the internally grouted specimens a lower w/c ratio of 57% was used. The clamp repaired specimen was tested at 14 days after grout placement. The resulting compressive strength of f_{cu} = 6103 psi at the time of the test is the average of three cubes and is noted in Table 2.3. A typical grout cube is shown in Figure 2.9(b).

2.2.3. Specimen Geometry

As already noted, the specimen geometry was selected to represent a large scale model of typical bracing member dimensions found in offshore platforms. Overall geometric parameters were discussed in Section 2.1 and given in Table 2.2.

2.2.3.1. Initial Geometry

Accurate measurements of diameter and thickness were carried out, the former by the means of caliper measurements at 90 degree spacings around the circumference of the cross section at five locations along the length of the tube. The thickness was determined from four micrometer readings at each end of the tube. Mean values and statistical parameters for all measurements taken are listed in Table 2.2. All measured values were found to be well within standard tolerances (API-RP-2A [4]).

Initial out-of-straightness along the length of the specimen was measured by placing the specimen in its horizontal test position, and a taut wire was strung along the length of the specimen. Deviations from this benchmark were measured through the use of a micrometer at 15 locations along the length of the specimen. At each of these locations measurements were taken at four positions, spaced at angles of 90 degrees around the circumference of the cross section, and originating at the weld. The location on the cross section where the weld is positioned is referred to herein as the bottom of the section, with the top at 180 degrees. Typical plots of out-of-straightness for the specimens prior to damage application are shown in Figure 2.10. Maximum values for out-of-straightness (δ_o) are reported in the last column of Table 2.2, and fall well below API tolerances of $\delta_o < L/960$ (API-RP-2A, Spec. 11.1.5i [4]).

2.2.3.2. Application of Damage

The targeted dent depth (d_d) of 0.10D was imposed on all damaged specimens. The dent was imposed at the centerspan of the tube and directly opposite of the weld. Global bending was minimized by uniformly supporting the tube throughout the middle section during the denting sequence.

The method of denting is shown in Figure 2.11 involved the use of a servo-valve controlled hydraulic overhead test machine. The dent was applied along the longitudinal surface directly opposite the weld for all specimens. Global bending damage was controlled during the denting process by supporting the tubes along the bottom across a 48 inch length centered about the dent section. The load was applied through a solid knife-edge device with a tip radius of approximately one-quarter of an inch, at the center span of the specimen. The sharp edge simulates the geometry of a sharp, rigid structure such as a ship bow. The load was increased until the dent depth (d_d) reached the targeted amount of 0.10D. A degree of elastic rebound was experienced when denting the tubes, thus several trials were necessary to carefully obtain the correct depth without exceeding it. The depth of each dent was monitored by the instrumented travel of the overhead test machine. These measurements are important for later use in idealizing the dent geometry for analysis. Measured dent depths are listed in Table 2.5 for each specimen, and exclude global bending. Included in Table 2.5 are the measured width w_d and length l_d of the dent.

The damaged out-of-straightness, or global bending (δ_p) after denting, was measured using the same means described for the initial out-of-straightness. These values are also reported in Table 2.5 and found to be very small. Dent profiles for each specimen were developed by similar means. A typical dented specimen profile is shown in Figure 2.12. These profiles include global bending. Figure 2.13 shows a photograph of a tube with D/t ratio of 34.5. Other specimen dent profiles are located in Appendix B.

2.3.   Repair   Methodologies

2.3.1.   Internal Grout Repair

The expected benefits when applying internal grout repair to dent-damaged bracing members arise from the arrest of a growth in the dent depth that has been shown to occur during loading of dented members in past experimental research [9].   Ultimate load capacity is thus increased by eliminating this mode of failure.   The ultimate capacity of internally grouted members can be estimated assuming composite action between the steel member and the grout.   A fiber based finite element program was employed to develop moment interaction curves.   The curves are shown in Figures 2.14, 2.15, and 2.16, and are based on the measured specimen material properties. These results provide an upper bound for the strength of internal grout repaired specimens.   Moment-curvature relationships corresponding to these analysis are provided in Appendix C.

2.3.1.1.   Internal Grout Application

Specimens for internal grout repair were first damaged through denting. Following this stage, each specimen was fitted with two end plates to provide a cap for the grout.   Holes were machined and tapped into each end cap to facilitate the installation of grout ports.   A standard gate valve was inserted into the inlet port to enable pressurized injection of the grout into the specimens.   The outlet port consisted of a three foot vertical standing pipe.   The end caps were tensioned together by the means of eight separate lengths of all thread rod brought together into four spans by the use of a turnbuckle coupler.   The grouting setup is shown in Figures 2.17(a) and (b).   A grout pump with a two inch diameter hose was utilized in the grout injection.   The specimens were inclined to simulate field conditions and the grout was injected from the low end and pumped to the upper end.   Grout was pumped under low pressure until it was flushed completely through the tube and overflowing from the stand pipe.   Grouting continued until a consistent mix was flowing from the outlet.   The inlet valve was closed and the grout pump stopped.   The grout filled specimens were shaded from the sun and kept cool with wet burlap during curing.

The grout strengths for these specimens were discussed previously in Section 2.2.2.4 and listed in Table 2.3.

2.3.2. Grouted Clamp Repair

A conservative design philosophy was taken in the design of the clamp to be installed and tested. The steel clamp was designed to replace the lost capacity of the dented member, by completely replacing the axial strength of a non-damaged section of the dented tube. The ultimate axial load transfer, P_t, between the member and the clamp was calculated by multiplying the contact area between the grout and steel surface of the dented specimen by the bond transfer stress f_{bu}, as determined by Krahl and Karsan [28];

$$f_{bu} = 167 + 1.72 \frac{h}{s} f_{cu} \quad \text{(psi)} \tag{2.1}$$

where f_{cu} is the unconfined grout compressive strength, h is the shear key height, and s is the shear key spacing. The ultimate axial transfer load P_t by the clamp thus becomes

$$P_t = \pi D L_c f_{bu} \tag{2.2}$$

where D is the outside diameter of the damaged member and L_c is the length of the clamp. Rearranging Equation (2.2) and equating the ultimate transfer load to the axial compressive yield capacity of the member's undented section, the required length L_c of the clamp to fully transfer the axial load is

$$L_c = \frac{P_t}{\pi D f_{bu}} = \frac{\sigma_y A}{\pi D f_{bu}} \tag{2.3}$$

where σ_y is the yield stress and A the cross sectional area of the non-damaged section of the member. No shear keys were used, except for a ring stiffener at each end of the clamp. This limited the bond stress transfer in Equation (2.1) to

$$f_{bu} = 167 \text{ psi} \tag{2.4}$$

Clamp cross section geometry was determined from consistent D/t ratios and available fabricated pipe. The lowest D/t ratio (34.5) was selected for the clamp to avoid local buckling. A grout annulus of 0.75 inch was used, subsequently setting the inside diameter of the clamp at approximately ten inches. Available stock with D/t ratios near 34.5 and an inside diameter of ten inches resulted in selection of a wall thickness of 0.307 inch.

The length L_c was compared with the dent profiles of the various specimens to ensure that the clamp extended past the end of the dented segment. The required length to cover the dent profile was found to be 3.5 diameters, or approximately 30 inches. The required clamp length L_c for Specimen C4 was also 30 inches, based on Equation (2.3), and therefore a length of 30 inches was used.

A full design of a working grouted clamp was completed for the required clamp length and specimen geometry of this test program. The clamp was modeled after standard clamp technology presently used in offshore applications. The design consists of two pieces mated together about the dented section through bolted flange plates. Stiffeners are spaced around the bolt holes to provide sufficient restraint against bending action of the flange plates. Fabrication drawings for all components of the designed clamp are included in Appendix D.

For the test program described herein, it was determined appropriate to test the grouted clamp repair philosophy, rather than a specific clamp design. To accomplish this objective, a sleeve with identical dimensions to the designed clamp was fabricated, see Figure 2.18. The use of the sleeve eliminated any need for flange plates and stiffeners. Construction practice enables the flange plates to be easily designed to sufficiently restrain unzipping of the mated sections of the clamp, thus modeling the tested sleeve. A ring stiffener was welded to the inside wall at each end of the sleeve to confine the grout and provide a sealing mechanism. A rubber material was placed between the stiffener and an end ring. The end ring was then tensioned to the stiffener, pinching and expanding the rubber, and thus providing a seal between the specimen and the sleeve. Figure 2.18(b) shows the end seal detail of the fabricated sleeve prior to installation on the damaged specimen. The sleeve contained two ports, one for injecting and the other for releasing the pressurized grout.

2.3.2.1. Annular Grout Injection

The sleeve and specimen surface areas which were in contact with the grout were sand blasted prior to installation of the sleeve to provide a consistent surface roughness as assumed in design calculations. The surface roughness was determined to be 3 mils. Figure 2.19 shows the blasted surface of the dented specimen. The sleeve was installed and positioned centrally about the dented section of the specimen and located symmetrically with fabricated placement bolts shown in Figure 2.20. The ends were sealed and the grout was injected. This specimen was also again set at an incline prior to grouting to simulate field conditions, as shown in Figures 2.20(a) and (b). No shrinkage was observed in the grout. The measured grout strength was described in Section 2.2.2.4 and listed in Table 2.3.

2.4. Test Frame

The 500 kip self-reacting test frame shown schematically in Figure 2.21 was designed and fabricated for the purpose of testing the specimens under compressive load. Care was taken in the development of the design criteria for the test frame to appropriately model assumed experimental parameters including pinned-end conditions; various combinations of applied axial load and bending; unrestrained rotation of specimen ends about any axis; and sufficient test frame capacity. Components of the test frame include: a reinforced concrete reaction block; a sliding load beam located on frictionless wheel casters and directed by a reinforced concrete guide block; two frictionless precision machined ball and socket bearing connections; and two high strength tension rods. A photograph of the test frame is given in Figure 2.22.

Compressive axial load was applied to the specimen through the use of a 150 ton capacity hollow plunger hydraulic cylinder attached to each tension rod (Figure 2.23). The pair of hydraulic cylinders were connected to a 10,000 psi hydraulic pump. The pressure to each cylinder was synchronized by the use of a common hydraulic line from the pump. A pressure relief valve was used to limit the pressure developed by the pump in the hydraulic line, thus limiting the force developed on the tension rods, and enabling load control

during testing. An in-line needle valve afforded the tight metering of flow into each cylinder, subsequently allowing displacement control in the post-ultimate region of loading.

The load collars displayed in Figures 2.24(a) and (b) applied the axial load to the specimen with a prescribed amount of eccentricity (e). For application of direct axial load, the center of the load collars coincided with the center of rotation of the spherical bearings. For combined loading, the center of the load collars was offset, to create the eccentricity (e) from the center of rotation of the spherical bearings and produce applied axial load and bending moment to the dent (Figure 2.25). This bending created additional longitudinal compressive stress in the saddle of the dent.

2.4.1. Design, Fabrication, and Construction

The ball and socket bearing connection, shown in Figure 2.25 was designed to effectively model true pinned-end conditions by allowing free rotation of the ends of the specimen. The spherical ball and socket were machined to a tolerance of 0.003 inch. The ball was coated with a high pressure grease before being fastened to the socket with high strength bolts. All welds designed for the fabricated pieces were sized from force and moment actions resulting from a specimen ultimate axial compressive load of 500 kips developing within the test frame. A reasonable factor of safety was applied to the required weld strengths to assure confidence and test frame endurance. All fabrication drawings produced for the designed spherical ball and socket are included in Appendix E.

The load beam, Figure 2.26, was designed to accommodate the ball and socket bearing connections and transfer the tension rod forces to the specimen. This beam was built up from two standard channel shapes, C15x50, placed back to back with a 3 inch gap providing passage for the tension rods, and secured by welded plates. Various stiffeners were located in the regions of applied load and reactions.

The 2 inch diameter high strength threaded tension rods are comprised of two lengths coupled together and extending a total of 20 feet. The rods had an ultimate load rating of approximately 250 kips each.

End platens were first inserted into each end of the specimen to provide uniform bearing pressure over the tube cross section, before placing the load

collars over the specimen's ends. Hydrostone was then injected into each load collar to provide a uniform bearing surface between the load collars and end platens as well as the outer wall of the specimen. Load collar fabrication drawings are also located in Appendix E.

Since the test frame was self-reacting, it did not require tie downs to a reaction floor. The reaction block of the test frame was designed to resist the moments and shears imposed on it by the two hydraulic cylinders. An added mat of steel was located in the block at points of load application (bearing connection, hydraulic cylinder) to resist concrete crushing under bursting stress. Figure 2.27 shows the reaction block during construction. The reaction block weighed approximately 6 tons after construction.

To eliminate any accidental eccentricities in the application of the load to the specimen, the load beam was placed and aligned on frictionless wheel casters and steered by the guide block. Care was taken in the framing of the guide block (Figure 2.28) to assure that the faces were orthogonal and parallel to the line of loading, thus eliminating possible wedging of the loading beam. The block was designed to withstand proportionally smaller loads than that of the reaction block. The guide block weighed approximately 8 tons after construction. Both the reaction and guide block were positioned and leveled in the test setup using hydrostone beneath each.

2.5. Instrumentation

Each specimen tested was instrumented to monitor its response under loading. Figure 2.29 shows the instrumentation setup employed for the non-repaired and internal grout repaired specimen tests. Axial end shortening was measured using two displacement transducers located at each end of the specimen on the horizontal neutral axis. The end shortening transducers were averaged to get the shortening at the centerline of the specimen. Electric inclinometers were mounted on each end of the specimen to monitor end rotation.

Vertical displacements in the plane of bending of the specimen were measured by five equally spaced transducers along the length of the specimen. The dent depth growth was monitored using two vertical displacement transducers, one measuring the displacement of the bottom of

44

the dented section while the other measuring the displacement of the saddle of the dent. These two readings were subtracted from each other to attain the dent depth growth.

Strain gages were placed around the circumference of the tube at the quarter points along the span to monitor both longitudinal and hoop strains. The longitudinal gages at each end location were used in the alignment of the specimen during installation into the test frame. These gages were also used in verification of the load readings obtained from the load cells. Figure 2.30 shows the results of the verification. Two strain gages were also placed longitudinally in the dent to monitor strain. Ovaling of the tube was monitored in both planes of the cross section. Four linear displacement transducers were fixed onto a specially fabricated bracket and mounted onto the specimen at the quarter points along the span of the specimen. Variations in the diameters were recorded to characterize the cross section ovaling. A displacement transducer placed at the dented section monitored any movement of the specimen out of the plane of bending as well.

A calibrated load cell was located at each hydraulic cylinder to record the load applied to each tension rod. The separate readings were combined to provide the total applied axial load.

The instrumentation scheme described above was modified slightly to monitor the response of the sleeve during testing of the grouted clamp repaired specimen. Figure 2.31 shows the modified instrumentation layout. The modification consisted of placing four additional linear transducers at each end of the sleeve to measure relative longitudinal displacement between the sleeve and the tube. Strain gages were placed at similar locations on both the tube and sleeve wall to monitor their longitudinal and transverse strains. In addition, a 0.25 inch hole was drilled through one side of the sleeve above the dent of the specimen and a conduit placed into the grout annulus, such that the end of the conduit bear against the saddle of the dent. This was done in order to allow the transverse displacement of the dent saddle to be monitored, placing the shaft of an LVDT through the conduit and in contact with the saddle. Figure 2.32 shows the instrumented sleeve on the specimen prior to testing.

Figures 2.33 shows a specimen installed into the test frame, instrumented for response, and ready for testing. Specimens were whitewash with a hydrated lime solution to display yield patterns.

2.6. Data Acquisition

2.6.1. Description of Software

The data acquisition system utilized in this experimental program is shown schematically in Figure 2.34. A 386 IBM PC compatible was used to run the DATACQ software written especially for this project. The PC was capable of scanning a total of 128 channels with 12 bit accuracy. This was accomplished by multiplexing a 16 channel National Instruments AT-MIO-16 A/D board by 8 National Instruments Multiplexing boards. A voltage source was provided for each bridge circuit (transducer) in the voltage/transducer cabinet, with signal conditioning for each strain gage channel. Each variable resistor (strain gage, transducer) located on the specimen was connected to the voltage/transducer cabinet.

The DATACQ program was developed to satisfy specified requirements of the test program. The following were key capabilities of the software:

- Real-time - In order to provide triggering and display of selected channels, the system was developed for real-time. This required small amounts of multi-tasking, listening for unsolicited keyboard input and also watching channels for triggering while continuously updating the display.

- Screen Formatting - The system utilized screen formatting to provide essential information at high speeds. The user was capable of modifying variables including displayed channels, triggering channels, and triggering deltas during acquisition.

- Manual Scanning - The system allowed the user to scan all channels at any instance during testing.

- Channel Display - The system provided channel display in real-time.

- Unlimited Scans - An unlimited scanning capability based on disk space was implemented to rid of pre-test predictions of total number of scans to be taken.

- Triggering on Multiple Channels - The system provided a capability to scan on its own, based on user specified values (deltas) on a number of different channels. Manual scans automatically reset old triggering values.

- Reliable Performance - The system was required to perform in case of possible user error. Known keyboard combinations causing program termination were watched for, and data was saved to disk upon detection.

- Safety Backup - The system provided a hard copy of user selected critical channels after each manual or triggered scan.

2.6.2. Procedure of Data Acquisition

After installation and instrumentation of the specimen, the data acquisition was configured. The program DATACQ was loaded and a zero scan of all channels was taken. The transducers were checked against known displacements to verify system operation. Another zero scan was taken and written to disk. A shunt calibration of the strain gages was performed to confirm known voltages input to the resistors. The next step was to define all channels and deltas to trigger on, and to select screen displayed channels. During loading of the specimen the screen displayed channels were watched to monitor specimen response. Manual scans were taken near the peak load to capture the maximum load. After the loading was discontinued, the data was saved to disk and the program was exited. The file created by DATACQ was then reduced to a group of individual channel files for subsequent analysis. A user's manual developed for use with the DATACQ program is located in Appendix F.

2.7. Testing Procedure

Prior to testing of a specimen, its alignment was verified by applying an initial load of approximately 10 kips. Longitudinal axial strains were monitored during alignment to check for uniformity in the plane of bending as well as out of the plane of bending. This ensured that no accidental eccentricity was introduced in the specimen from installation into the test frame. The alignment loading also provided an initial seating force to firmly seat all components of the test frame and ready the system for testing.

All instruments were zeroed in the data acquisition program prior to testing. A compressive axial load was applied at an approximate rate of 1 ksi/min. The loading rate was controlled by limiting the pressures developed by the pump and released to the hydraulic cylinders. Load control was attained in the ascending branch of the load-shortening curve by slowly increasing the pressure in the system through the use of a pressure relief valve. This increase in pressure increased the force developed in the hydraulic cylinders and subsequently applied to the tension rods.

Scan triggers were set within the data acquisition software to scan all instrumented channels at increments of 7 kips applied load and/or end shortening displacement increments of 0.03 inches. An end shortening signal was fed into an XY recorder together with the load cell signals to provide a real-time graphic load-shortening curve.

The loading was halted frequently to allow the load to stabilize and static readings to be scanned. The load stabilization in the ascending portion of the load-shortening curve was accomplished by locking in the current pressure in the system. The loading was continued until the ultimate capacity of the specimen was reached and a maximum static value recorded. Beyond the ultimate capacity, displacement control was introduced into the loading by the tight metering of an in-line needle valve in the hydraulic system. With the pressure decreasing, increased hydraulic fluid flow into the hydraulic cylinders was allowed, subsequently increasing the cylinder stroke. The data acquisition software typically began scanning on end shortening displacements at, or just prior to, attaining the peak load.

The test was continued until the specimen's strength reached zero, or a total displacement of five times the displacement at peak load was reached.

48

(This page intentionally blank)

Table 2.1 - Experimental Test Matrix.

Spec. No.	$\dfrac{D}{t}$	End Eccentricity e	Dent Depth d_d	Description of Specimen
A1	34.5	0	0.10D	Damaged, Non-repaired
B1	46	0	0.10D	Damaged, Non-repaired
C1	64	0	0.10D	Damaged, Non-repaired
A2	34.5	0.20D	0.10D	Damaged, Non-repaired
B2	46	0.20D	0.10D	Damaged, Non-repaired
C2	64	0.20D	0.10D	Damaged, Non-repaired
A3	34.5	0.20D	0.10D	Damaged, Internal Grout Repair
B3	46	0.20D	0.10D	Damaged, Internal Grout Repair
C3	64	0.20D	0.10D	Damaged, Internal Grout Repair
C4	64	0.20D	0.10D	Damaged, Grouted Clamp Repair
A5	34.5	0.20D	0	Non-damaged
B5	46	0.20D	0	Non-damaged
C5	64	0.20D	0	Non-damaged

Table 2.2 - Measured Specimen Geometry.

Spec. No.	Diameter, D (in.)		Thickness, t (in.)		Length, L (in.)	Mean Initial Ovality $\frac{D_{max} - D_{min}}{D_{mean}}$	$\frac{\delta_0}{L}$
	Mean	COV	Mean	COV			
A1	8.626	0.0002	0.247	0.0232	178.8	0.0004	0.0004
A2	8.624	0.0002	0.246	0.0119	178.8	0.0006	0.0001
A3	8.625	0.0003	0.247	0.0210	178.8	0.0005	0.0001
A5	8.636	0.0011	0.248	0.0210	178.8	0.0006	0.0002
B1	8.631	0.0041	0.186	0.0120	178.9	0.0029	0.0003
B2	8.636	0.0011	0.186	0.0384	178.9	0.0038	0.0005
B3	8.634	0.0025	0.187	0.0215	178.9	0.0032	0.0006
B5	8.642	0.0810	0.134	0.0200	178.9	0.0320	0.0001
C1	8.642	0.0810	0.134	0.0200	180.1	0.0320	0.0001
C2	8.643	0.0396	0.136	0.0127	180.1	0.0152	0.0004
C3	8.643	0.0413	0.135	0.0152	180.1	0.0264	0.0002
C4	8.642	0.0522	0.136	0.0261	180.1	0.0211	0.0008
C5	8.643	0.0396	0.136	0.0127	180.1	0.0152	0.0009

Table 2.3 - Averaged Specimen Measured Material Properties from Tensile Coupon Tests and Grout Cubes

Spec. No.	Young's Modulus	Static Yield Stress σ_y	Strain Hardening Modulus E_{sh}	Strain Hardening ε_{sh}	Ultimate Stress σ_u	Elongation at Fracture $\Delta_\%$	Compressive Grout Strength
	(ksi)	(ksi)	(ksi)	(in/in)	(ksi)	(%)	(psi)
A1	29071	34.8	0.0162	518	46.5	33.1	-
A2	29071	34.8	0.0162	518	46.5	33.1	-
A3	29071	34.8	0.0162	518	46.5	33.1	4375
A5	29071	34.8	0.0162	518	46.5	33.1	-
B1	30714	33.4	0.0089	764	42.9	32.9	-
B2	30714	33.4	0.0089	764	42.9	32.9	-
B3	30714	33.4	0.0089	764	42.9	32.9	3885
B5	30714	33.4	0.0089	764	42.9	32.9	-
C1	30800	39.4	0.0111	1145	57.9	28.9	-
C2	30800	39.4	0.0111	1145	57.9	28.9	-
C3	30800	39.4	0.0111	1145	57.9	28.9	6894
C4	30800	39.4	0.0111	1145	57.9	28.9	6103
C5	30800	39.4	0.0111	1145	57.9	28.9	-

52

Table 2.4 - Tensile and Compressive Measured Specimen Static Yield Stress

Spec. No.	Tensile Yield Stress σ_y (ksi)	Compressive Yield Stress σ_y (ksi)
A1	34.8	33.3
A2	34.8	33.3
A3	34.8	33.3
A5	34.8	33.3
B1	33.4	31.4
B2	33.4	31.4
B3	33.4	31.4
B5	33.4	31.4
C1	39.4	38.2
C2	39.4	38.2
C3	39.4	38.2
C4	39.4	38.2
C5	39.4	38.2

Table 2.5 - Test Specimen Parameters Based on Measured Specimen Geometry

Spec. No.	$\dfrac{D}{t}$	$\dfrac{L}{r}$	$\lambda = \dfrac{L}{r\pi}\sqrt{\dfrac{\sigma_y}{E}}$	$\dfrac{\delta_p}{L}$	d_d (in)	w_d (in)	l_d (in)
A1	34.9	60.4	0.745	0.0007	0.868	5.0	26.0
A2	35.1	60.6	0.747	0.0006	0.861	5.0	26.0
A3	35.1	60.6	0.747	0.0006	0.857	5.0	24.0
A5	34.8	60.5	0.746	-	-	-	-
B1	46.4	60.0	0.730	0.0009	0.862	5.0	24.0
B2	46.4	60.0	0.730	0.0026	0.861	5.0	24.0
B3	46.5	60.1	0.731	0.0011	0.863	5.0	24.0
B5	46.3	60.1	0.731	-	-	-	-
C1	64.5	59.8	0.743	0.0012	0.861	5.0	24.0
C2	63.6	59.6	0.743	0.0007	0.861	5.0	24.0
C3	63.9	59.7	0.744	0.0009	0.860	5.0	24.0
C4	64.5	59.8	0.743	0.0012	0.861	5.0	24.0
C5	63.6	59.6	0.743	-	-	-	-

Note: Dent is located at midspan of each specimen, and is subjected to compression with respect to bending when loaded by combined loading
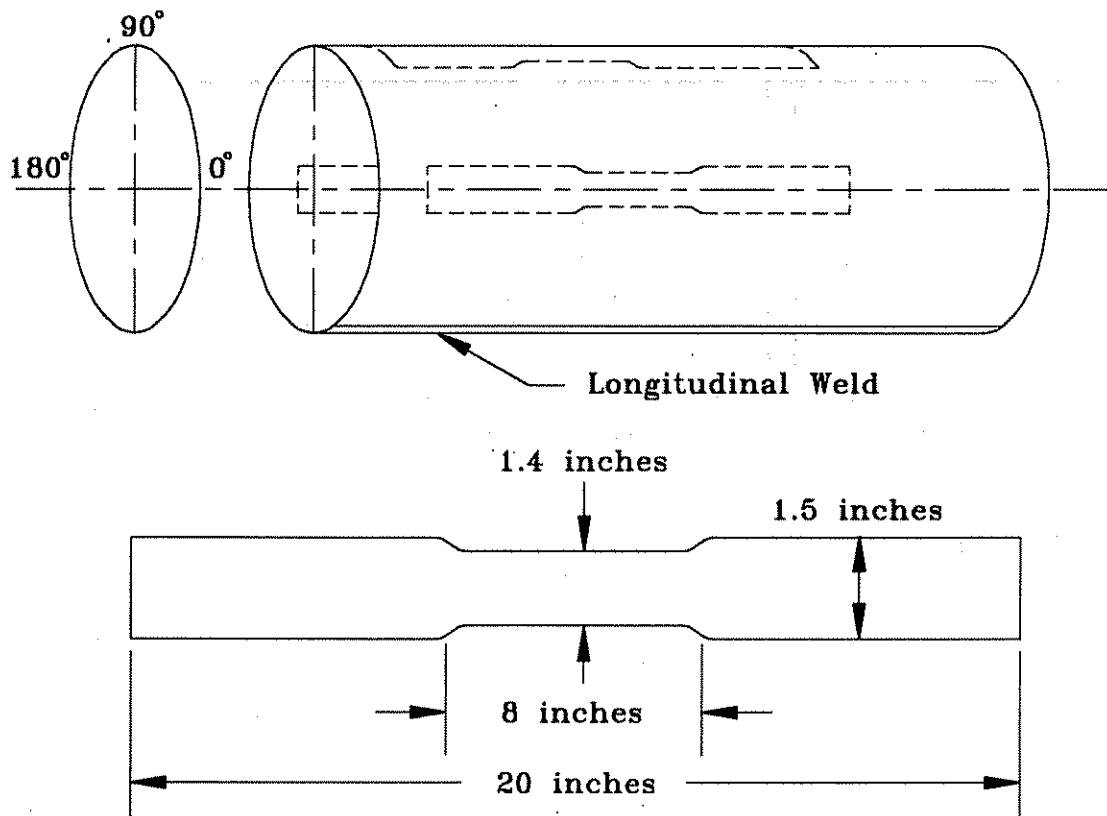
Figure 2.1: Tensile Coupons
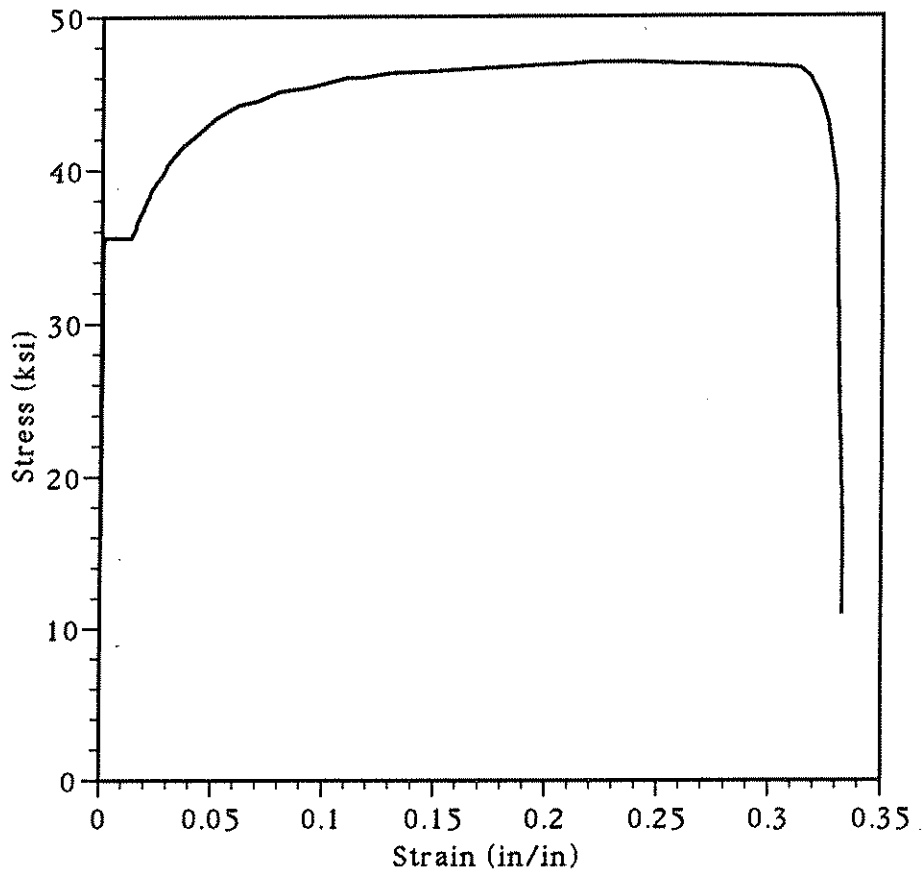
Figure 2.2. Stress-Strain Curve for a Tensile Coupon of D/t=34.5

56
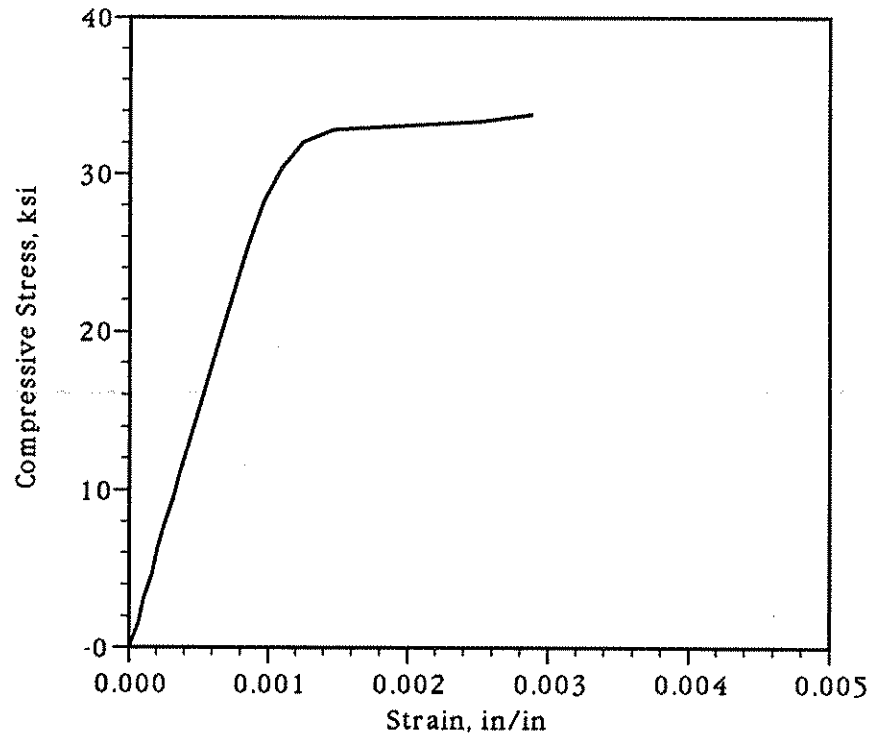
Figure 2.3. Stub-Column Stress-Strain Curve for Specimens with D/t=34.5.
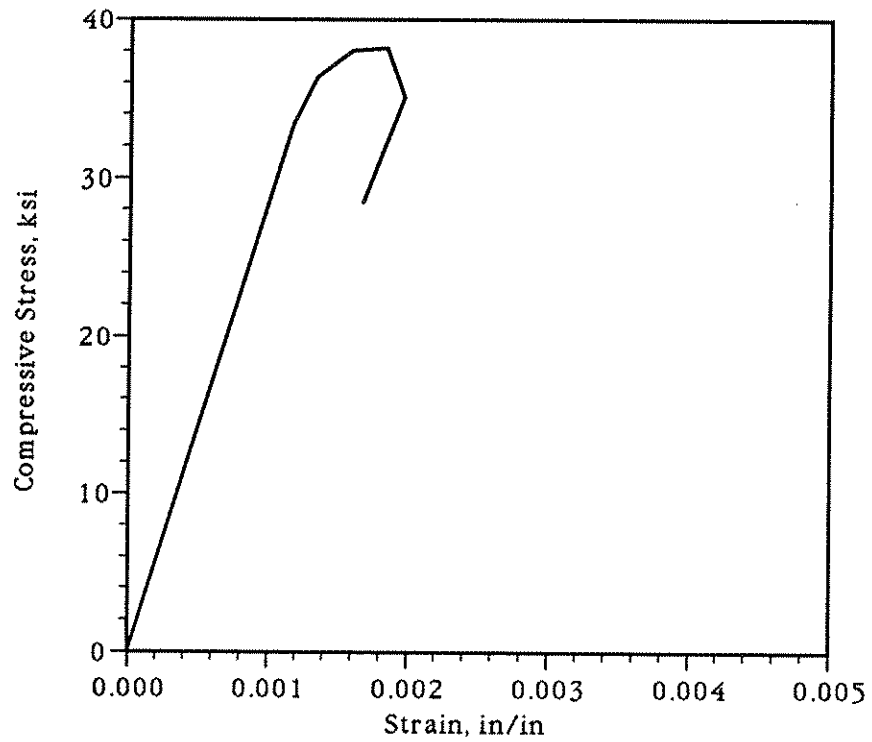
Figure 2.4. Stub-Column Stress-Strain Curve for Specimens with D/t=64.
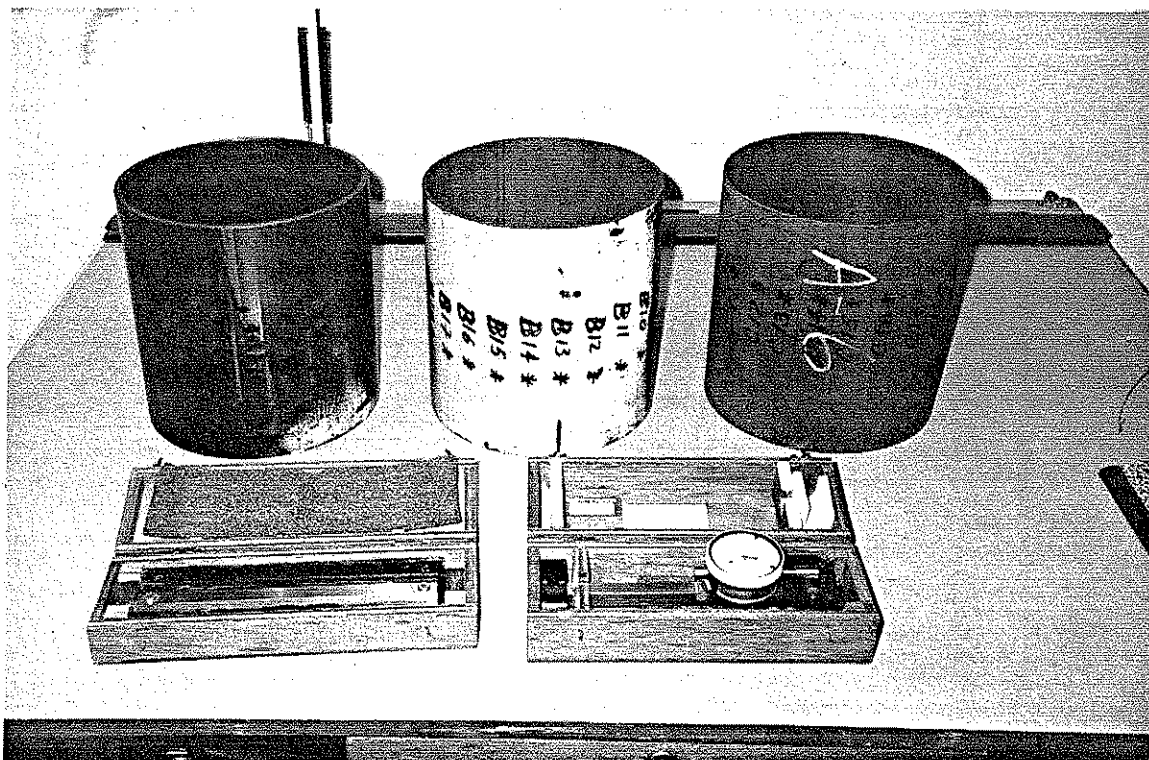
Figure 2.5.   Sections marked on tubes for determining residual stresses by the method of sectioning.   Mechanical extensometer was used for measurement.
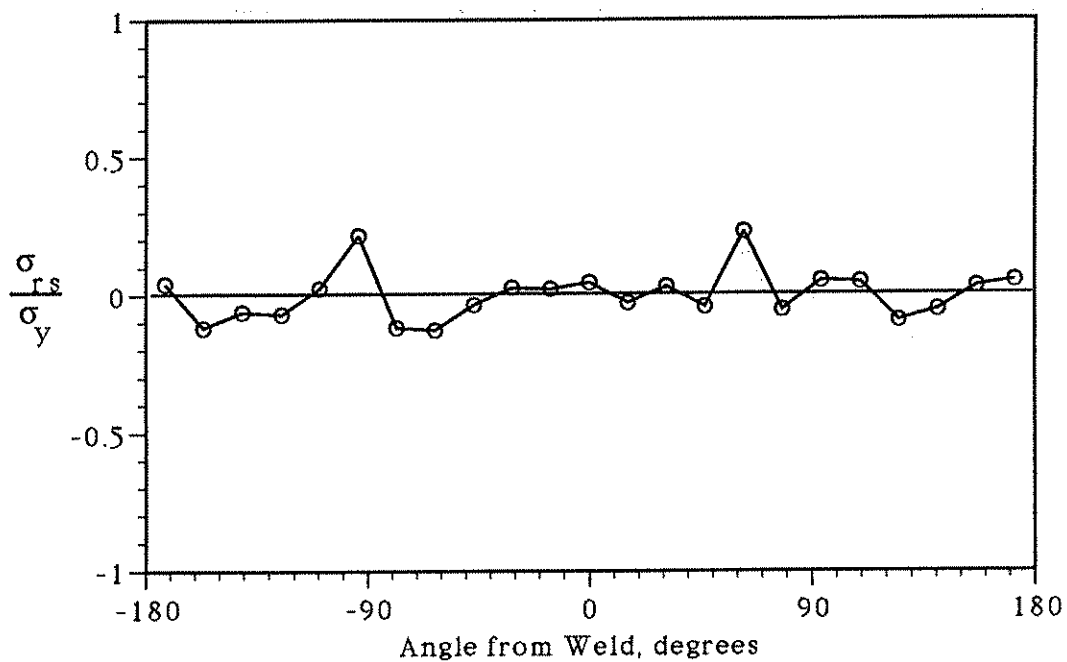
Figure 2.6.   Longitudinal Residual Stress Distribution from Sectioning Method for Specimens with D/t=34.5.

58
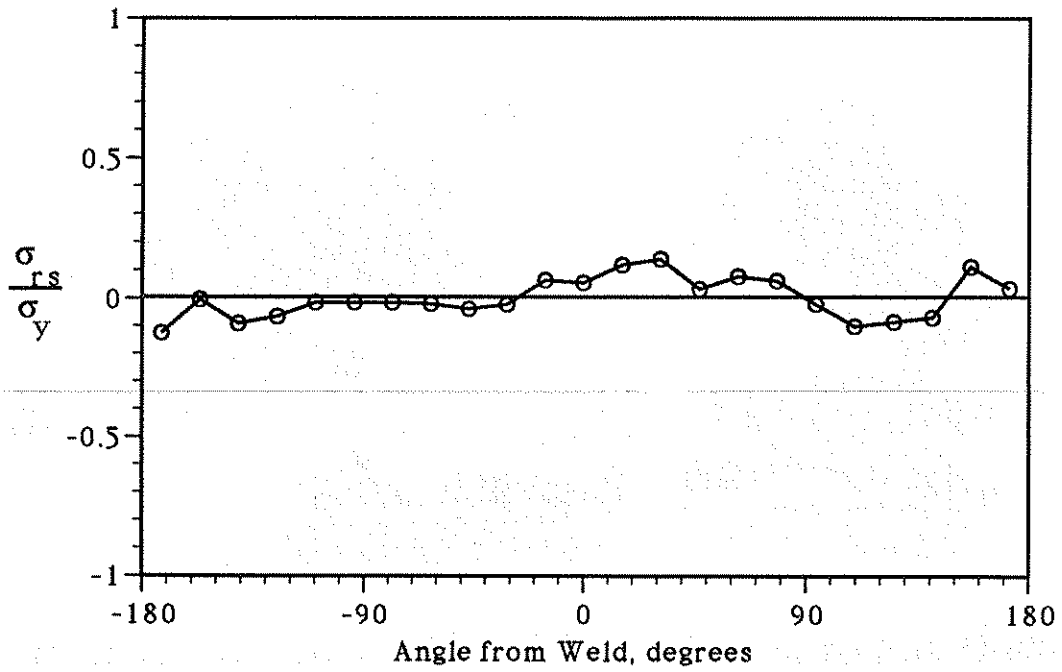
Figure 2.7.   Longitudinal Residual Stress Distribution from
Sectioning Method for Specimens with D/t=46.
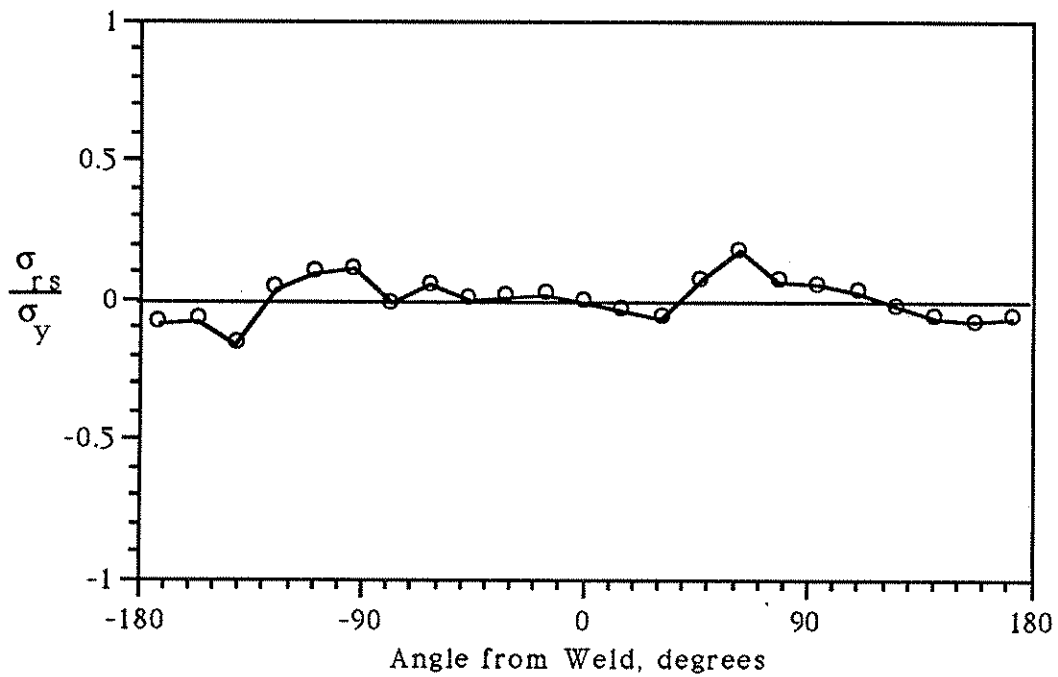
Figure 2.8.   Longitudinal Residual Stress Distribution from
Sectioning Method for Specimens with D/t=64.
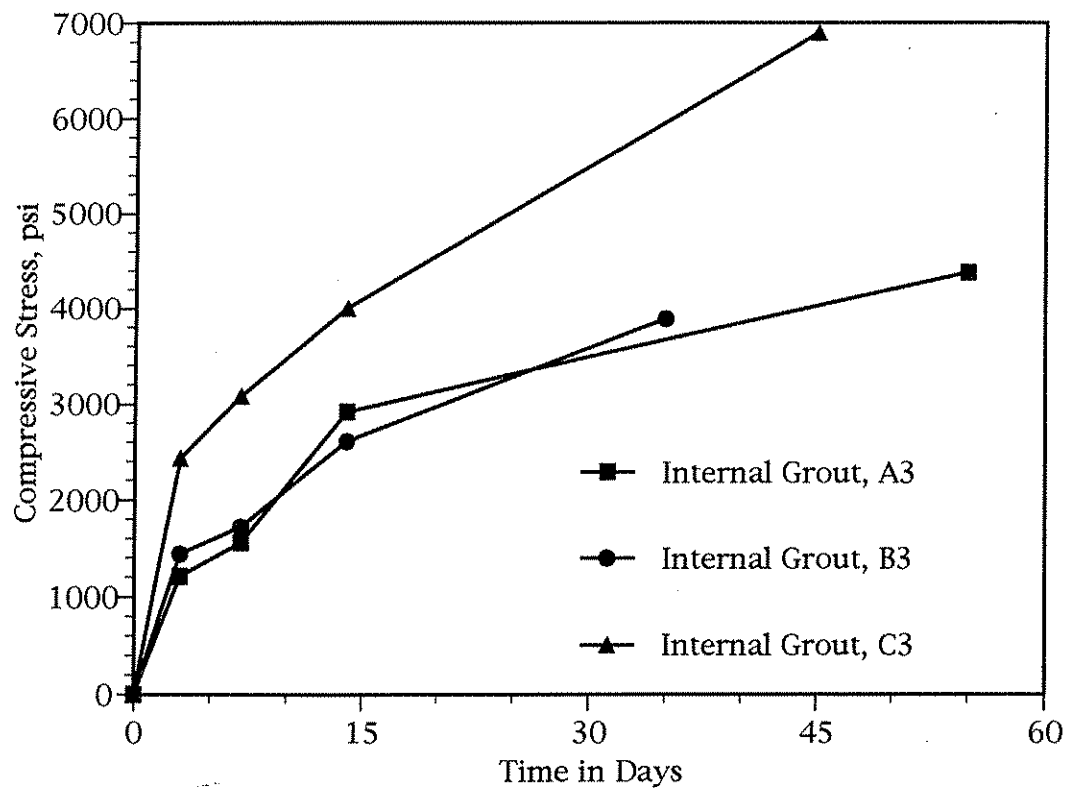
Figure 2.9(a). Compressive Strength Curves for Internal Grout Repaired Specimens. Last Data Point Represents the Grout Strength at Time of Testing.
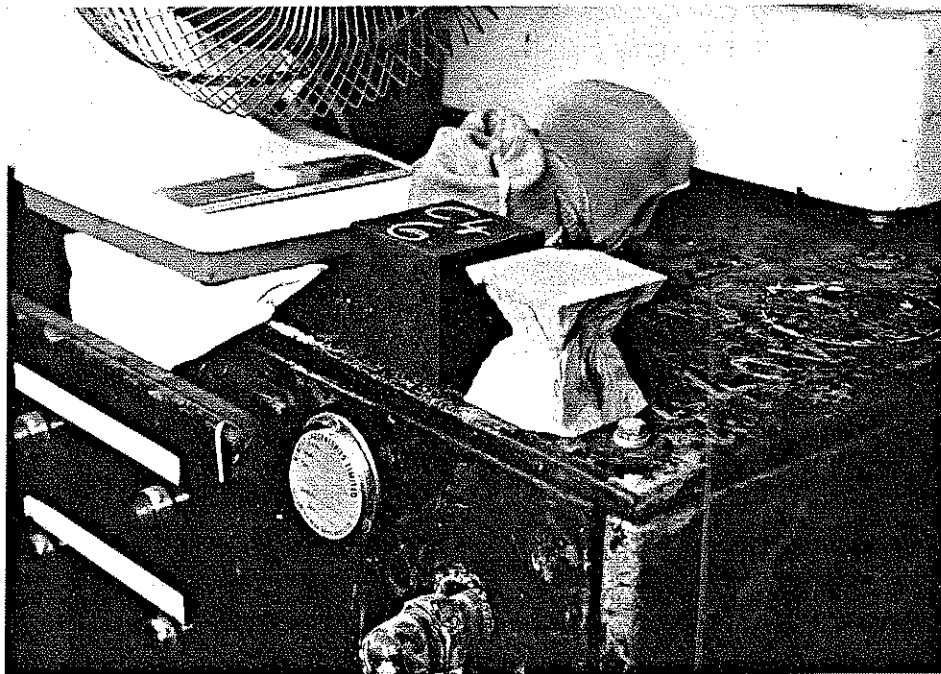
Figure 2.9(b). Typical grout cube utilized for compressive strength tests.
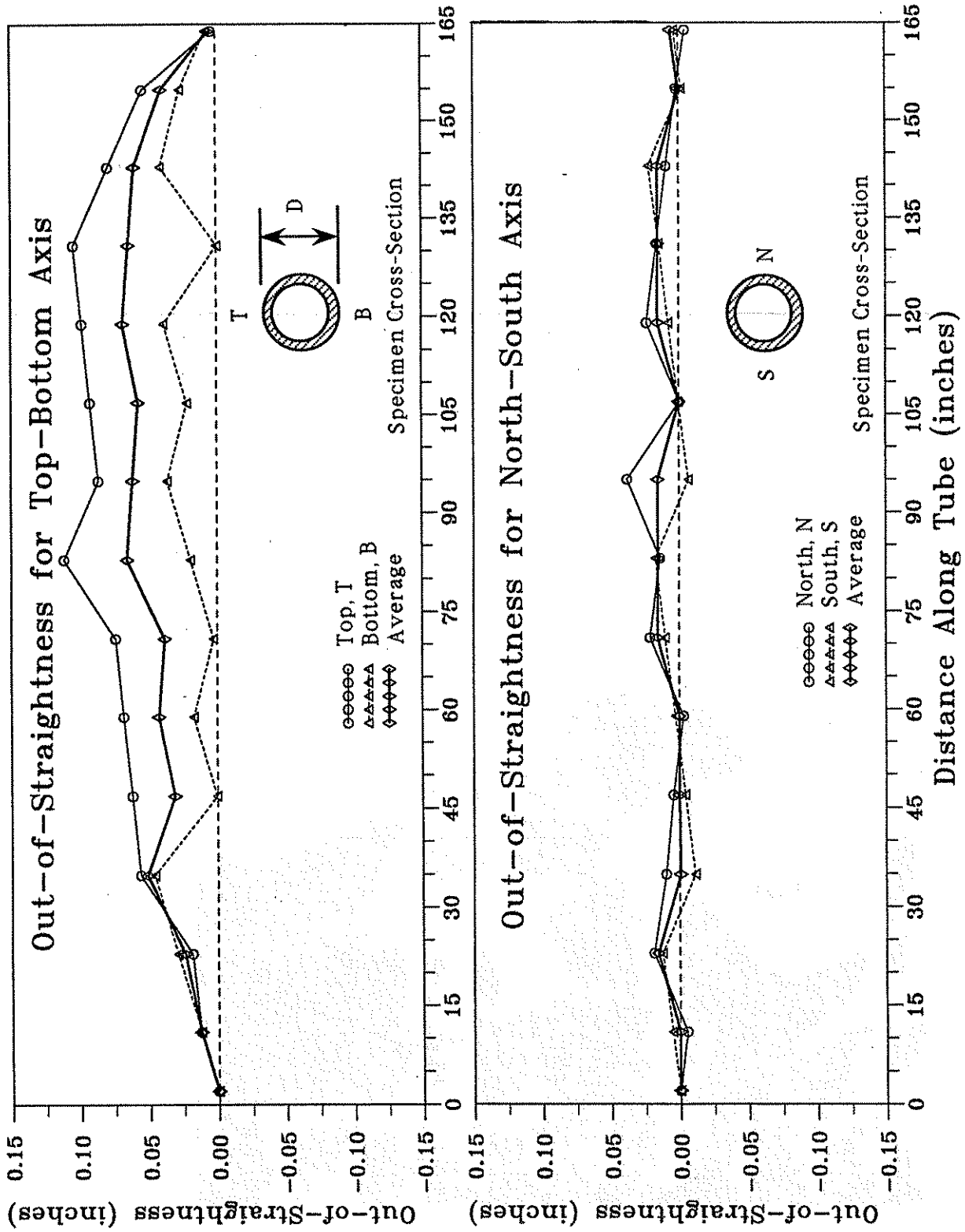
Figure 2.10. Initial Out-Of-Straightness for Specimen A1.

Imposing Controlled Dent Damage to a Specimen

P, Load Applied by Overhead Test Machine

Hydrostone Support Bed

48 in.

A A

P

Section A-A
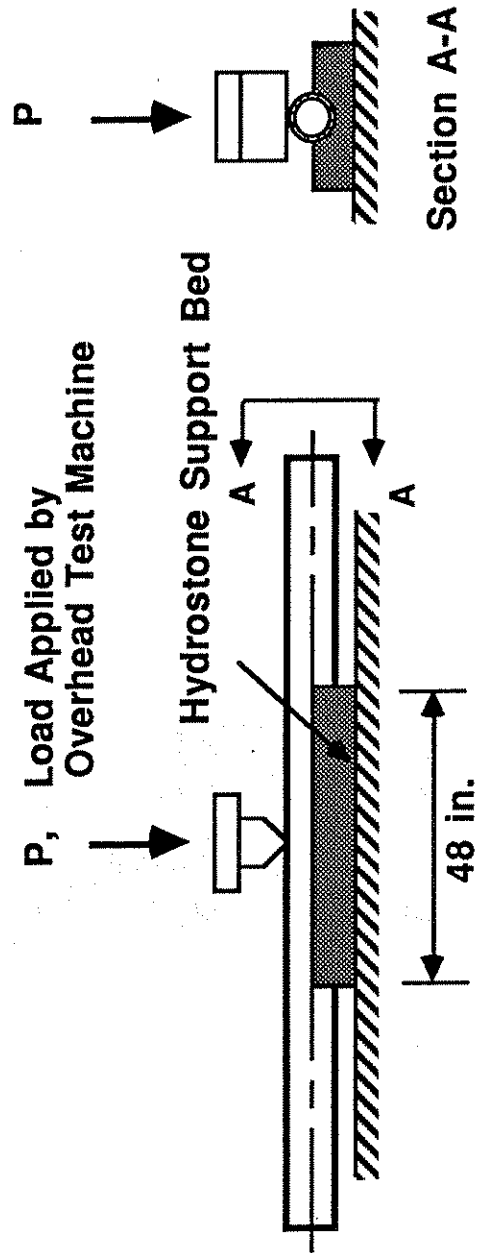
Figure 2.11. Indentation Device
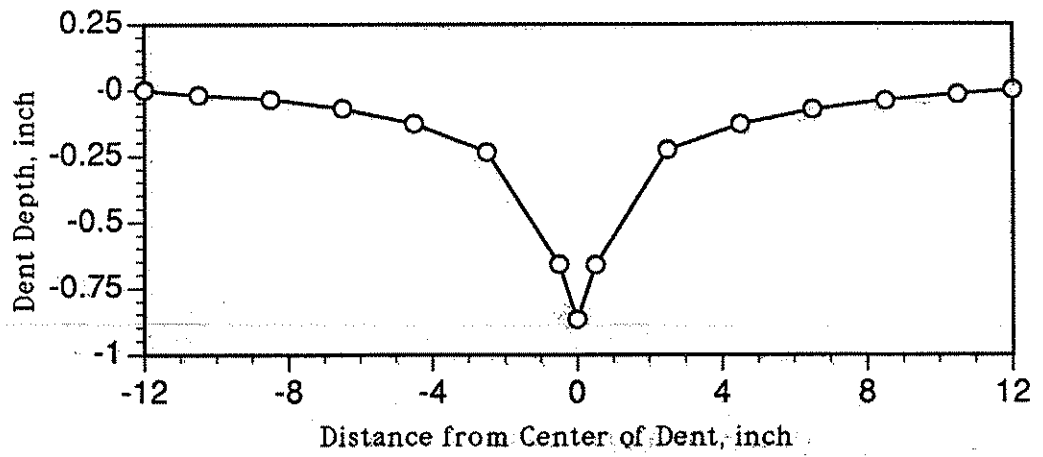
Figure 2.12. Dent Profile for Specimen A1.
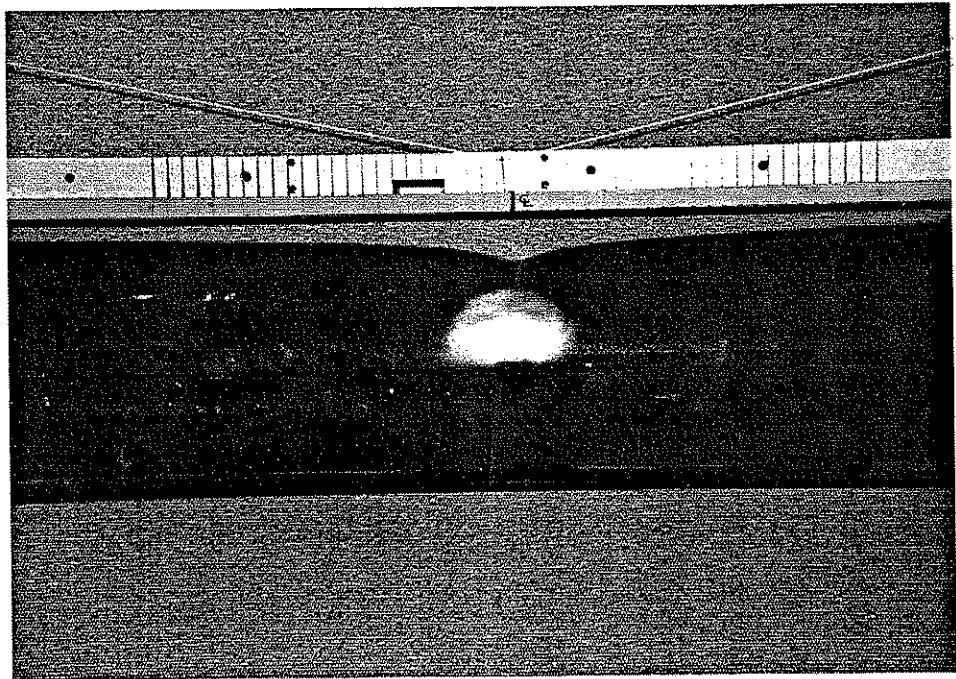
Figure 2.13. Photograph of dent damaged Specimen A1.
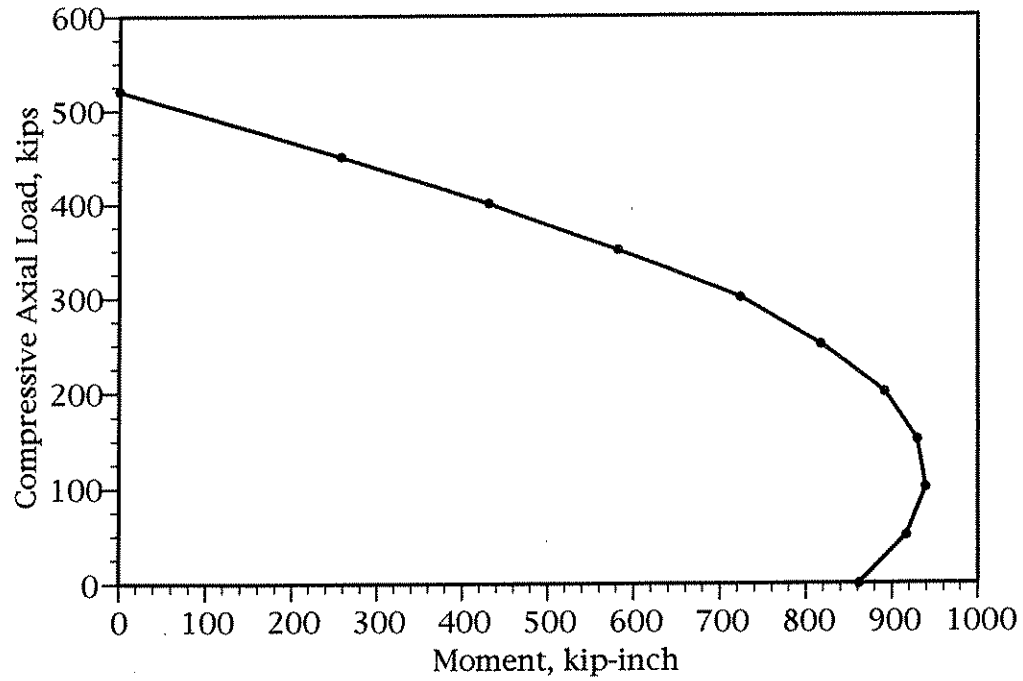
Figure 2.14. Moment-Axial Load Interaction Surface for Full Composite Action of Internal Grout Repaired Specimen A3.
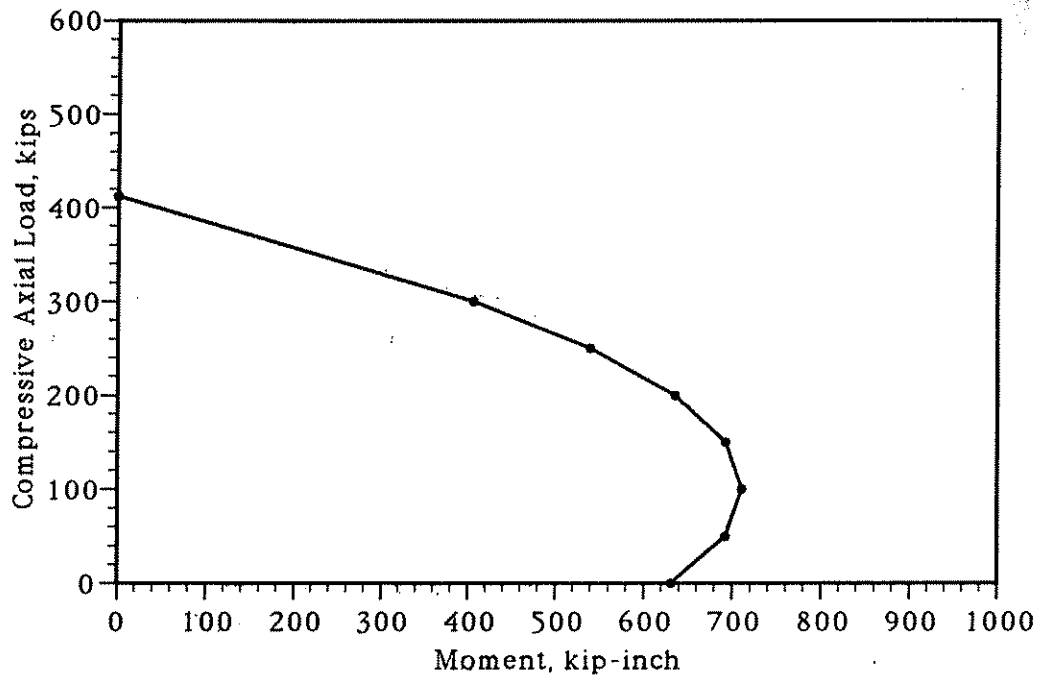
Figure 2.15. Moment-Axial Load Interaction Surface for Full Composite Action of Internal Grout Repaired Specimen B3.

64
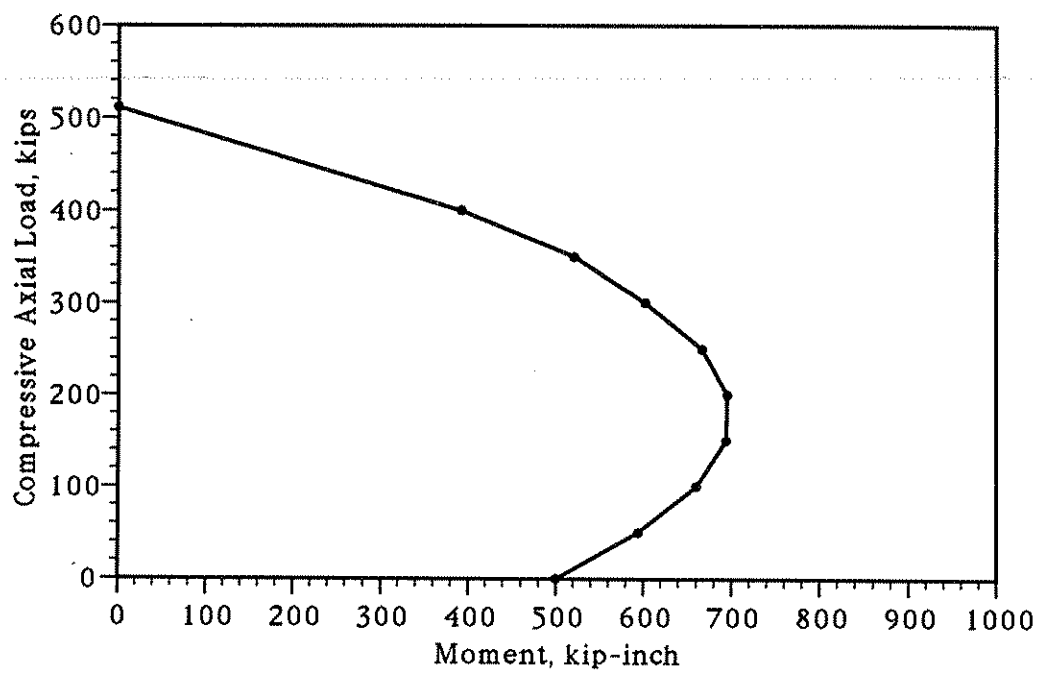
Figure 2.16.   Moment-Axial Load Interaction Surface for Full
Composite Action of Internal Grout Repaired Specimen C3.
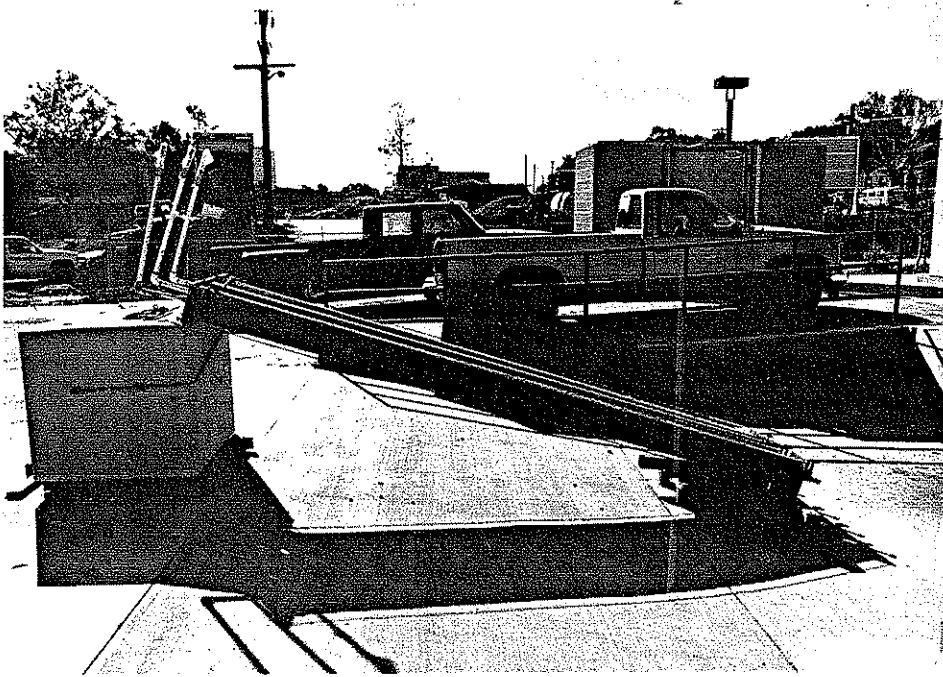
Figure 2.17(a) and (b). Setup for the internal grouting of Specimens A3, B3 and C3.
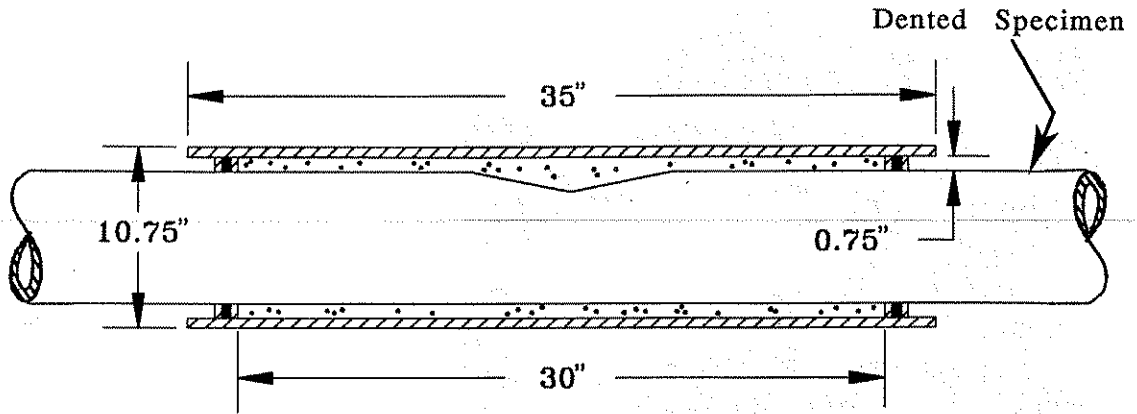
Figure 2.18(a). Section of Sleeve Designed to Simulate a Grouted Clamp.
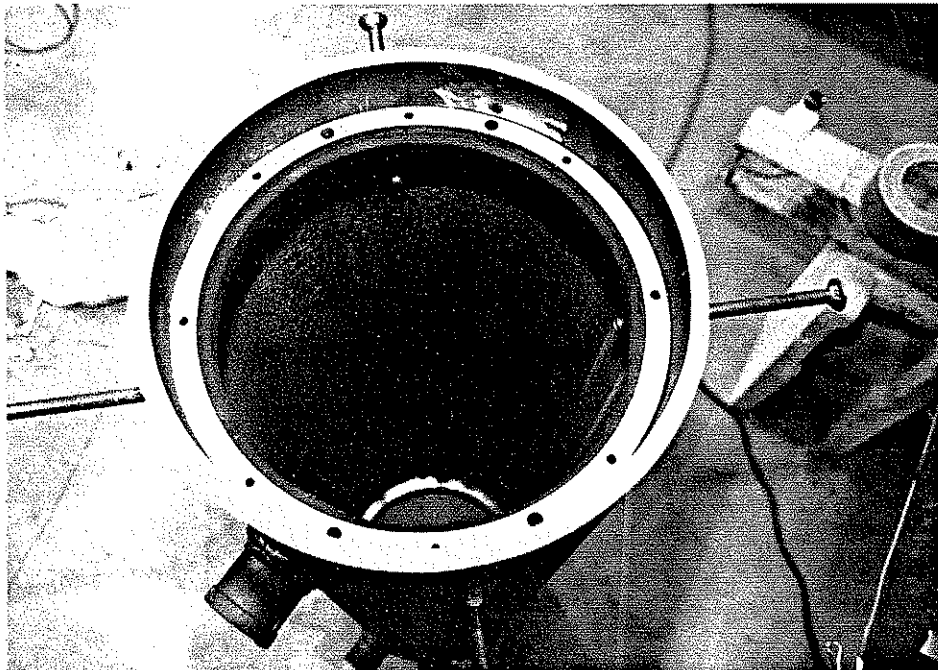
Figure 2.18(b). View of sleeve showing ring stiffener and rubber seal.
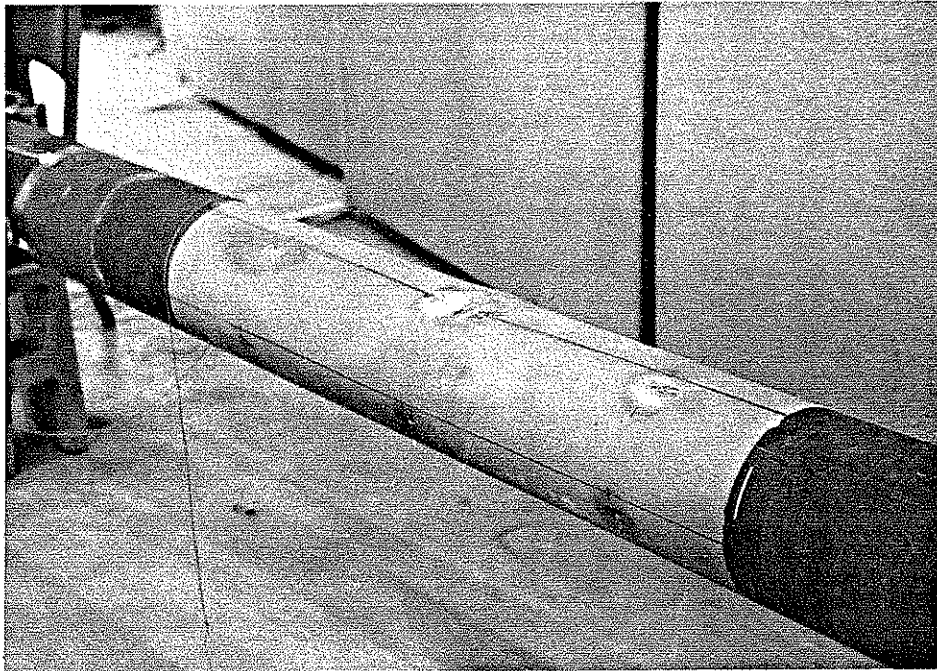
Figure 2.19. Sand-blasted region of Specimen C4 prior to installation of grouted sleeve.
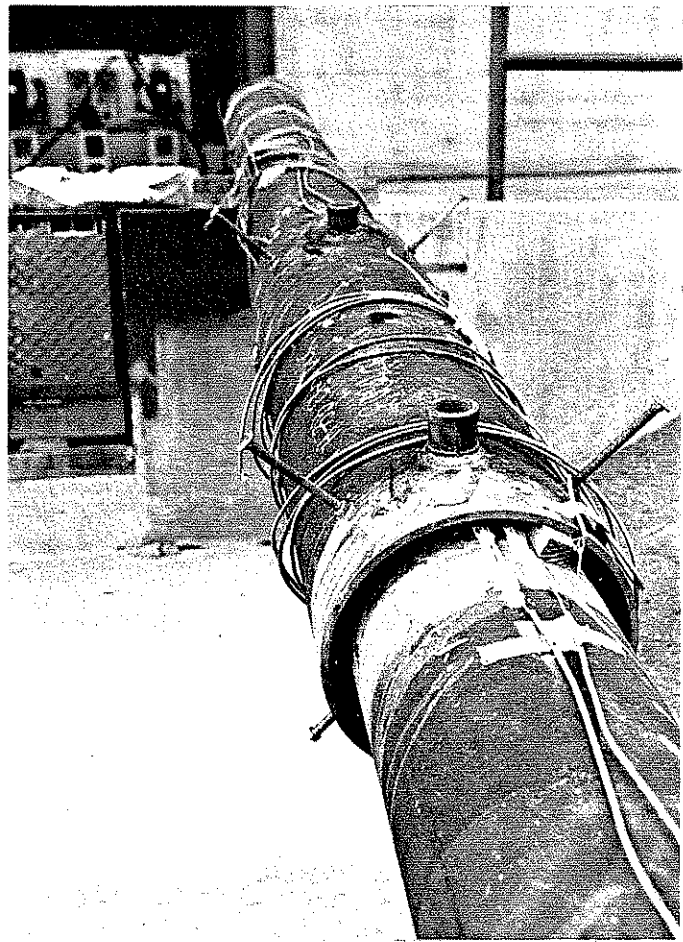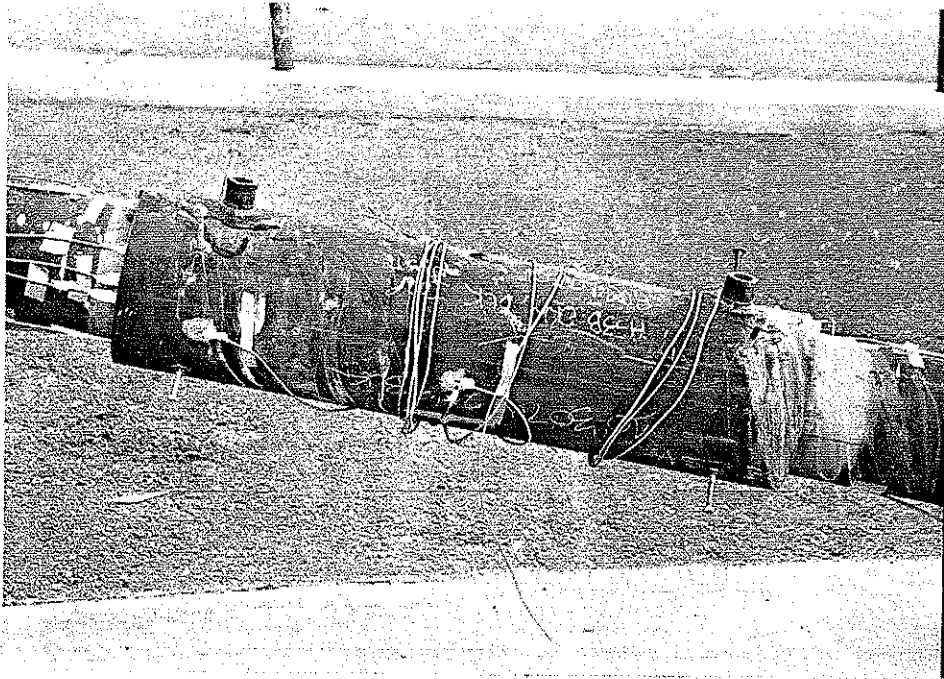
Figure 2.20(a) and (b).   Grouted sleeve installed on Specimen C4.
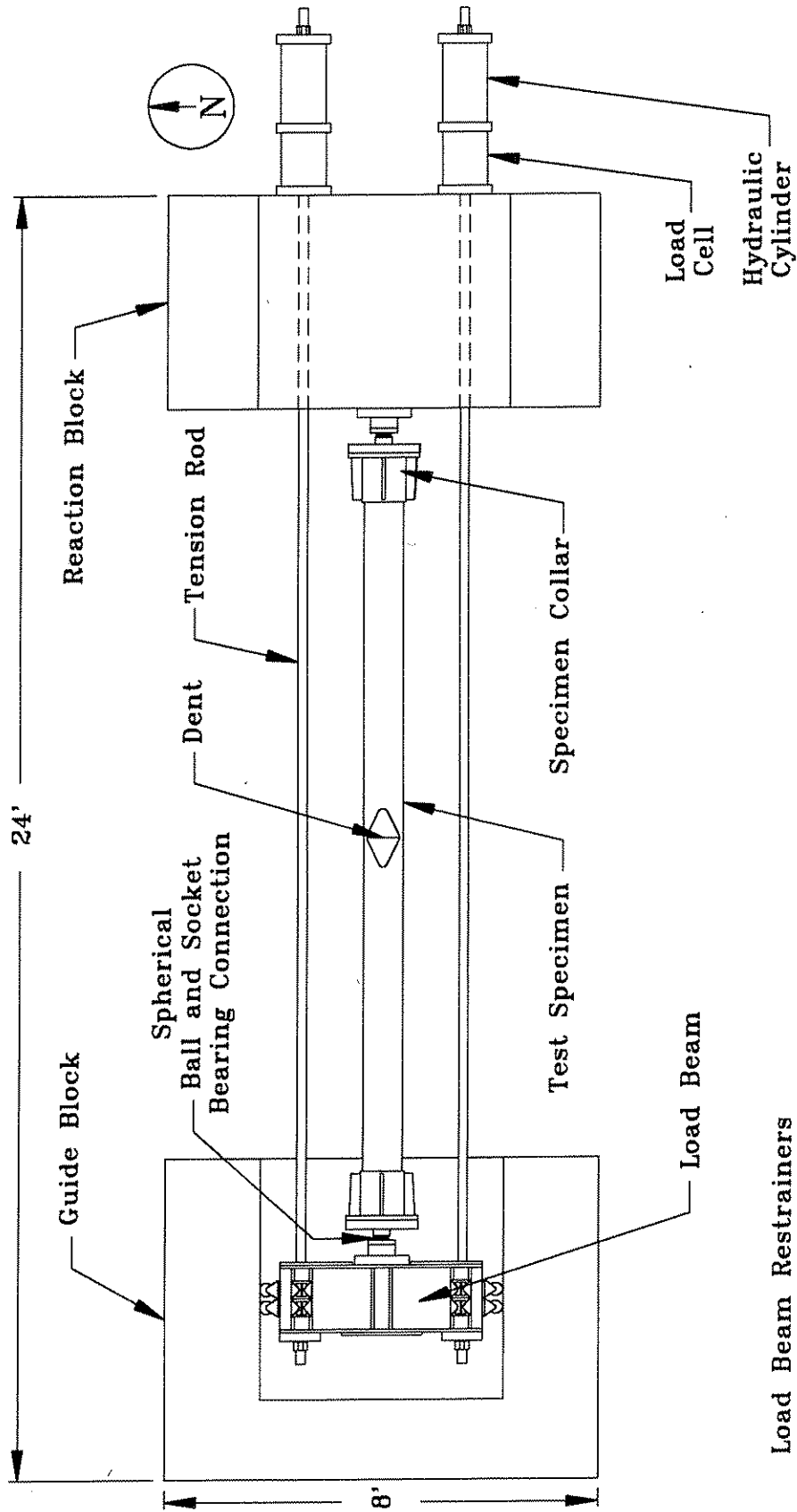
Figure 2.21. Plan View of Test Frame.
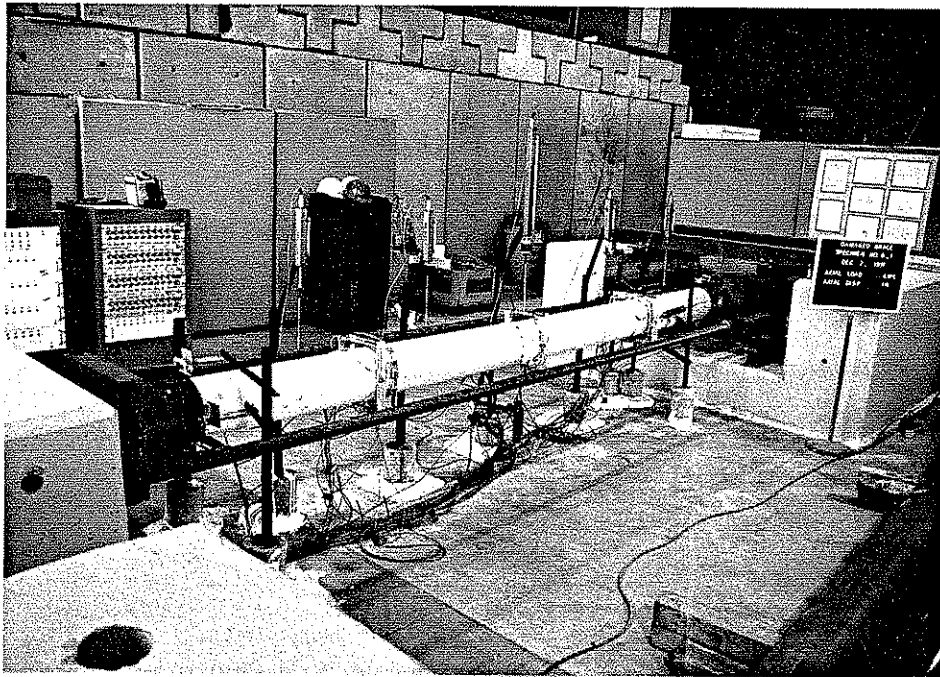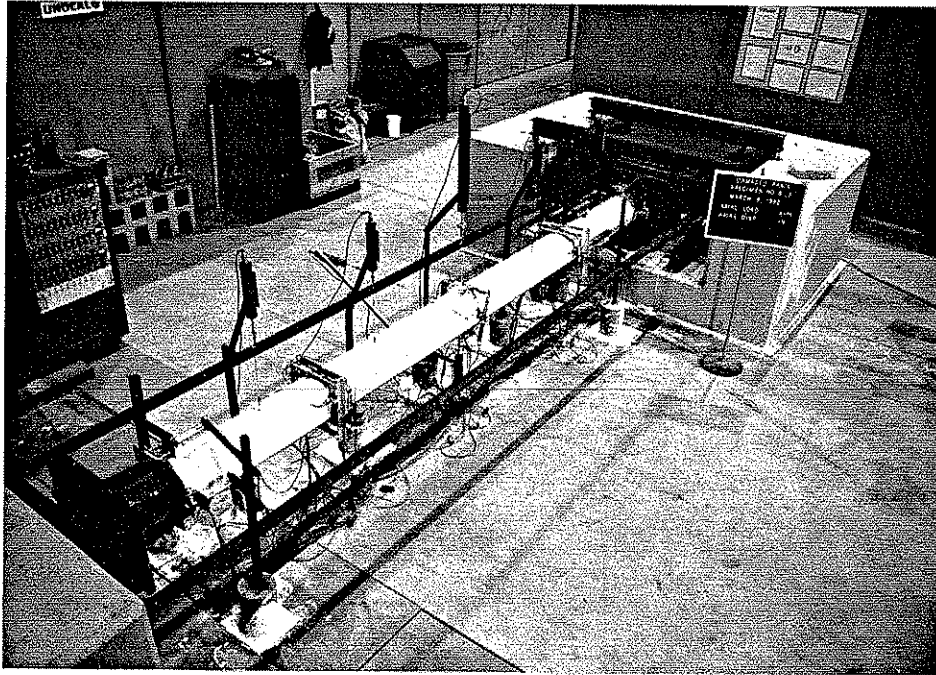
Figure 2.22(a) and (b). 500 kip self reacting experimental test frame.
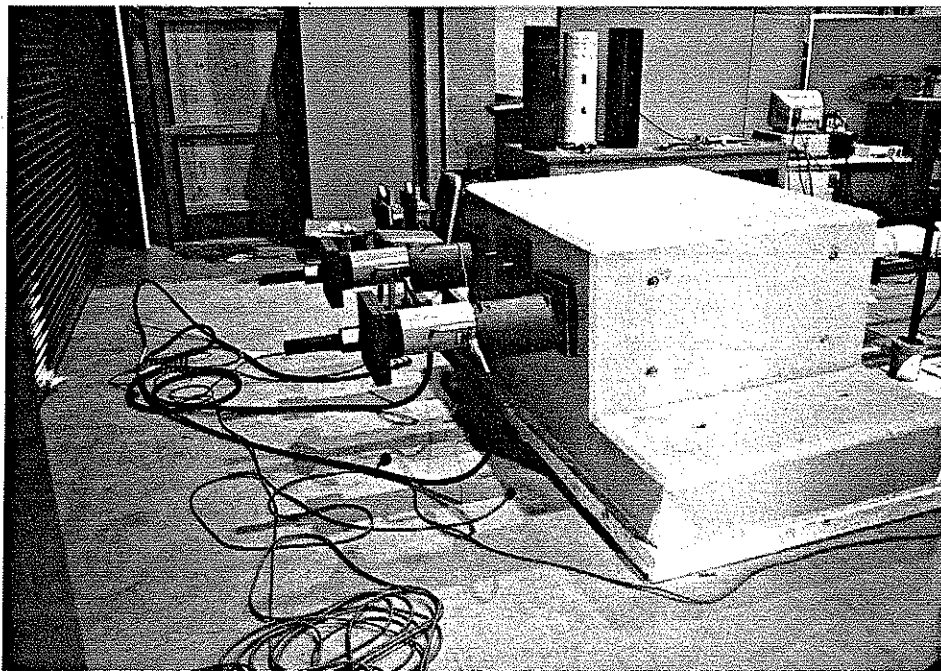
Figure 2.23. Two 150 ton hydraulic cylinders attached to the tension rods and located at the backside of the reaction block.
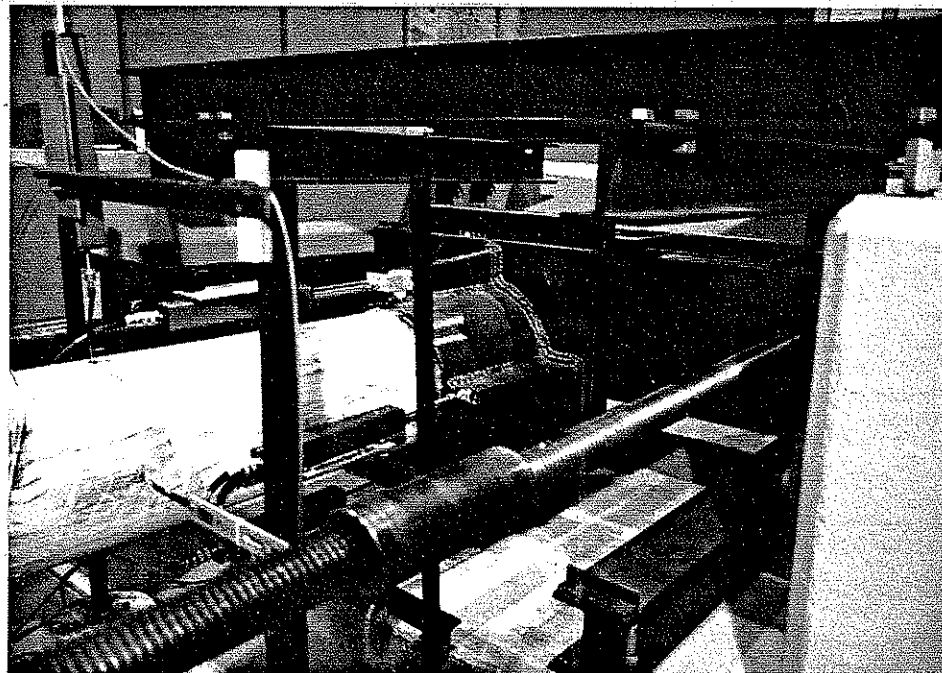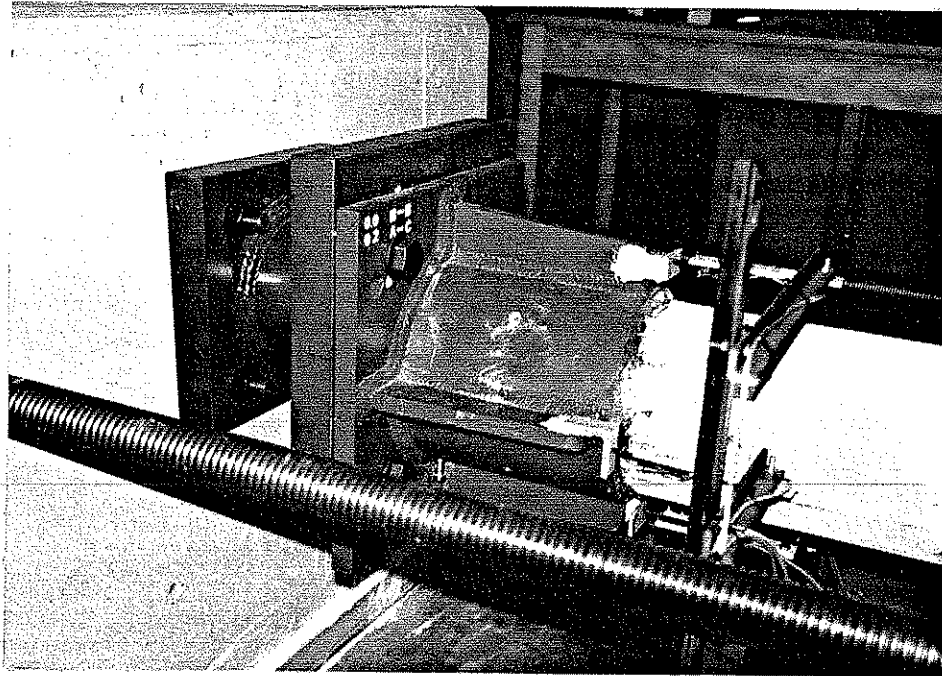
Figure 2.24(a) and (b). View of load collars at either end of specimen.
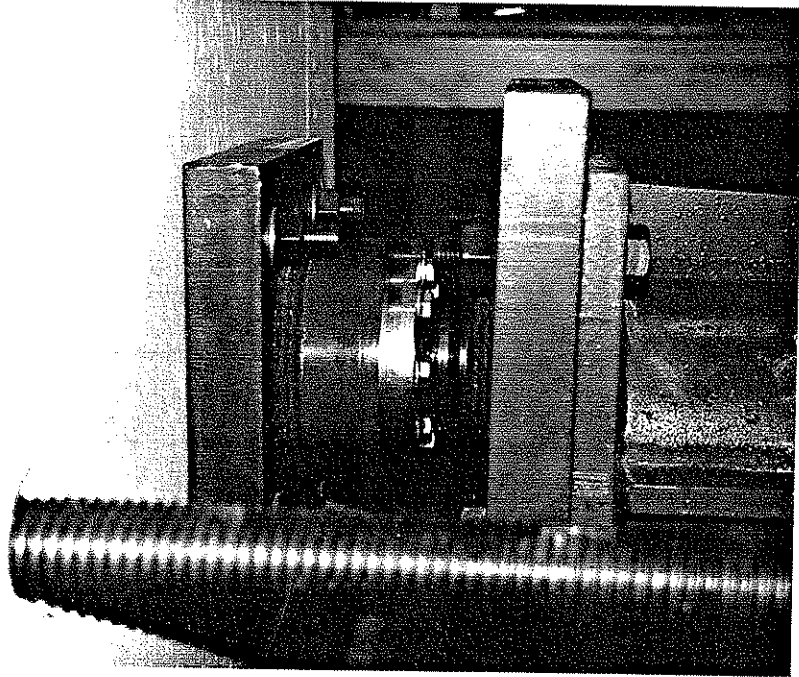
Figure 2.25.   Frictionless ball and socket bearing connection allowing free rotation of ends of specimen.

Side View

High Strength
Tension Rod

Frictionless
Wheel Casters

Top View

Front View
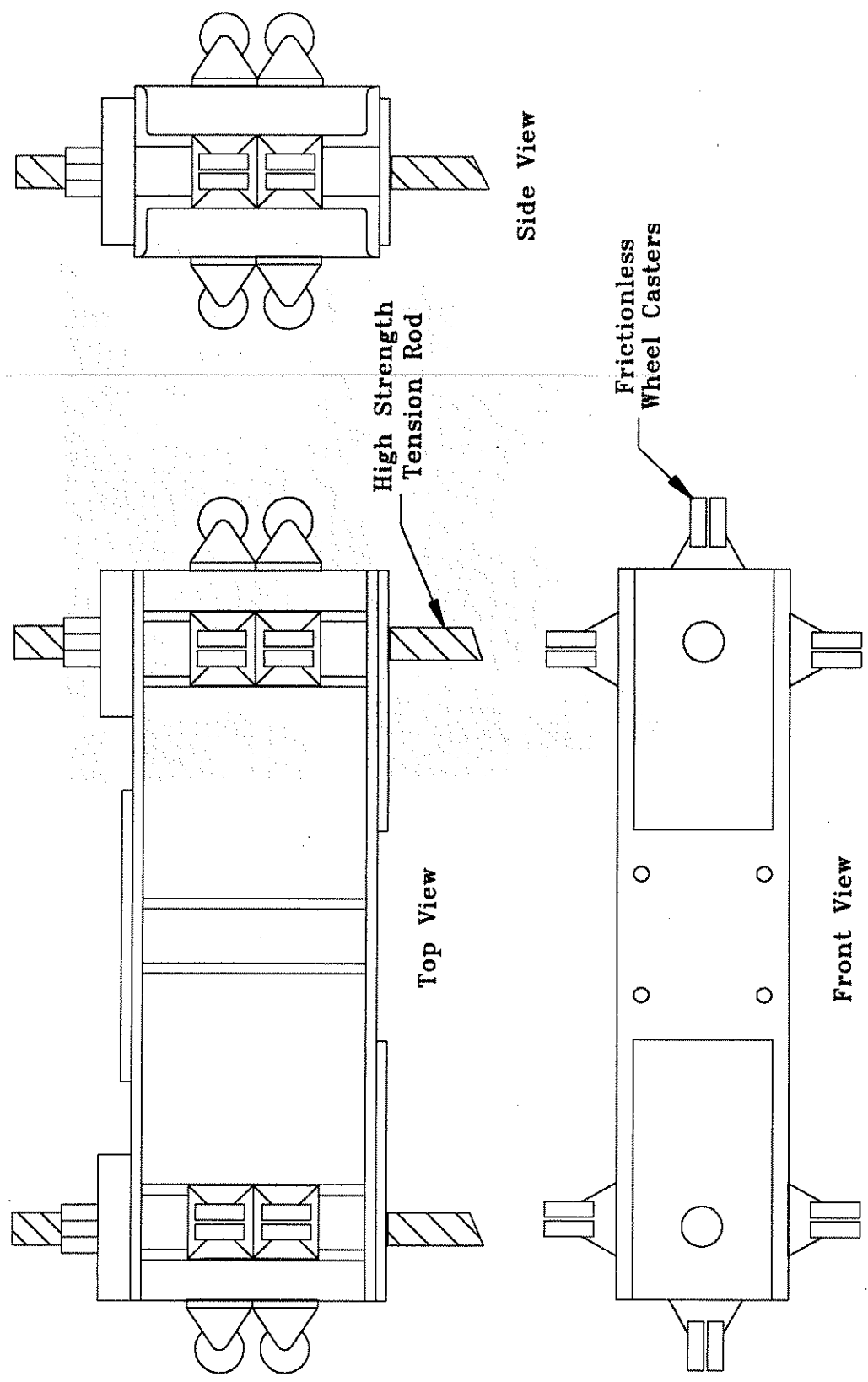
Figure 2.26: Load Beam Details
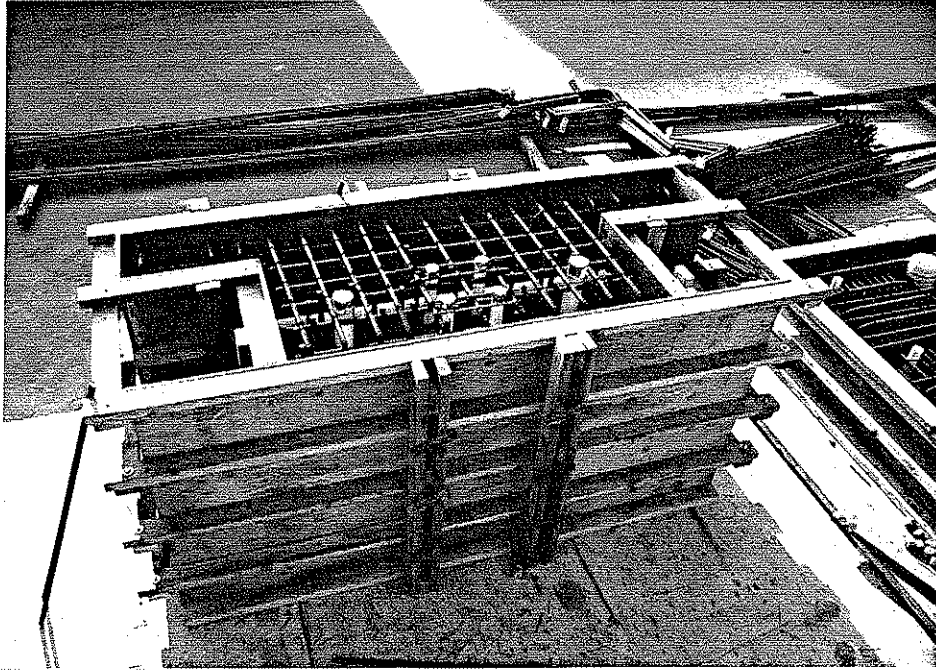
Figure 2.27. Formwork and steel reinforcement for the reaction block prior to casting.
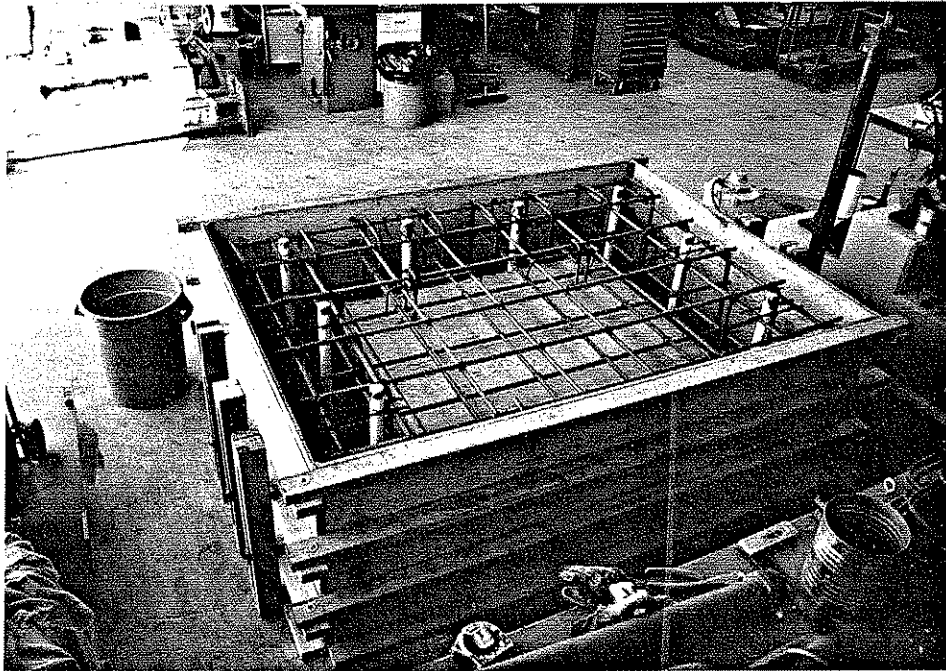
Figure 2.28. Formwork and steel reinforcement for the guide block prior to casting.
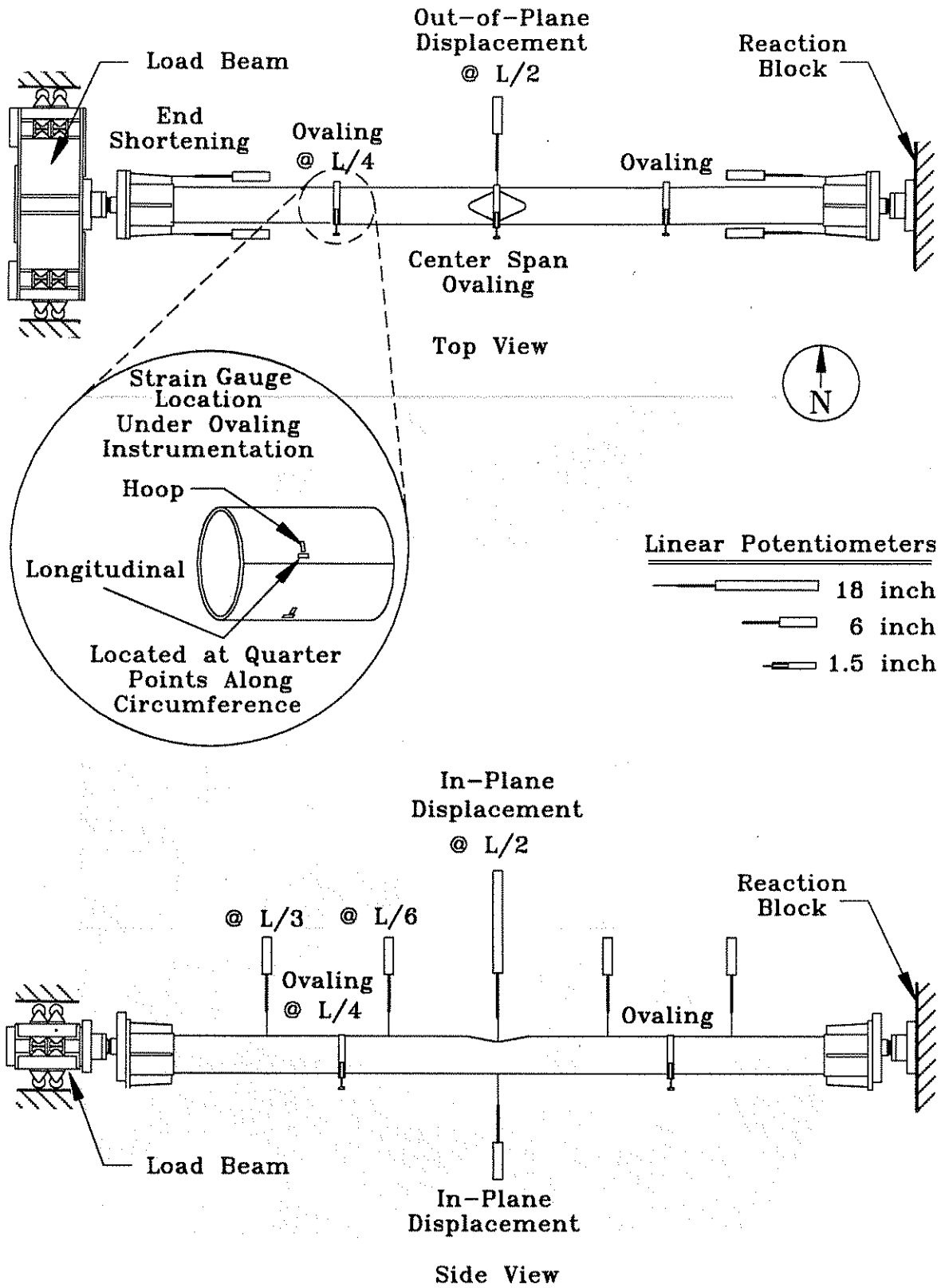
Figure 2.29. Instrumentation for Unrepaired and Internally Grout Repaired Specimens.
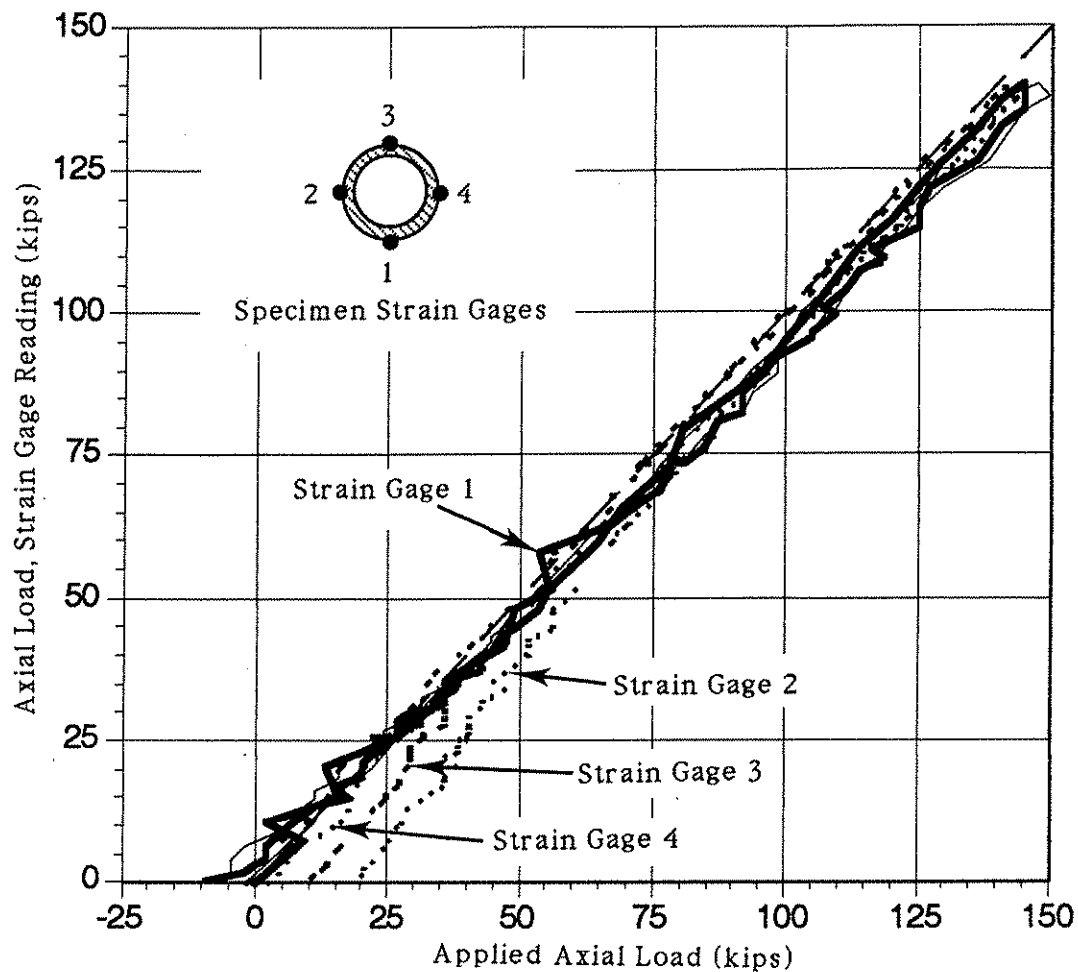
Figure 2.30. Verification of Monitored Load by Comparison of Load Cell Readings with Load Calculated from Measured Longitudinal Strains, Specimen A1.
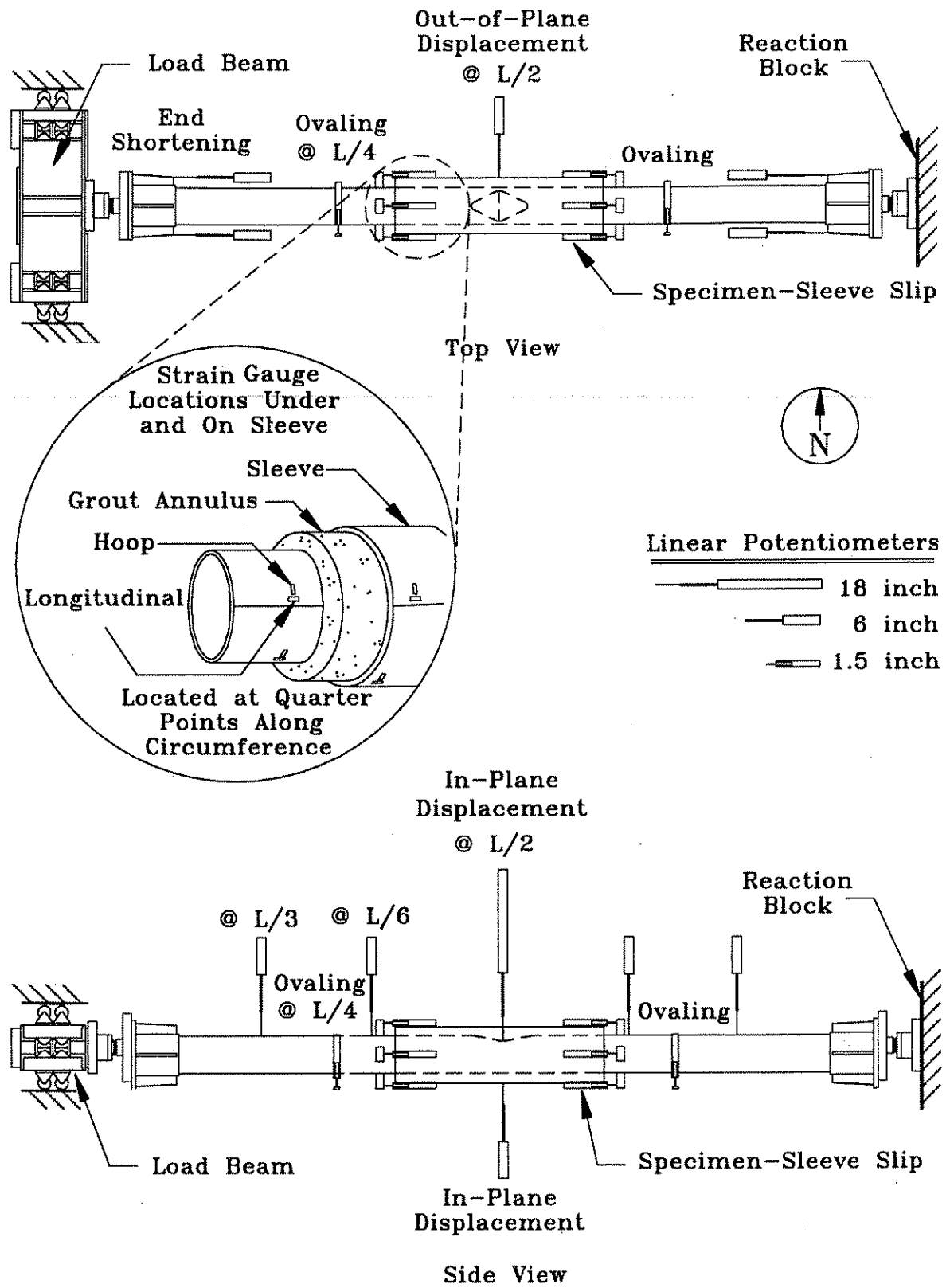
Figure 2.31. Instrumentation for Grouted Clamp Repaired Specimen C4.
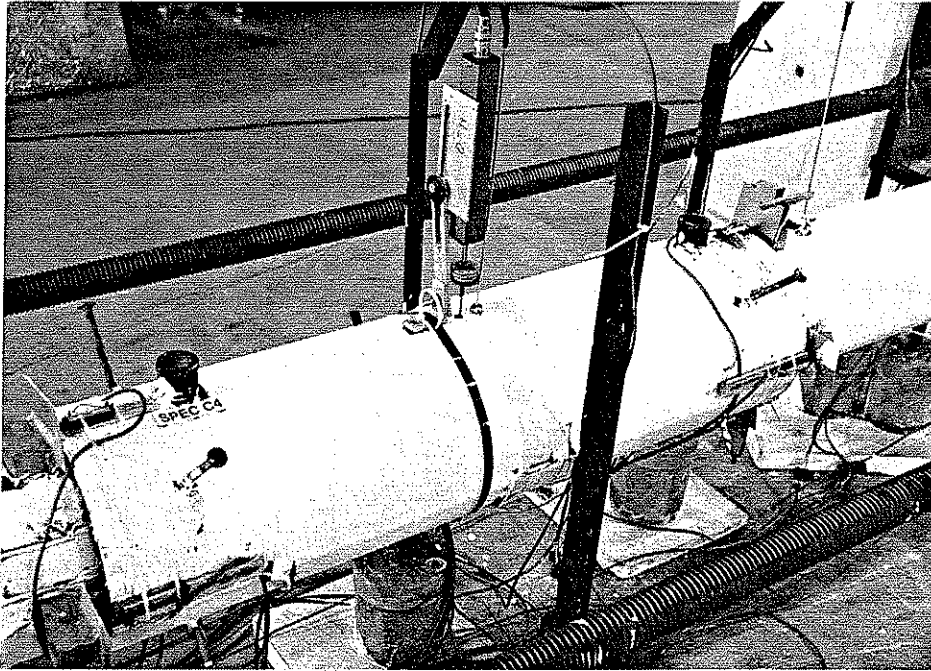
Figure 2.32. Instrumentation of grouted sleeve on Specimen C4.
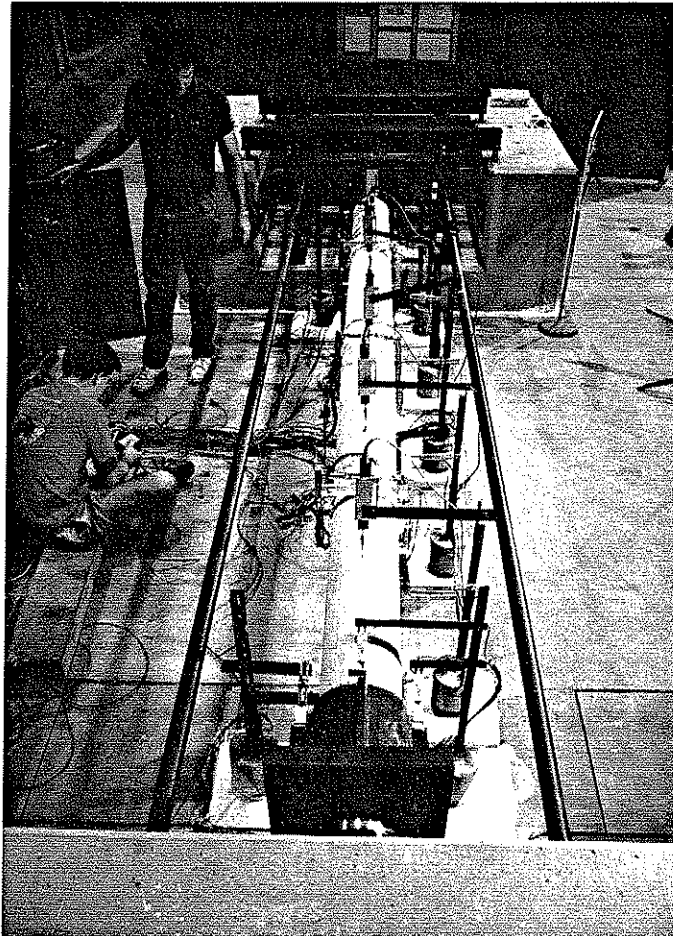
Figure 2.33. A specimen installed in test frame and instrumented for response.

Variable Resistors: Strain Gauges, Transducers

8 Channels
Per Cable

Gauge 1

Gauge 2

Gauge 128

Voltage/
Transducer
Cabinet

Neff Jr.
Cabinet

386 PC

The Neff Jr. Contains
8 National Intruments
Multiplexer Boards.
Making Each
AT-MIO-16 Channel
Equal to 8 Channels
For a Total of 128

The 386 PC Contains a
National Intruments
AT-MIO-16 Board
12 Bit 16 Channel Board
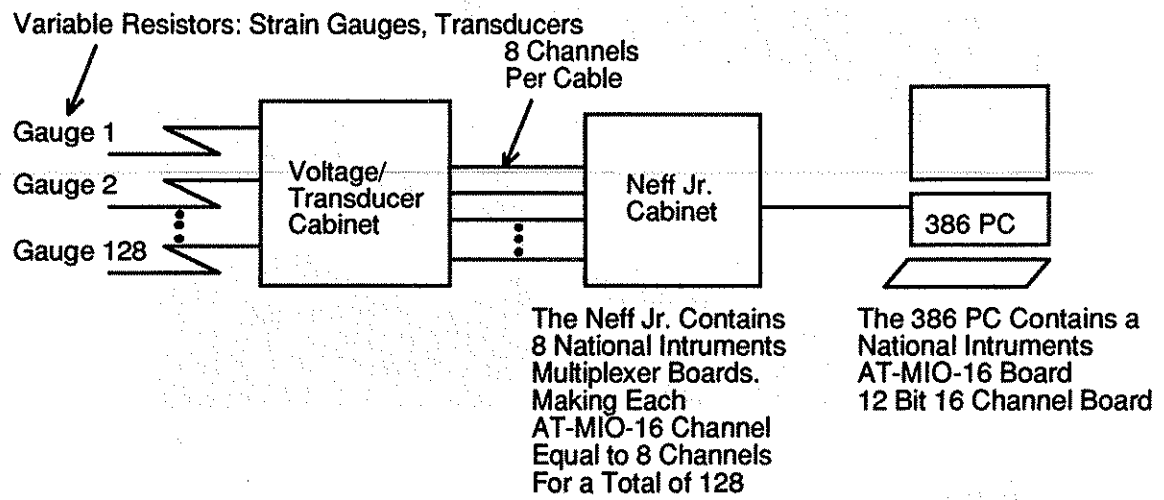
Figure 2.34: Data Acquisition Setup

CHAPTER 3

EXPERIMENTAL BEHAVIOR

This chapter discusses the behavior of the damaged bracing members tested. Each of the thirteen tests is described under sections pertaining to each test series. Observations and specimen response are presented along with a summary of the experimental behavior for each series.

3.1. Non-damaged Specimen Behavior (Series 5)

Three specimens were tested without damage and subjected to combined axial and bending loads to provide baseline comparisons for damaged member tests. This series provided a means to evaluate present design criteria, including API's allowable stress design (ASD) method, and the load and resistance factored design (LRFD) method. Instrumentation was a minimum and included monitoring of axial load-shortening response, and longitudinal strain development at the ends of each specimen for alignment purposes.

Test Specimen A5 - Specimen A5 simulated a non-damaged bracing member with a D/t ratio of 34.5. Geometric parameters including initial out-of-straightness are listed in Table 2.2 of Chapter 2. The specimen was subjected to combined axial and bending loads, by introducing the applied axial load at an end eccentricity of 0.20D.

Figure 3.1 shows the load-shortening curve with axes normalized by yield strength P_y and the specimen length L. P_y was obtained based on the measured tensile yield stress (see Table 2.3). The load-shortening curve was essentially linear up to the peak load of 155 kips, developing a slight deviation from linearity near the peak load. Although the 0.20D eccentric axial load was applied, the ascending branch closely follows theoretical calculations for an elastic member, based on shortening stiffness of AE/L, subjected to direct axial load. Compressive loading and unloading cycles are displayed at the tail end of the load-shortening curve to observe specimen response under cyclic loading.

82

Yielding of Specimen A5 was noticed by flaking of the whitewash at the peak load. The yielding pattern was fairly symmetric along the compression face of the tube, centered about the midspan. The pattern ranged from ten inches on the west end of the midspan to approximately seventeen inches on the east, and is shown in Figure 3.2. The load diminished at a consistent rate after reaching the peak load. At approximately 55% of the peak load following failure, a slight buckle formed on the compression face of the specimen at approximately four inches to the east of the midspan. The buckle quickly propagated to a second, smaller buckle at the midspan of the tube. Figure 3.3 shows the general yielding and local buckle formation. The descending load rate increased in slope after the formation of a buckle. The specimen had displaced a total of 6.5 inches in the plane of bending at the onset of this stage of failure, corresponding to a normalized axial displacement of 1% of the members length L. Figures 3.4 and 3.5 show the in-plane displacement pattern of Specimen A5 at 72% of ultimate and 41% of the maximum load following failure, respectively. The loading was discontinued at an axial shortening approximately 7.5 times that of the shortening at peak load.

Test Specimen B5 - Specimen B5 examined the ultimate strength of a non-damaged bracing member of D/t ratio of 46, subjected to combined axial and bending loads. Initial out-of-straightness values were well within API tolerances for this member and are listed in Table 2.2 of Chapter 2.

Specimen B5 responded to the applied loads in the behavior shown in the normalized load-shortening curve of Figure 3.6. Deviation from linearity during the ascent to maximum load was observed before the development of the peak load of 104 kips. Slight yielding and only slight curvature along the length of the specimen was noticeable at peak load (see Figure 3.7). Yielding was symmetric across the compression face of the tube for a span of approximately 24 inches. A local buckle (Figures 3.8 and 3.9) formed in the tube wall at a location three inches to the east of the midspan of the tube. This buckle occurred at 67% of the post peak load, corresponding to a normalized axial displacement of 0.65% of the specimen length L, and resulted in a sharp increase in the slope of the descending load-shortening curve (Figure 3.6). The depth of the buckle measured 0.07D when the loading was discontinued at a total shortening of seven times that measured at the maximum load.

Test Specimen C5 - Specimen C5 was the final test for Series 5. The D/t ratio of 64 for Specimen C5 is in the region where members are susceptible to local buckling as designated by API design criteria. Negligible initial out-of-straightness values were measured for this member and are reported in Table 2.2. Combined axial and bending loads were applied to the specimen, using the procedure as previously discussed.

The load-shortening response (Figure 3.10) shows a very slight deviation from linearity and theoretical predictions in the elastic region of loading. Figure 3.11 shows that only slight curvature existed in the specimen at the ultimate axial load capacity of 65 kips. Local yield was noticed at the maximum load. A local buckle formed at 85% of the post peak load, corresponding to a normalized axial displacement of 0.25% of the specimen length L, at a location five inches from the midspan (Figure 3.12). This buckle initiated a sharp descent in the load resistance of the member (see Figure 3.10) and propagated as shown in Figure 3.13. The residual load capacity after loading the member beyond failure was comparatively lower than that of Specimens A5 and B5 due to the buckling of the tube. Only 10% of the maximum load was resisted by Specimen C5 at the discontinuation of the loading. Corresponding in-plane curvature for the member at the completion of testing is shown in Figure 3.14.

Summary - Yielding initiated along the compression face near peak axial load. The non-damaged specimens all developed a local buckle in the tube wall at or near the midspan on the compression face after reaching a peak load. Slight curvature occurred in the specimens until after the peak load was reached. The local buckle of Specimen C5 transformed into major cross section distortion because of the high D/t ratio. This failure mode is safeguarded against in API design by designating substitution of local buckling stresses into column buckling equations for members with D/t ratios greater than 60. Residual load capacity was reduced to less than 30% for all specimens at a shortening of seven times the value observed at the maximum load.

3.2. Damaged, Non-repaired Specimen Behavior (Series 1 and 2)

A total of six tests were conducted to assess the affect of combined axial and bending loads and direct axial load on damaged specimen behavior. One specimen of each D/t group was tested under direct axial load, and one under combined axial and bending load.

The instrumentation scheme used was described in Section 2.5 and shown in Figure 2.29. The behavior of each specimen is described herein by the response of axial load-shortening, growth in dent depth, in-plane (e.g. in the plane of bending) displacement, and longitudinal strain developing in the dented section.

Test Specimen A1 - Specimen A1 modelled a bracing member of D/t 34.5, damaged, and subjected to direct axial load. An approximate dent depth of 0.10D existed at midspan on the compression face of the tube. All geometric and material properties for Specimen A1 are listed in Tables 2.2, 2.3, and 2.4 of Chapter 2.

The load-shortening response shown in Figure 3.15 was linear up to 67% of maximum load, closely following theoretical predictions in the elastic region. Yielding occurred in the bottom of the dent saddle just prior to the attainment of the peak load of 141 kips. Very little increase in the dent depth occurred, as indicated in Figure 3.16, until after the ultimate capacity of the member was reached. At yielding of the dent section, outward bulges of the tube's wall formed at each side of the dent saddle. Flaking of whitewash revealed symmetric yielding on each side of the specimen's cross section, centered about the newly formed bulges. Following yielding of the dent saddle and development of the ultimate capacity of the member, the dent grew rapidly inwards, leading to specimen failure and subsequent load shedding. Figures 3.17 and 3.18 show the dent region before testing and at peak load of the specimen, respectively.

The history of the longitudinal strain developed in the dent is shown in Figure 3.19. These strains due not include the residual strains developed in the section during denting and are the average from two strain gages, each placed one inch to the side of the dent saddle. Prior to reaching the peak load the exterior surface of the tube in the dent saddle region developed compressive strain under the applied axial load. As the dent grew inwards, curvature

developed through the wall in the strain gaged dented region, leading to tensile strain. The strain eventually reversed sign, leading to compressive strain as the dent depth growth exceeded 0.15 times the member's diameter.

Increased axial shortening beyond failure resulted in the formation of a plastic hinge at the dented section. Measured in-plane displacements along the specimen (Figure 3.20 and 3.21) revealed curvature in the plane of bending at the peak load. Second order bending effects became more apparent at 75% of the peak load (141 kips) following failure, where curvature was concentrated in the dented section due to the formation of a plastic hinge (Figure 3.21).

Test Specimen A2 - Specimen A2 simulated a bracing member, damaged and subjected to combined axial and bending loads. Specimen A2 was the second damaged member to be tested in the 34.5 D/t group. A 0.10D dent depth was introduced at midspan of the tube, on the bending compression face. Material and geometric properties were measured and are listed in Tables 2.2 through 2.5.

The normalized load-shortening response (Figure 3.22) displays linearity in the elastic region with a slight deviation from theory. Yielding in the dent saddle was first observed at the maximum load of 91 kips. A slight increase in dent depth (Figure 3.23) was present at this stage. Bulges again began to form on both sides of the dent as the saddle continued to yield. Both sides of the specimen yielded symmetrically about the deformed dent section. The dent depth grew rapidly inward as the loading continued, leading to failure and load shedding. Figure 3.24 shows the dented segment of the specimen after failure.

A review of the history of the longitudinal strain (Figure 3.25) developed in the dent shows similar trends as that observed in Specimen A1. The dent resisted the initial applied axial load through development of compressive strain. Just prior to reaching the peak axial load, an increment in tensile strain was formed as the dent saddle yielded and the dent grew inwards. Further shortening created more compressive strain, before the final unloading of the specimen.

The In-plane displacements are shown in Figure 3.26. Again, some curvature existed in the specimen at the peak load. Second order bending

effects became more apparent after achieving peak axial load in the specimen. Following the application of peak load, a concentration of curvature (e.g. the formation of a plastic hinge) developed at the dented section, similar to that observed in Specimen A1. The concentration of curvature across the dented section increased as the axial shortening continued (see Figure 3.27).

Test Specimen B1 - Specimens B1 simulated a damaged bracing member having a D/t ratio of 46. Specimen B1 was subjected to direct axial loading, and had a dent depth of 0.10D at its midspan on the compression face.

The load-shortening curve (Figure 3.28) of Specimen B1 displayed a deviation from linearity near the peak axial load of 99 kips. Initial yielding occurred simultaneously with the attainment of ultimate capacity of the member. Yielding was located in the saddle of the dented section. Following saddle yielding, bulges formed (Figure 3.29) on each side of the saddle. The sides of the specimen yielded symmetrically about this deformed section. Figure 3.30 shows that the dent grew quickly inwards as the section failed and load shed. Very little load capacity remained in the damaged member, approximately 10% of the maximum load, when the loading was discontinued at a value five times the shortening reached at the peak load (see Figure 3.28).

Longitudinal strain history in the dented section (Figure 3.31) differed from Specimens A1 and A2 in that no tensile strain developed as the dent section failed and the dent grew inwards. The magnitude of the compressive strain at maximum axial load corresponded well with the yield strain of the material. After reaching peak load, the compressive strain rapidly increased as the shortening continued and shed load.

A plastic hinge again developed across the dented section, as displayed in Figures 3.32 and 3.33. Larger curvature developed in the specimen following peak load, particularly at the dented section .

Test Specimen B2 - Specimen B2 examined the affect of combined axial and bending loads on the D/t ratio of 46. The specimen was damaged with a dent placed at midspan on the compression face, with a depth of 0.10D.

The ascending branch was linear as shown in the normalized load-shortening curve of Figure 3.34. Yielding again initiated in the bottom of the dent saddle, where the specimen's cross section formed two bulges at both sides

of the dent. Dent growth was minimal up until 90% of the peak axial load (52 kips) of the member occurred, at which point the dent grew inwards at a rapid rate (Figure 3.35). The increased dent depth following failure is shown in Figure 3.36.

The longitudinal strain history of the dented section again displayed strain reversal characteristics (Figure 3.37). Compressive strain developed while resisting the initial applied axial and bending load. At the onset of rapid inward dent growth in the dented section, tensile strains formed. Increments of compressive strains again developed as the dent eventually grew deeper.

Soon after reaching the peak load, second order bending effects became more pronounced, and the formation of a plastic hinge at the dented section became apparent (Figure 3.38). Measured in-plane displacement profiles at various stages of loading are given in Figure 3.39, where also the second order effects are shown to be evident.

Test Specimen C1 - A bracing member of D/t ratio 64, damaged and subject to direct axial load was simulated with the testing of Specimen C1. The dent was again located at midspan on the compression face, and measured approximately 0.10D.

The ascending load-shortening relationship (Figure 3.40) of Specimen C1 was linear and in close agreement with elastic theory. At the peak load of 97 kips an abrupt loss of capacity was observed, where a rapid descent to approximately 40% of the peak load occurred before the axial load stabilized. Yielding initiated in the bottom of the dent saddle just prior to failure of the specimen, at which point the dent grew rapidly inwards as shown in Figure 3.41. Yielding spread to the sides of the specimen as the cross section of the dented segment began to oval. Continued shortening beyond failure resulted in the formation of a distinct local buckle on both sides of the deepened dent saddle (Figure 3.42).

The longitudinal strains developed near the saddle in the dent section (see Figure 3.43) displayed a compressive-tensile history on the exterior surface, similar to earlier specimens. The dent saddle again resisted the initial applied axial load through the development of compressive strains up until failure. At peak load the dent saddle depth increased, resulting in tensile strain. With continued growth in dent depth, increments of compressive

88

strain developed until the load was discontinued at ten times the shortening observed at failure.

Specimen C1 was unique in that at 75% of the peak load, prior to failure, no measurable in-plane curvature existed. Former specimens all recorded measurable curvature at this stage. The plotted curve for the displacement at the ultimate load in Figure 3.44 is markedly smaller than in the previous specimens. Although meticulous care was taken to align the specimen, it appeared that a slight accidental eccentricity in the form of upward hogging was introduced into the specimen during installation into the load frame. The upward hogging afforded the specimen additional resistance and thus increased the ultimate capacity of the specimen while decreasing its curvature under loading. All curvature profiles monitored and presented in Figure 3.44 display the effects of negative curvature at the specimen ends, furthering the misalignment assumption. The displaced tube is shown in Figure 3.45.

Test Specimen C2 - Specimen C2 was the final of the damaged, non-repaired specimen tests. The specimen again modelled a dent damaged bracing member with the dent residing at midspan on the compression face and measuring to a depth of approximately 0.10D. The specimens D/t ratio was 64. Geometric measurements are listed in Tables 2.2 and 2.5 of Chapter 2.

The normalized load-shortening response of Specimen C2 (Figure 3.46) was initially linear and aligned well with theory at low levels of axial load. Yielding initially occurred at the bottom of the dent saddle prior to reaching maximum capacity corresponding to an axial load of 46 kips. The yielding then spread to the sides of the specimen at the dented section, and the cross section ovaled with the formation of bulges at both sides of the dented section in similar fashion to other damaged specimens. The dent increased in depth only slightly prior to reaching the peak applied load. Following application of the peak load, the dent again grew quickly inwards as the load was shed (Figure 3.46 and 3.47). Figures 3.48 and 3.49 show the formation of a plastic hinge at the dented section occurring during continued shortening beyond peak load.

Summary - The specimens which were subjected to direct axial load attained higher ultimate capacities than their counterparts, which were subjected to combined axial and bending loads through an end eccentricity. The dent

initially resisted applied loads through development of compressive strain. Up until peak load of the specimens, very slight growth in dent growth was measured. All six specimens failed shortly after yielding occurred in the saddle of the dent, where the axial load resistance deteriorated with continued axial shortening. Upon failure, the dent consistently was shown to rapidly grow inwards. An outward bulging formed on the sides of the specimen at the dent. The yielding spread from the dent saddle to the sides of the cross section, and longitudinally along both sides of the member. Most specimens displayed a longitudinal strain history in the dent that transformed from initial compressive strains to the development of tensile strain as the dent grew inward. After continued shortening was applied to the specimen, further compressive strains developed. In-plane displacements became large after peak load was reached, where second order bending effects became prominent, resulting in the formation of a plastic hinge at the dented cross section.

3.3. Damaged, Internal Grout Repaired Specimen Behavior (Series 3)

Three damaged specimens were tested after having been repaired by internal grouting. The grout extended the full length of the specimen. One specimen from each D/t group was repaired and tested under combined loading to assess the performance of this technique. Respective compressive grout strengths are reported in Table 2.3. Grout strength curves are given in Figure 2.9(a). All specimens were initially damaged through the introduction of a 0.10D deep dent at the midspan on the compression face of the tube. Initial and damaged state geometry for these specimens are listed in Tables 2.2 and 2.5. Steel material properties are listed in Tables 2.3 and 2.4.

Instrumentation remained the same for this series of tests as in the non-repaired series described earlier. The load-shortening relationship, dent growth, longitudinal strain in the dent section, and the in-plane displacements of the specimen are discussed.

Test Specimen A3 - Specimen A3 simulated a damaged bracing member of D/t ratio 34.5, which was subsequently repaired using internal grout. The

damage existed in the form of a dent of depth 0.10D located at the midspan on the compression face. The grout strength was 4375 psi at the day of testing.

The load-shortening response of Specimen A3 is normalized with respect to the yield strength P_y of the steel tube cross section and specimen length L in Figure 3.50. The figure indicates that the specimen was able to absorb a large amount of energy due to the addition of grout. Specimen A3 developed a peak load of 191 kips. The curvature existing in the specimen at peak load (see Figure 3.51) was larger than that of the non-repaired specimens. The effect of second order bending was pronounced as indicated by Figures 3.52 and 3.53.

Yielding initiated in the tube at the bottom of the dent saddle. This yielding quickly spread along a wide pattern on the compression face (Figure 3.54). At this point in previous damaged non-repaired specimen tests, the dent depth was observed to rapidly grow as the specimen failed and load was shed. Figure 3.55 shows that for Specimen A3, the grout resisted and arrested the growth of the dent into the member's cross section. This arrest was further verified by reviewing the longitudinal strain history developed in the dented section during loading (Figure 3.56), where only compressive strain increments developed. The measured compressive strain of 1189 microstrains at peak load of the specimen correlated well with the yield strain of the material, confirming that failure occurred after plastification of the dented section.

Further shortening of the specimen beyond peak load resulted in large curvature in the plane of bending along the specimen length. A local outward buckle formed on the compression face of the tube at each end of the dent (Figure 3.57). It was determined that the material had yielded prior to buckling. The location of the buckle was near the location of maximum bending moment. The peak load, and residual load capacity displayed by the specimen beyond peak load was significantly higher than the corresponding response of the non-repaired specimen (Specimen A2).

Test Specimen B3 - Specimen B3 was the second in the internal grout repair sequence and was used to assess the performance of the repair technique on a damaged member (dent depth 0.10D) of D/t ratio 46 and subjected to combined axial and bending loads through an end eccentricity. The grout was again

placed along the full length of the specimen. The grout strength was 3885 psi at the day of testing.

The load-shortening response (Figure 3.58) again shows a more significant amount of energy absorption than that of the corresponding non-repaired specimen (Specimen B2). The curve is very flat at its peak load of 117 kips, in contrast to the sharper decline of the non-repaired specimens. Curvature was noticed and measured along the specimen at the peak load (Figure 3.59).

Figure 3.60 shows that the internal grout arrested the dent growth, subsequently increasing the member's capacity. The history of the longitudinal strains in the dent, Figure 3.61, shows that plastification of the dent occurred at peak load as the yield strain of 1139 microstrains of the steel material was surpassed. Compressive strains further developed as the grout resisted dent growth and bending actions in the wall of the specimen.

Yielding was noticed to have initiated at the peak load in Specimen B3, on the top sides of the compression face, Figure 3.62. The yield pattern eventually grew longitudinally approximately 29 inches, and was centered about the dent. The yielding occurred along this region of the tube due to the compression in this segment developed under combined loading.

Increased shortening of the specimen after ultimate load resulted in large curvature in the plane of bending along the specimen length, see Figures 3.63 and 3.64. As in Specimen A3, a local buckle formed on the compression face of the tube at the each end of the dent of Specimen B3, Figure 3.65, following the application of the peak load. Residual load capacity displayed by the specimen beyond failure was significantly higher than the corresponding response of the non-repaired specimen (Specimen B2).

Test Specimen C3 - Specimen C3 was the final damaged member to be repaired with internal grout. The specimen had a D/t ratio of 64 and a dent depth of 0.10D at midspan on the compression face. It was repaired with internal grout, and was subjected to combined axial and bending loads through an end eccentricity. All geometric and material properties are listed in Tables 2.2 through 2.5.

The load-shortening relationship given in Figure 3.66 shows a significantly higher load carrying capacity compared to the corresponding

unrepaired Specimen C2, (Figure 3.46), where specimen C3 developed 75% of the compressive yield load P_y. Near the peak load of 122 kips the load-shortening curve was very flat. The descending branch of the curve was steeper than both Specimens A3 and B3, and will be discussed more later.

Peak load of the specimen occurred with yielding at the dent region. Yielding initiated in the bottom of the dent saddle and quickly spread longitudinally along the compression face of the tube. The yielding did not span as long of a length as in the two earlier repaired tests (Specimens A3 and B3).

The dent growth was once again arrested by the internal grout. Beyond peak load, Figure 3.67 shows that very little increase in depth occurred in the dent. The longitudinal strain history within the dented section (Figure 3.68) shows the development of compressive strain on the exterior surface of the tube wall as the grout resisted the inward growth of the dent. Again, the peak load of the specimen correlated well with the yielding of the material in the dented section. The yield strain for Specimen C3 is approximately 1336 microstrains. A local outward buckle formed at each end of the dent with continued deformation beyond the peak load, initiating at a load of 93% of specimen axial load capacity. The capacity diminished more rapidly than the previous tests due to development of a crack in the tube wall at the bottom tension face of the specimen, leading to a loss of resistance in the member. This crack was initiated when the load had diminished to 80% of the peak load, originating at a hole drilled in the wall of the specimen for instrumentation.

Second order bending effects were noticed in the specimen before and at the peak load. Continued shortening, following failure, resulted in the development of a plastic hinge. A concentration of curvature developed at the dented section due to the formation of the plastic hinge and tearing, see Figure 3.69.

Summary - Internal grout repair significantly restored the load carrying capacity of the tested specimens through the arrest of the dent growth. The grout supported the dented section, thus eliminating this mechanism of failure. The specimens developed their peak axial load as the steel wall yielded in the dent saddle and along the compression face of the tube. An outward local buckle formed at each end of the dent after the peak load was developed

in the specimen. The repaired specimens were capable of withstanding very large in-plane displacements while resisting the axial load with less strength deterioration than the unrepaired specimens.

3.4. Damaged, Grouted Clamp Repaired Specimen Behavior (Series 4)

One damaged specimen was repaired by placement of a grouted steel sleeve around the damaged section of the member. The repair technique was assessed by testing the specimen under combined axial and bending loads through end eccentricity. The grout mix and compressive strength were described in Section 2.2.2.4. The specimen was initially damaged through the introduction of a 0.10D deep dent at the midspan on the compression face of the tube. Initial and damaged state geometry for this specimen are listed in Tables 2.2 and 2.5. Table 2.3 and 2.4 lists the steel material properties. The sleeve geometry was discussed in Section 2.3.2 and simulated the method of grouted clamp repair used presently in offshore applications.

Instrumentation remained the same as for the non-repaired and internal grout repaired specimens, with additional instrumentation included for the sleeve-tube interaction monitoring. The setup used was described in Section 2.5 and shown in Figure 2.31. Monitored and included here to describe the specimen behavior under loading were the load-shortening relationship, dent growth, and the in-plane displacements.

Test Specimen C4 - Specimen C4 simulated the grouted clamp repair of a damaged bracing member with a D/t ratio of 64. The high D/t ratio was selected due to susceptibility to local buckling. As noted previously, if this specimen D/t group could be repaired by this means, the repair was assumed to be effective on members with smaller D/t ratios.

The normalized load-shortening curve given in Figure 3.70 shows the response of the specimen during loading. The ascending branch of the curve is linear and follows theoretical predictions very well. This theoretical prediction is based on a bare steel specimen, and ignores the grouted clamp. The descending relationship following failure is much steeper than viewed in the internal grout repair technique. The residual load capacity at the termination of shortening was very low as well, due to the mode of failure.

94

No signs of yielding were present in the clamp at the maximum load of 74 kips. Likewise, very little dent growth was measured up to and at the peak load. Figure 3.72 shows that for Specimen C4 the grouted sleeve was able to arrest the dent growth into the member's cross section by restricting the cross section ovaling that typically accompanies the increased dent growth. This resistance to ovaling was supplied by hoop confinement to the dented section by the clamp. Consequently, this increased the specimen capacity by eliminating this mechanism of failure. The curvature existing in the specimen at peak load is shown in Figure 3.71.

Yielding initiated outside of the clamped section. At peak load, flaking of the whitewash was noticed at a location 30 inches to the west of the midspan of the specimen, 10 inches from the edge of the clamp. A local buckle formed at this location following first yield of the material (Figure 3.73). The buckle initiated as a simple wave, and as axial shortening was increased beyond peak axial load, it propagated into the same cross section distortion observed in the non-damaged specimen of this same D/t group (see Figures 3.13 and 3.74).

The in-plane displacements (Figures 3.75 and 3.76) reveal that the clamped section of the tube remained relatively stiff during loading. The displacements before and at peak load are composed of sloped spans to each side of the grouted clamp. The local concentration of curvature at x/L=0.35 is evident following the development of peak load P_{max}, and is associated with the local buckling.

Summary - The grouted sleeve was effective in repairing the damaged specimen of D/t ratio 64 by restoring the load carrying capacity. The sleeve averted the mechanism of failure observed in non-repaired specimens by resisting the dent growth through containment of the tube cross section. Ovaling of the cross section was observed to follow dent growth in the earlier non-repaired specimens. By resisting the ovaling, the dent was not allowed to grow and the mode of failure was transferred to outside the clamp. The failure of Specimen C4 was identical to that of non-damaged Specimen C5, and consisted of the formation of a local buckle in the tube wall outside the clamp. The buckle propagated into a major distortion of the cross section, diminishing the load carrying capacity of the member.

3.5   Dissection of Grout Repaired Specimens

Following the completion of all testing, the grout repaired specimens were cut open in the dent zone to in order to expose the grout. The exposed grout of the internally grout repaired specimens is shown in Figures 3.77 through 3.79.   The wall of each specimen was rather easily removed, where it was noted that a weak bond had developed between the grout and the inside of the steel wall.   No grout voids were found.   In all cases, the area immediately around the dent saddle contained loose material, as attested by the cracks and flakes of grout appearing in Figure 3.80(a).   This grout was easily removed (see Figure 3.80(b)).   A one inch wide strip of grout under the dent saddle however remained intact.   It is speculated that the grout failure pattern shown in Figure 3.80 is caused by the outward buckling of the wall discussed previously under specimen behavior, at 3 to 4 inches to each side of the dent saddle.   This outward movement left the grout unconfined and caused it to fail under compression.   The dent saddle always remained in contact with the 1 inch strip of grout beneath the saddle, thereby maintaining its confinement.

The cutting open of the grouted sleeve (Specimen C4) indicated that no crushing or cracking of the grout had occurred.   Furthermore, the surface roughness produced by the sand blasting resulted in an appreciable increase in bond between the grout and steel.
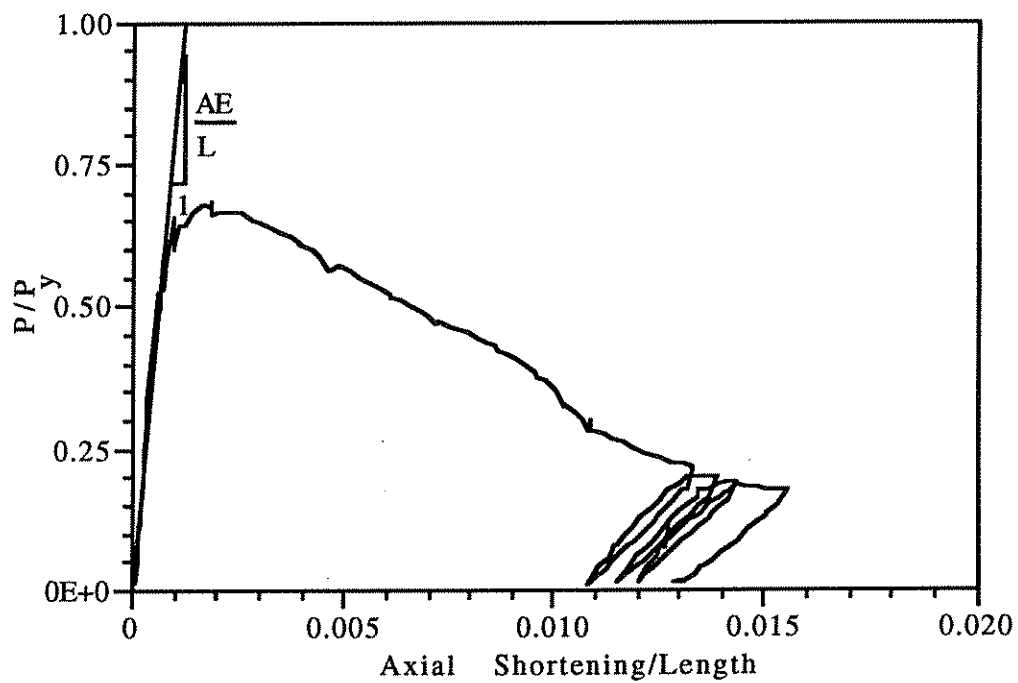
(This page intentionally blank)

Figure 3.1.   Axial Load - End Shortening Relationship for Specimen A5.
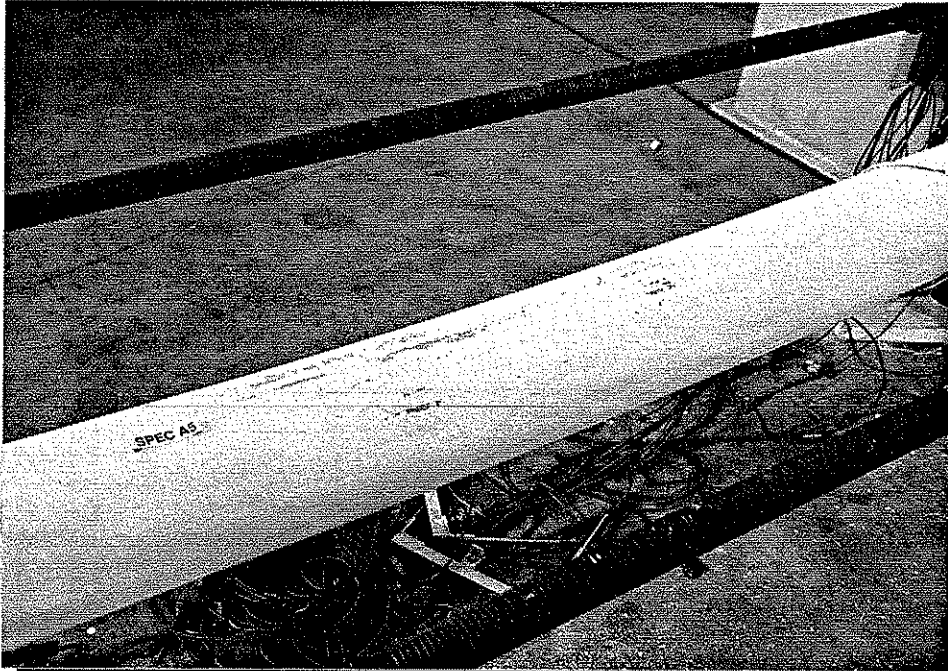
Figure 3.2. Initial yielding along compression face of Specimen A5.

Figure 3.3. Formation of a local buckle on the compression face of Specimen A5.
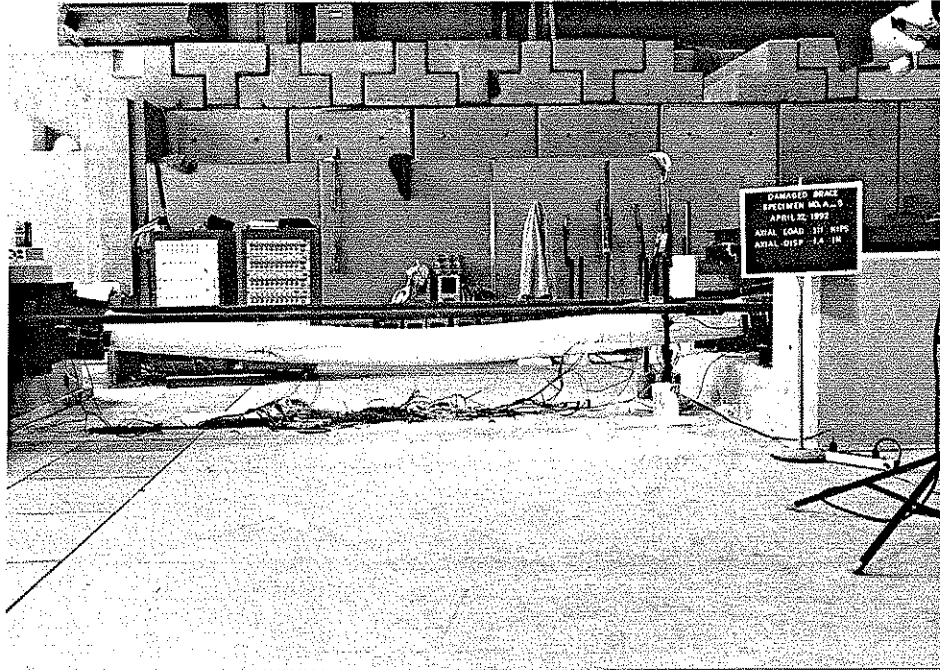
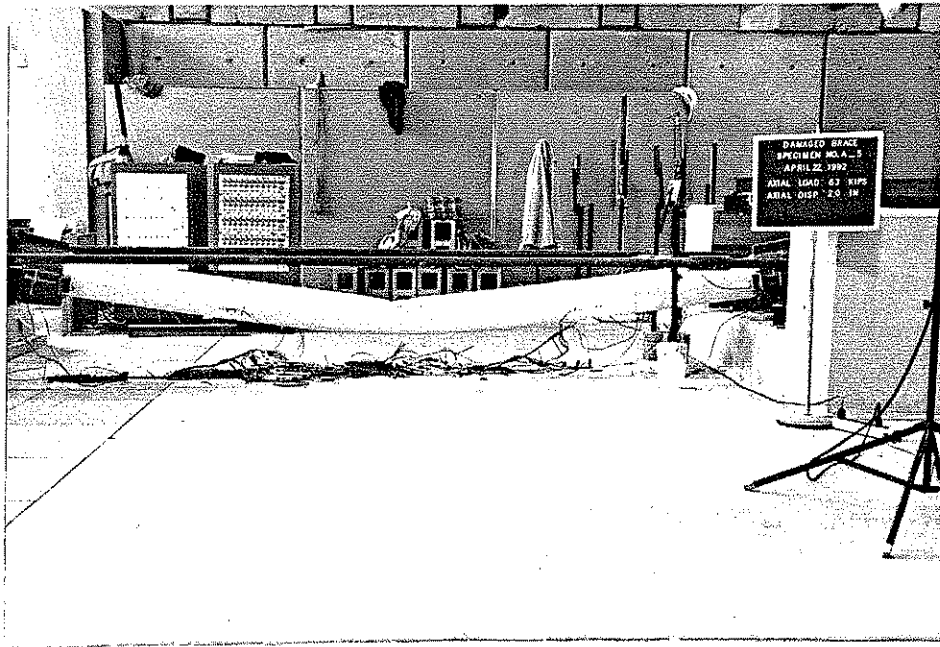Figure 3.4. Displacement of Specimen A5 in the plane of bending following peak load $(P=0.72P_{max})$.

Figure 3.5. Displacement of Specimen A5 in the plane of bending following peak load $(P=0.41P_{max})$.
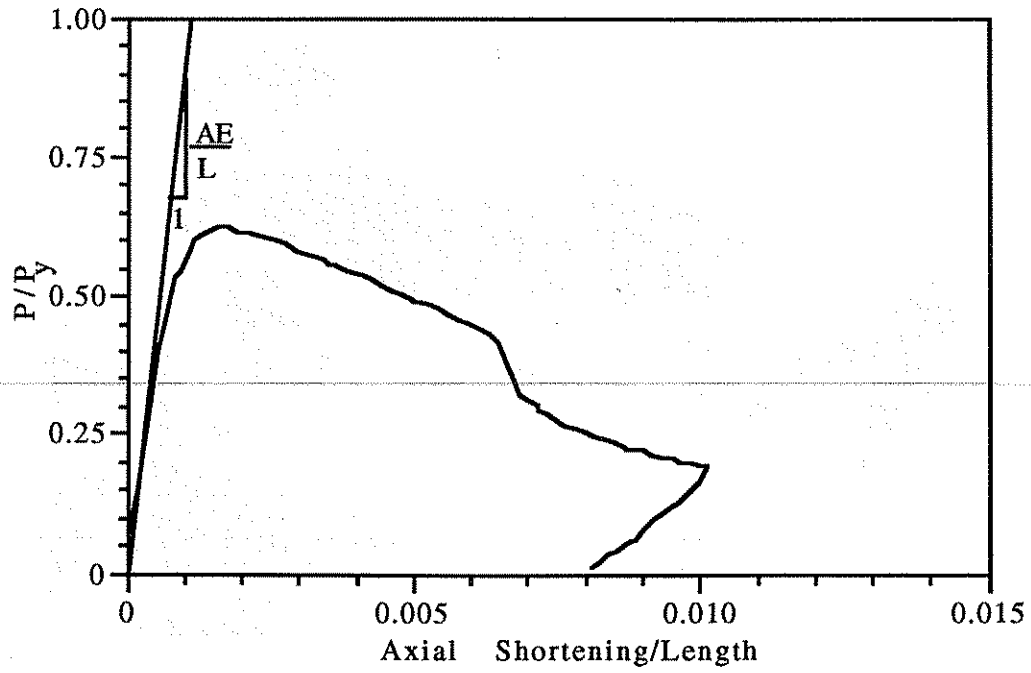
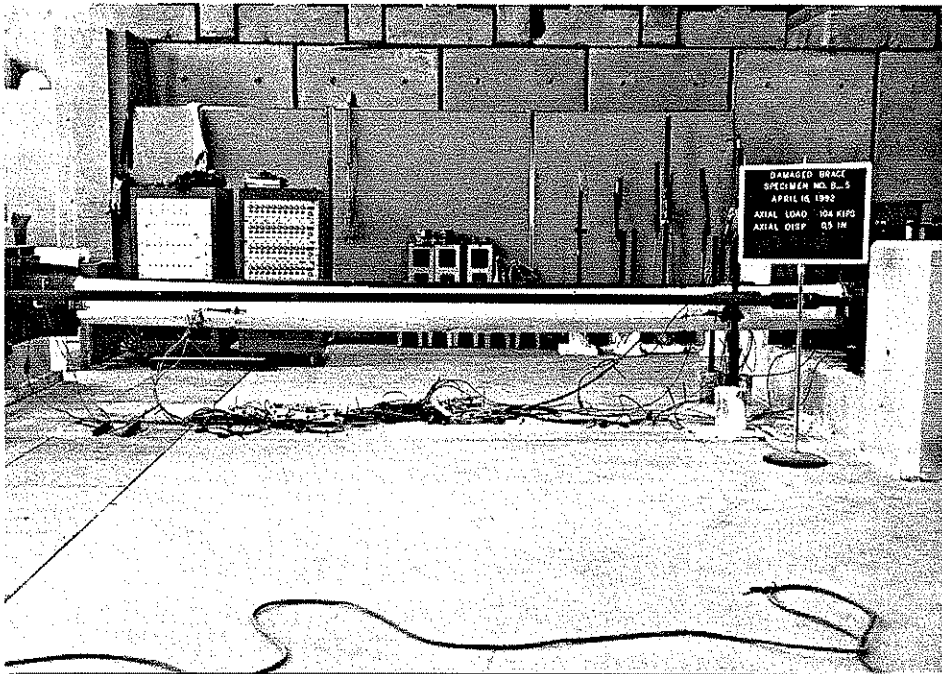Figure 3.6.   Axial Load - End Shortening Relationship for Specimen B5.

Figure 3.7.   Displacement of Specimen B5 in the plane of bending at its peak load.

Figure 3.8. Formation of a local buckle on the compression face of Specimen B5.
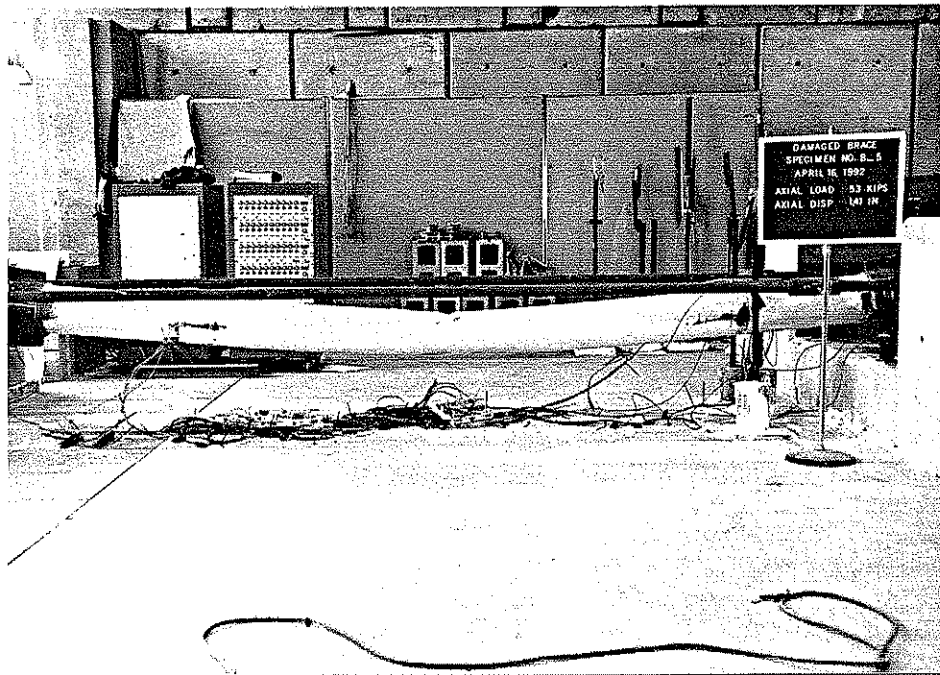

Figure 3.9. Displacement of Specimen B5 in the plane of bending following the formation of the local buckle and subsequent failure.
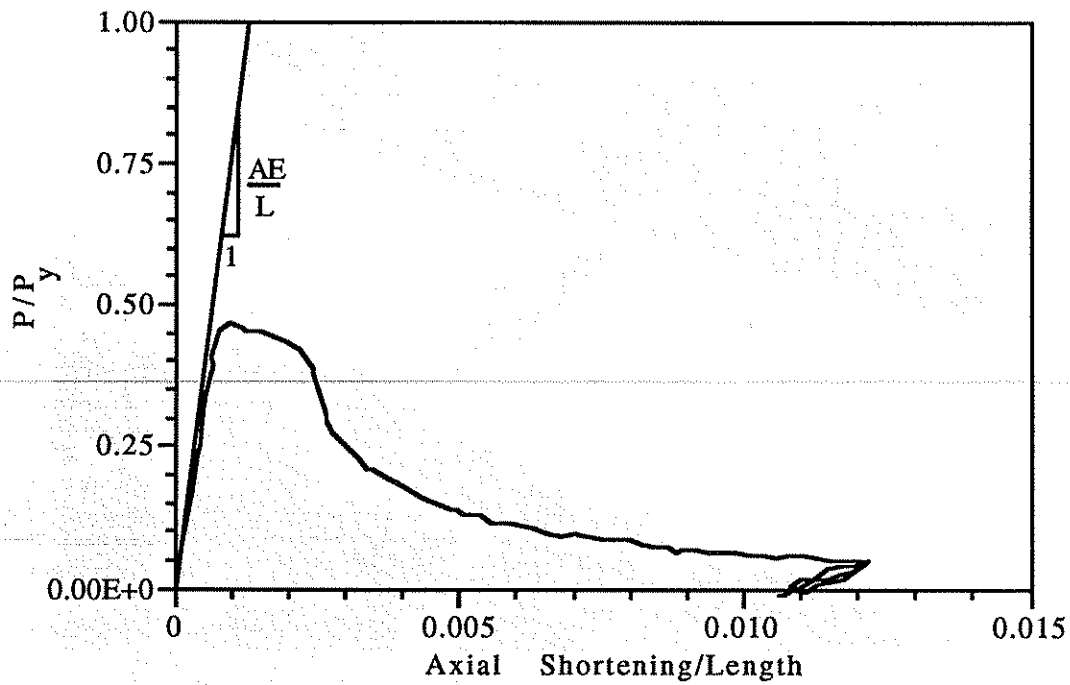
Figure 3.10.   Axial Load - End Shortening Relationship for Specimen C5.
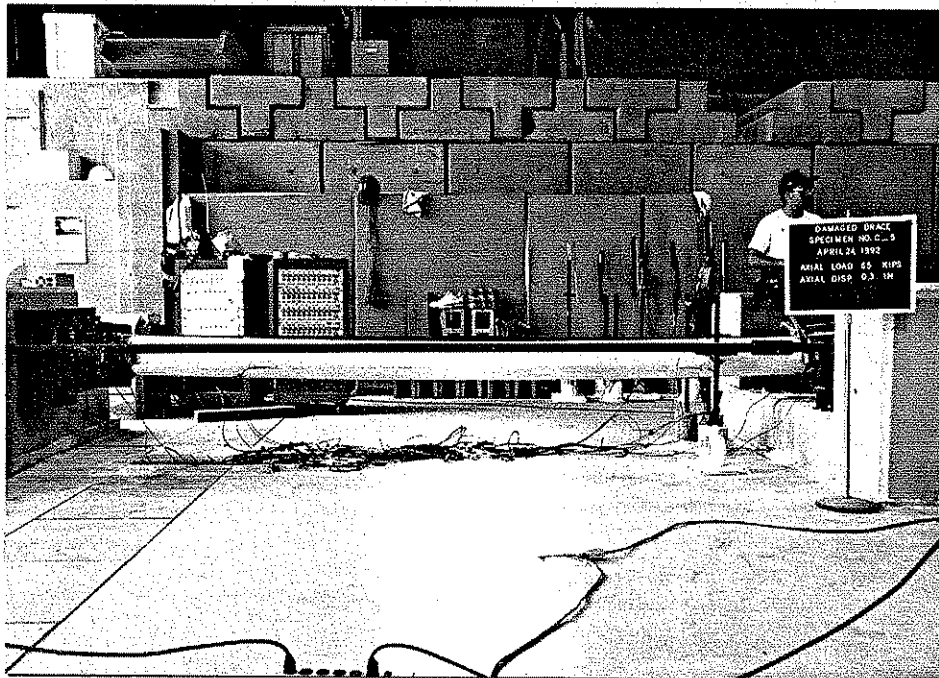
Figure 3.11.   Displacement of Specimen C5 in the plane of bending at its peak load $(P=P_{max})$.
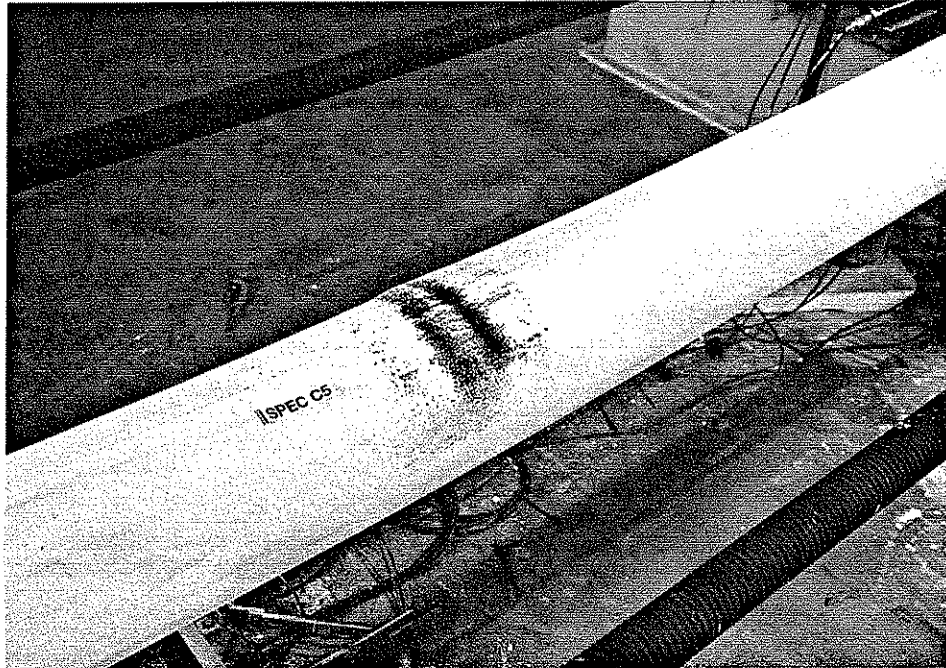
Figure 3.12.   Formation of a local buckle on the compression face of Specimen C5.
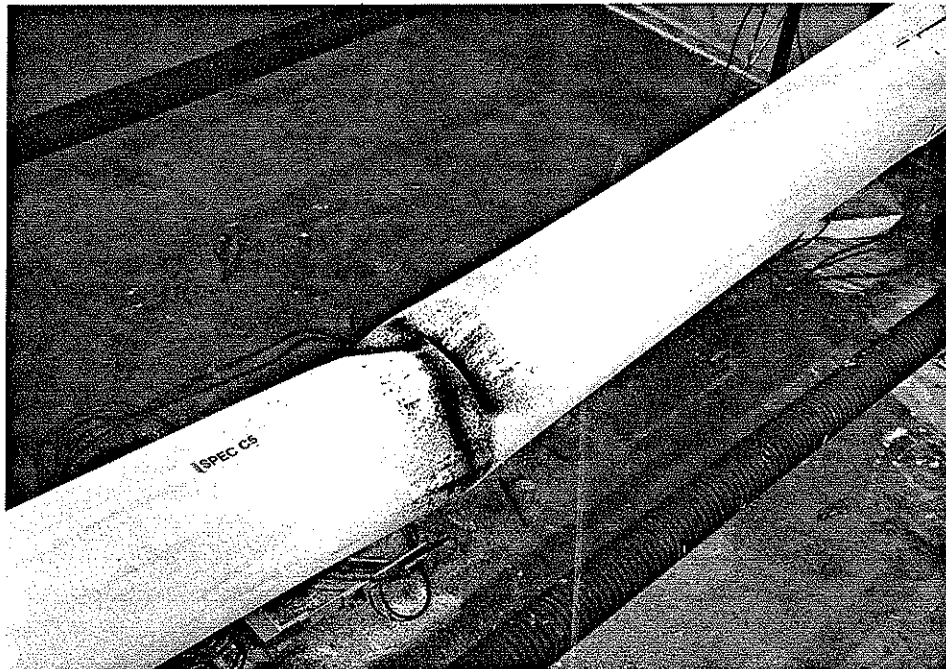
Figure 3.13.   Deterioration of the buckled region following continued shortening.

Figure 3.14. Corresponding in-plane displacement of Specimen C5 after continued shortening.
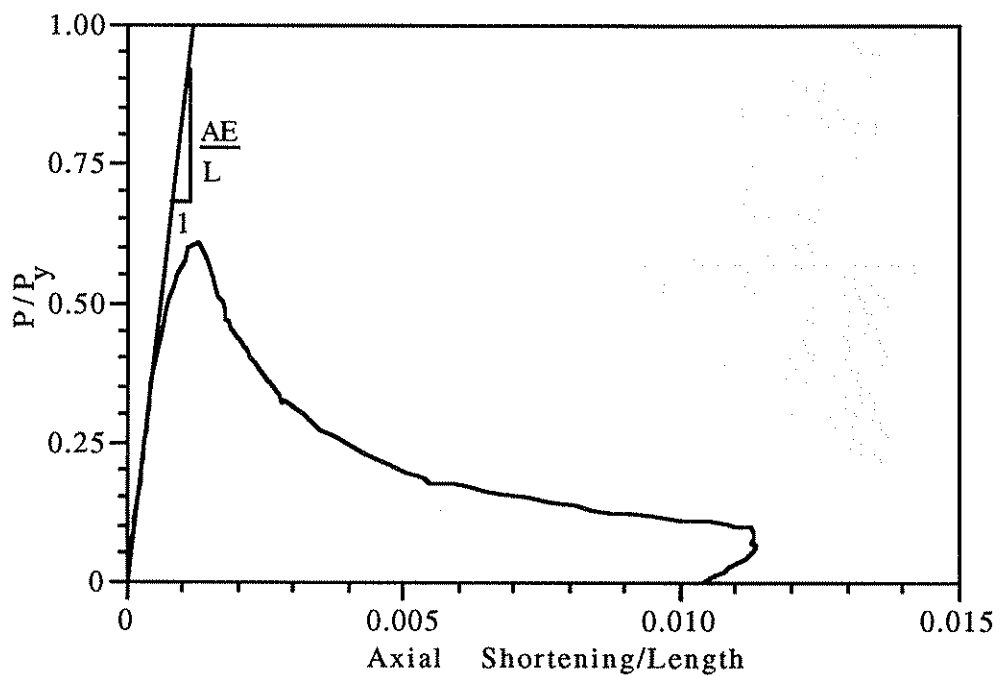
Figure 3.15. Axial Load - End Shortening Relationship for Specimen A1.
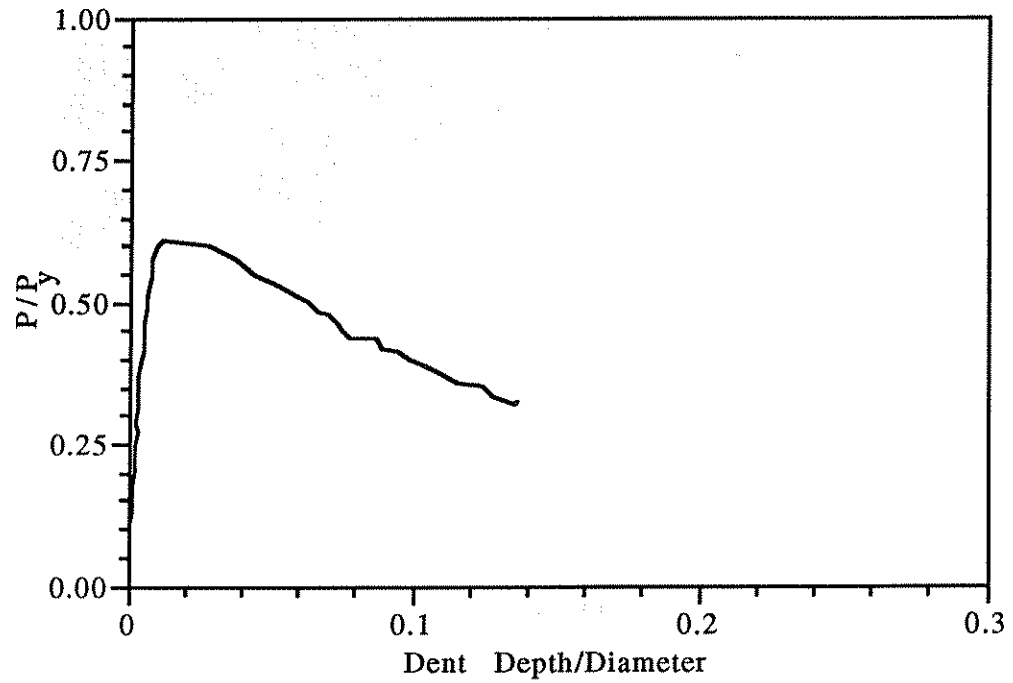
Figure 3.16. Axial Load - Dent Growth Relationship for Specimen A1.
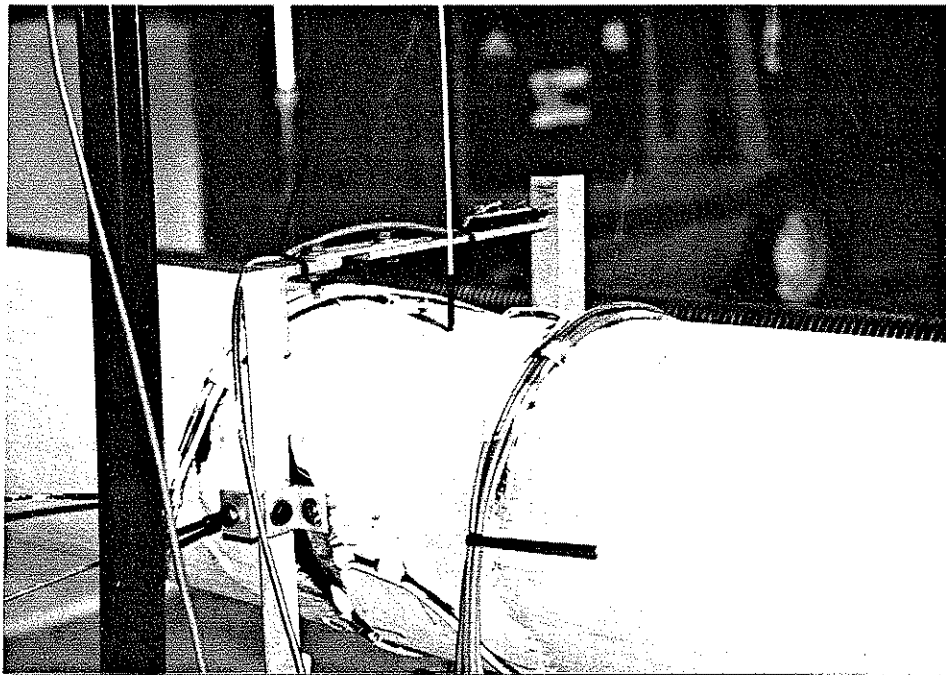
Figure 3.17. View of dented region of Specimen A1 prior to testing.

106
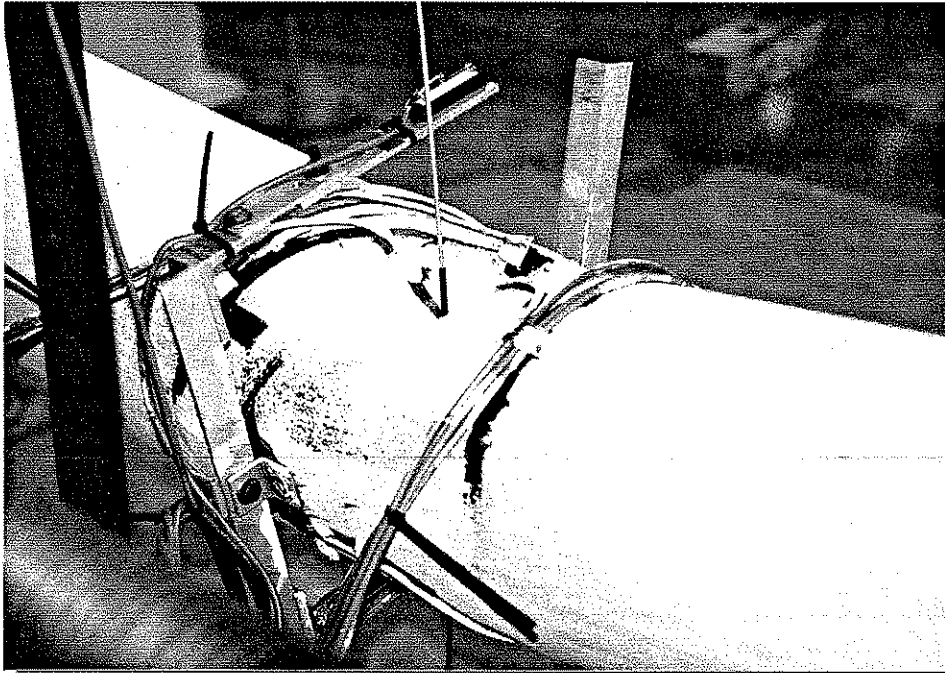
Figure 3.18. View of dented region of Specimen A1 at peak load.
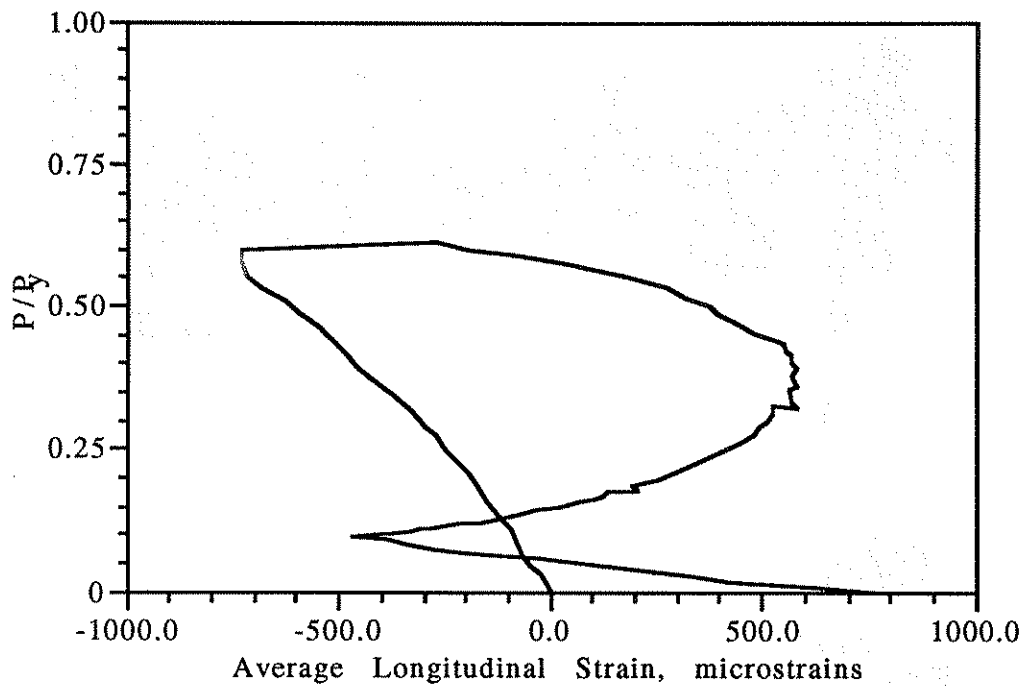
Figure 3.19. History of Longitudinal Strain Developed in the Dent, Specimen A1.
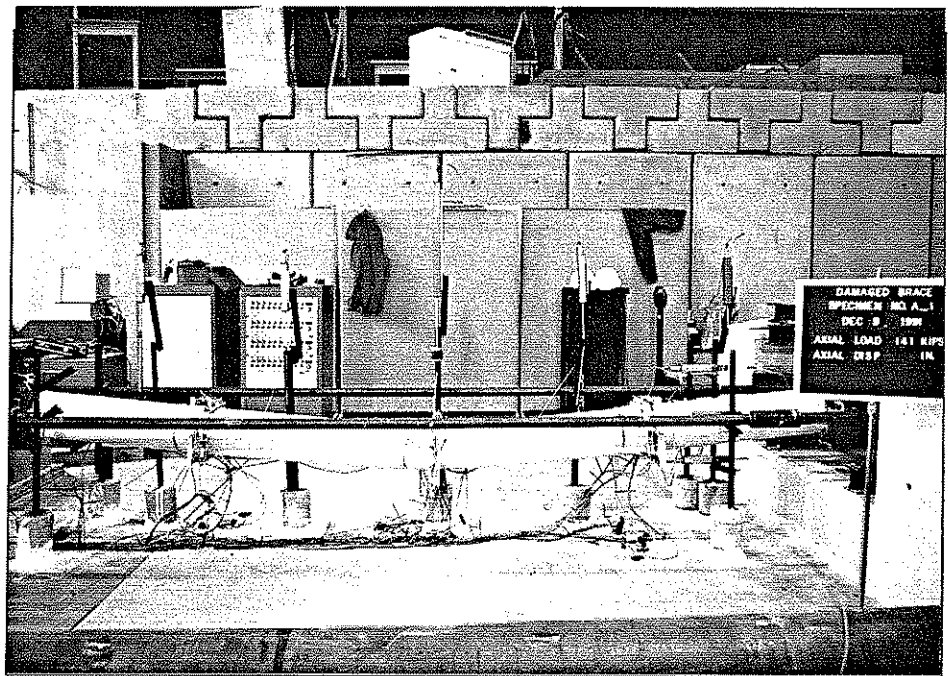
Figure 3.20. Displacement of Specimen A1 in the plane of bending at its ultimate capacity.

Figure 3.21. Measured In-plane Displacements of Specimen A1 at Various Stages of Loading.

Figure 3.22. Axial Load - End Shortening Relationship for Specimen A2.

Figure 3.23. Axial Load - Dent Growth Relationship for Specimen A2.
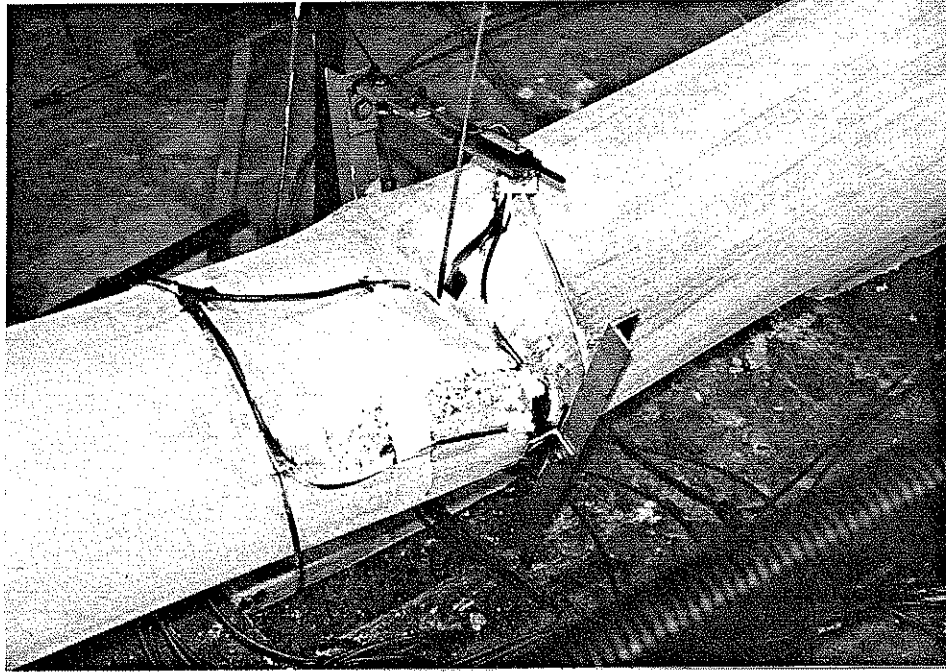
Figure 3.24. View of the deformed cross section after failure of Specimen A2.
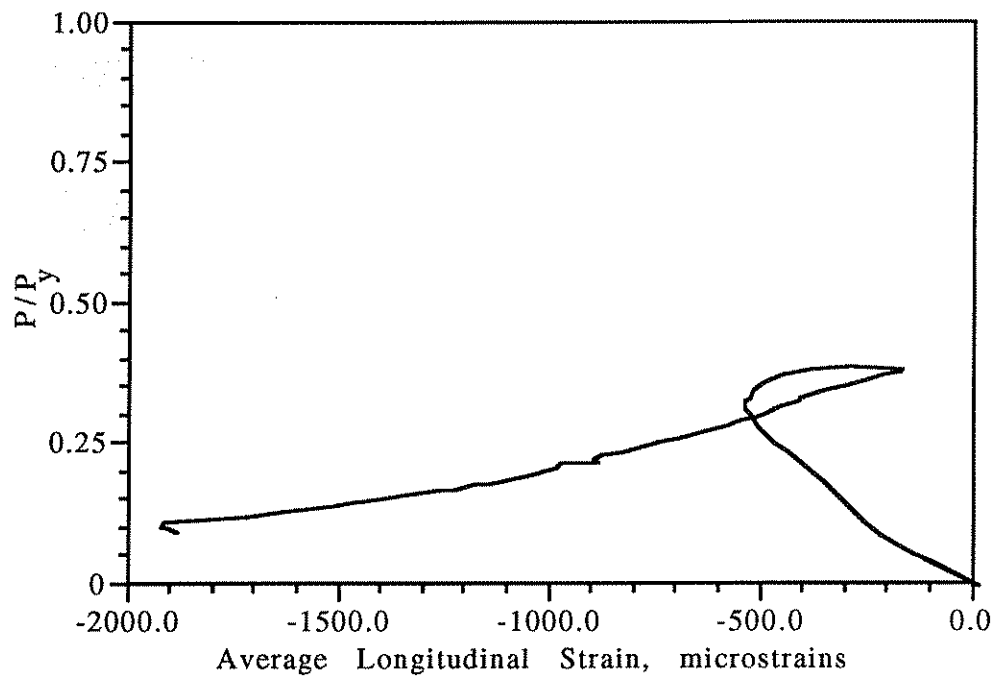
Figure 3.25. History of Longitudinal Strain in Dent for Specimen A2.
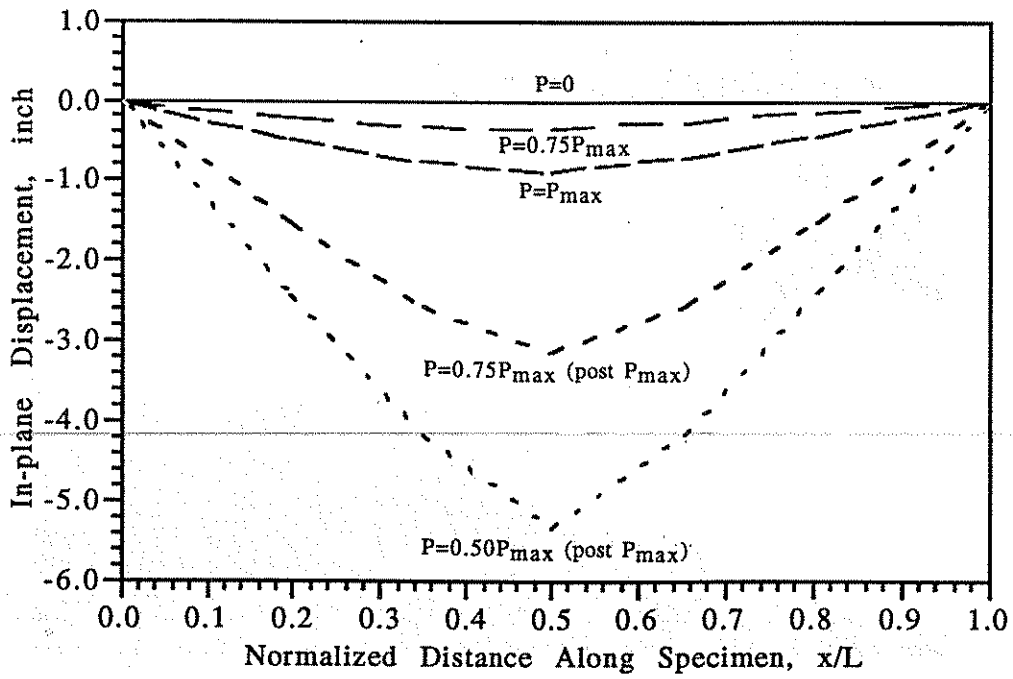
Figure 3.26.   Measured In-plane Displacements of Specimen A2 at Various Stages of Loading.
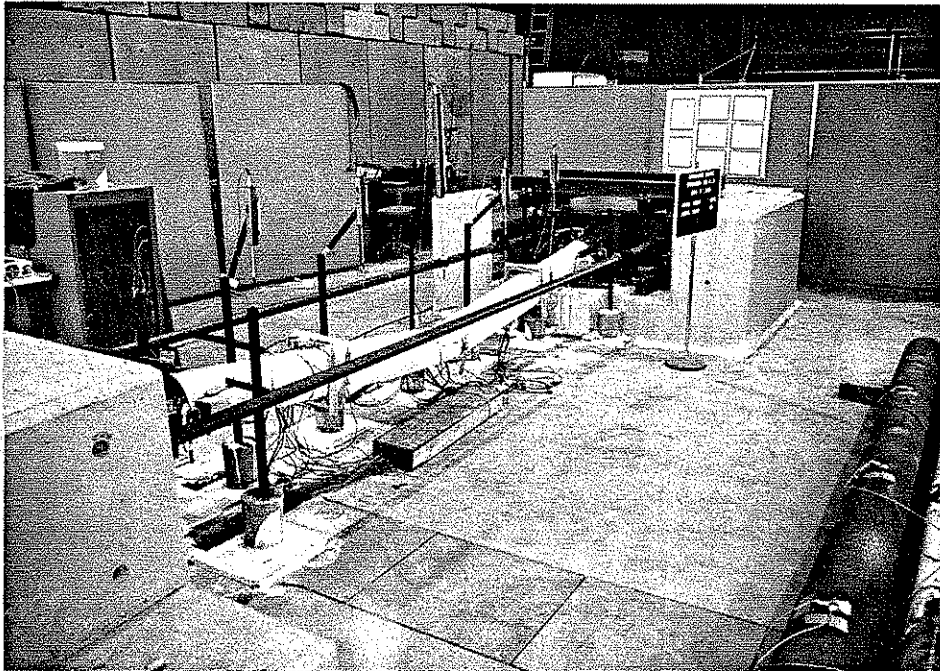
Figure 3.27.   View of the failed Specimen A2 showing the concentration of curvature at the dented section.
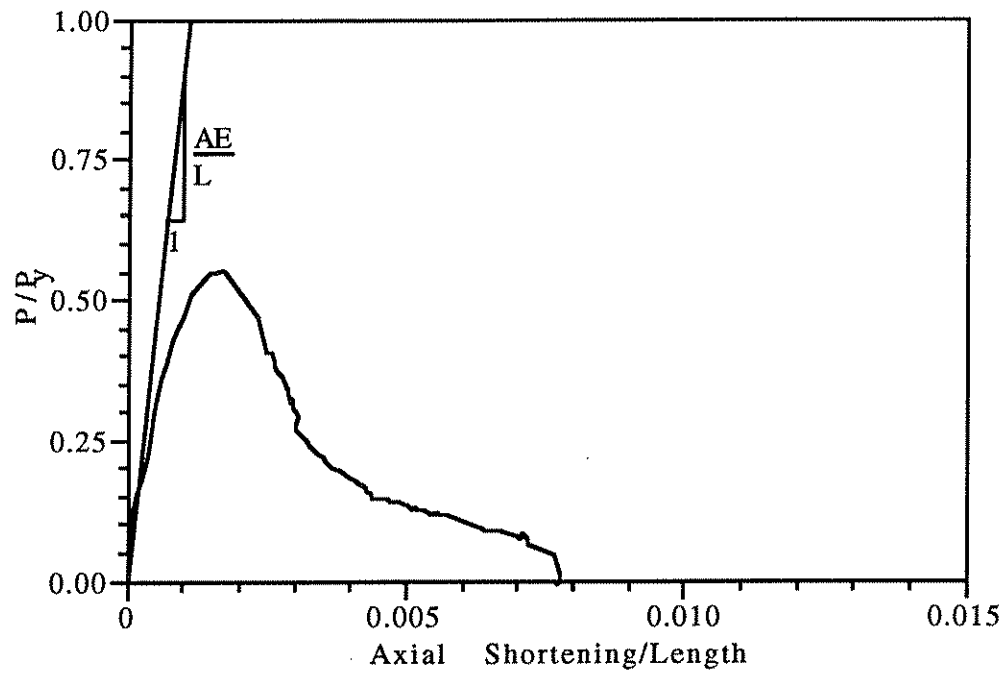
Figure 3.28. Axial Load - End Shortening Relationship for Specimen B1.
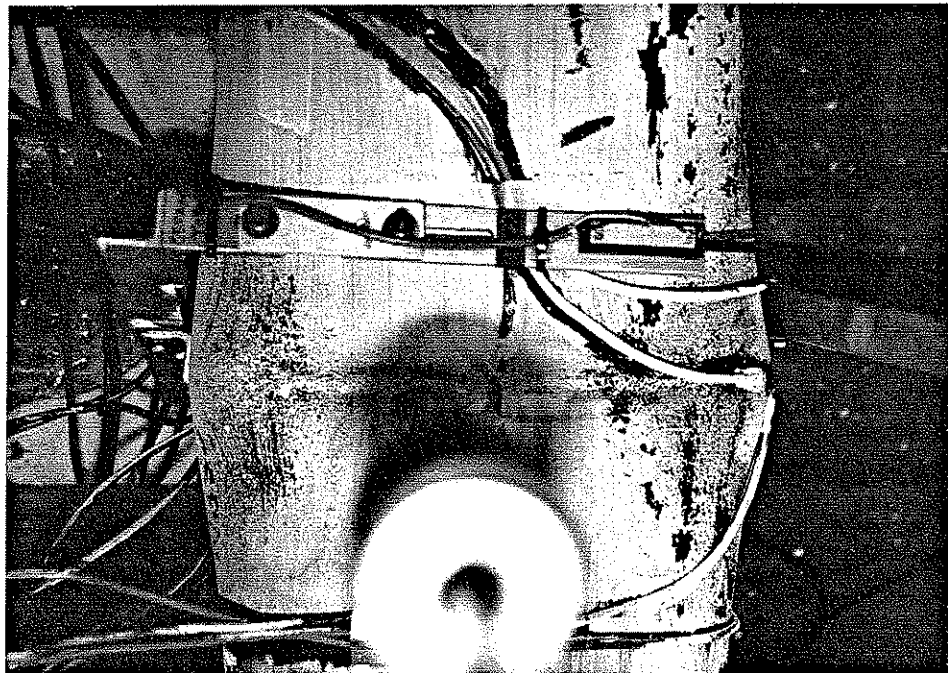
Figure 3.29. Yielding in the dented region showing deformed cross section of Specimen B1.

Figure 3.30. Axial Load - Dent Growth Relationship for Specimen B1.

Figure 3.31. History of Longitudinal Strains in Dented Region of Specimen B1.

Figure 3.32. Measured In-plane Displacements of Specimen B1 at Various Stages of Loading.
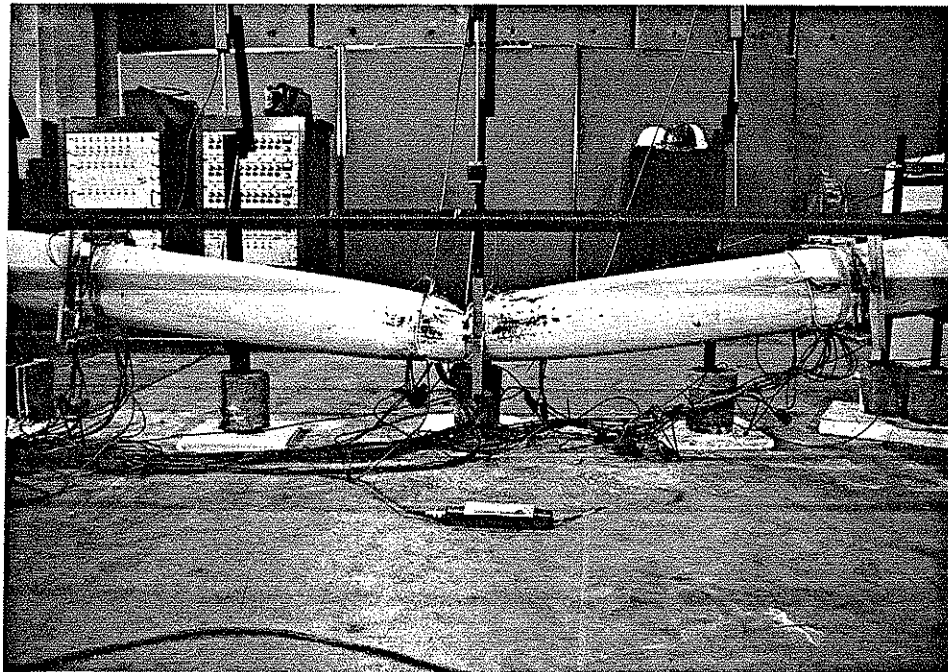
Figure 3.33. View showing formation of a plastic hinge across the dented region in Specimen B1.
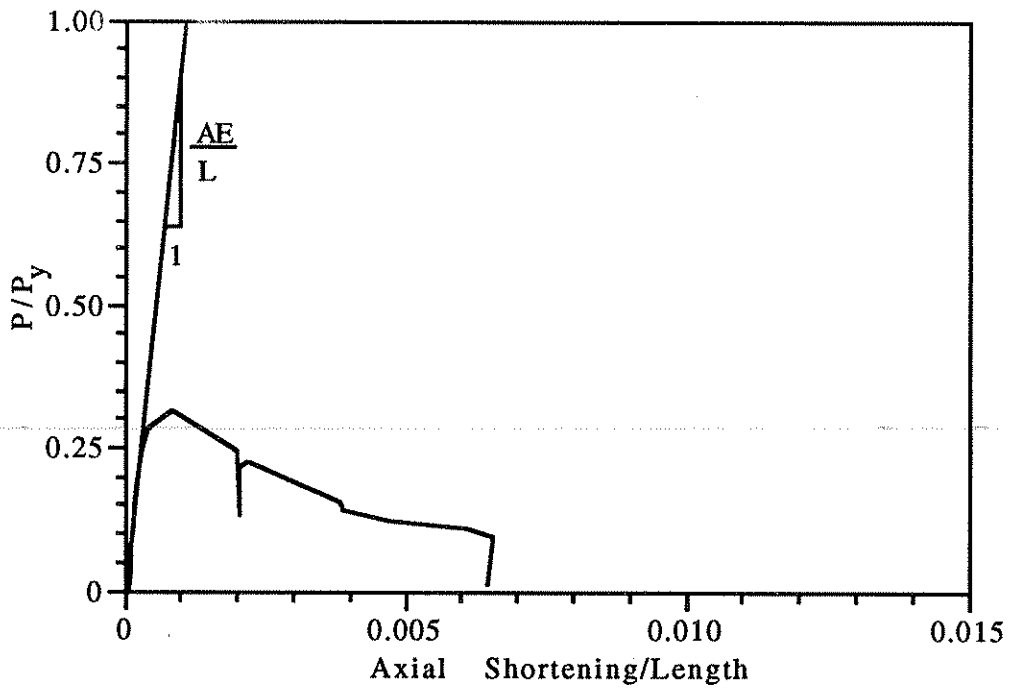
Figure 3.34. Axial Load - End Shortening Relationship for Specimen B2.
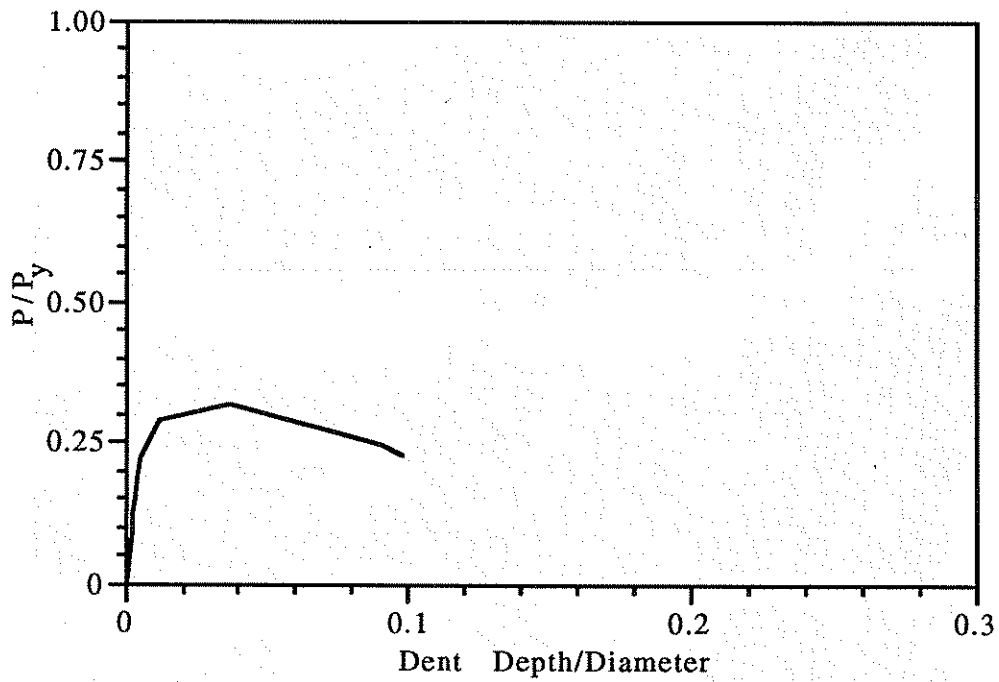
Figure 3.35. Axial Load - Dent Growth Relationship for Specimen B2.
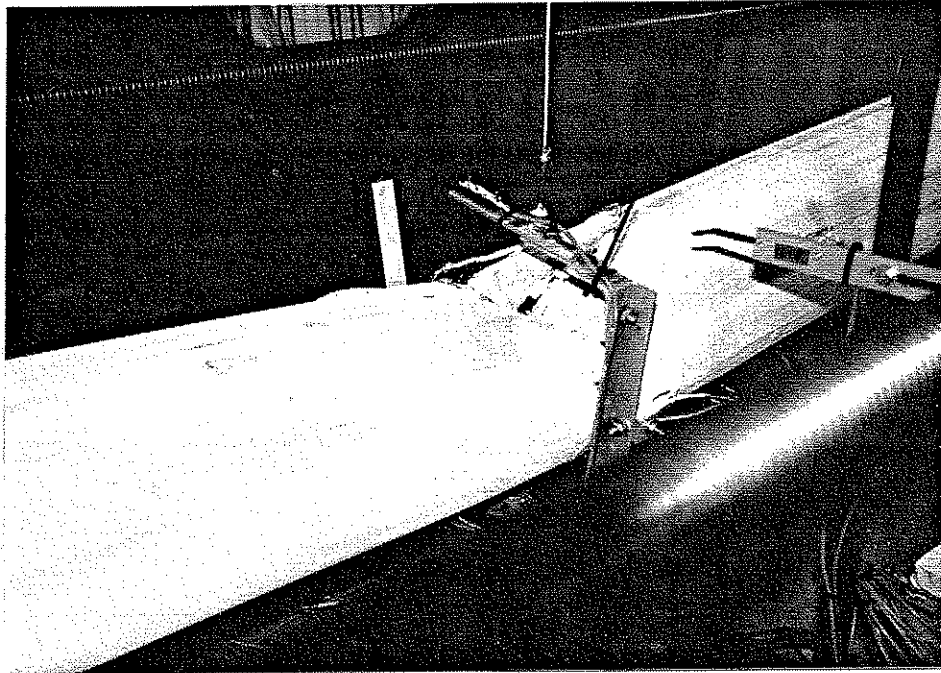
Figure 3.36. Dented Region of Specimen B2 Following Displacement Past its Peak Load P_{max}.
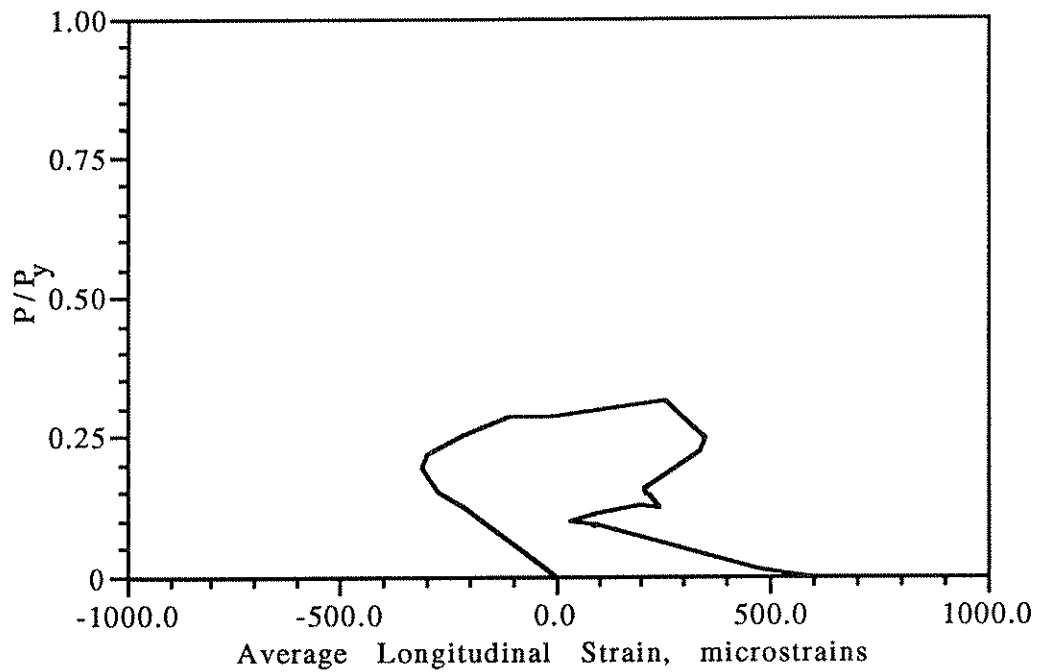
Figure 3.37. History of Longitudinal Strains in Dented Region of Specimen B2.

116
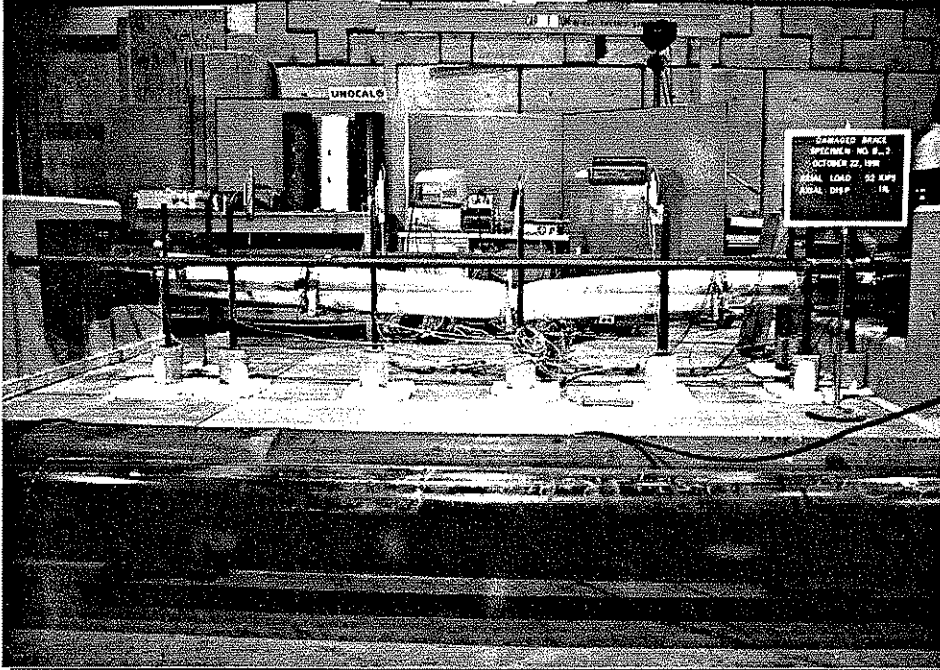
Figure 3.38. View of Specimen B2 following formation of a plastic hinge at the dented section.
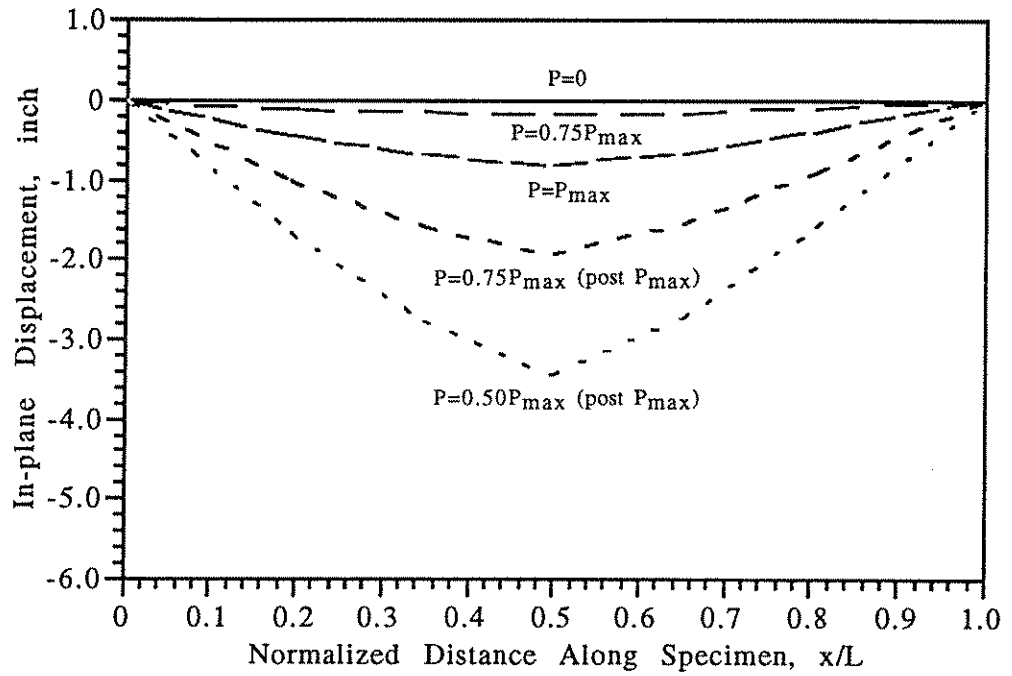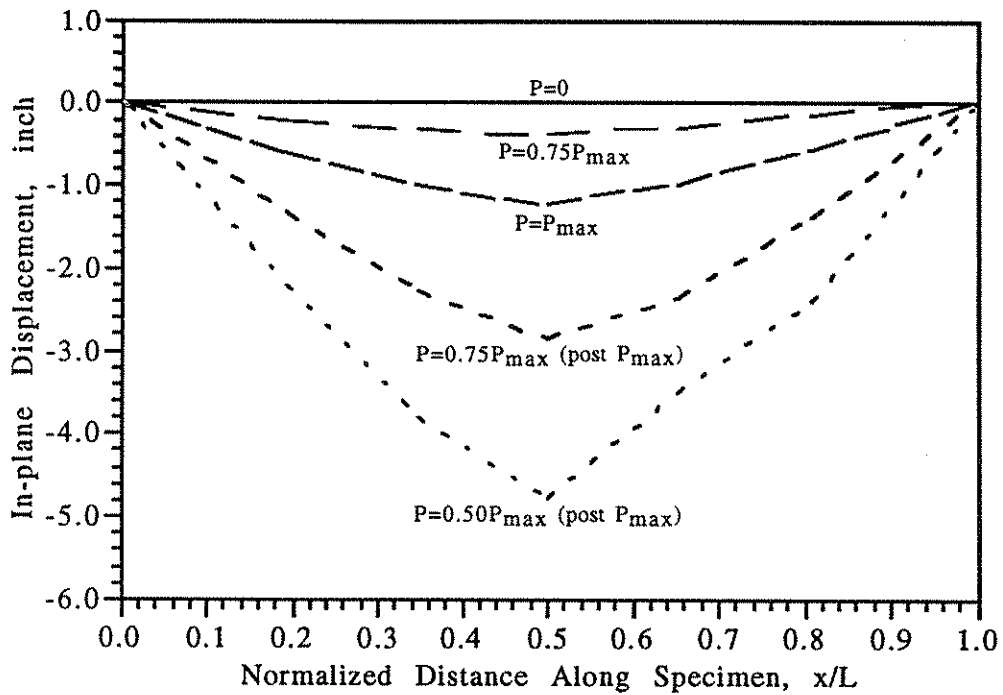

Figure 3.39. Measured In-plane Displacements of Specimen B2 at Various Stages of Loading.
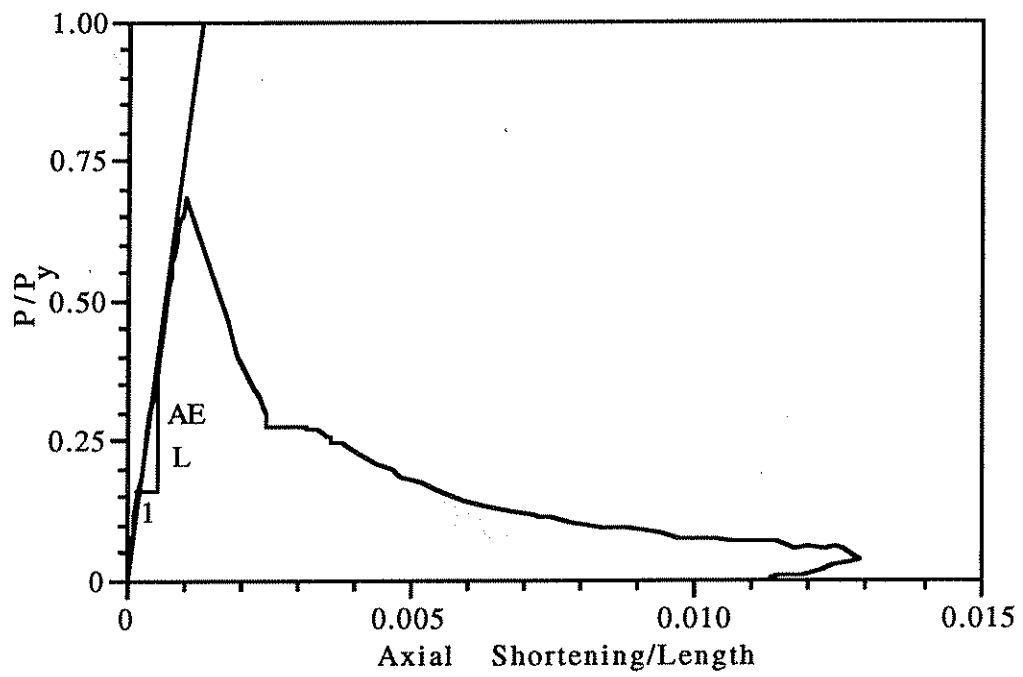
Figure 3.40. Axial Load - End Shortening Relationship for Specimen C1.
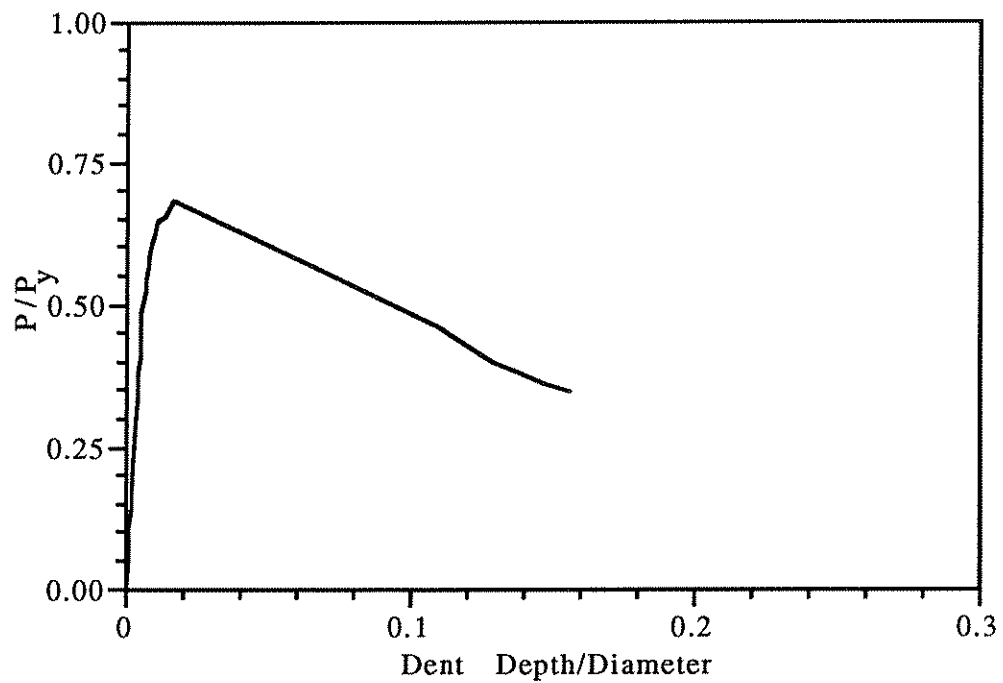
Figure 3.41. Axial Load - Dent Growth Relationship for Specimen C1.
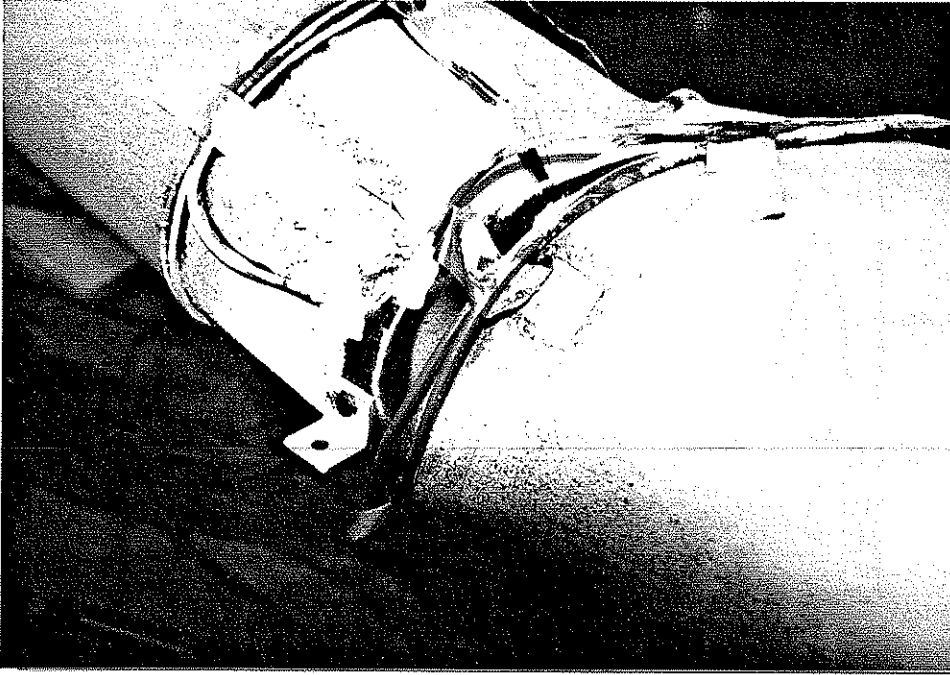
Figure 3.42. Formation of a Local Buckle on the Side of Specimen C1 at the Dented Section.
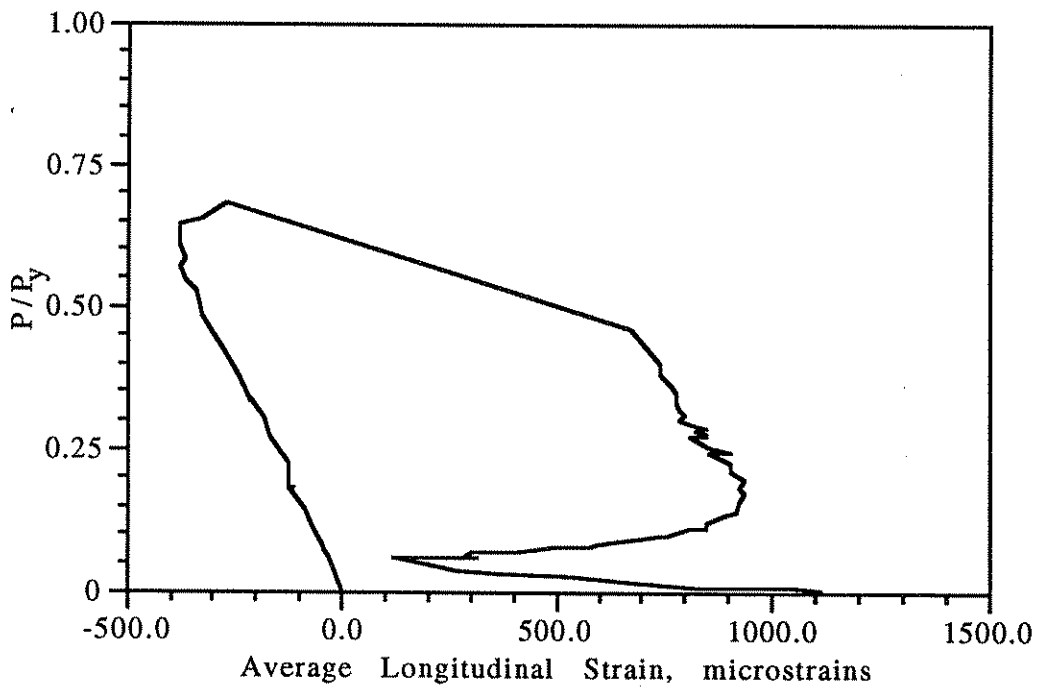
Figure 3.43. History of Longitudinal Strains in Dented Section of Specimen C1.
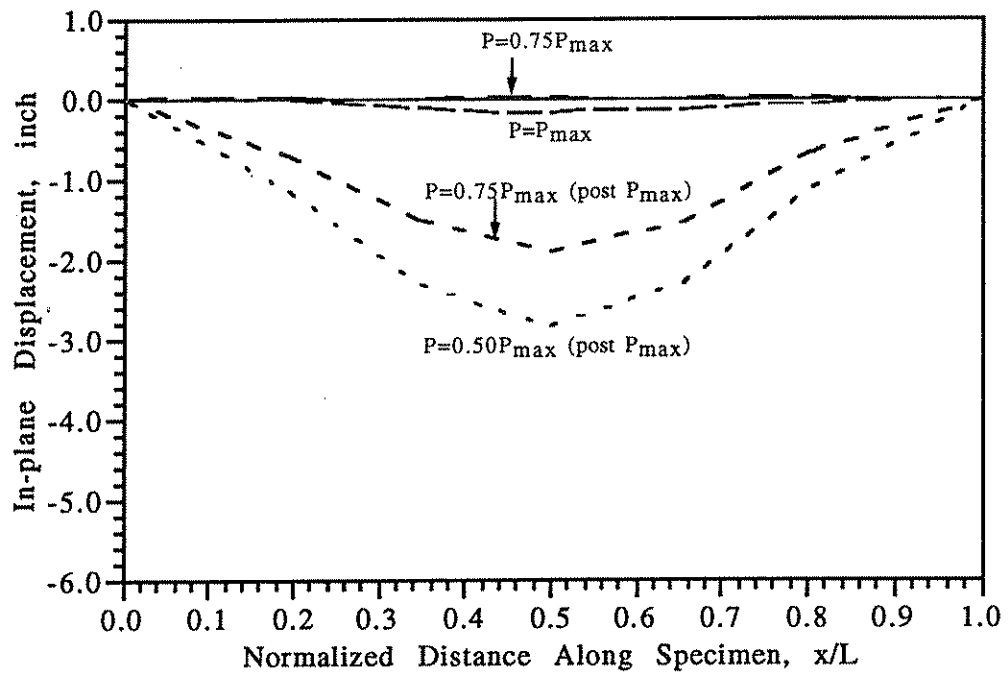
Figure 3.44. Measured In-plane Displacements of Specimen C1 at Various Stages of Loading.
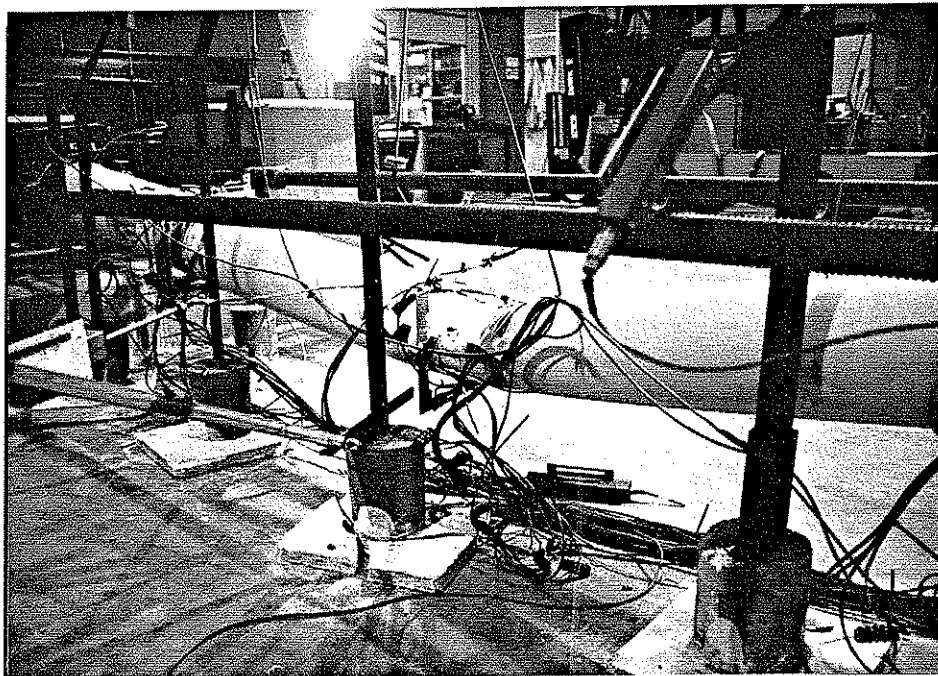
Figure 3.45. View of Specimen C1 following testing showing a plastic hinge formation across the dented section.
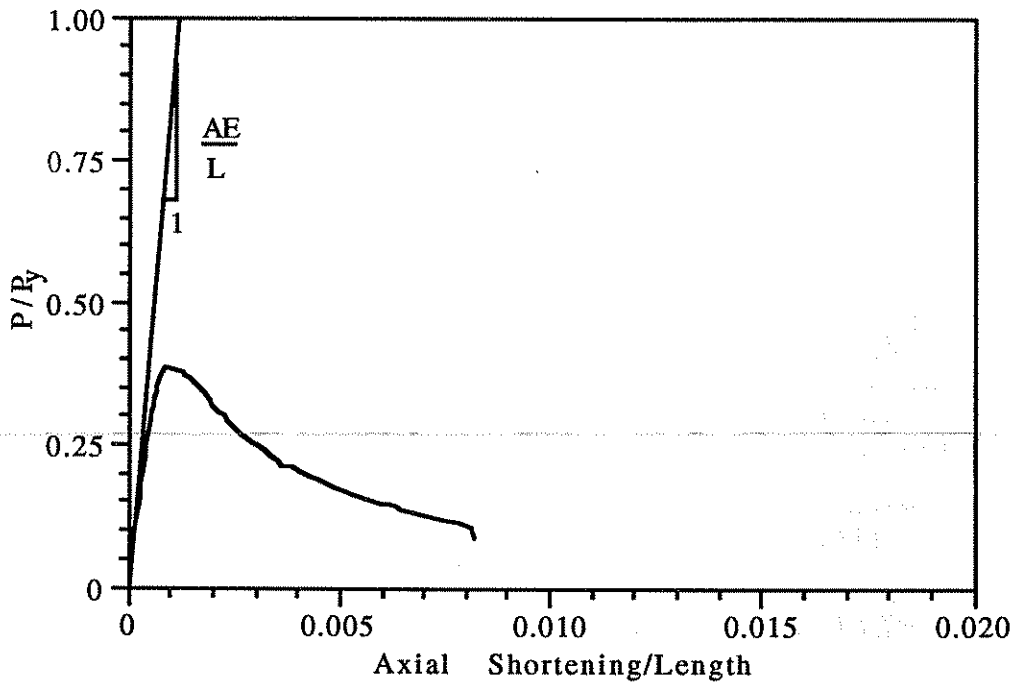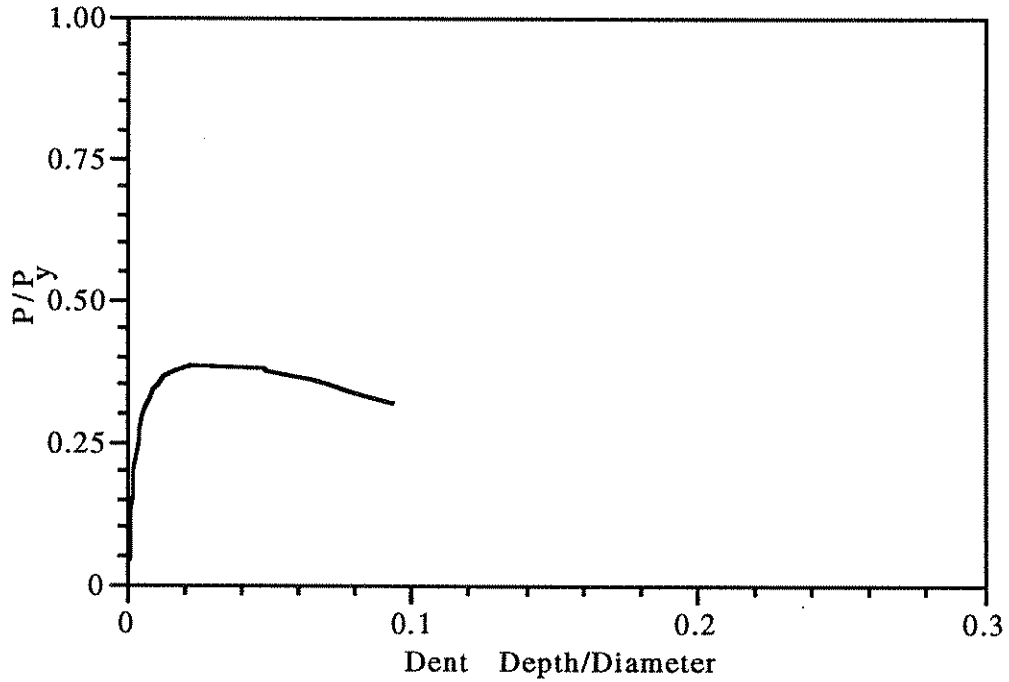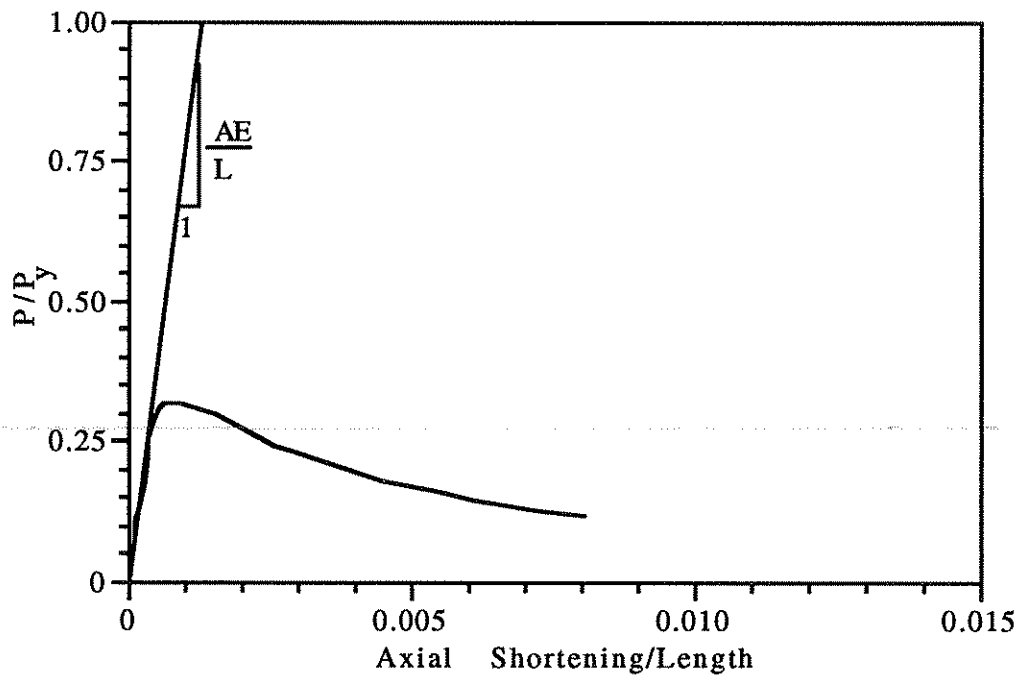
Figure 3.46.   Axial Load - End Shortening Relationship for Specimen C2.
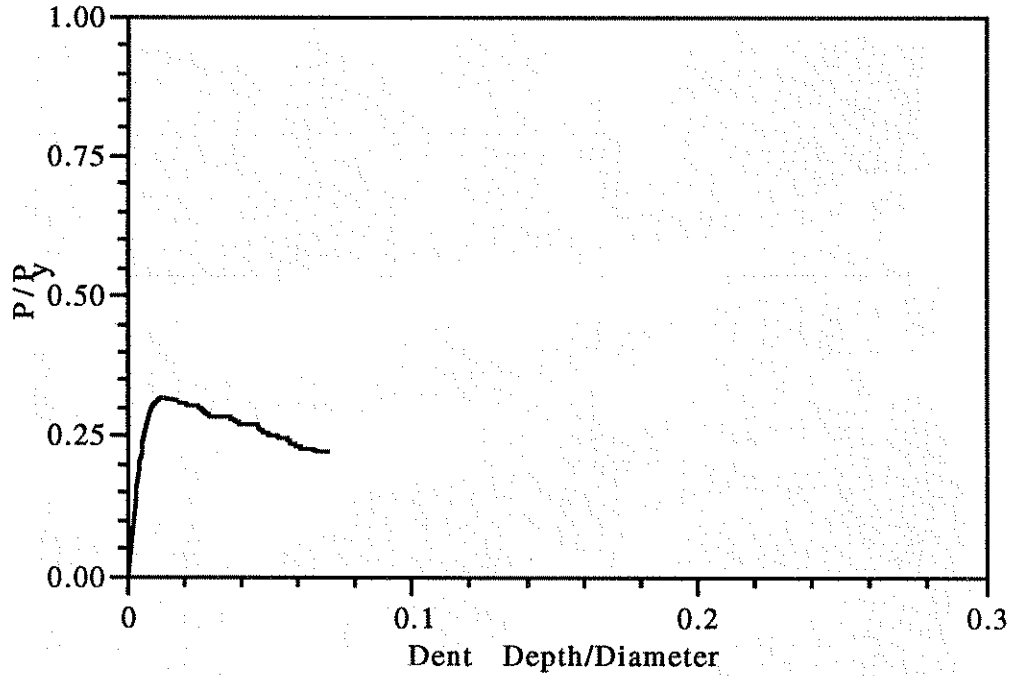
Figure 3.47.   Axial Load - Dent Growth Relationship for Specimen C2.
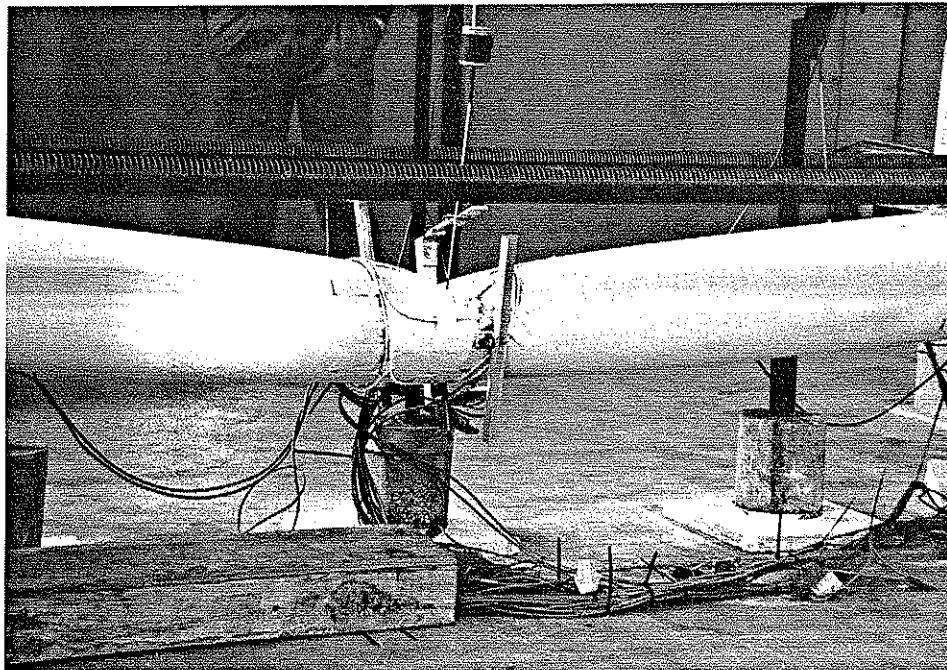
Figure 3.48. View of the Dented Section of Specimen C2 Following Failure.
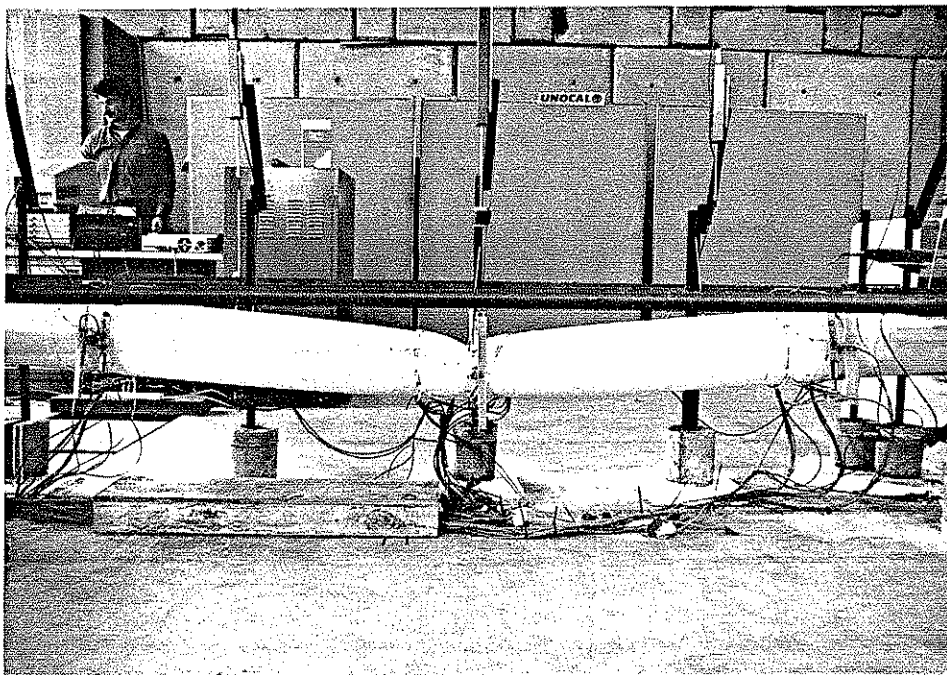
Figure 3.49. Formation of a Plastic Hinge Across the Dented Section of Specimen C2.

122
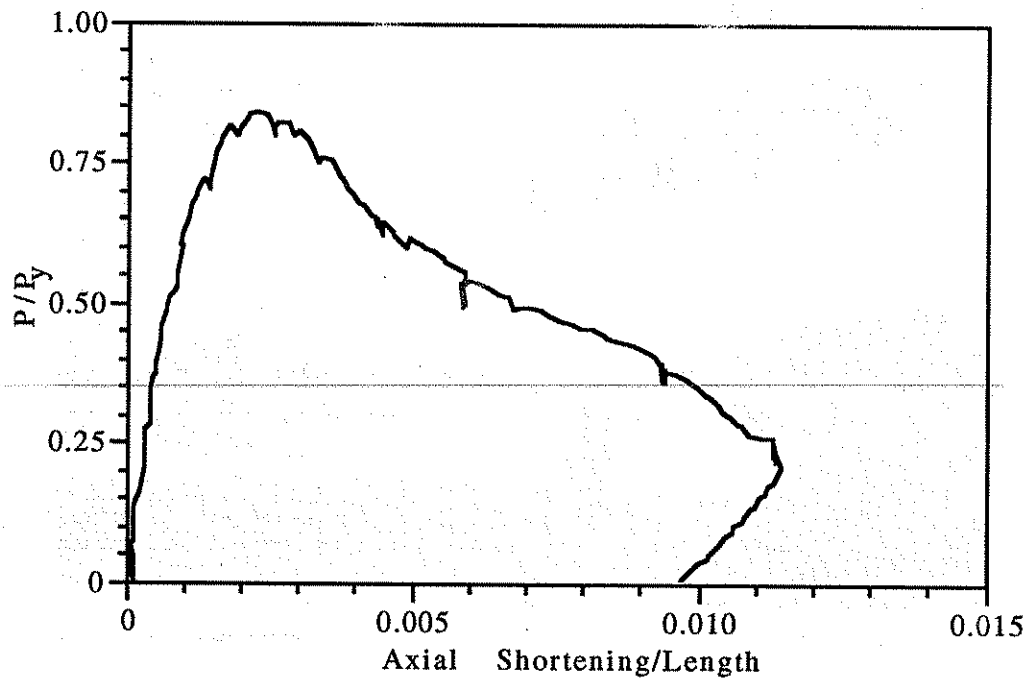
Figure 3.50.   Axial Load - End Shortening Relationship for Specimen A3.
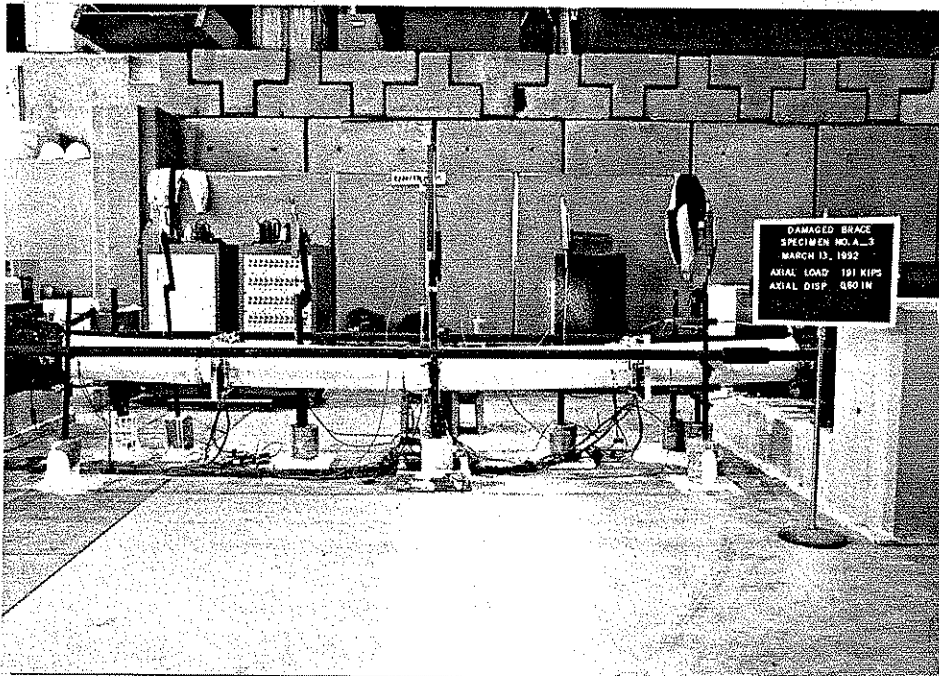
Figure 3.51.   View of the In-Plane Displacement of Specimen A3 at its Peak
Load.
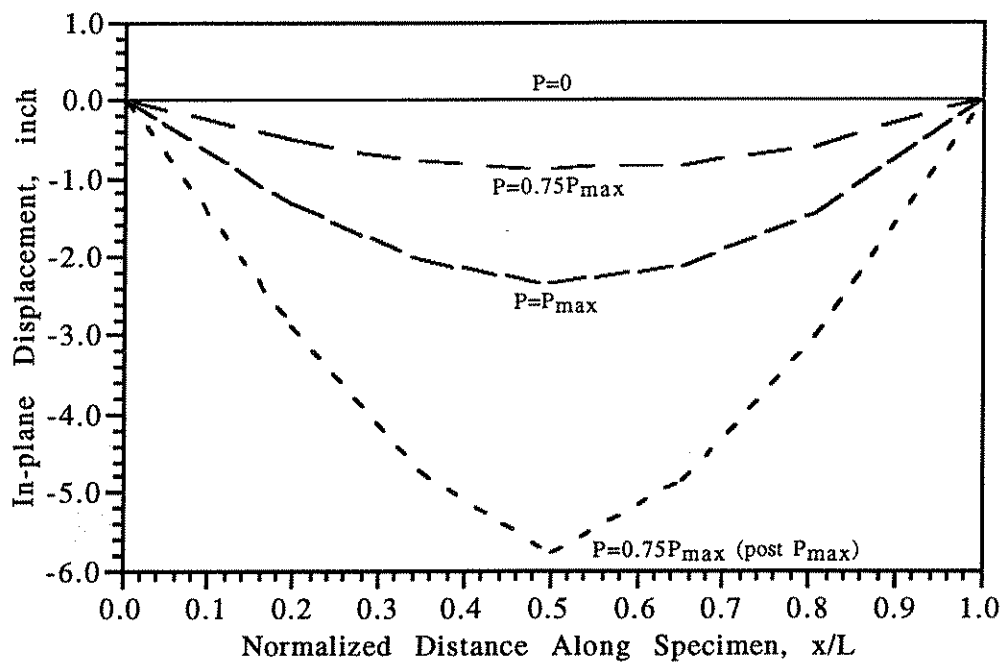
Figure 3.52.   Measured In-plane Displacements of Specimen A3 at Various Stages of Loading.
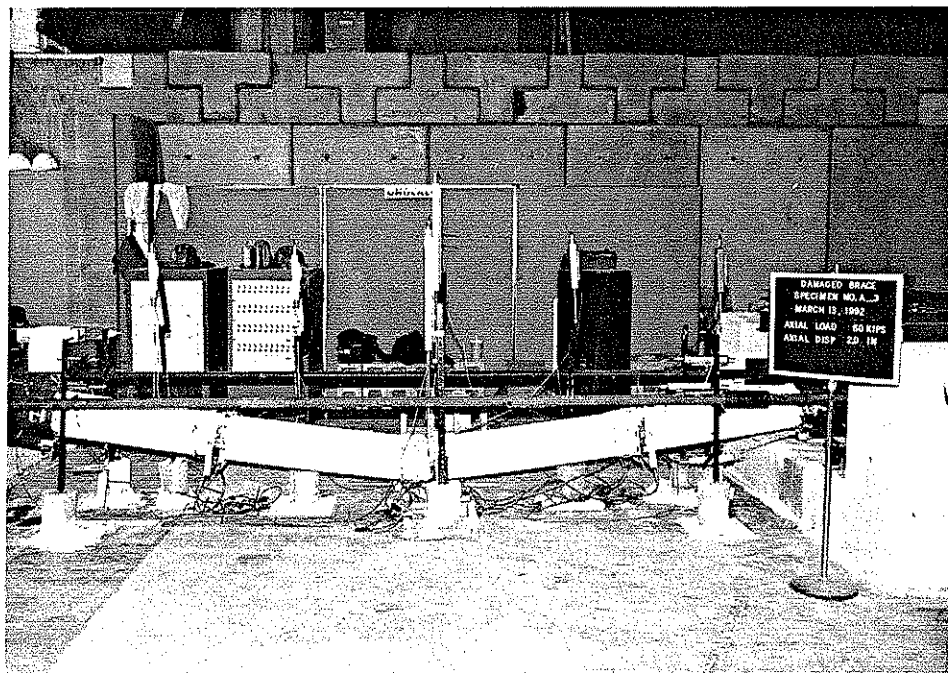
Figure 3.53.   Specimen A3 after testing.

124
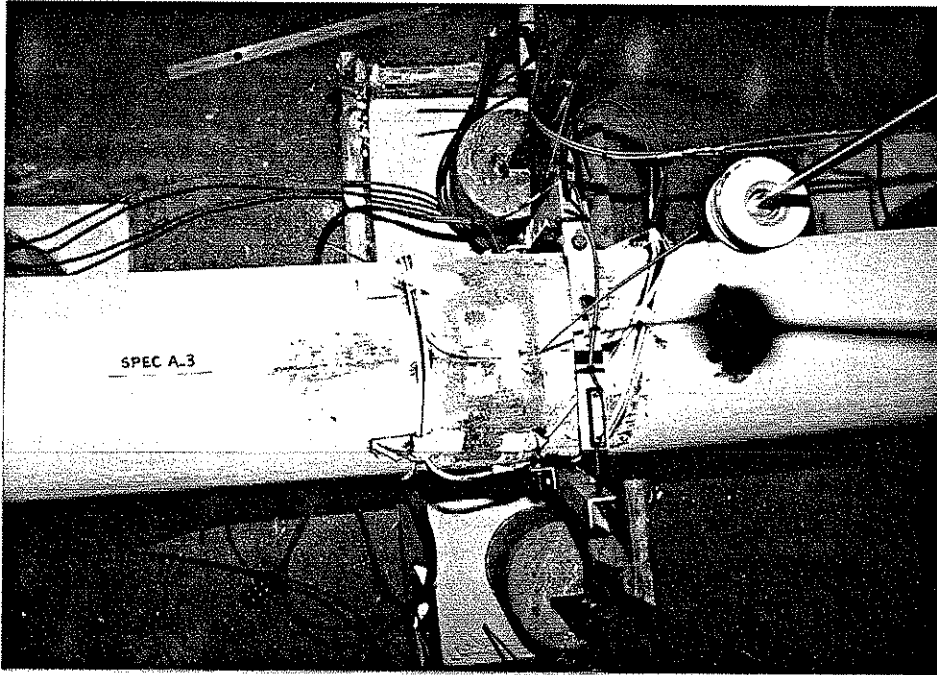
Figure 3.54. Initial Yielding of Specimen A3 Along the Compression Face.
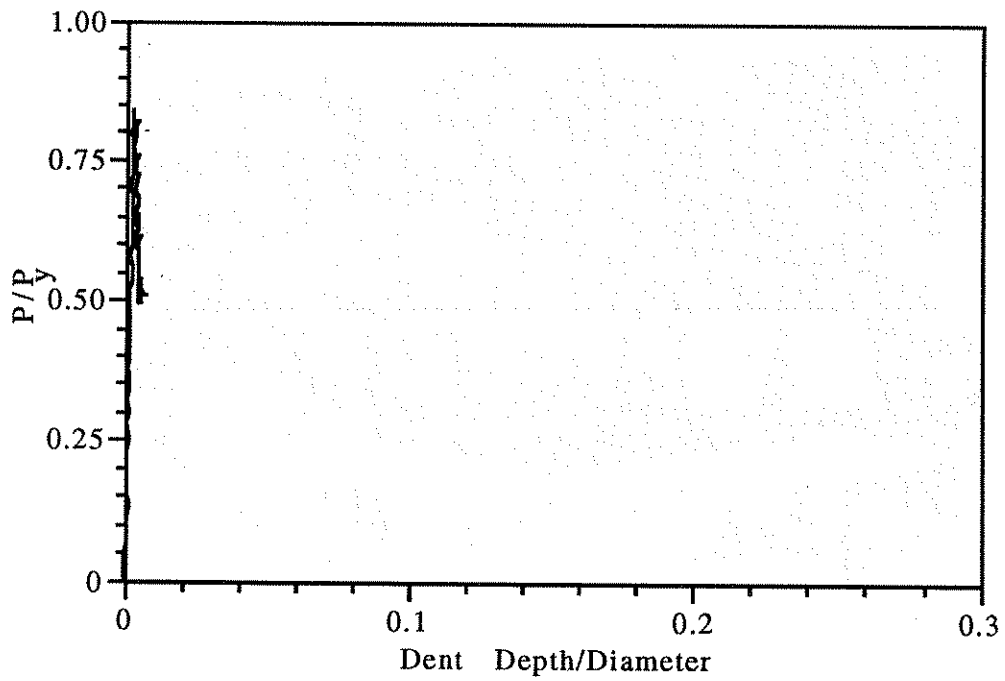
Figure 3.55. Axial Load - Dent Growth Relationship for Specimen A3.
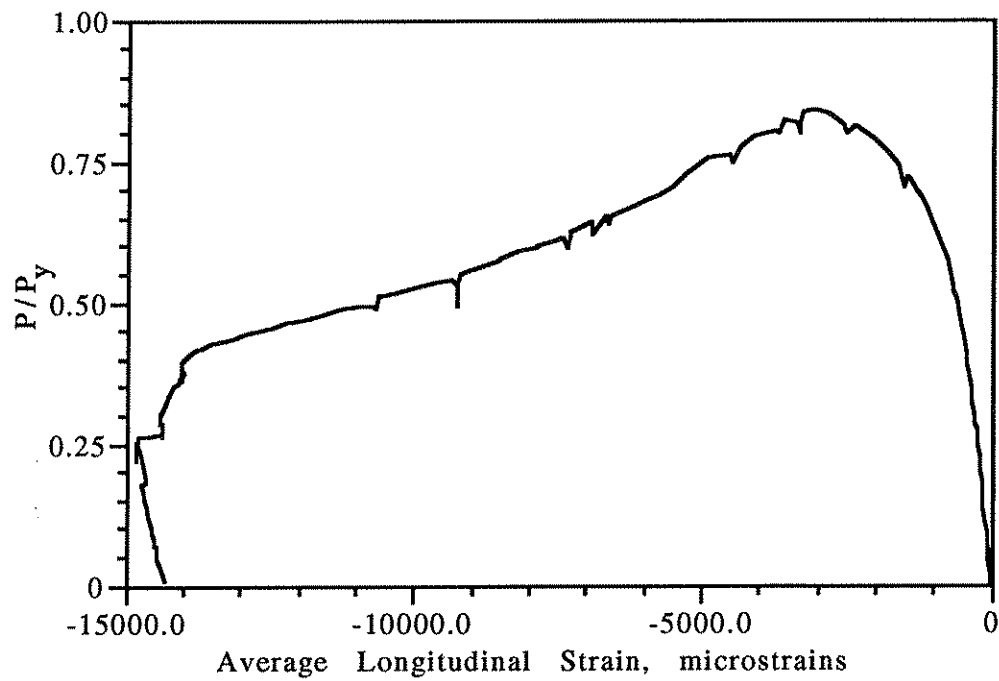
Figure 3.56. History of Longitudinal Strains in Dented Section of Specimen A3.
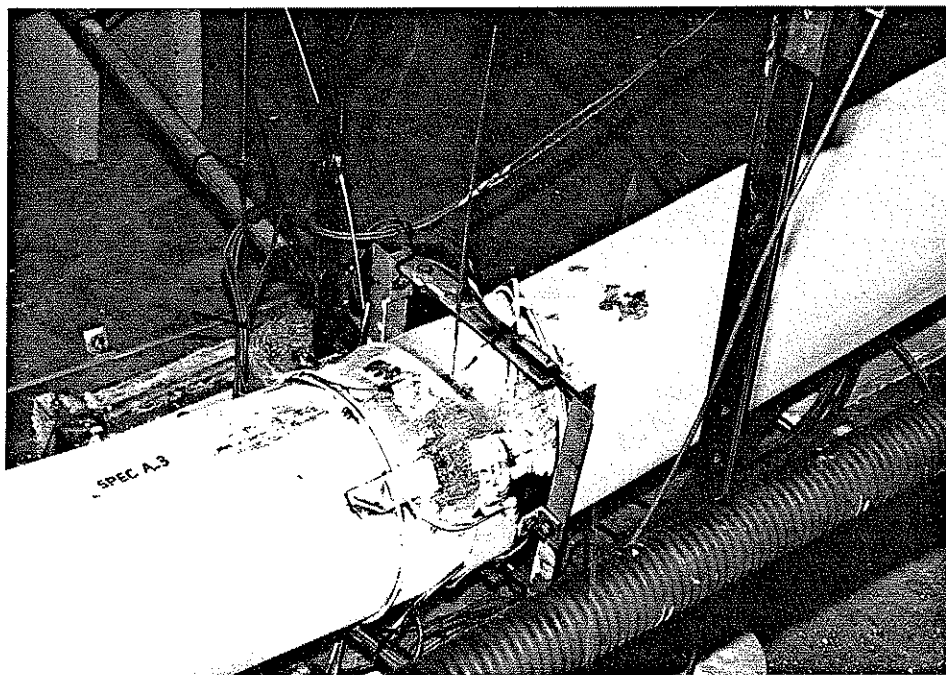
Figure 3.57. Formation of a Local Buckle on the Compression Face of Specimen A3 Following Yielding of the Steel Tube.
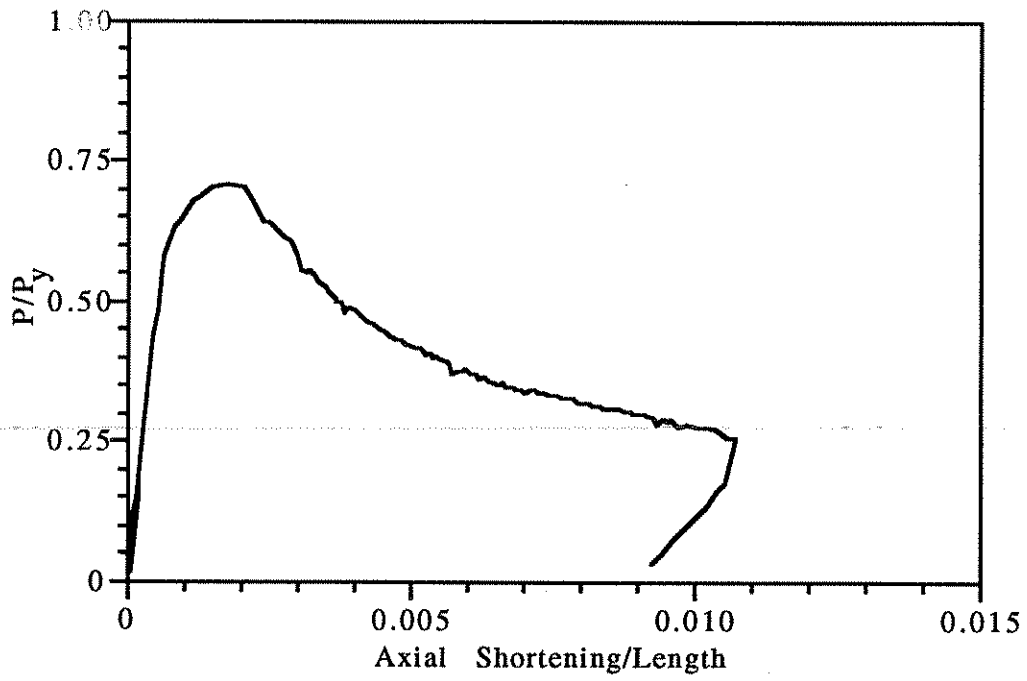
Figure 3.58.   Axial Load - End Shortening Relationship for Specimen B3.
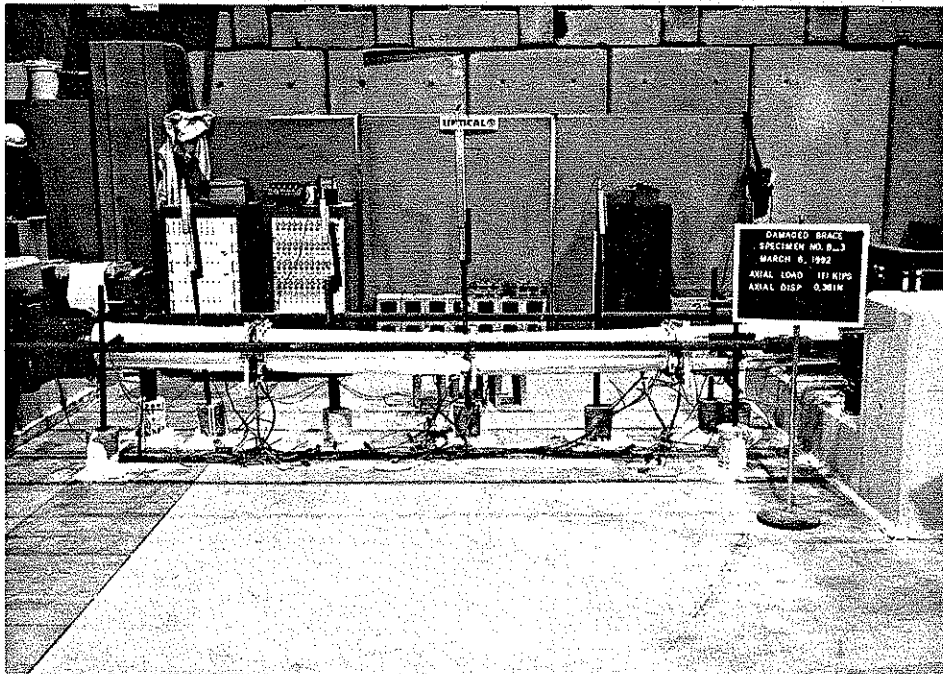
Figure 3.59.   View of Curvature Existing in Specimen B3 at its Peak Load P_{max}.
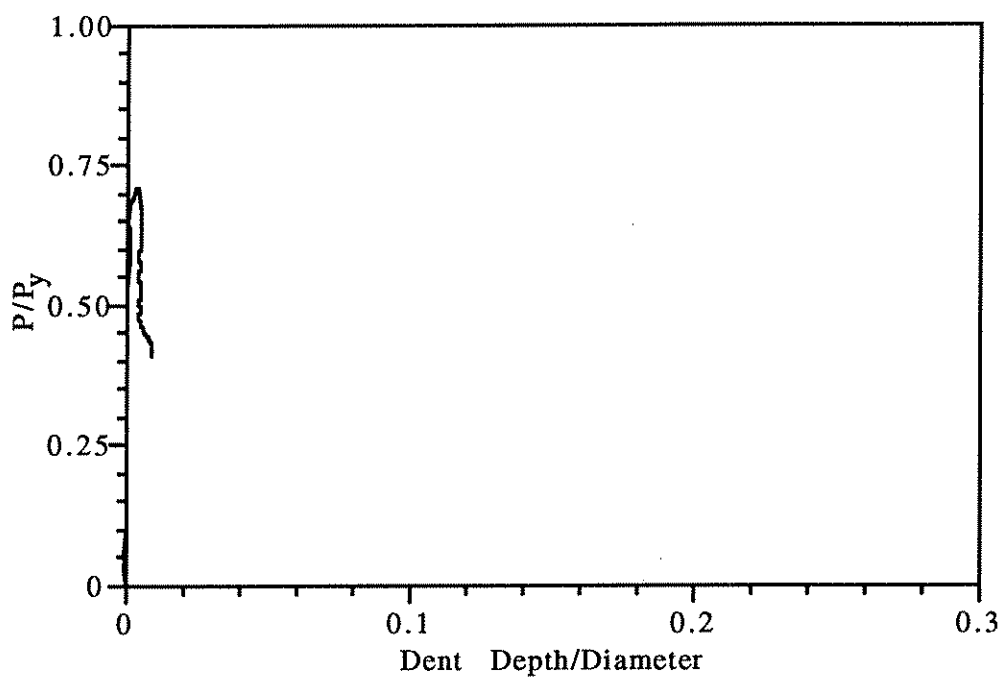
Figure 3.60. Axial Load - Dent Growth Relationship for Specimen B3.
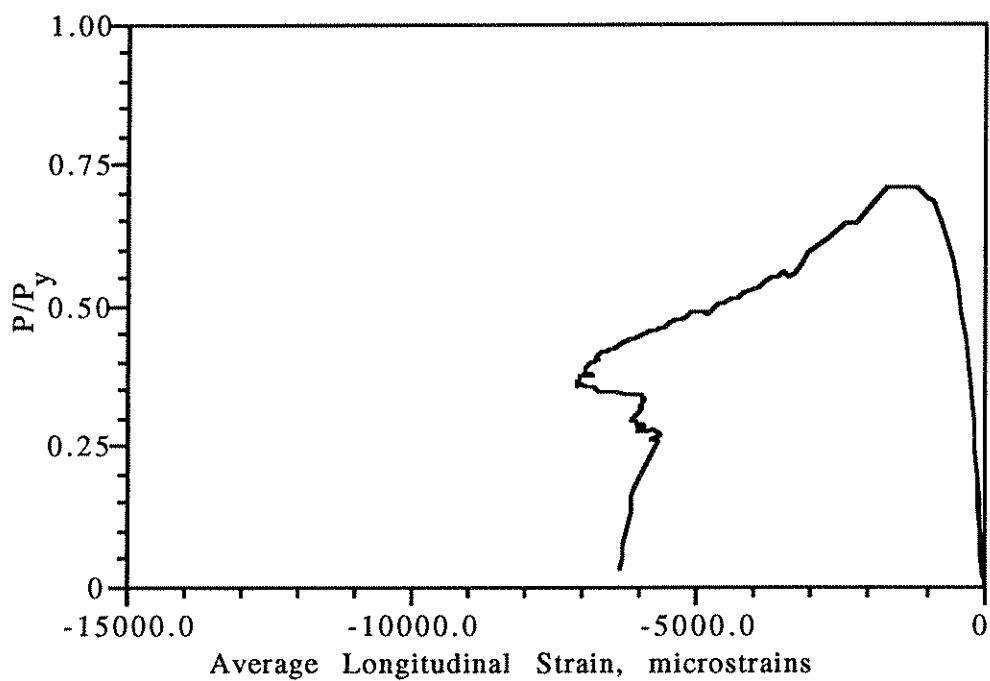
Figure 3.61. History of Longitudinal Strains in Dent for Specimen B3.
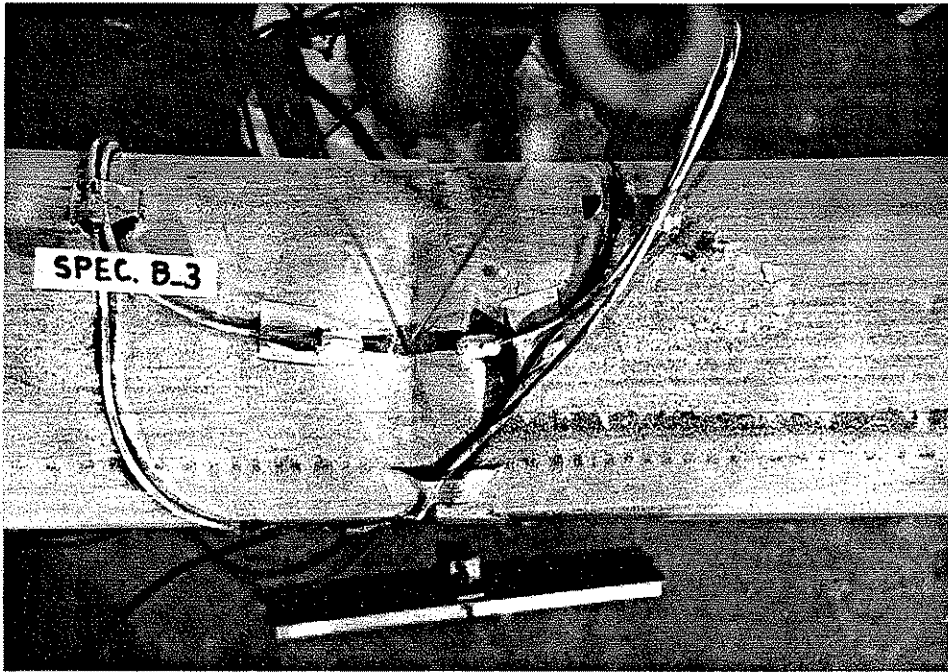
Figure 3.62. Initial yielding along compression face and centered about the dented section of Specimen B3.
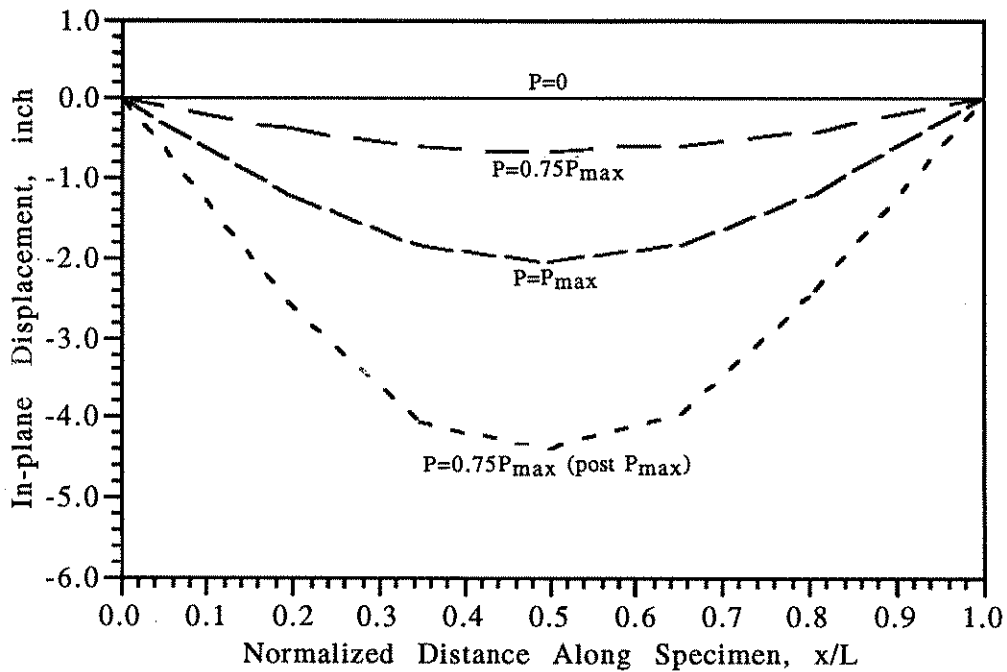
Figure 3.63. Measured In-plane Displacements of Specimen B3 at Various Stages of Loading.
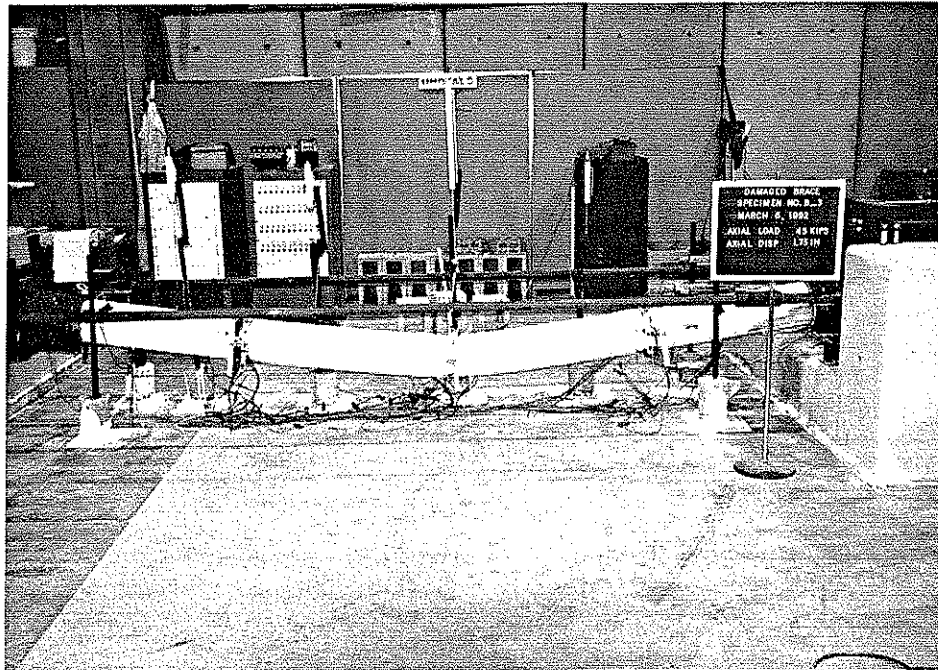
Figure 3.64.   View of Large Curvature Existing in Specimen B3 Following Test.
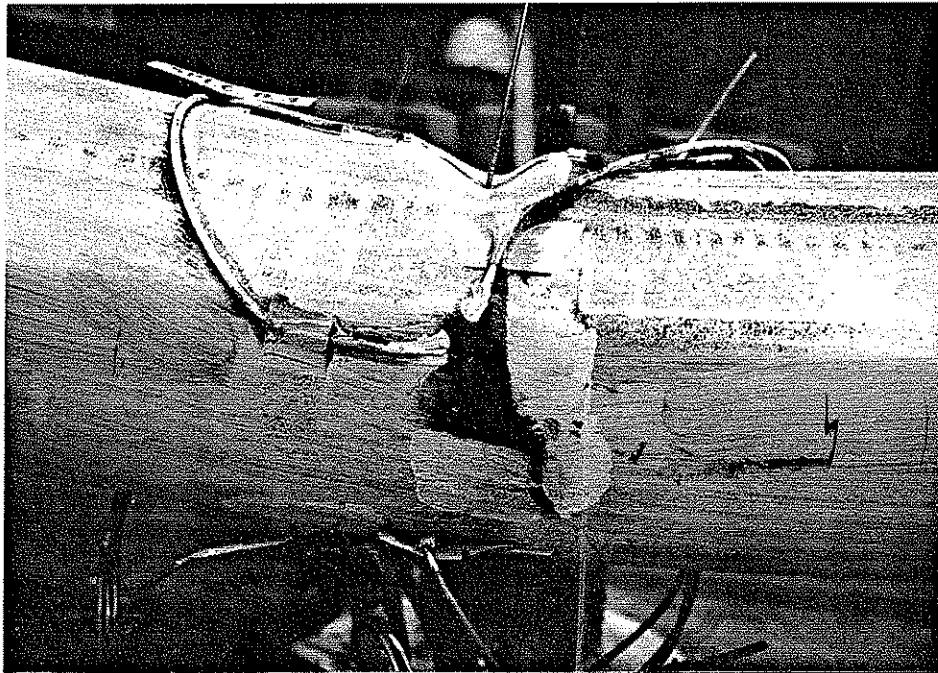
Figure 3.65.   Local Buckle on Compression Face of Specimen B3.   Arrest of Dent Growth is Noticeable.
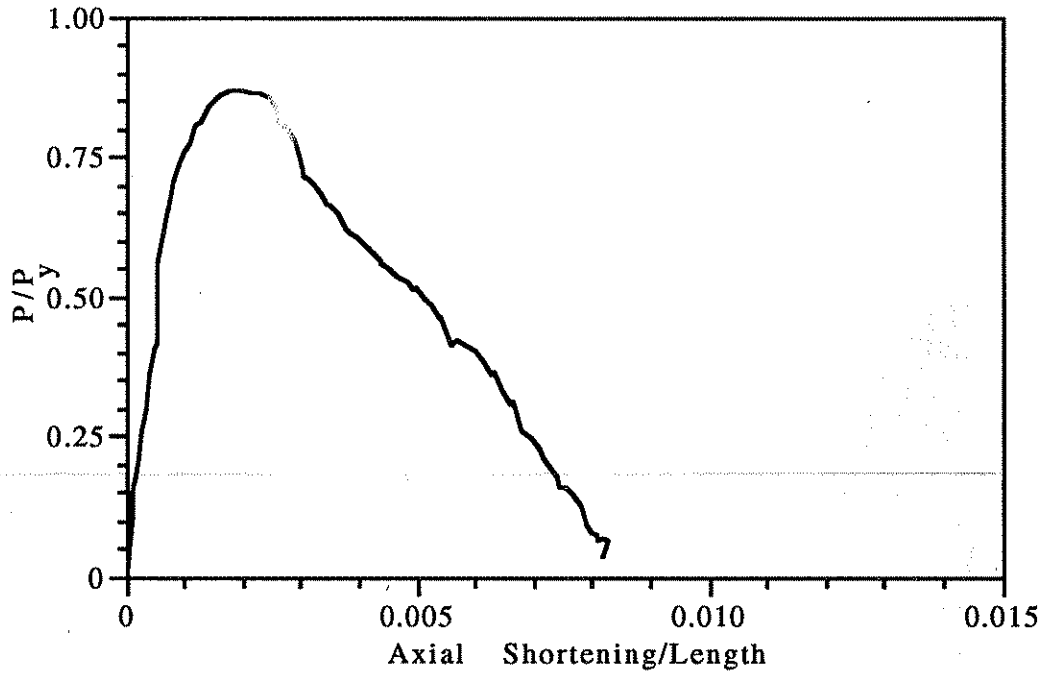
Figure 3.66.   Axial Load - End Shortening Relationship for Specimen C3.
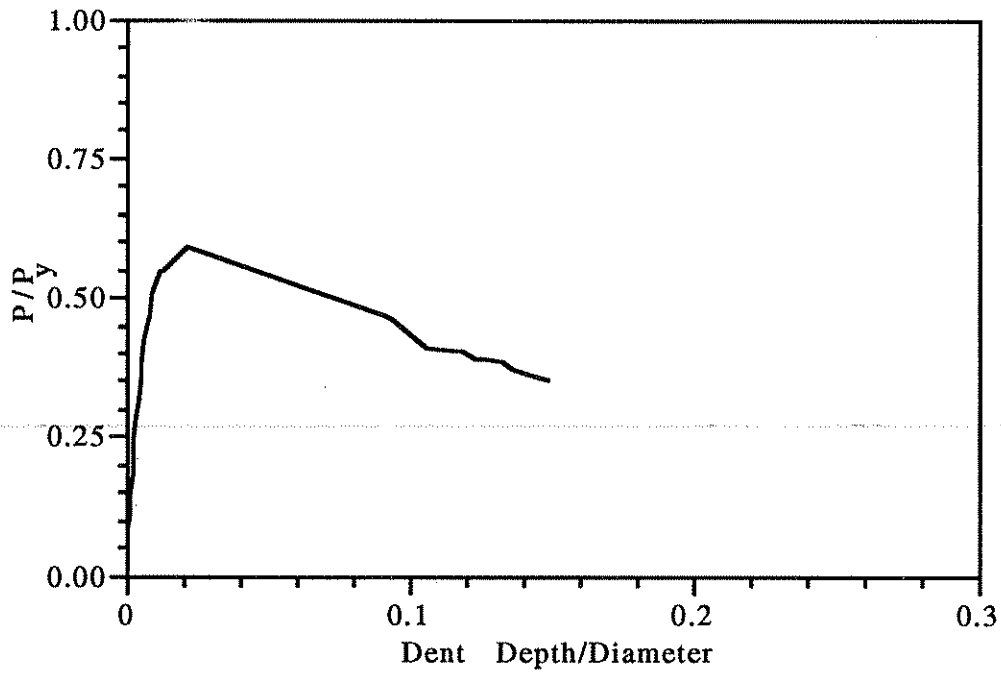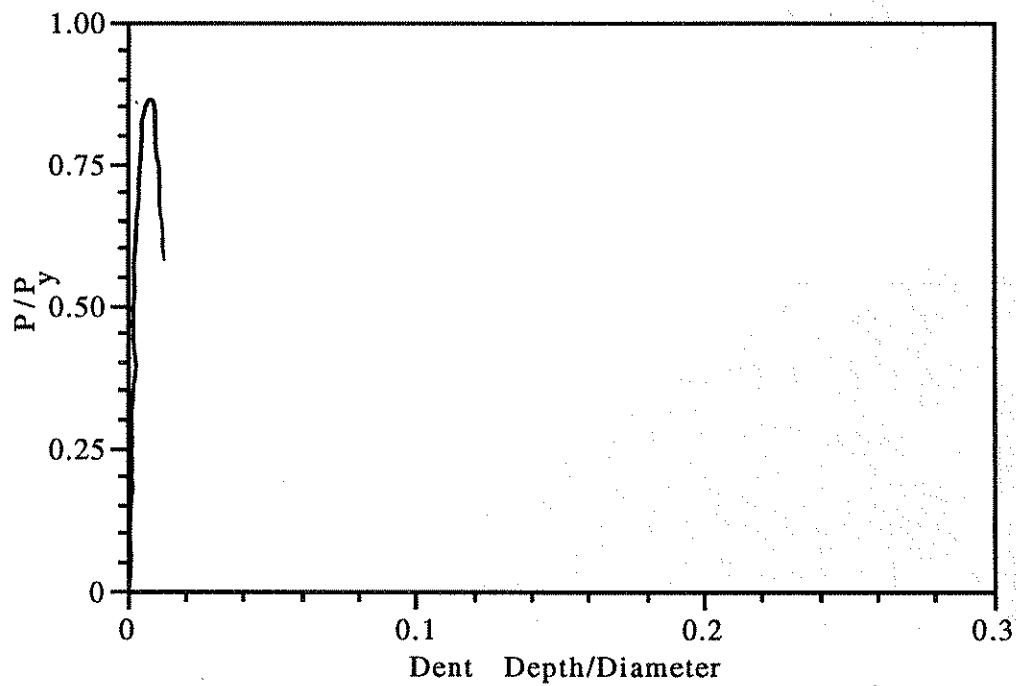

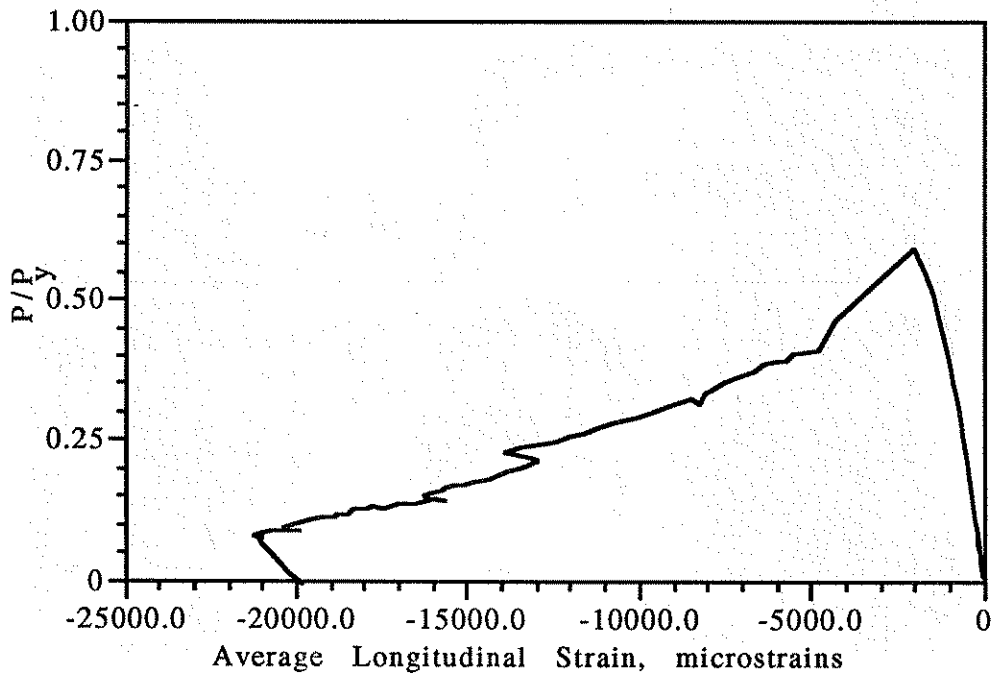Figure 3.67.   Axial Load - Dent Growth Relationship for Specimen C3.
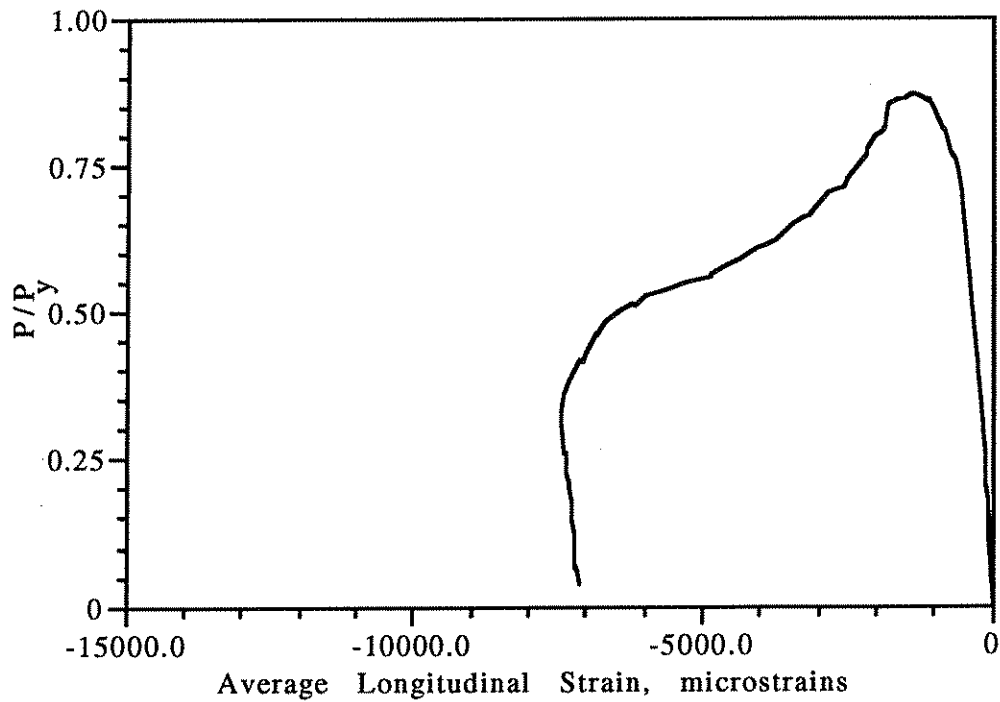
Figure 3.68. History of Longitudinal Strains in Dented Section of Specimen C3.
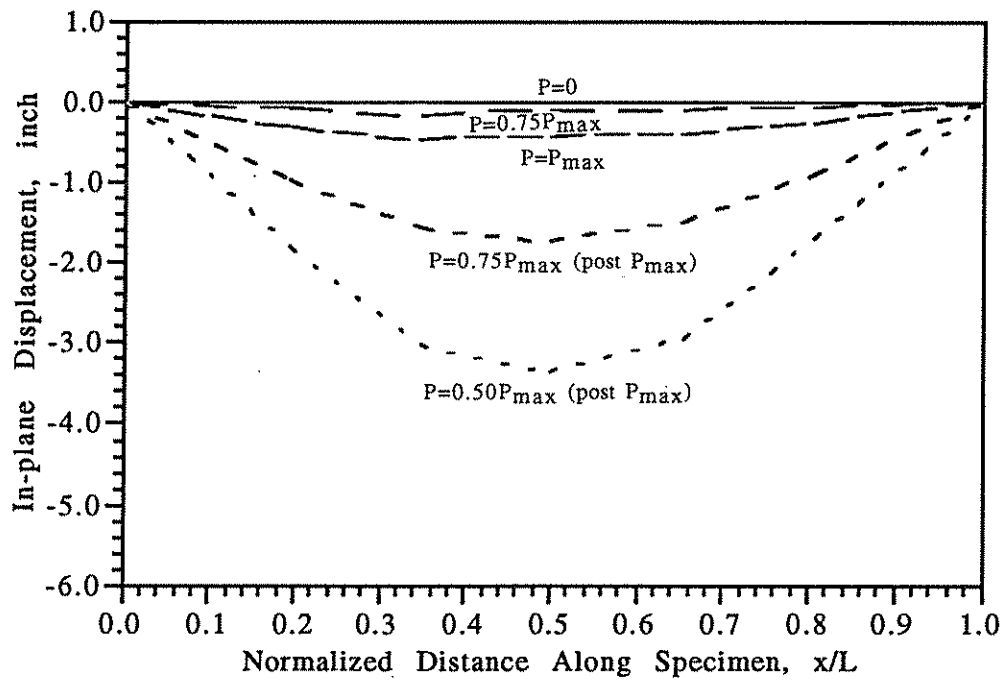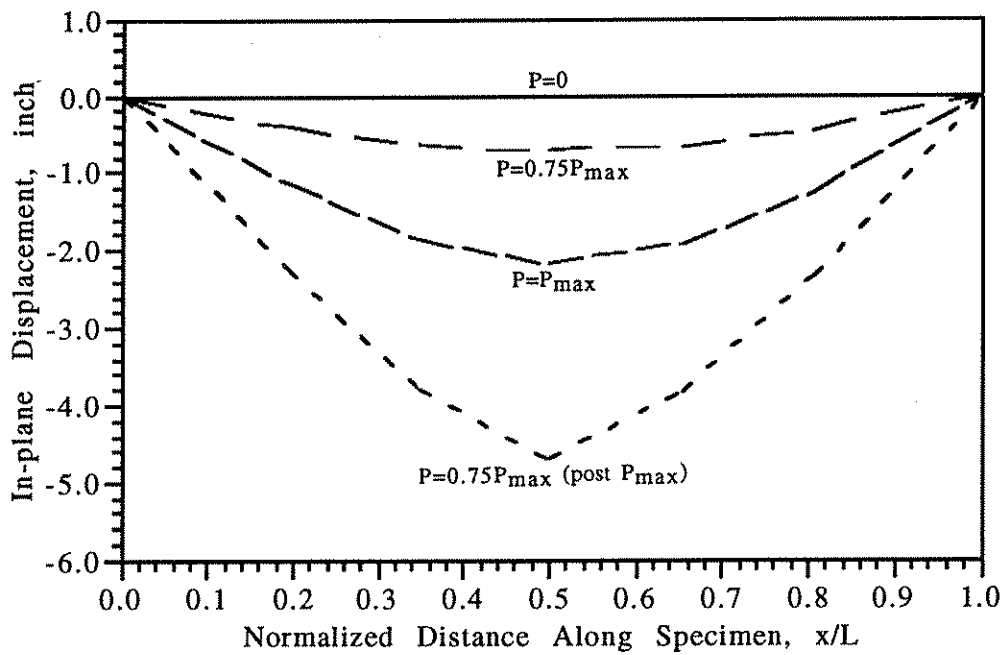

Figure 3.69. Measured In-plane Displacements of Specimen C3 at Various Stages of Loading.
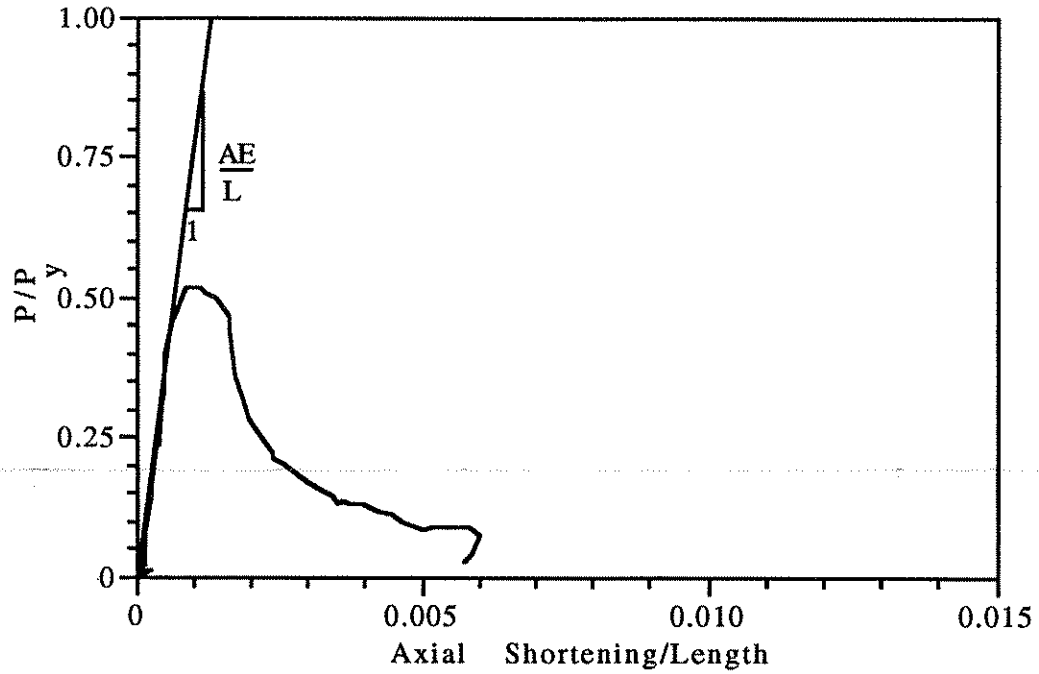
Figure 3.70. Axial Load - End Shortening Relationship for Specimen C4.
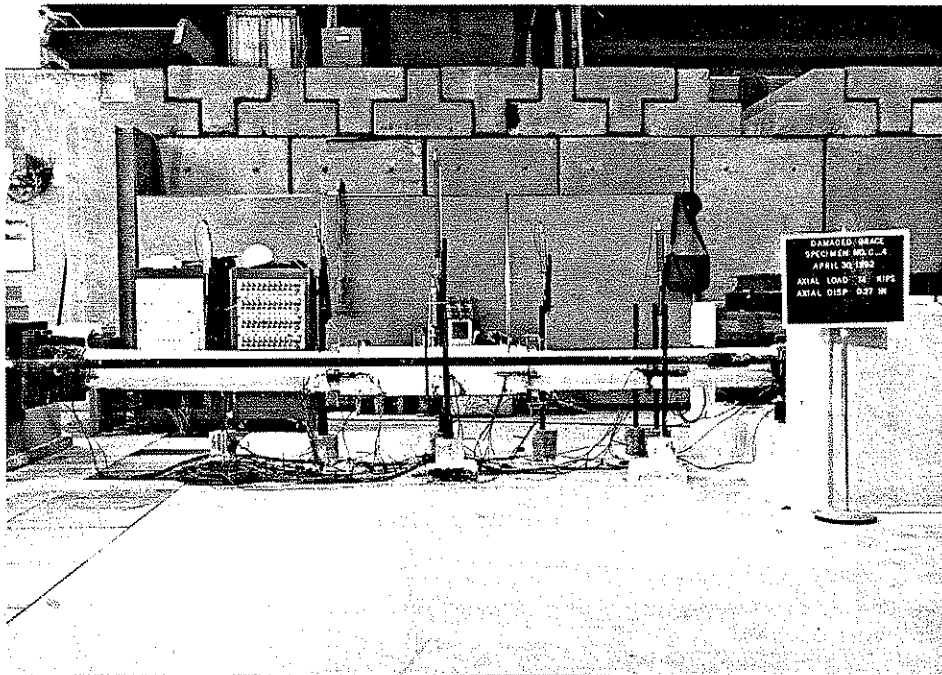
Figure 3.71. Curvature in Specimen C4 at Peak Load P_{max}.
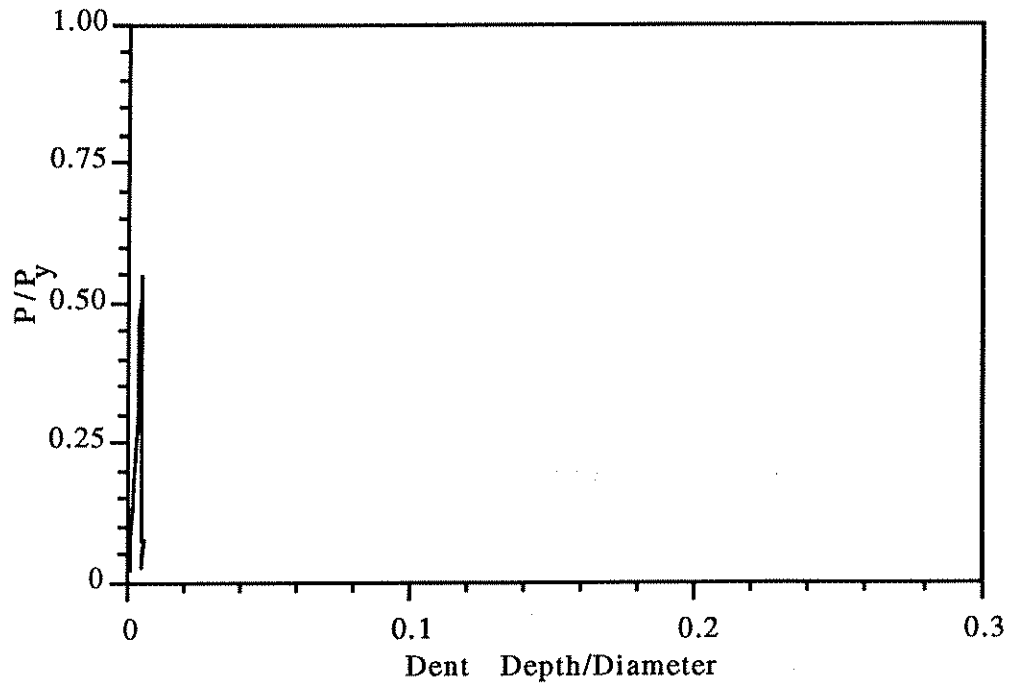
Figure 3.72. Axial Load - Dent Growth Relationship for Specimen C4.
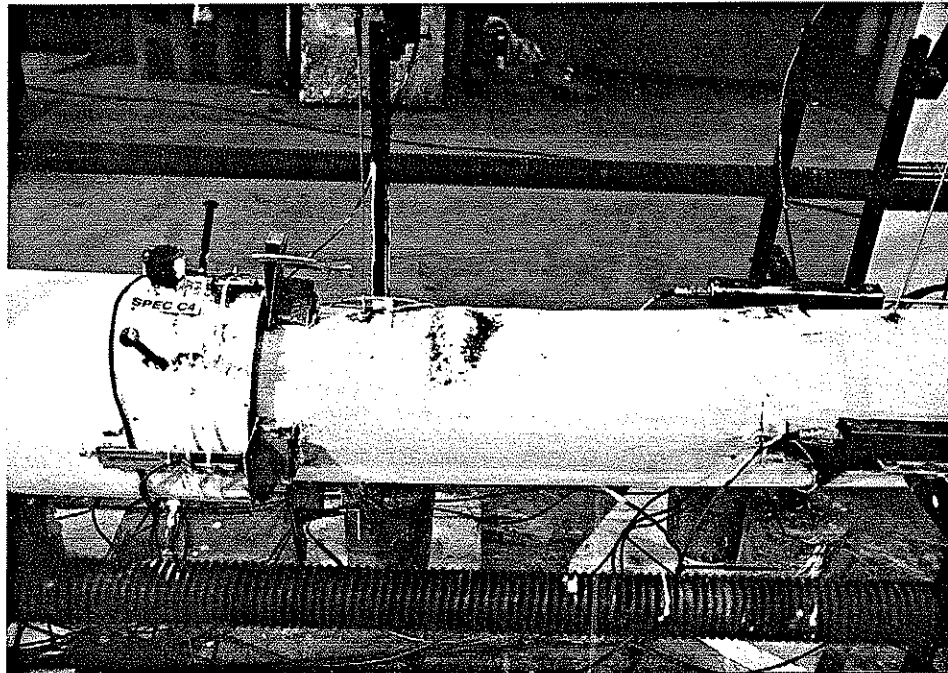
Figure 3.73. Formation of Local Buckle Outside Grouted Clamp Region of Specimen C4.

134
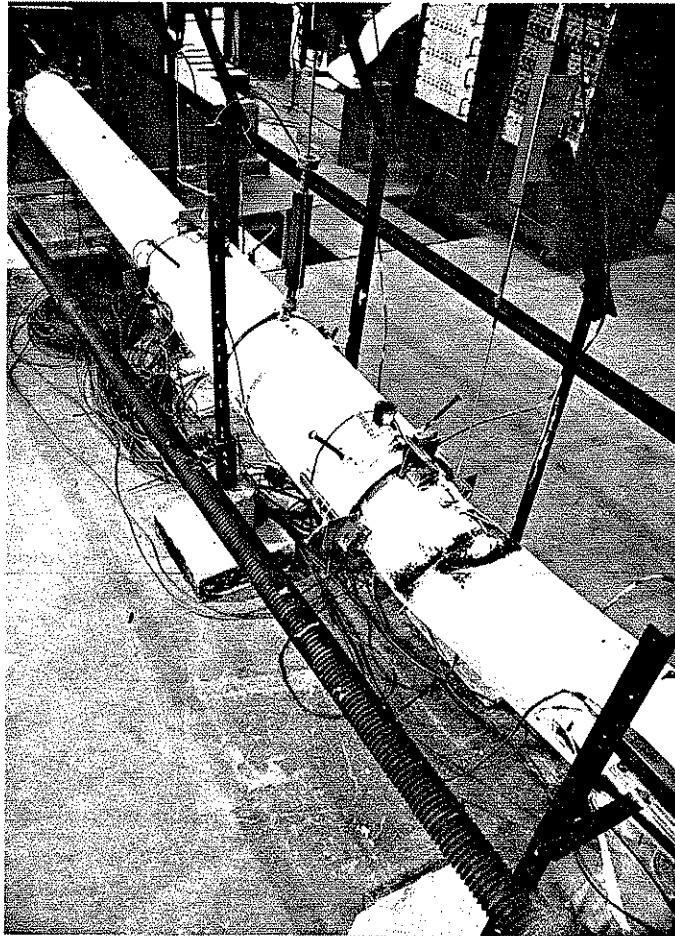
Figure 3.74. View of deteriorated buckled region outside of grouted clamp region.
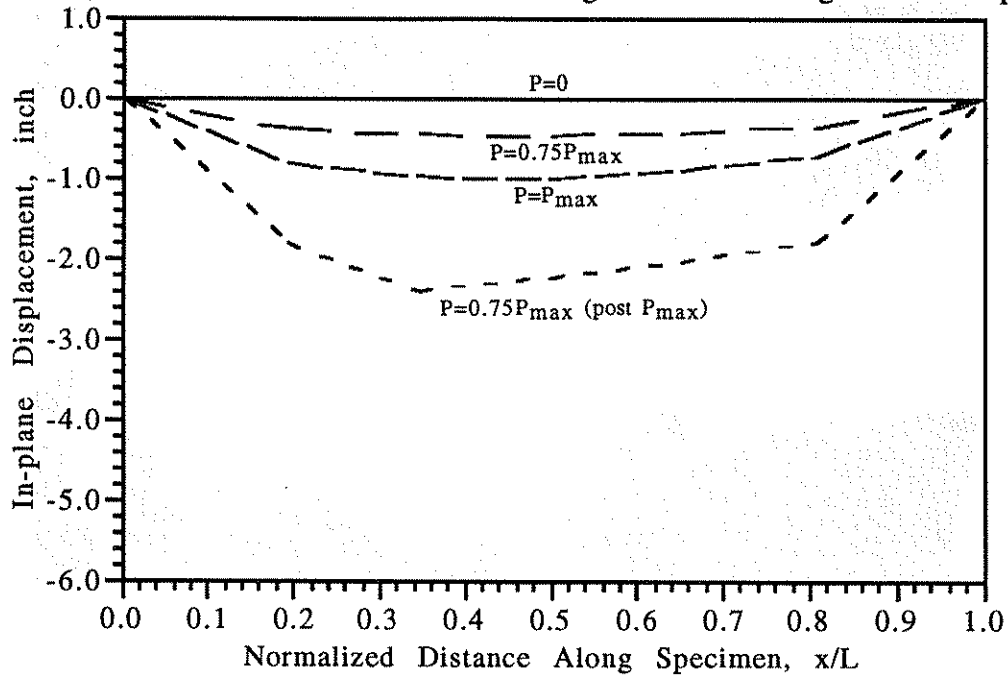
Figure 3.75. Measured In-plane Displacements of Specimen C4 at Various Stages of Loading.
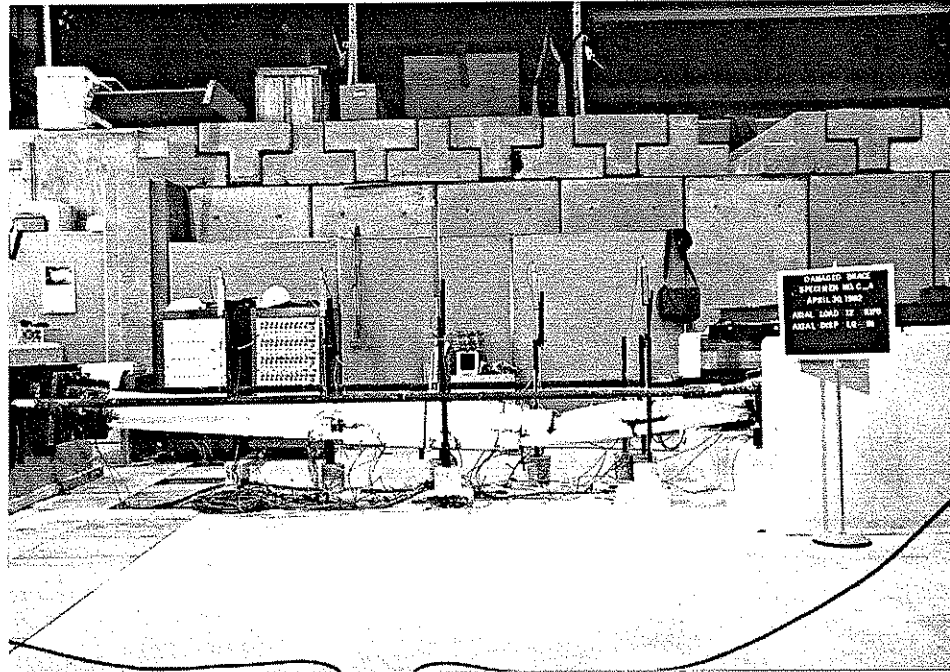
Figure 3.76. Curvature Existing in Specimen C4 Following Testing.
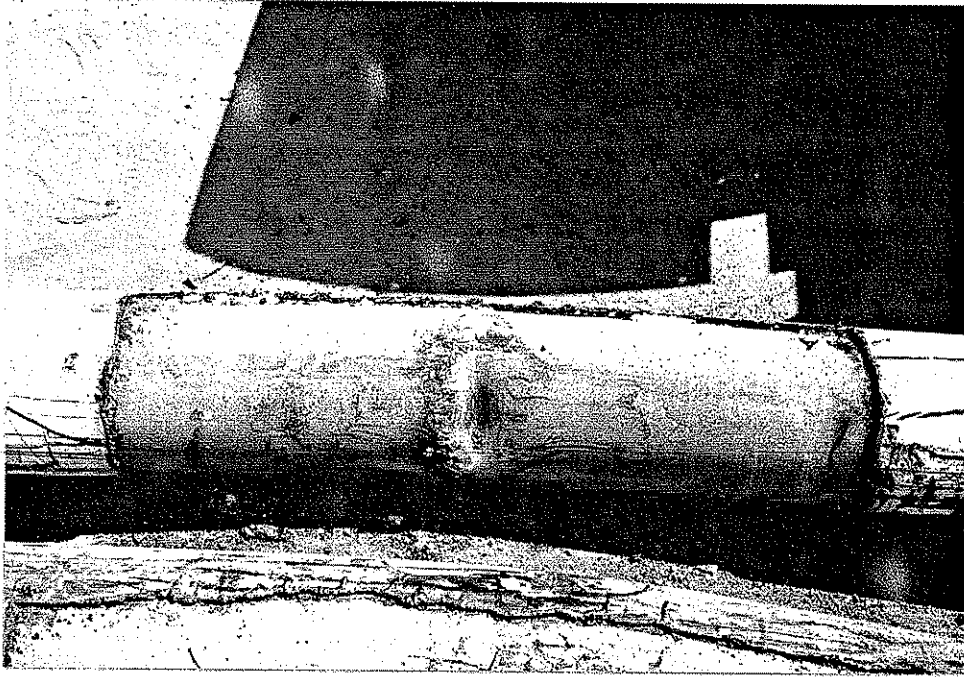
Figure 3.77.   Exposed Grout Beneath Dent, Specimen A3.
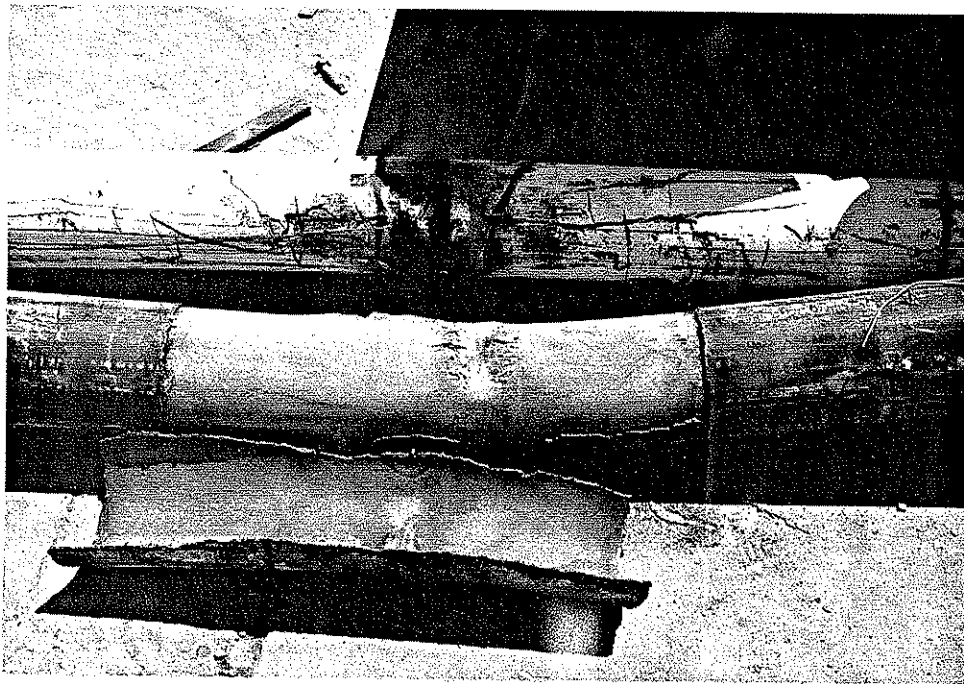
Figure 3.78.   Exposed Grout Beneath Dent, Specimen B3.

Figure 3.79.   Exposed Grout Beneath Dent, Specimen C3.

(a)
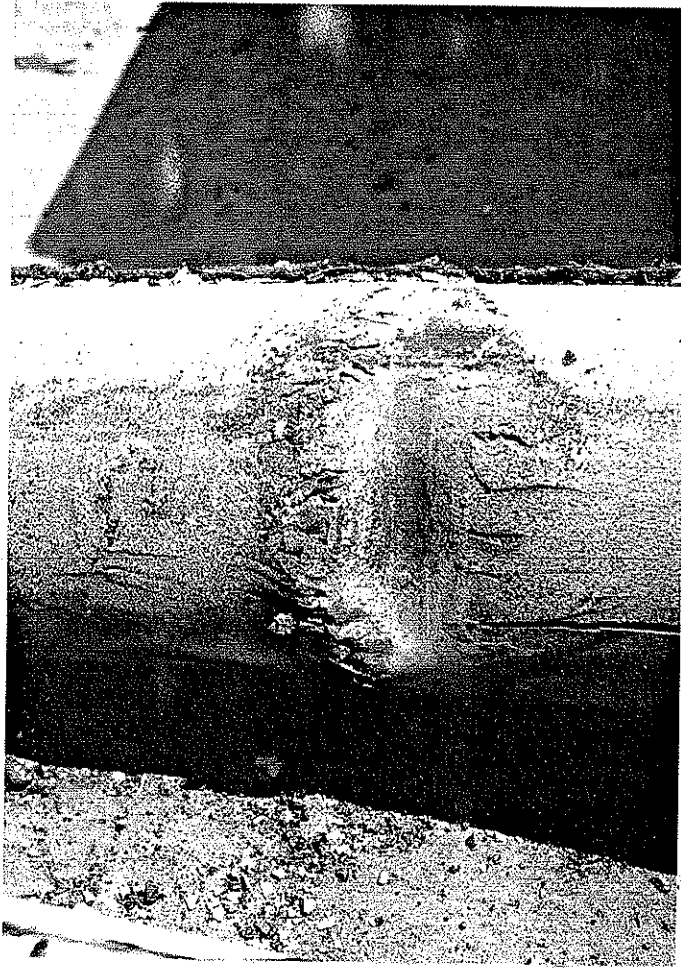
(b)

Figure 3.80.   Closeup View of Exposed Grout Beneath Dent (a) Before, and (b)
After Removing Loose Grout, Specimen A3.

CHAPTER 4

ANALYSIS OF EXPERIMENTAL RESULTS

4.1. General

In Chapter 3, observations of the experimental behavior of each of the 13 specimens were discussed. Based on these observations general remarks were made for each series of tests. In Chapter 4 a detailed evaluation of the experimental behavior will be performed by analyzing the measured data for each specimen. The peak axial load P_{max} of each of the specimens is summarized in Table 4.1. Results will be compared between series of tests to determine the effect of damage to the member on the ultimate load carrying capacity, the effect of combined axial load and bending on the capacity, and the increase in strength of damaged specimens produced by the grouted repairs. Moment-axial load interaction analyses are used to explain the failure of the non-repaired and repaired specimens. The experimental capacity of the undamaged as well as the damaged, unrepaired specimens is compared with the API design criteria discussed in Chapter 1 for undamaged beam-columns. Finally, comparisons are made with the theoretical formulations laid out in Chapter 1, to show the most effective methods for assessing the residual strength of dent-damaged bracing members. Preliminary nonlinear finite element analysis is also presented and discussed.

4.2. Moment-Axial Load Interaction

4.2.1. Non-repaired Specimens

During the testing of the damaged, non-repaired specimens, data was gathered which enabled the force path to be determined. For purposes of comparing the moment-axial interaction theory with the force path, the bending moment at the dented section (midspan) was computed for each increment of axial load. The value, which included second order effects, was determined from the following expression

$$M = P\left(e + e_d + \Delta\right) \qquad (4.1)$$

where M is the current moment at the dented section, P is the current axial load, e is the initial end eccentricity, e_d is the current eccentricity due to damage in the dented cross section, and Δ is the current displacement in the plane of bending.

For comparison with the member force path, plastic hinge theory was utilized to develop the moment-axial load interaction surface. The following relationship was used to determine the moment-axial load interaction surface [10], and is based on full plasticity of the dented section

$$\frac{M}{M_p} - \cos\left[\frac{\pi}{2}\left(\frac{P}{P_p} - \frac{F_{dp}}{P_p}\right) + \frac{\alpha}{2}\right] + \frac{1}{2}\sin\alpha - \frac{\pi F_{pd}}{2P_p}\left(\cos\alpha + \frac{2\eta}{D}\right) + 0 \qquad (4.2)$$

where P and M, are current axial load and bending moment, respectively. P_p and M_p are the fully plastic axial load and the fully plastic moment capacity, respectively, and are defined in the nomenclature section of this report. The parameters α, η, and F_{dp} are related to the dent depth and have been defined previously in Chapter 1 and are also located in the nomenclature section. Equation (4.2) is only valid for members with the dent located on the compressive side of the bending moment and the axial load in compression.

The interaction surface was computed using the static yield stress determined from the testing of the tensile coupons. Figures 4.1 through 4.5 show the force path of the non-repaired damaged members plotted against their moment-axial load interaction surfaces. Specimen C2 is not included because of a malfunctioning transducer that was measuring the displacement Δ.

All specimens, except Specimen C1, are shown to reach their peak load at or very near the interaction surface. The capacity of Specimens A1 and B1 (Figures 4.1 and 4.2) are predicted quite well by the moment-axial load interaction surface. Specimens A2 and B2 (Figures 4.4 and 4.5) fail near the interaction surface, but not exactly at it. Specimen C1 surpasses the interaction surface, which was noted in Chapter 3 to have incorporated an initial eccentricity when loaded into the test frame. Test data showed that the specimen resisted higher load due to this upward hogging at the dented

section, decreasing the compression in the dented section. Consequently, the force path extends outside the interaction surface.

The peak load attained by each specimen was indicated in Chapter 3 to occur just after yielding in the saddle of the dent, with a subsequent large inward growth in dent depth. Overall, the interaction surface analyses for the dented members based on Equation (4.2) with static yield stress provides a good estimate of the residual strength of dent damaged members subjected to concentric as well as eccentric axial loading.

4.2.2. Internal Grout Repaired Specimens

The success of the above analysis, suggested that it be carried forward to the internal grout repaired specimens to see if failure could be described by the moment-axial load interaction surface for the repaired members as well. A fiber analysis technique was employed to develop the interaction surface, using the measured material properties. An upper bound on the strength was established by assuming full composite action. This analysis involves describing the dented cross section and grout by several individual fibers, each with its own stress strain relationship. Assuming plane sections remain plane, the stress resultant for moment corresponding to a prescribed level of axial load is determined. In addition to computing moment, curvature was determined. The moment-curvature relationship for the grout repaired specimens for several levels of axial load are given in Appendix C. Specimen force paths were again determined by Equation (4.1) and plotted against the developed interaction surfaces. Figures 4.6, 4.7, and 4.8 show the resulting comparisons.

Figure 4.6 indicates that the peak load for Specimen A3 was attained near the intersection of the force path with the moment-axial load interaction surface. First yield of the steel material was observed to have occurred just prior to reaching the interaction surface. The formation of a local buckle in the tube wall is shown to occur at a point past the interaction surface and just before decrease of the force path.

Specimen B3 developed its maximum axial load just prior to reaching the interaction surface (see Figure 4.7). The points of first yielding and local buckle occur somewhat closer together than in Specimen A3, where the formation of the local outward buckle in the tube wall induced failure of the

specimen before reaching it full composite strength. The nominal diameter-to-thickness (D/t) ratio of Specimen A3 is 34.5, while that of Specimen B3 is 46. Both of these specimens have a theoretical local buckling stress equal to their yield stress.

Figure 4.8 shows that Specimen C3 (D/t = 64) was even more susceptible to local buckling of the tube wall, where local buckling formed almost immediately after yielding developed. The theoretical local buckling stress for this specimen is equivalent to 98% of the yield stress. The maximum load corresponds to a point which is further from the interaction surface than previous specimens. After reaching maximum capacity the specimen force path sharply diminishes due to the formation of a local buckle. Full composite strength was again not attained because of the formation of the local buckle in the tube wall.

In summary, the internal grout is effective in arresting the dent growth and subsequently increases the residual strength of the dented member. The internal grout repaired specimens of higher D/t ratio (Specimens B3 and C3) did not all exhibit full composite strength. The local buckling of the tube walls for the specimens of higher D/t ratio diminished the resistance of the member.

4.3. Comparisons of Experimental Results

4.3.1. Effect of Damage on Ultimate Capacity

The experimental testing of non-damaged members (Series 5) along with damaged members (Series 2) allowed for direct comparisons of ultimate capacities. Figures 4.9 through 4.11 show the decrease in the ultimate capacity of members due to the presence of a dent of depth 0.10D. All specimens in Series 2 and 5 were subjected to combined axial and bending loads through end eccentricity.

The damaged tube with a D/t ratio of 34.5 (Specimen A2) was found to have an ultimate capacity which was 41% less than corresponding nondamaged Specimen A5 (see Figure 4.9). The damaged tube with a D/t ratio of 46 (Specimen B2) showed a 50% reduction in capacity compared to corresponding nondamaged Specimen B5, and a 29% loss in capacity for dented

Specimen C2 (D/t=64) compared to corresponding nondamaged Specimen C5. These results are tabulated in column 3 of Table 4.2 and summarized in Figures 4.10 and 4.11.

4.3.2. Effect of Combined Axial and Bending Loads on Ultimate Capacity

Direct comparisons were also made between Series 1 and 2 of the experimental tests to measure the effect of the additional bending moment through an end eccentricity of 0.2D on dented members. Both series tested specimens with approximately the same dent depth located on the compression side of bending, where Series 1 involved concentric loading and Series 2 eccentric loading.

The effect of combined loading resulted in a 35% lower peak axial force resistance in Specimen A2 compared to corresponding concentrically loaded Specimen A1. Specimens A1 and A2 both had D/t=34.5. The axial load-shortening relationship for these specimens are compared with each other in Figures 4.12. For specimens with D/t=46 (concentrically loaded Specimen B1 and eccentrically loaded Specimen B2) the effect of end eccentricity resulted in a 47% reduction in peak axial load (see Figure 4.13). Finally, the comparison of the resistances of concentrically loaded Specimen C1 and eccentrically loaded Specimen C2, both with D/t=64, indicates that the peak axial load is reduced by 53% due to the end eccentricity (see Figure 4.14). A summary of the capacities of the above eccentrically loaded specimens relative to the concentrically loaded specimens is given in column 4 of Table 4.2.

4.3.3. Effectiveness of Grouted Repairs

4.3.3.1. Internal Grout Repair

The use of grouted repairs were intended to restore the residual strength of a damaged member back to its original non-damaged strength. The experimental tests conducted on the internal grout repaired specimens resulted in a dramatic increase in capacity over that of the damaged, non-repaired specimens.

Figure 4.15 shows a comparison of the axial load-axial shortening relationship for repaired Specimen A3 with non-repaired Specimen A2 and

non-damaged Specimen A5. Specimen A3 was repaired back to a strength of 23% greater than the original non-damaged strength of Specimen A5. This strength represents a large increase (110%) in strength over the non-repaired specimen. The grout compressive strength for this repair was determined to be 4375 psi. The increase in strength produced from this repair technique was observed in Chapter 3 to be due to the arrest of the dent growth normally associated with the non-repaired specimens, which allowed the steel tube of the repaired section to develop full yielding. Figure 4.16 shows the dent growth measured for the repaired and non-repaired specimens. It is very clear that the dent was effectively stabilized, which resulted in restoring the residual strength.

Specimen B3 was also effectively repaired by the application of internal grout. The axial load-shortening relationship for repaired Specimen B3 is compared with that of Specimens B2 (unrepaired) and B3 (non-damaged) in Figure 4.17. The repaired strength (Specimen B3) was 13% greater than the non-damaged axial load capacity of Specimen B5. A 125% increase in capacity was developed over that of the non-repaired specimen. The arrest of the dent growth is shown in Figure 4.18 to have also occurred in repaired Specimen B3. The compressive strength of the grout was determined to be 3885 psi for this repair.

The internal grout repair technique was also effective in rehabilitating the high D/t ratio members as well, Specimen C3 (D/t=64). Figure 4.19 illustrates an 88% and 165% increase in capacity over that of the non-damaged and non-repaired specimens, respectively. As with the other repaired specimens, the grout was able to resist the inward growth of the dent, as shown in Figure 4.20. The increase in restored strength in Specimen C3 relative to the undamaged strength is higher than in Specimens A3 and B3 due to the increased compressive grout strength of 6894 psi in Specimen C3. The capacity P_R of the internal grout repaired specimens, as well as a comparison with the damaged residual strength P_{max} and non-damaged strength P_o of corresponding specimens are summarized in Table 4.3.

4.3.3.2. Grouted Clamp Repair

The use of the grouted clamp on damaged Specimen C4 was also very effective in restoring the residual strength of the dented specimen. A

comparison of the load-shortening relationships for non-repaired Specimen C2, grouted clamp repaired Specimen C4, and non-damaged Specimen C5 is given in Figure 4.21. The grouted clamp repair increased the capacity 61% over that of the non-repaired specimen, and 14% over the original non-damaged specimen. This technique was also able to effectively stabilize the inward growth of the dent by confining the dented cross section from the resulting outward deformation (see Figure 4.22). The compressive strength of the grout utilized in this repair was 6103 psi.

4.4. Comparison of Experimental Results with Theory

4.4.1. Design Criteria for Non-damaged Members

4.4.1.1. API Allowable Stress Design (ASD)

The allowable stress design (ASD) format applies a factor of safety to the axial compressive stress and the flexural bending stress. For the members studied herein the computed factors of safety were approximately 1.83 and 1.67 for the axial and bending stress, respectively using the formulas outlined in Chapter 1. The computed allowable stress, f_a, for the cross section and the subsequent allowable load P_a are shown in Table 4.4 along with the safety factors (column 7) present when comparing specimen capacities (P_{max}) for Series 1 (damaged, non-repaired, direct axial load), Series 2 (damaged, non-repaired, combined loading), and Series 5 (non-damaged, combined loading), with the allowable design load (P_a). Results obtained for the non-damaged specimens (Specimens A5, B5, and C5), indicate a factor of safety from 1.63 to 2.28. A reduction in the factor of safety is evident when comparing the capacity of the damaged specimens to the allowable stress design load P_a. The comparisons show that little or no safety factor exists in a member with existing dent damage of the parameters studied in this report, where the values are from 1.05 (Specimen B2) to 1.43 (Specimen C1). Figure 4.23 graphically displays the reduction in safety for the damaged specimens (see API-ASD).

4.4.1.2. API Load and Resistance Factored Design (LRFD)

The load and resistance factored design method is a format for assessing ultimate capacities of members. The ultimate axial load carrying capacity of the section P_u was determined using the formulas outlined in Chapter 1. The resulting ultimate compressive stress, f_c, and ultimate compressive axial load, P_u are given in Table 4.4. The ratio of experimental axial load capacity (P_{max}) to P_u show a range in value from 0.61 to 1.34 (see column 8). For the eccentrically loaded specimens subjected to combined loading (Specimens A2, B2, C2), this ratio is 0.61 (Specimen B2) to 0.79 (Specimen A2) , while for concentrically loaded Specimens A1, B1, C1 the ratio is 0.78 (Specimen B1) to 0.92 (Specimen C1). The non-damaged specimens (A5, B5, and C5) have ratios of 0.97 (Specimen C5) to 1.34 (Specimen A5). The ratios for the damaged specimens fall below sufficient levels of safety, where the eccentrically loaded specimens in Series 2 have a lower level of safety. Figure 4.23 graphically displays the reductions in strength relative to the API-LRFD criteria for specimens with D/t ratios of 34.5, 46, and 64, respectively.

4.4.2. Analysis of Non-repaired Specimens

Presented herein are analysis of the dented specimens without repair. These analysis are based on the semi-empirical methods discussed in Chapter 1. Nonlinear finite element analyses are discussed in Appendix G.

4.4.2.1. Modified Ellinas Strength Equation

The modified Ellinas design equation of Chapter 1 (Equation 1.29) was utilized to predict the ultimate strength of the damaged, non-repaired specimens. The method had been shown in earlier experimental findings [23] to provide a lower bound for results (see Figure 1.4). The ultimate axial load capacity P_{th} computed from the ultimate stress of the damaged section (σ_{ud}) found in Equation (1.30) are compared against the maximum experimental axial loads (P_{max}) in column 3 of Table 4.5. Figure 4.24 plots the theoretical ultimate stress values (σ_{ud}), determined from Equation (1.30), against the experimental ultimate stress values. Included in this figure are the previous comparisons with experimental results [23]. In general, Table 4.5 and Figure

4.24 show that the modified Ellinas formula provides similar lower bounds for the strength prediction as in the comparisons with the previous experimental results. An exception in the comparison to present data is Specimen C1, which tends to fall outside the cluster of data. This phenomena is associated with the accidental eccentricity and upward displacement that gave Specimen C1 additional strength.

4.4.2.2. UC-DENT Analysis

The quadratic equation implemented in UC-DENT (Equation 1.44) gives the load at first yield of the dented section of the damaged member for dented members with initial imperfection δ_0 and end eccentricity e. The program was run to assess the strength of the test specimens. Input included the existing end eccentricity of the applied axial load, measured specimen imperfections, material yield stress, and geometric properties. Numerical values showing the exactness of the method are listed in Table 4.5. The predicted results, in terms of ultimate stress σ_{ud}, are compared with the stress σ_{exp} corresponding to the specimen peak axial load in the scatter diagram of Figure 4.25. The method is shown to provide a close lower bound for the residual strength. A knock-down factor of $\phi = 0.88$ [10] was used for Specimen C5 to account for interaction of the residual strength with local buckling. Specimen C1 again falls outside the main distribution of the data for the rest of the specimens, due to the accidental eccentricity introduced into Specimen C1 during installation into the test frame.

4.4.2.3. DENTA Analysis

DENTA includes three stages of analysis: loading to first yield; inelastic response to ultimate load; and a post ultimate load and displacement relationship. The model restricts any increase in the dent growth until after reaching the ultimate load. The DENTA model predicts an increase in strength beyond first yield of the dented cross section, but experimental findings of this study show only a small increase in axial load beyond initial yield of the specimen in the dent saddle. The experimental results also show that there exists a growth in dent depth prior to developing the peak load. Despite these contradictions, results from DENTA correlate extremely well with experimental results, as shown in Figures 4.26 through 4.31. Excluding Specimen C1, the

ultimate load capacity of the specimens is well predicted by DENTA, as well as reasonable post ultimate behavior. As noted previously, Specimen C1 has a higher resistance because of the initial upward displacement before failure. Numerical comparisons between DENTA and experimental axial load capacity are given in column 5 of Table 4.5, where it is indicated that the ultimate experimental load capacity is within a range of 0.93 to 0.99 times the capacity predicted by DENTA. The experimental ultimate load capacity for Specimen C1 is within 1.29 times that predicted by DENTA.

4.4.2.4. Damaged Member Unity Checks

4.4.2.4.1. Strength Check

Strength checks for the failure of the dented section of a damaged member were discussed in Chapter 1 (Equation 1.47). These checks incorporate LRFD criteria along with reduced section properties resulting from the damage. Table 4.5 lists the values for the unity checks for the non-repaired damaged specimens. The strength unity checks range in value from 0.78 to 1.16.

4.4.2.4.2. Stability Check

Stability checks incorporate the column buckling effects as stated in Chapter 1 (Equation 1.56). Table 4.5 shows that the stability unity checks range from 0.90 to 1.30 for the damaged, non-repaired specimen tests. The stability unity checks result in a larger value, and hence control the load carrying capacity associated with the residual strength of each damaged specimen. In column 8 of Table 4.5 the axial load based on the stability unity check P_{uc} is compared to the peak axial load P_{max} for each specimen. The average value of the stability unity check for all damaged specimens is 1.04. If one excludes Specimen C1, which had higher resistance due to the initial upward displacement, the average of the stability unity checks is 0.99. Overall, the unity check appears to provide a good prediction of the residual strength of the damaged specimens.

4.4.3.   Analysis of Repaired Specimens

The strength of the internally grout repaired specimens (A3, B3, and C3) were compared to the predicted strength using Parsanejad's formulation. Table 4.5, column 9, summarizes the ratio of peak experimental axial load (P_{max}) to theoretical ultimate axial load capacity (P_{th}). P_{th} was computed from the ultimate stress σ_{ud} of the repaired member using Equation (1.26). The results for the present experiments are compared with previous small scale experiments from Reference 30 in Figure 4.32. Specimen A3 tends to fall outside the other present and previous range of data. The repaired strength of Specimens B3 and C3 are well estimated by Parsanejad's method and fall within the deviation between the previous experimental results and their theoretical predictions.

150

(This page intentionally blank)

Table 4.1. - Peak Axial Loads (P$_{max}$) Developed in Specimens.

Spec. No.	Exp. P$_{max}$ (kips)
A1	141
B1	99
C1	97
A2	91
B2	52
C2	46
A3	191
B3	117
C3	122
C4	74
A5	155
B5	104
C5	65

152

Table 4.2. - Comparison of Damaged Residual Strength (P_{max}) with Non-damaged (P_o) and Concentrically Loaded (P_{axial}) Specimen Strengths.

Spec. No.	P_{max}	$\dfrac{P_{max}}{P_o}$	$\dfrac{P_{max}}{P_{axial}}$
A2	91	0.59	0.65
B2	52	0.50	0.53
C2	46	0.71	0.47

Table 4.3. - Comparison of Grout Repaired Strength (P_R) with Non-repaired (P_{max}) and Non-damaged (P_o) Specimen Strengths.

Spec. No.	P_R	$\dfrac{P_R}{P_{max}}$	$\dfrac{P_R}{P_o}$
A3	191	2.10	1.23
B3	117	2.25	1.13
C3	122	2.65	1.88
C4	74	1.61	1.14

Table 4.4. - Experimental Peak Loads and Comparisons with Design Criteria for Damaged, Non-repaired and Non-damaged Specimens.

Spec. No.	Exp. P_{max} (kips)	API ASD		API LRFD		$\dfrac{P_{max}}{P_a}$	$\dfrac{P_{max}}{P_u}$
		f_a (ksi)	P_a (kips)	f_c (ksi)	P_u (kips)		
A1	141	17.3	113	26.8	174	1.25	0.81
B1	99	16.6	82	25.8	127	1.21	0.78
C1	97	18.9	68	29.6	106	1.43	0.92
A2	91	10.5	68	17.7	115	1.34	0.79
B2	52	10.0	49	17.4	86	1.05	0.61
C2	46	11.0	40	18.7	67	1.15	0.69
A5	155	10.5	68	17.7	115	2.28	1.34
B5	104	10.0	49	17.4	86	2.10	1.21
C5	65	11.0	40	18.7	67	1.63	0.97

154

Table 4.5. Analytical Comparisons for the Residual Strength of Damaged, Non-Repaired and Repaired Specimens.

Spec. No.	Exp. P_{max} (kips)	Mod'fd Ellinas $\dfrac{P_{max}}{P_{th}}$	UC-DENT $\dfrac{P_{max}}{P_{UC\text{-}DENT}}$	DENTA $\dfrac{P_{max}}{P_{DENTA}}$	Unity Check Strength	Unity Check Stability	Unity Check $\dfrac{P_{max}}{P_{uc}}$	Parsanejad $\dfrac{P_{max}}{P_{th}}$
A1	141	1.47	0.84	0.99	0.82	0.93	0.93	-
B1	99	1.41	0.82	0.95	0.87	0.96	0.96	-
C1	97	1.77	0.70	1.29	1.16	1.30	1.30	-
A2	91	1.59	0.84	0.96	0.91	1.04	1.04	-
B2	52	1.26	0.96	0.93	0.78	0.90	0.90	-
C2	46	1.40	0.89	0.93	0.93	1.12	1.12	-
A5	155	-	0.80	-	-	-	-	1.43
B5	104	-	0.87	-	-	-	-	1.17
C5	65	-	0.96	-	-	-	-	1.12
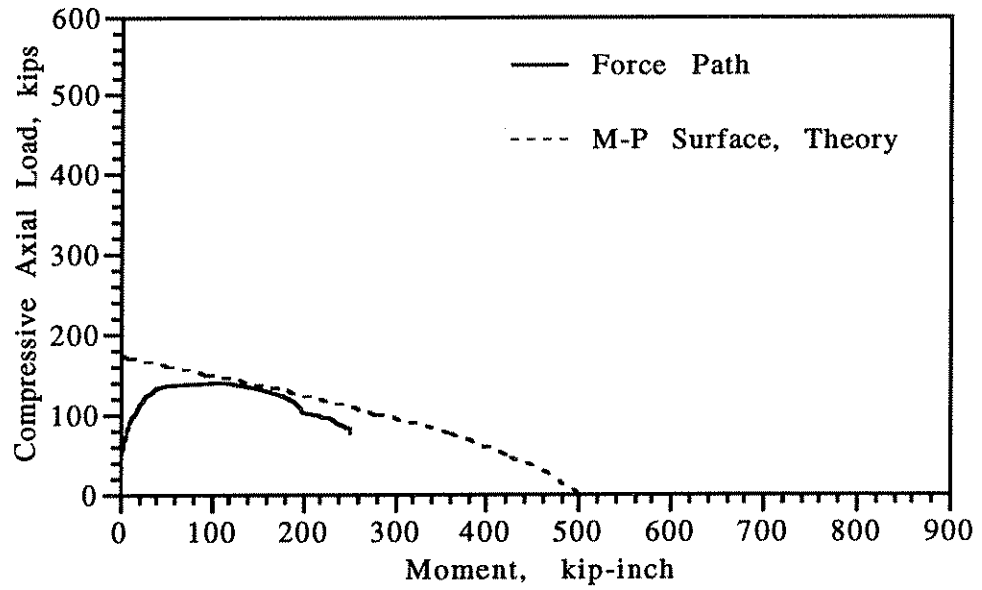
Figure 4.1. Moment-Axial Load Interaction, Specimen A1.
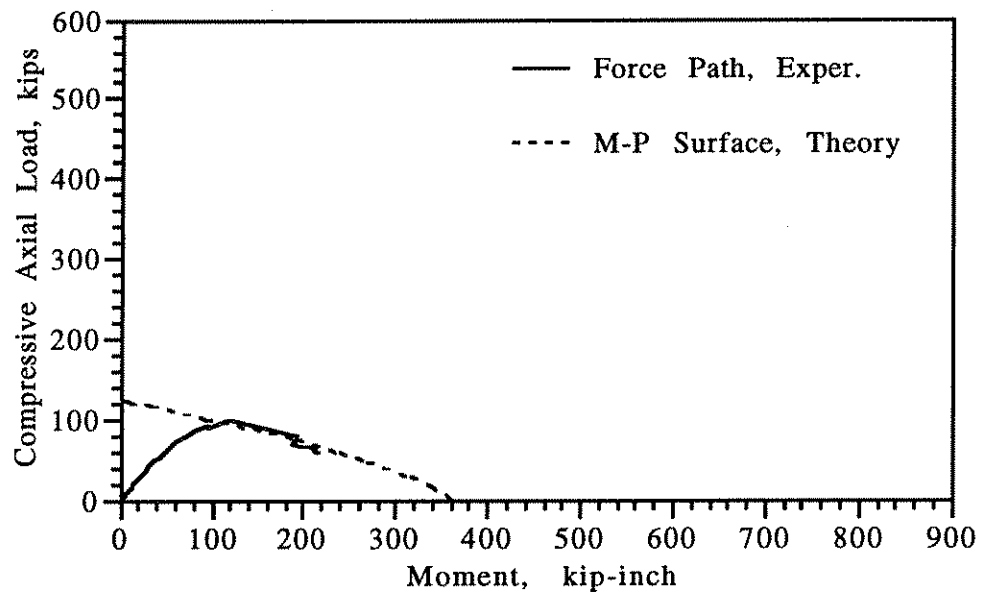
Figure 4.2. Moment-Axial Load Interaction, Specimen B1.
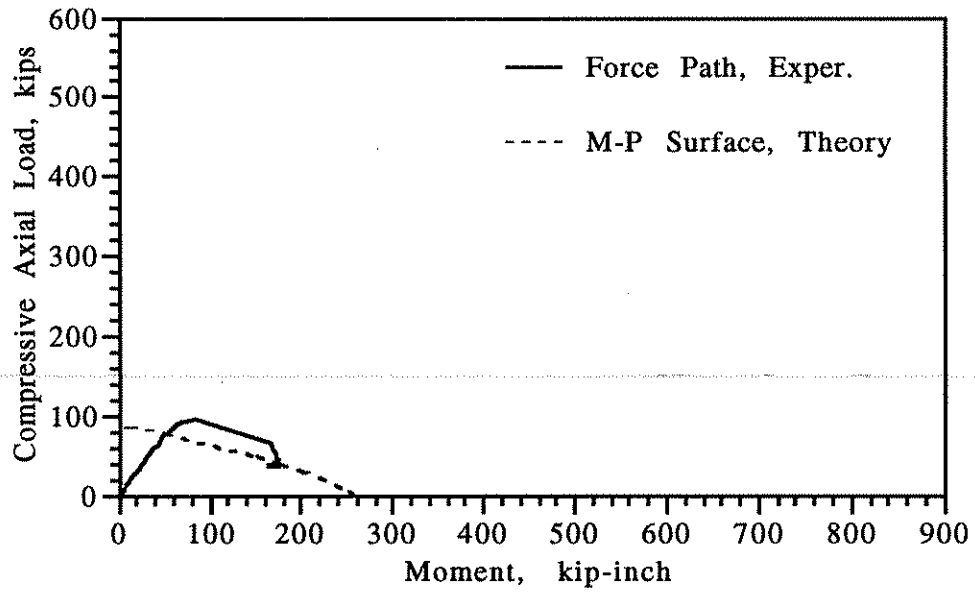
Figure 4.3.   Moment-Axial Load Interaction, Specimen C1.
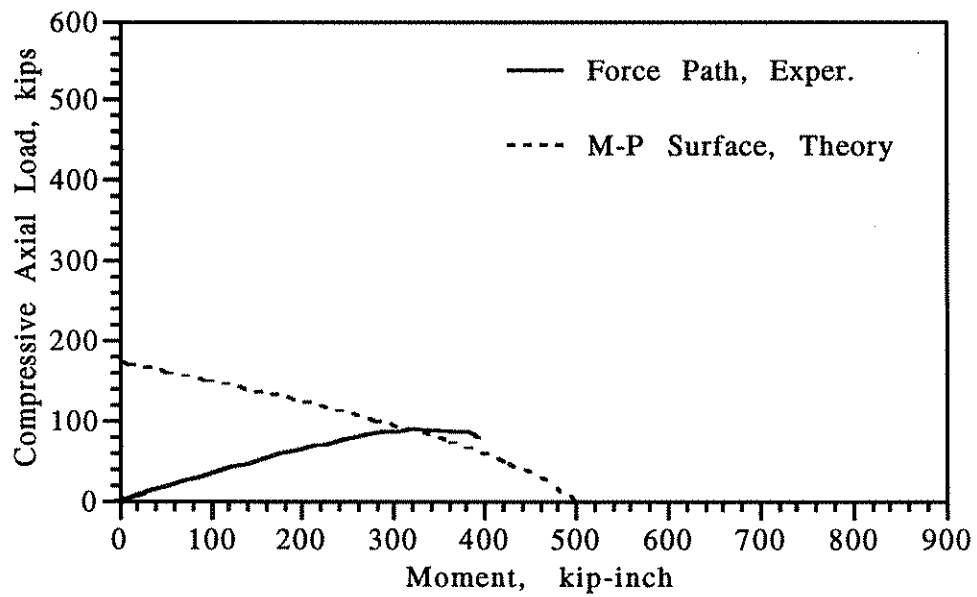
Figure 4.4.   Moment-Axial Load Interaction, Specimen A2.
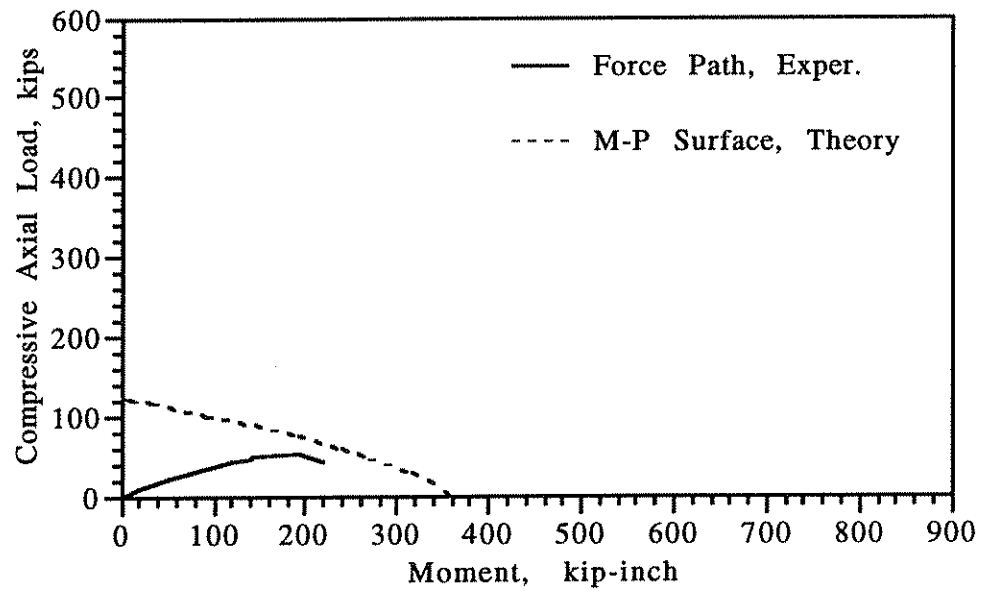
Figure 4.5. Moment-Axial Load Interaction, Specimen B2.
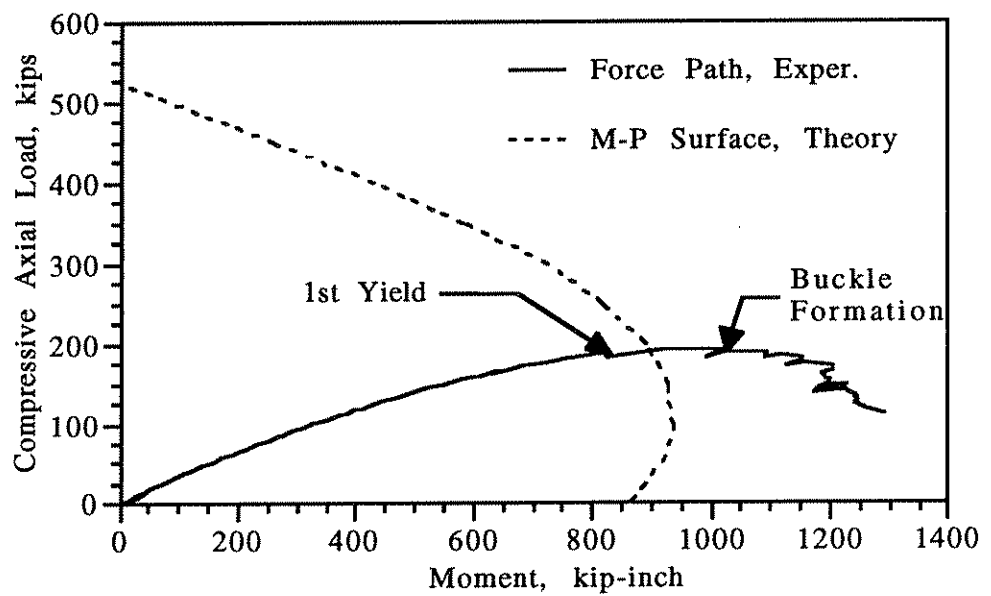
Figure 4.6. Moment-Axial Load Interaction, Specimen A3.
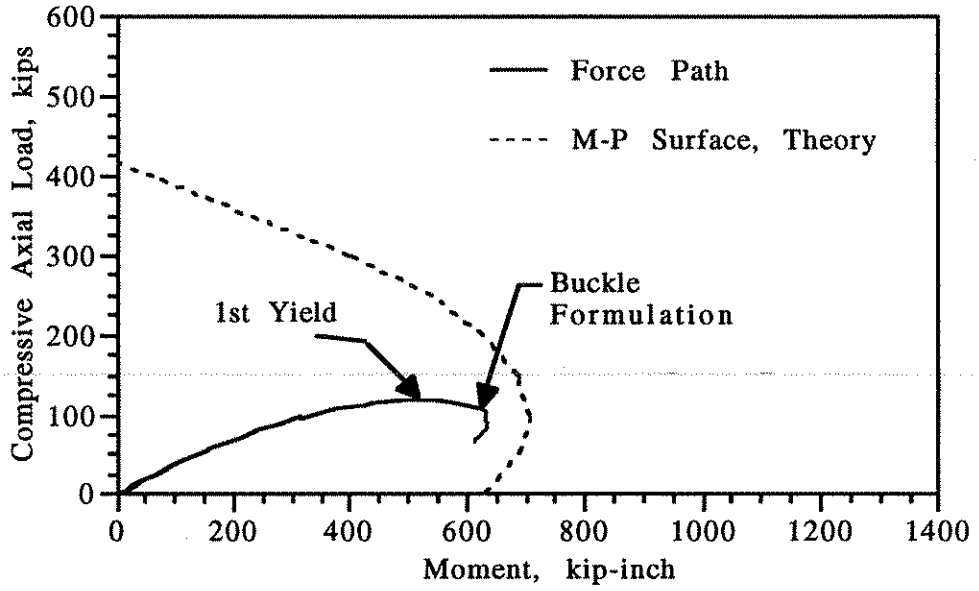
Figure 4.7. Moment-Axial Load Interaction, Specimen B3.
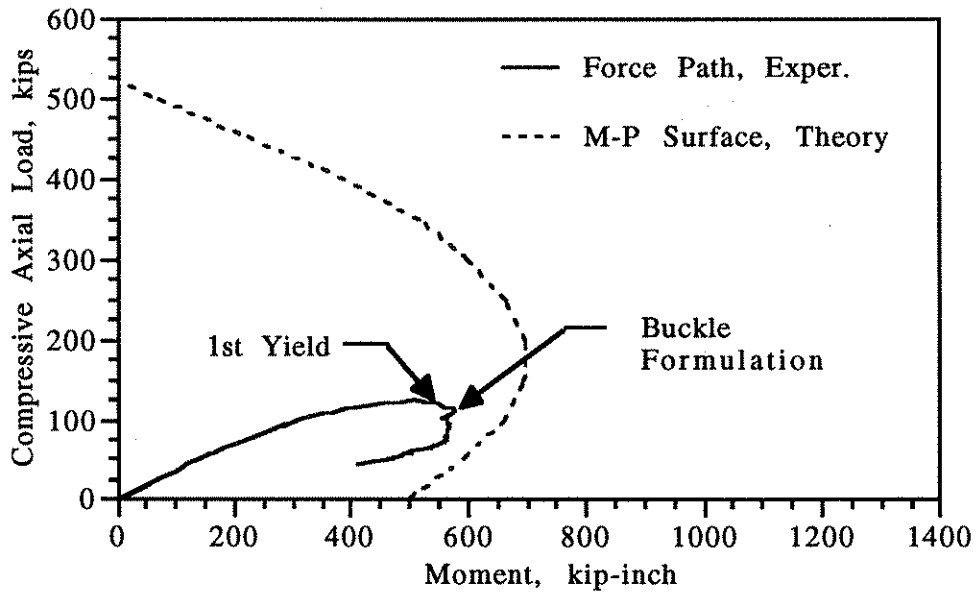
Figure 4.8. Moment-Axial Load Interaction, Specimen C3.
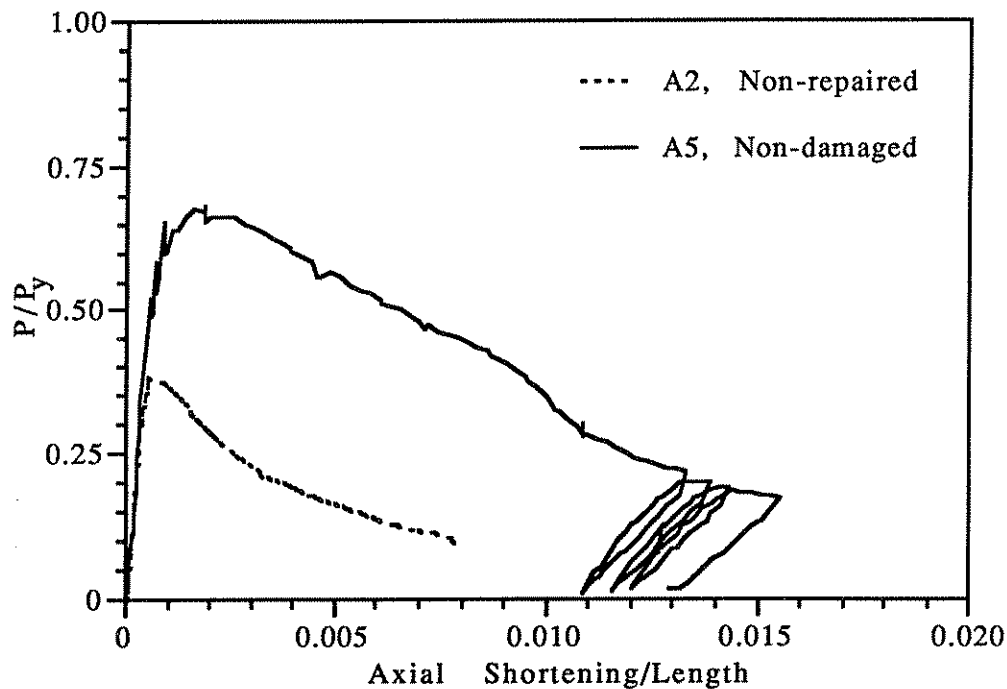
Figure 4.9.   Axial Load - Shortening Relationship for Repaired and Unrepaired Specimens with D/t=34.5, Showing Loss in Capacity Due to Damage.
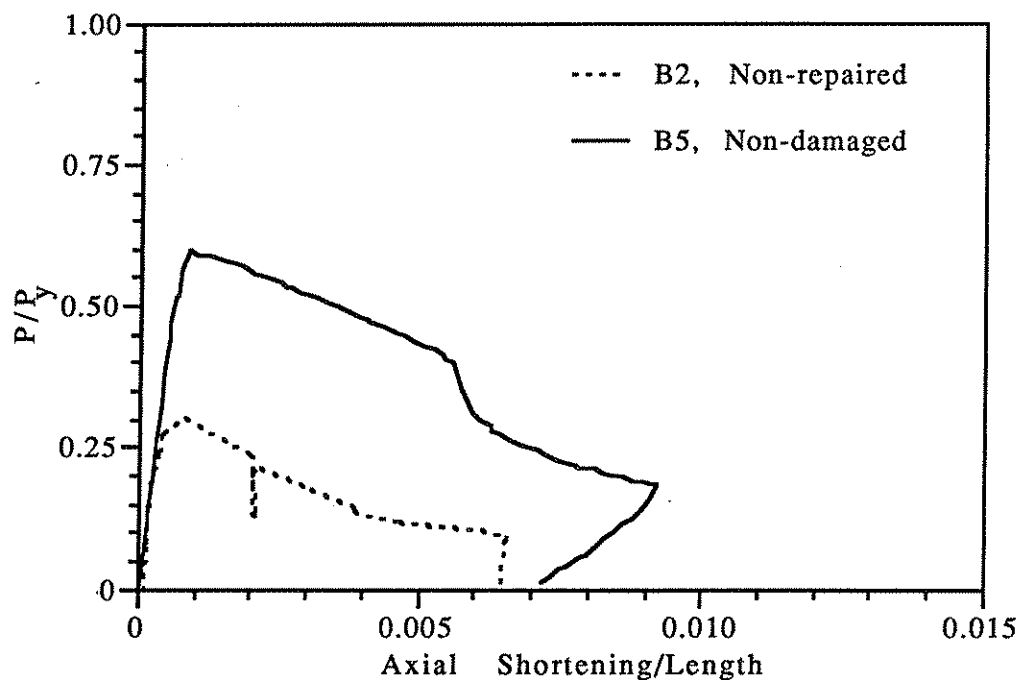
Figure 4.10.   Axial Load - Shortening Relationship for Repaired and Unrepaired Specimens with D/t=46, Showing Loss in Capacity Due to Damage.
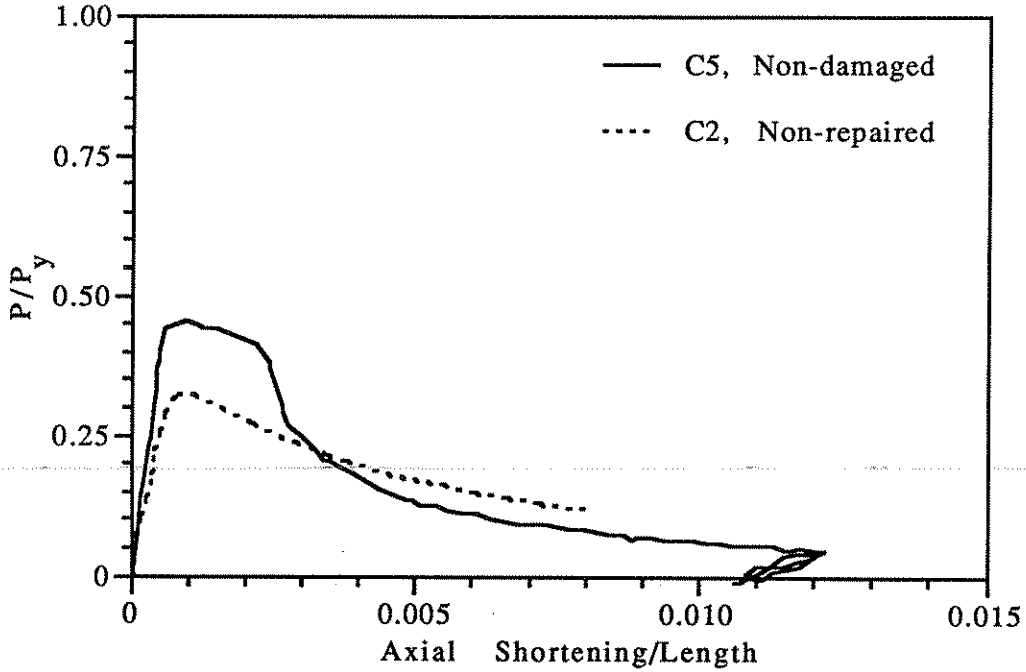
Figure 4.11. Axial Load - Shortening Relationship for Repaired and Unrepaired Specimens with D/t=64, Showing Loss in Capacity Due to Damage.
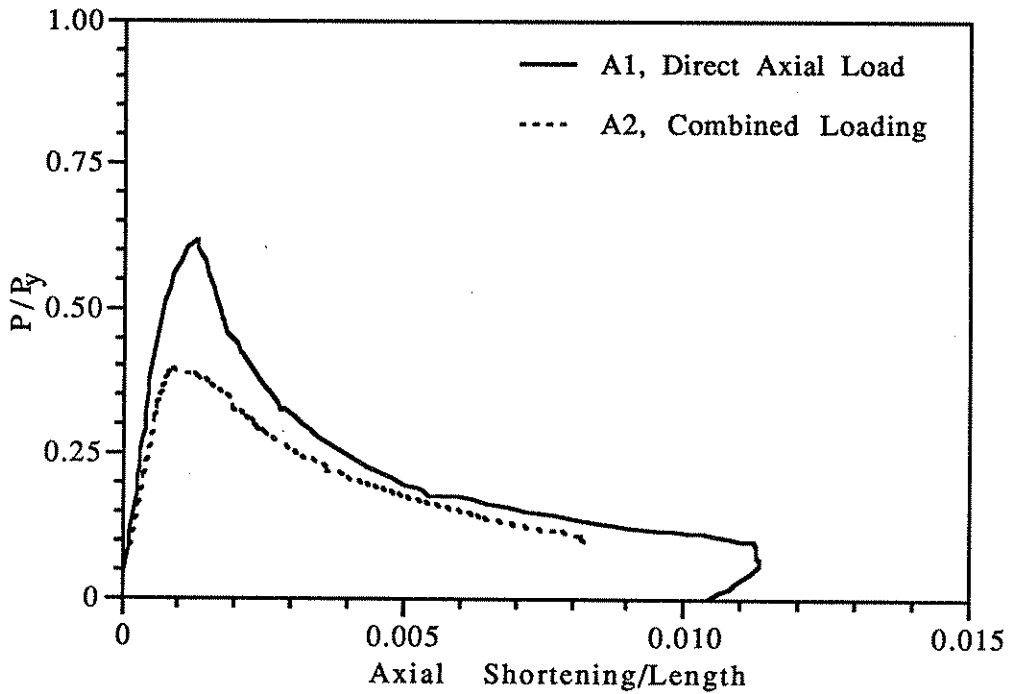
Figure 4.12. Axial Load - Shortening Relationship for Unrepaired Specimens with D/t=34.5, Showing Effect of Combined Loading.
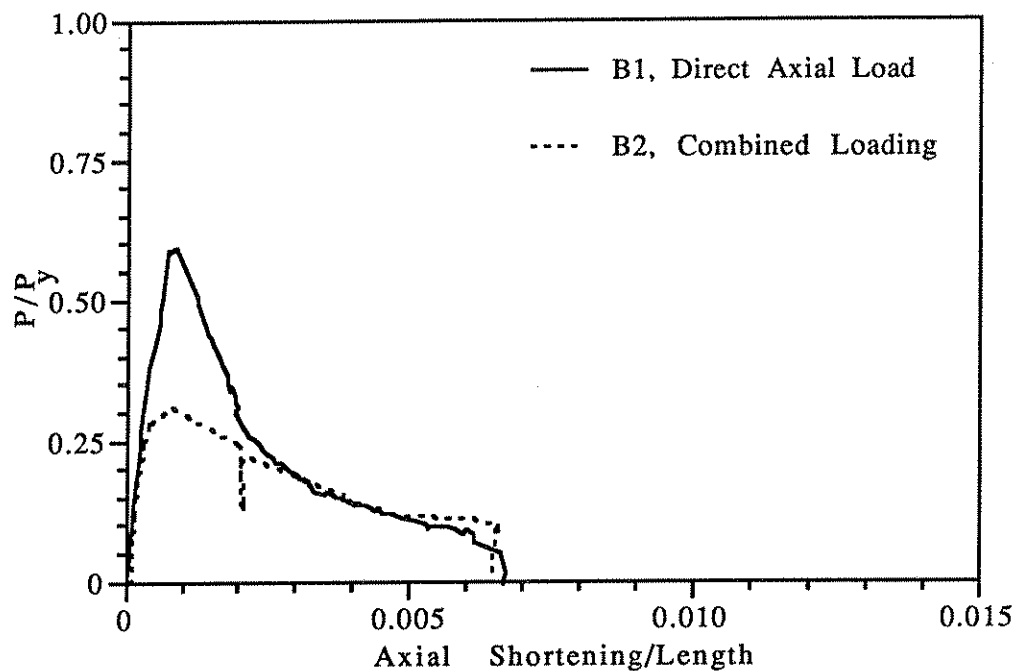
Figure 4.13. Axial Load - Shortening Relationship for Unrepaired Specimens with D/t=46, Showing Effect of Combined Loading.
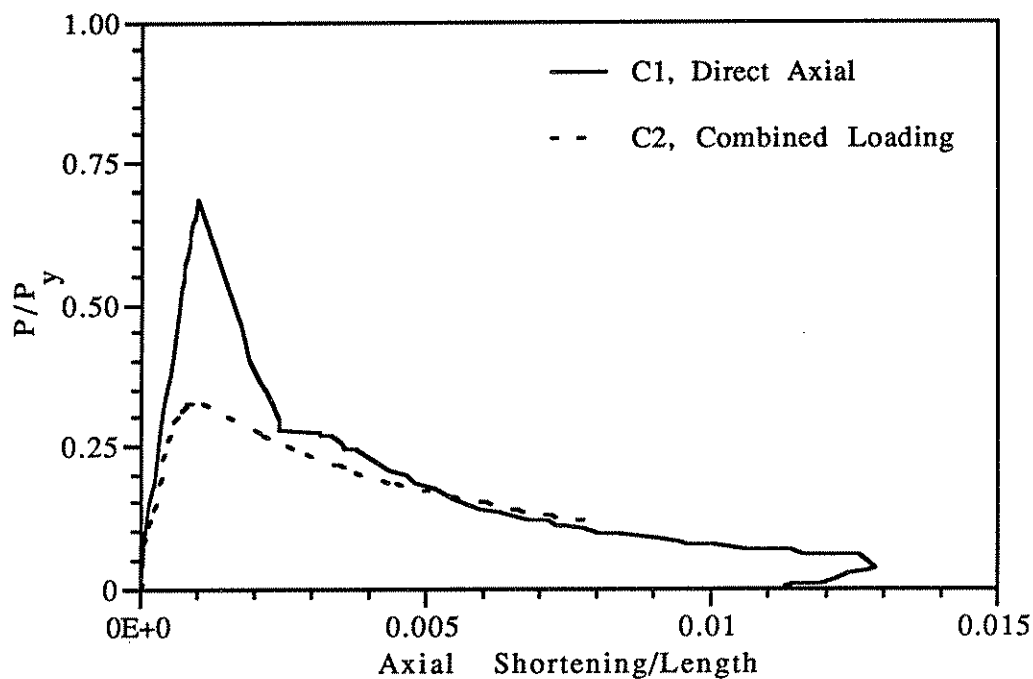
Figure 4.14. Axial Load - Shortening Relationship for Unrepaired Specimens with D/t=64, Showing Effect of Combined Loading.
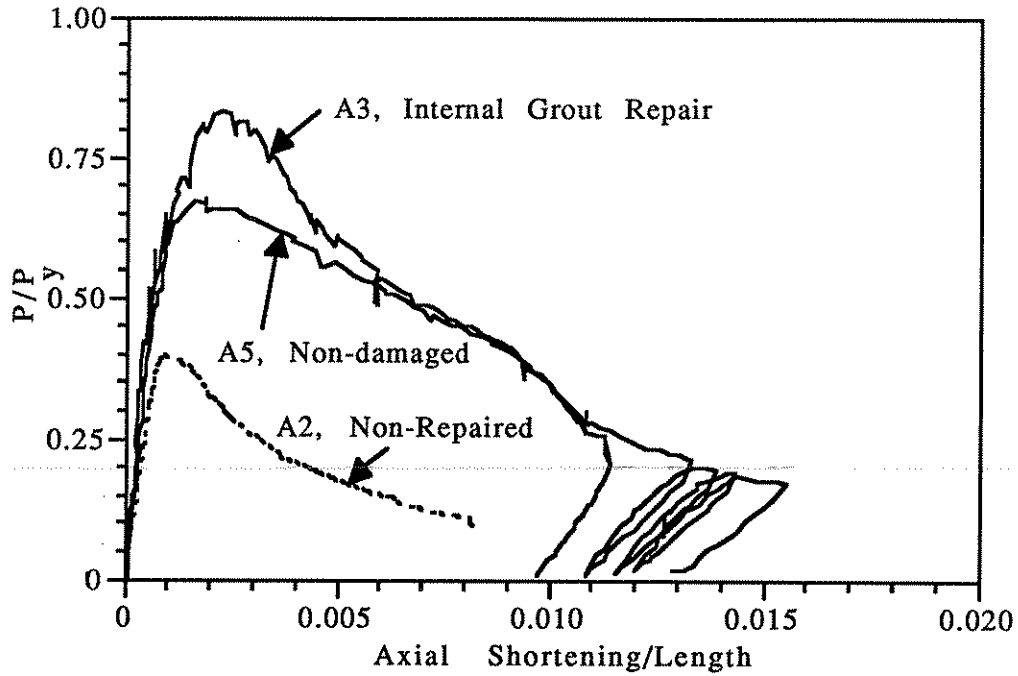
Figure 4.15   Axial Load - Shortening Relationship for Specimens with D/t=34.5, Showing Effectivness of Internal Grout Repair .
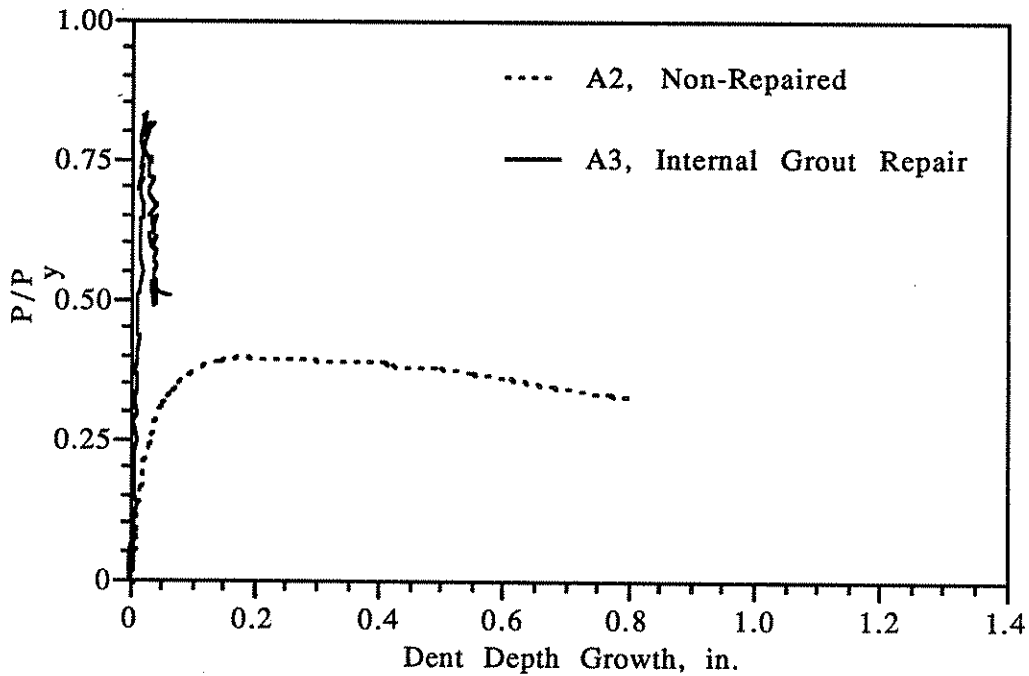
Figure 4.16   Axial Load - Dent Depth   Relationship for Specimens with D/t=34.5, Showing the Arrest of Dent Growth by Internal Grout Repair .
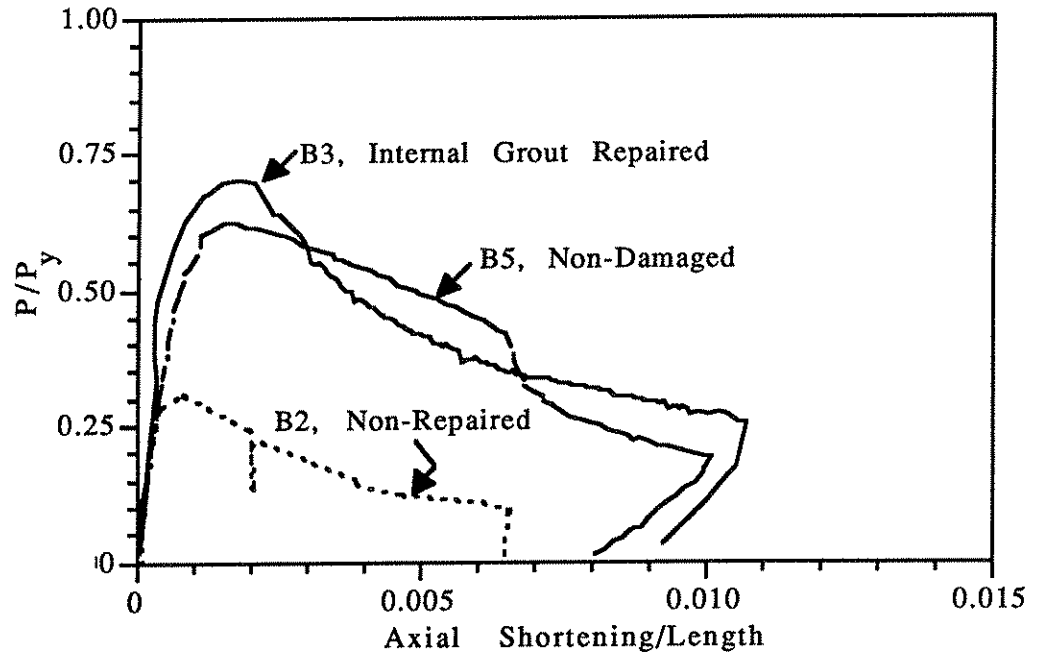
Figure 4.17   Axial Load - Shortening Relationship for Specimens with D/t=46, Showing Effectivness of Internal Grout Repair.
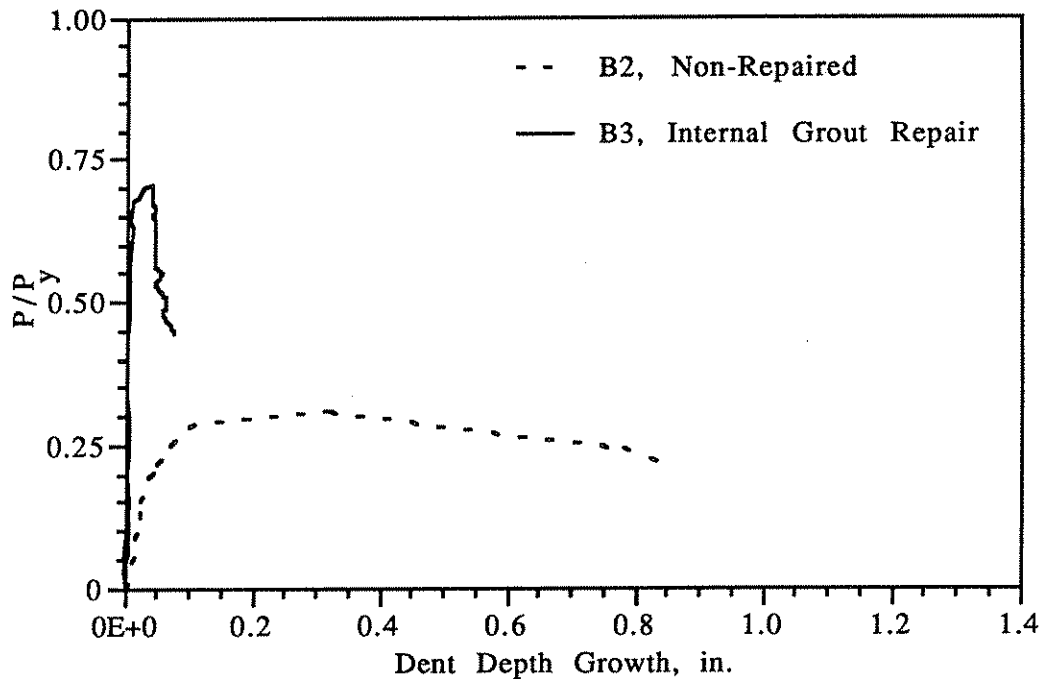
Figure 4.18   Axial Load - Dent Depth   Relationship for Specimens with D/t=46, Showing the Arrest of Dent Growth by Internal Grout Repair .
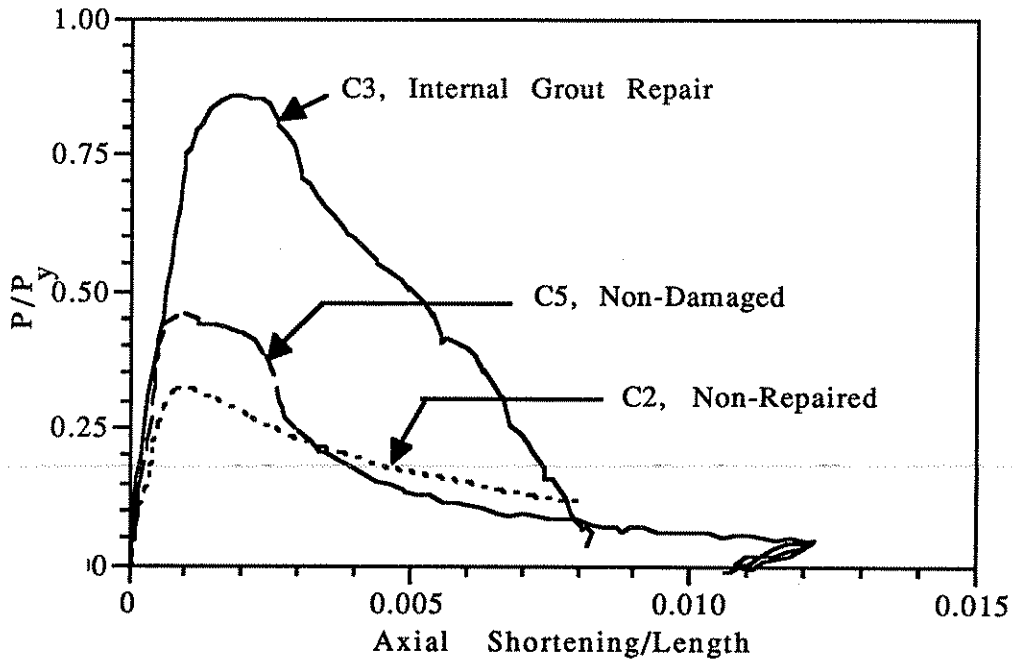
Figure 4.19   Axial Load - Shortening Relationship for Specimens with D/t=64, Showing Effectivness of Internal Grout Repair.
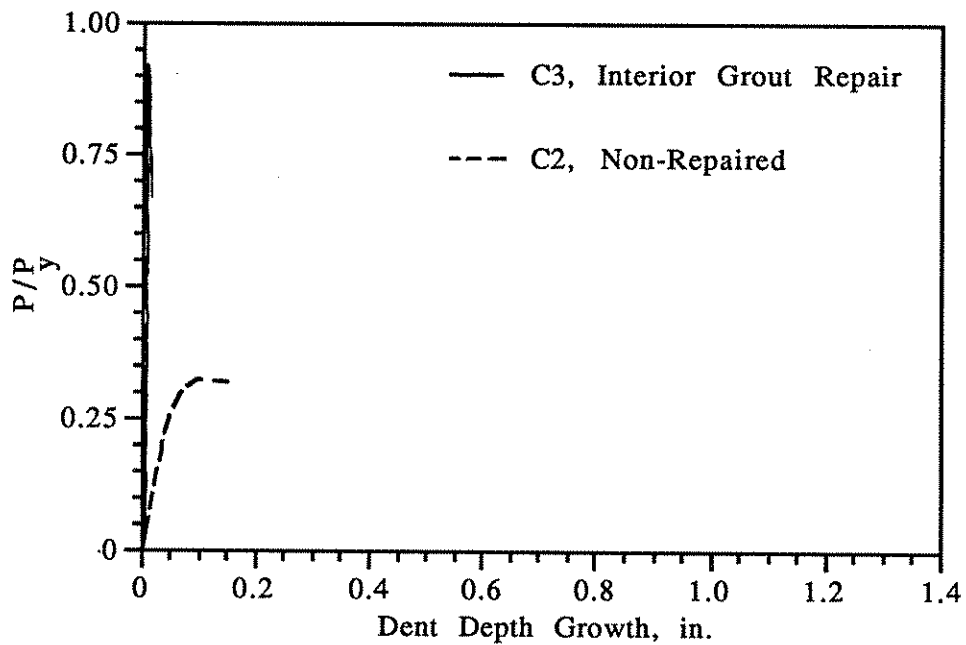
Figure 4.20   Axial Load - Dent Depth   Relationship for Specimens with D/t=64, Showing the Arrest of Dent Growth by Internal Grout Repair .
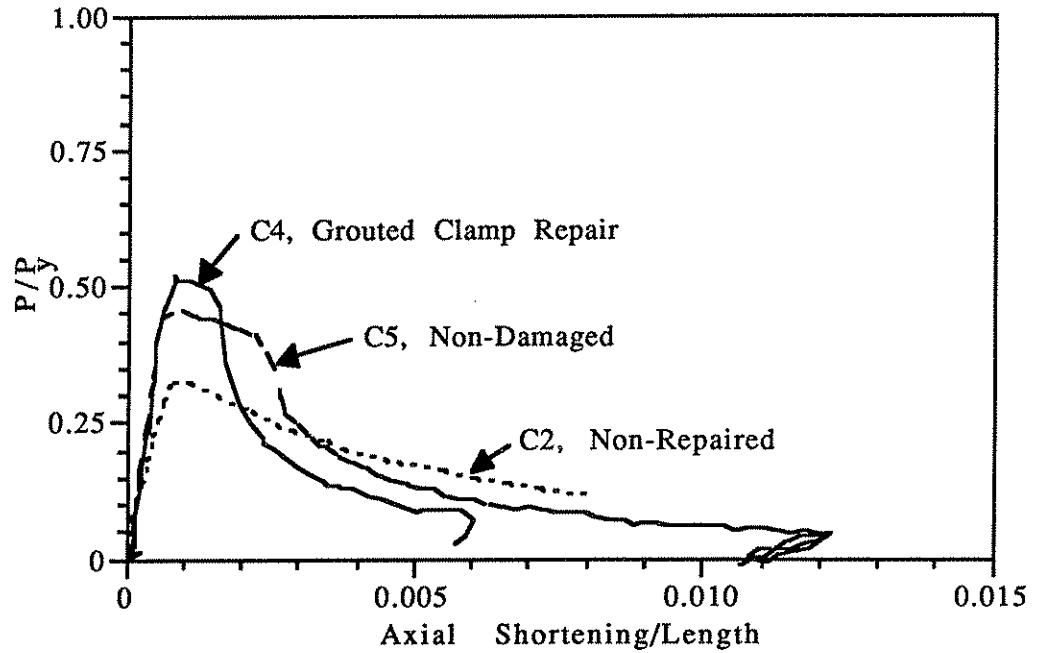
Figure 4.21   Axial Load - Shortening Relationship for Specimens with D/t=64, Showing Effectivness of Grouted Clamp Repair.
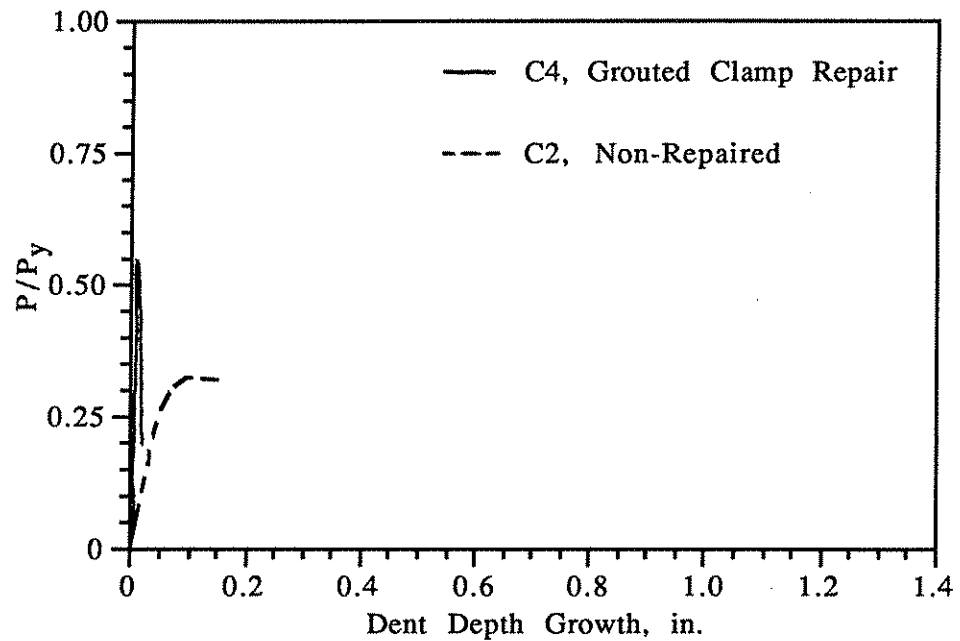
Figure 4.22   Axial Load - Dent Depth   Relationship for Specimens with D/t=64, Showing the Arrest of Dent Growth by Grouted Clamp Repair .
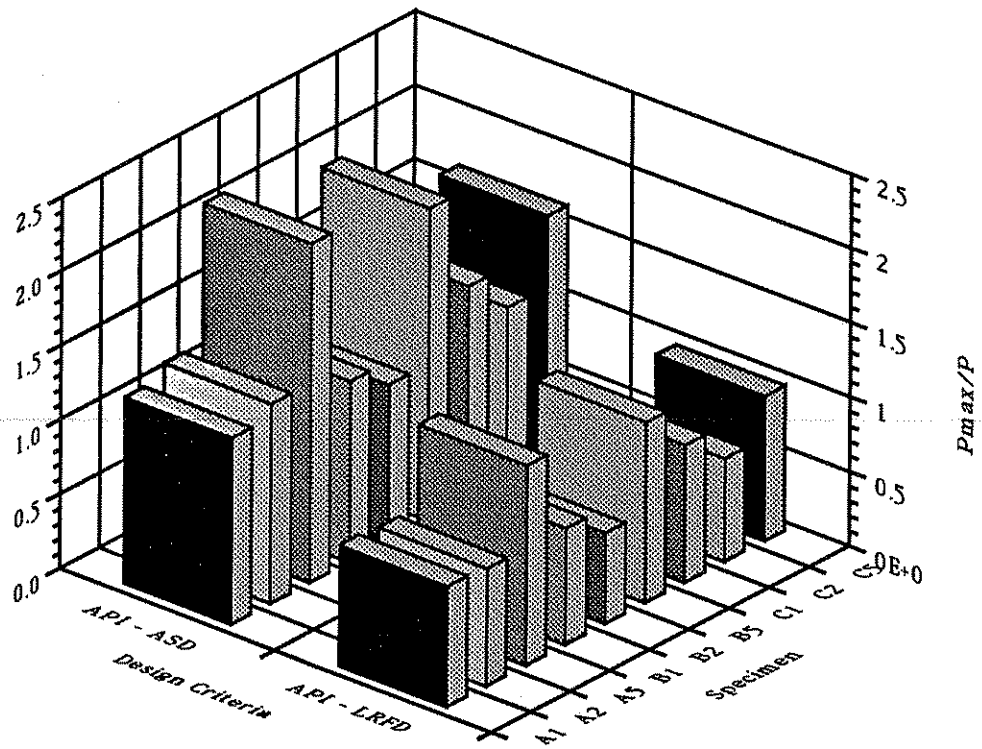
Figure 4.23. Comparison of API Design Criteria (P) With Specimen Capacity Pmax, Showing Reduced Margin of Safety for Damaged, Non-Repaired Specimens.
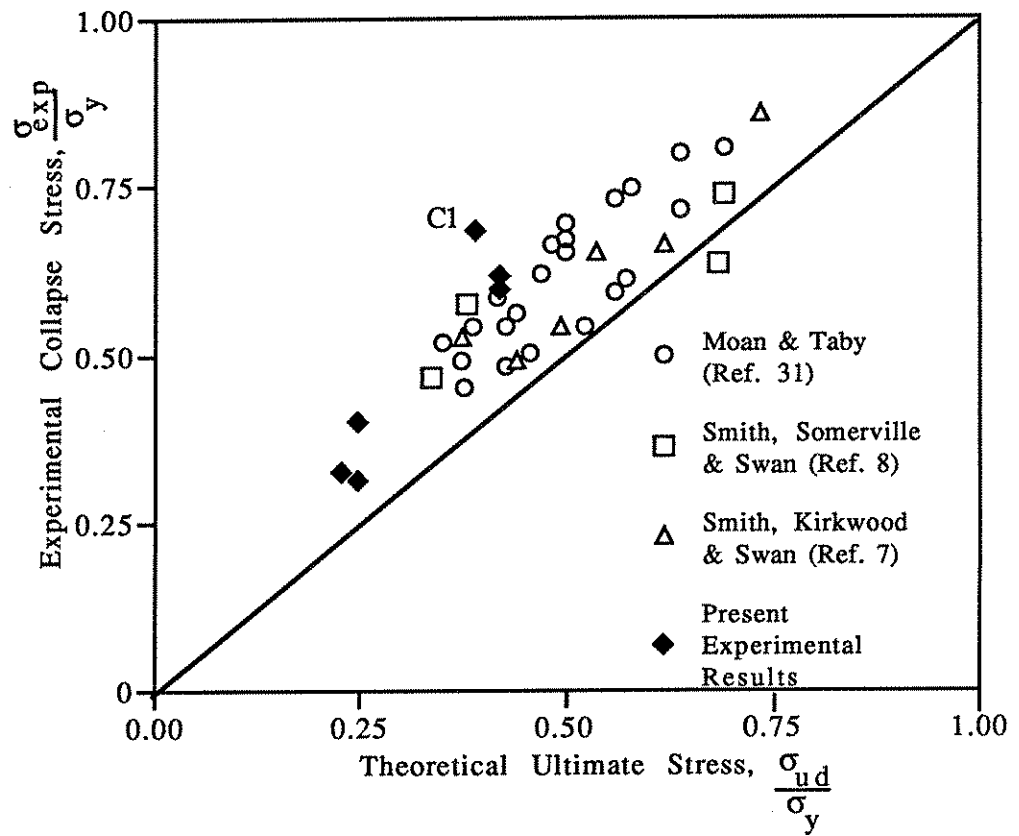
Figure 4.24.   Comparison of Experimental Results With Modified Ellinas' Design Equation.
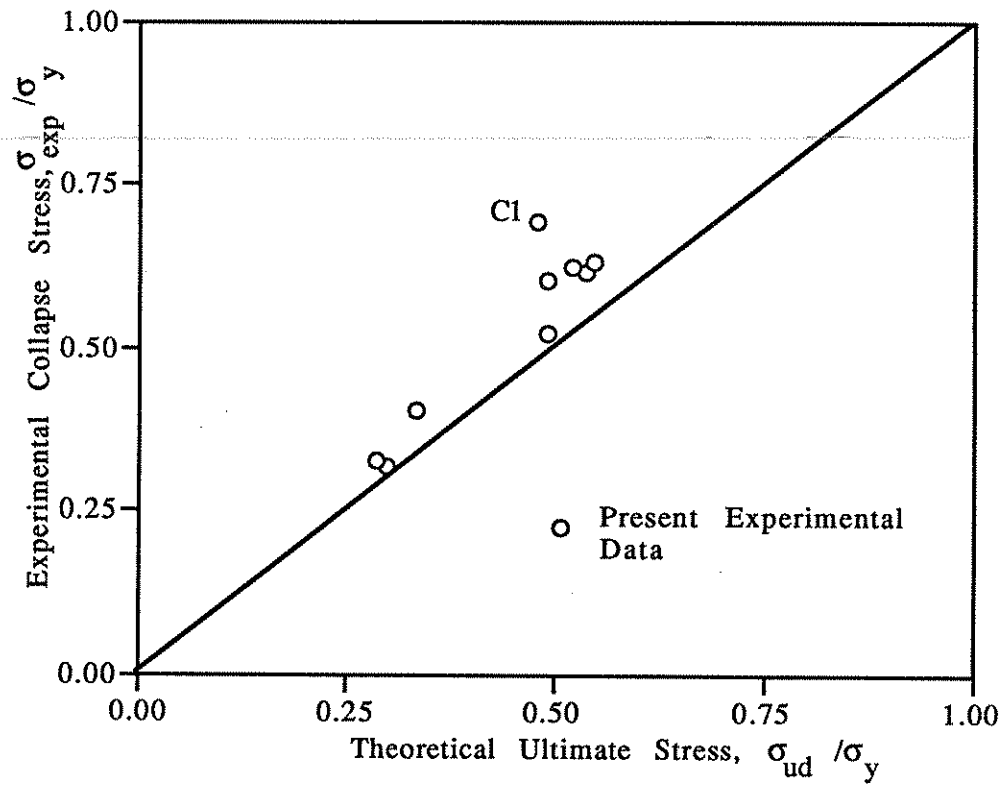
Figure 4.25. Comparison of Experimental Results with UC-DENT Analysis, Non-Repaired Members.
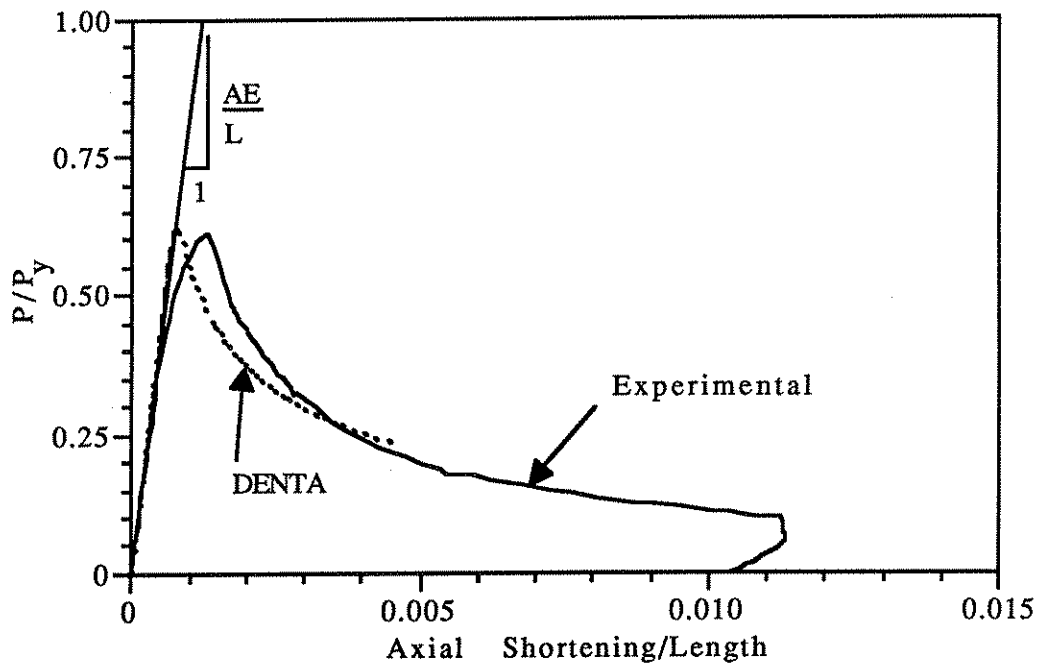
Figure 4.26. DENTA and Experimental Comparisons for the Axial
Load - Shortening Relationship of Specimen A1.
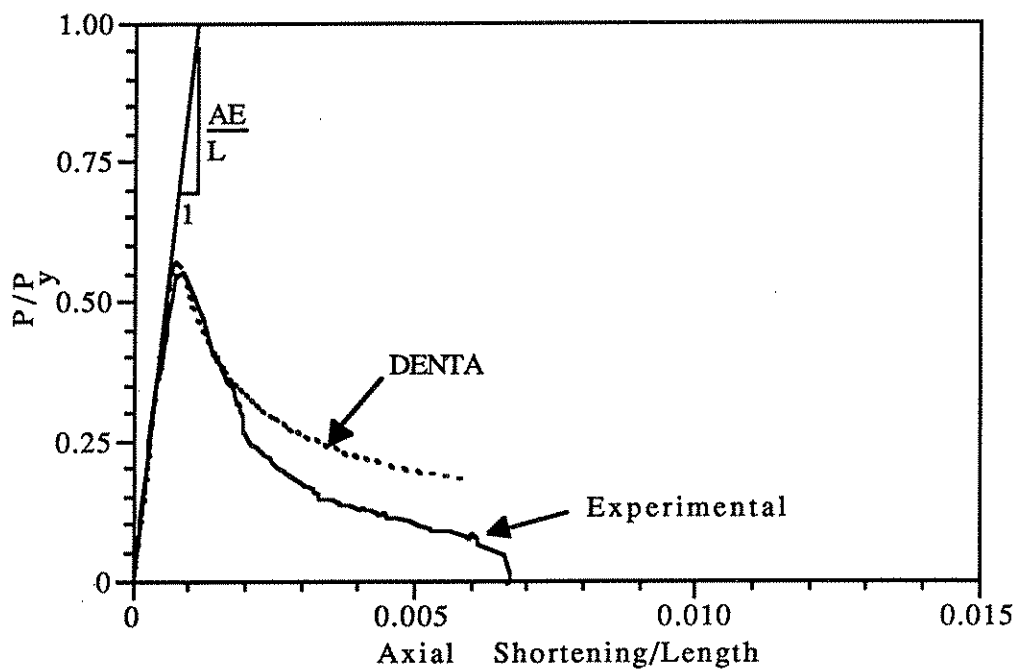
Figure 4.27. DENTA and Experimental Comparisons for the Axial
Load - Shortening Relationship of Specimen B1.
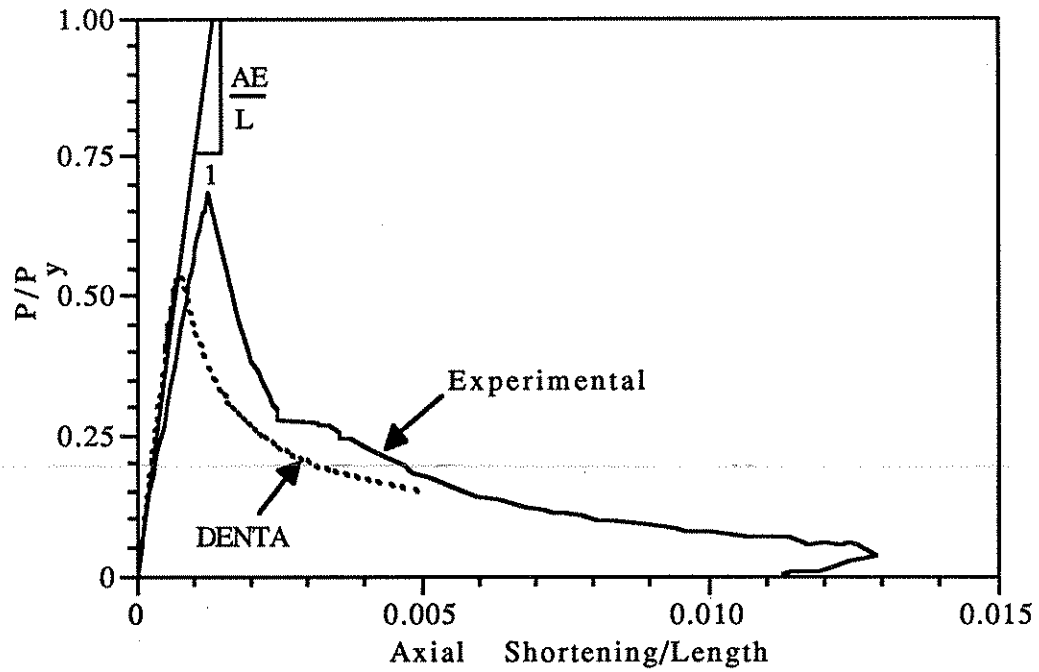
Figure 4.28. DENTA and Experimental Comparisons for the Axial Load - Shortening Relationship of Specimen C1.
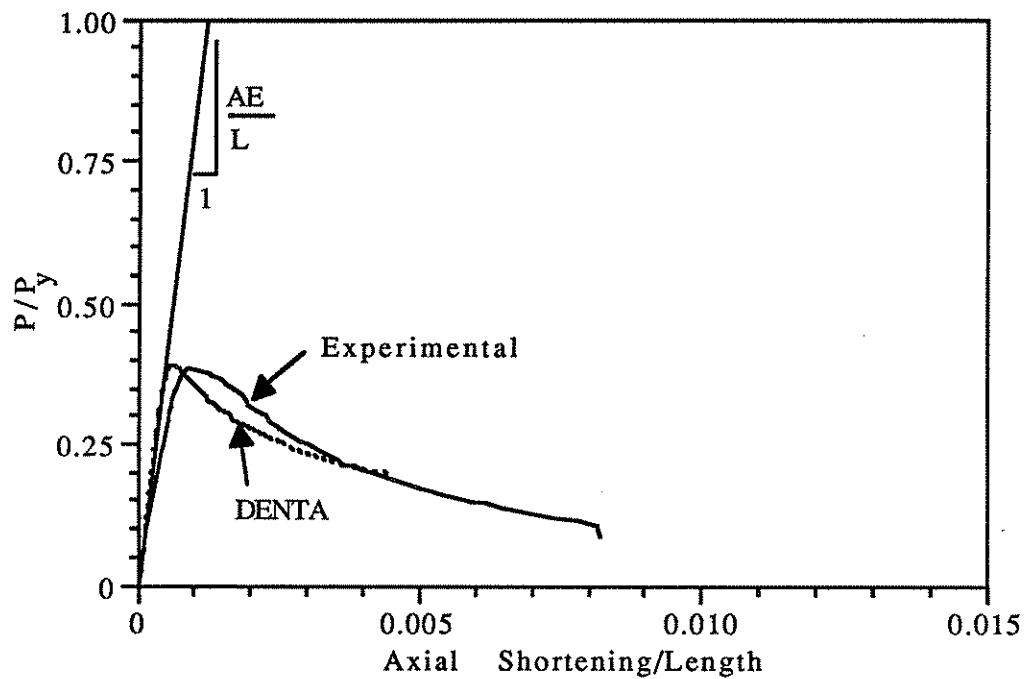
Figure 4.29. DENTA and Experimental Comparisons for the Axial Load - Shortening Relationship of Specimen A2.
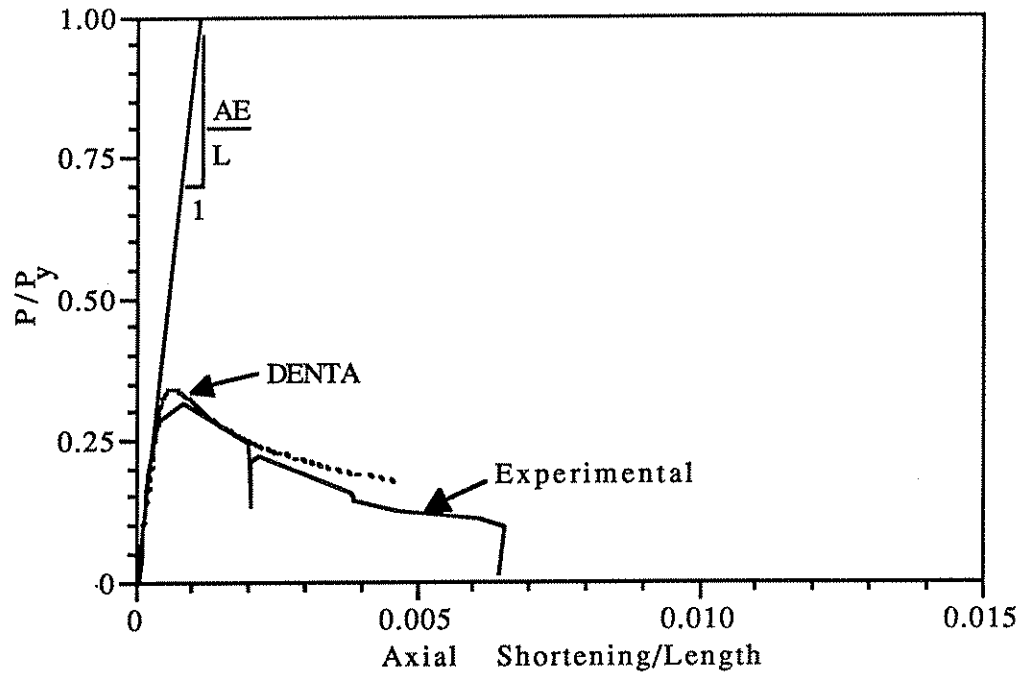
Figure 4.30. DENTA and Experimental Comparisons for the Axial Load - Shortening Relationship of Specimen B2.
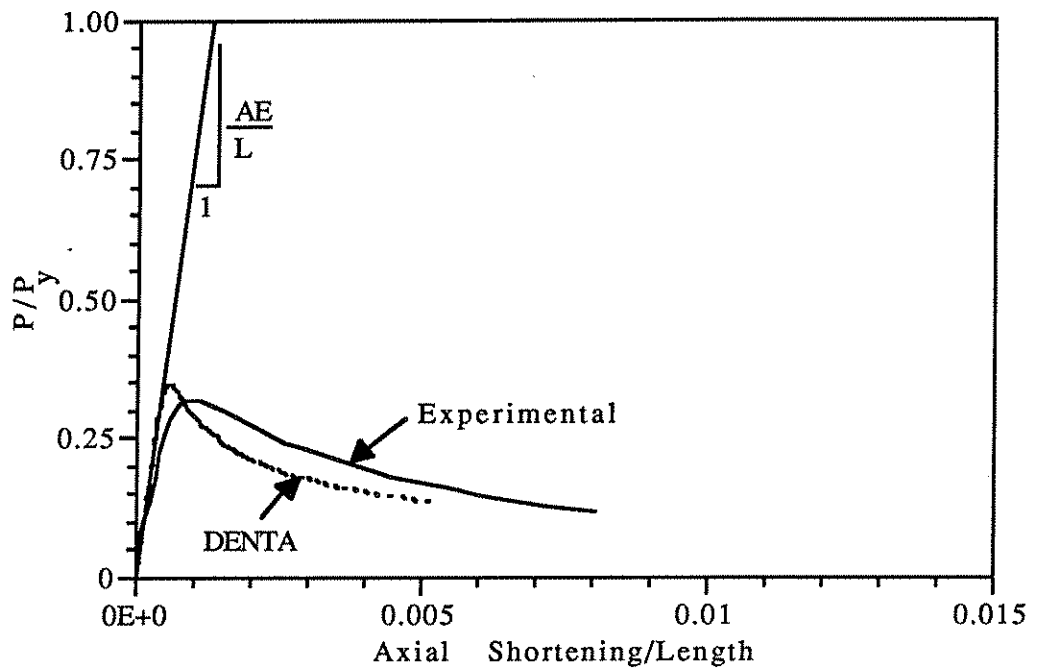
Figure 4.31. DENTA and Experimental Comparisons for the Axial Load - Shortening Relationship of Specimen C2.
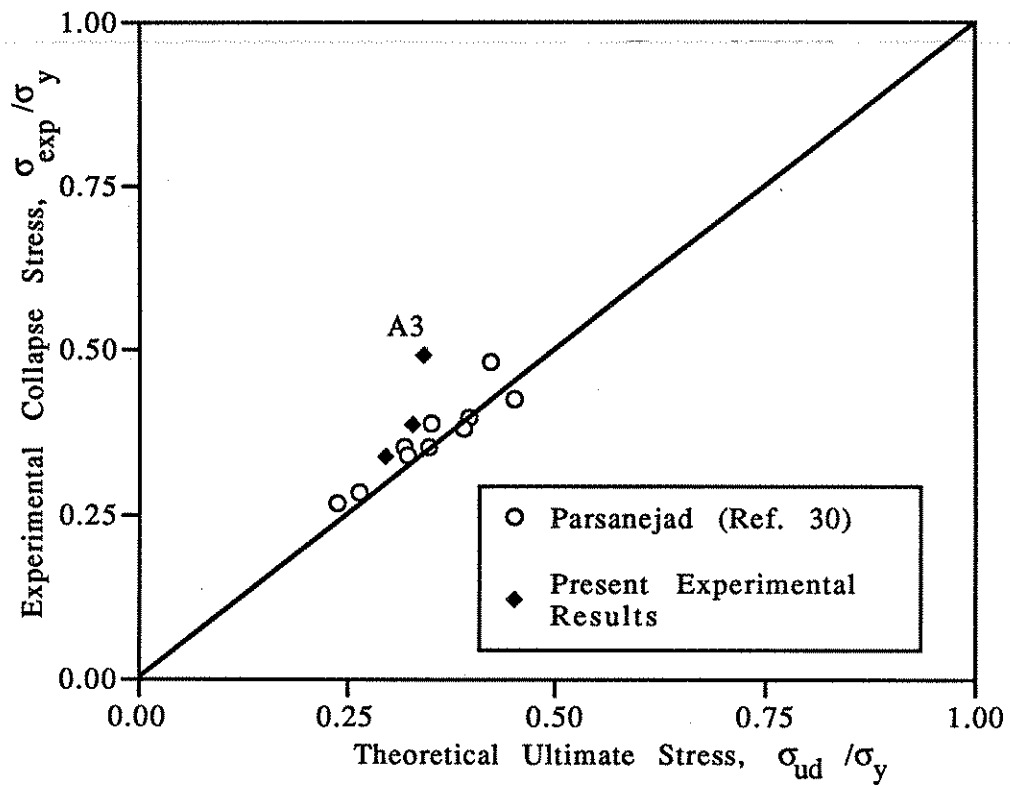
Figure 4.32.   Comparisons of Experimental Results with Parsanejad's
Method, Internally Grout Repaired Members.

CHAPTER 5

5.1.   Summary

Five series of tests, consisting of thirteen steel tubular braces of various diameter to thickness (D/t) ratio were tested to examine the effect of a dent damage of 0.10D depth on their residual strength and to assess the effectiveness of internal grout repair and grouted steel clamp repair techniques.   The braces were subjected to either direct axial loading or combined axial and bending loads through an end eccentricity of 0.20D. Comparisons between the test series allowed direct evaluation of the effect of the dent damage on specimens subjected to concentric and combined loading, the repaired residual strength of internal grout repaired specimens, and the repaired strength of a grouted steel clamp repaired specimen.   Various existing analytical techniques and newly developed formulations used for predicting the residual strength of dent damaged tubular braces were also assessed through comparison with experimental results.

5.2.   Conclusions

Based on the results of the study presented here, the following are given:

(1) A dent depth of 0.10D leads to significant loss of strength.

(2) Effects of an end eccentricity of 0.20D on the residual strength
     is pronounced.

(3) Internal grout repair of a 0.10D dent damaged brace is
     successful in reinstating the original non-damaged member
     strength by arresting the dent from growing inwards.   Extent
     of strength enhancement is limited by the D/t ratio of the
     damaged member due to susceptibility to local buckling in
     higher D/t ratio specimens.

(4) Grouted steel clamp repair of a 0.10D dent damaged brace is successful in reinstating the original non-damaged member strength by restraining the cross section from ovaling, thereby preventing the dent from growing inwards.

(5) Modification of Ellinas' strength equation for additional eccentricity of the applied axial load provides a lower bound on residual strength.

(6) UC-DENT agrees reasonably well with test results, providing a lower bound prediction for ultimate load capacity, and shows correct trends in residual strength - dent growth relationships.

(7) Preliminary nonlinear finite element analyses show that the method is effective in modelling the experimental tests, but care must be taken in the description of the material properties and refinement of the mesh.

(8) The residual strength of the nonrepaired, damaged specimens is closely predicted by DENTA.

(9) The unity check method for dented members was found to agree closely with the experimental results, where the stability check controlled.

(10) Parsanejad's formulation for predicting the strength of internally grout repaired members was found to provide a reasonable close lower bound for the strength of the internally grout repaired specimens.

Additional studies are currently continuing under the second phase of work, involving the assessment of the effects of deeper dent depth on residual strength and repair. In addition, refined nonlinear finite element analysis of nonrepaired and repaired specimens are being performed.

Appendix A -
UC-DENT Source Code

UC-DENT SOURCE CODE LISTING

```
c.....................................................................
c    Program UC_DENT -
c               Determination of the residual strength
c               of dent damaged tubular members.
c               Revisions based on reduced euler buckling,
c               limit on plastification stress, as well as
c               proper second order deflection.
c
c               Developed by
c               Professor James Ricles and Troy Gillum
c
c               Version 1.3
c               April, 1992
c.....................................................................
C
      program dent
      implicit real*8(a-h,o-z)
      common /xmat/emod,sigy
      common /geom/dia,t,xl,ende,area,gyr,alpha,xi,deltad,del0
      common /dprop/theta,si,eta,aread,ed,rd,sd,deld,es,ddepth,xld,
     $          xid,xldent,xl1,xl2
      common /dmat/sigpd,sige
      common /var/paxial
      character*80 title(2)
      character*1 iquiz,ians
      data ians/'Y'/
      write(6,100)
100   format(5x,
     &      'Program Dent - Determination of the residual strength',/,
     &   5x,'            of dent damaged tubular members.',//,
     &   5x,'            Version 3.0 - May, 1992',/,
     &   5x,'              Developed by',/,
     &   5x,'           Professor James Ricles',/,
     &   5x,'                  and',/,
     &   5x,'               Troy Gillum',/,
     &   5x,'           Department of AMES',/,
     &   5x,'     University of California San Diego',//)
      open(1,file='dent.out',status='new')
      rewind 1
C
C    Enter input data
C
      write(6,120)
120   format(5x,
     &      'Enter title lines for identifying output file dent.out')
      read(5,150) (title(i),i=1,2)
150   format(a80)
1     continue
      write(6,125)
125   format(5x,
     & 'Enter member: diameter, effective length, wall thickness,',/,
     &5x,'yield stress,Young`s mod, end eccentricity,',/,
     &5x,' midspan imperfection, length of dent,',
```

```
      &   ' dent location, maximum dent depth',/,
       &   5x,'>',$)
        read(5,*) dia,xl,t,sigy,emod,ende,del0,xldent,xdent,dmax
        write(6,300) (title(i),i=1,2),dia,xl,t,sigy,emod,ende,
       &            del0,xldent,xdent,dmax
        write(6,375)
  375   format(5x,'Is input data okay [Y,N]?')
        read(5,250) iquiz
        write(6,250) iquiz
  250   format(a1)
        if(iquiz.ne.ians) go to 1
        write(1,300) (title(i),i=1,2),dia,xl,t,sigy,emod,ende,
       &            del0,xldent,xdent,dmax
        write(1,350)
  300   format(1x,2(a80,//),
       &     5x,'Member Diameter         = ',f8.3,/,
       &     5x,'Member Effective Length   = ',f8.3,/,
       &     5x,'Member Wall Thickness     = ',f8.3,/,
       &     5x,'Member Yield Stress     = ',e11.4,/,
       &     5x,'Member Young`s Modulus     = ',e11.4,/,
       &     5x,'Member End Eccentricity    = ',f8.3,/,
       &     5x,'Initial Midspan Imperfection = ',f8.3,/,
       &     5x,'Length of Dent        = ',f8.3,/,
       &     5x,'Dent Location, x       = ',f8.3,/,
       &     5x,'Maximum Dent Depth       = ',f8.3,/)
  350   format(1x,'dent depth/Diameter    Sigu/Sigy  Pu')
C
C    Initialize parameters
C
        ptol=1.0d-02
        xl1=xdent-xldent
        xl2=xl-xl1-xldent
        deldep=dmax/30.0
        call sectprop
        ddepth=0.0
C
C    Compute normalized residual strength
C
  2     continue
        deld=ddepth/dia
        call dentprop
        call sigmae
        call sigpdd
        call eccen
c.... set initial guess of axial load to p = area*sigy
        paxial=sigy*area
        ncount =0
  4     continue
        call secdefl
        if(si.lt.1d-06) then
        term =0.0
        else
        term=sigpd/si/dia/t
        endif
        a1=(1.0/aread + (ende+ed)/sd)/sige/aread
        a2=(ende+ed)/sd + deltad/sd + 1/aread +
       &  (term +sigy + sigpd*es/sd)/sige/aread
```

```
      a3=sigy+sigpd + sigpd*es/sd
      temp=a2*a2 - 4.0*a1*a3
      paxnew=(a2-dsqrt(temp))/2.0/a1
      sigud=paxnew/sigy/area
      temp=paxial-paxnew
      if(dabs(temp).lt.ptol) go to 3
      paxial=(paxnew+paxial)*0.5
      ncount=ncount+1
      if(ncount.gt.1000) then
      write(6,1000)
1000  format(5x,'Convergence not achieved during second order',/,
     &      5x,'deflection calculation')
      stop
      else
      go to 4
      endif
3     continue
      write(1,500) deld,sigud,paxial,a1,a2,a3
500   format(2(1x,f7.3,2x,f7.3),4(2x,e11.4))
      ddepth=ddepth+deldep
      if(ddepth.le.dmax) go to 2
      write(6,600)
600   format(5x,'Computation completed, results are saved in dent.out')
      stop
      end
C
C.............................................................
C
C     subroutine sectprop - compute section properties of
C                  undamaged state of member
C
C.............................................................
C
      subroutine sectprop
      implicit real*8(a-h,o-z)
      common /geom/dia,t,xl,ende,area,gyr,alpha,xi,deltad,del0
      common /xmat/emod,sigy
      pi=4.0*datan(1.0d0)
      area=pi*dia*t
      gyr=dia*0.5/dsqrt(2.0d0)
      xi=gyr*gyr*area
      return
      end
C
C.............................................................
C
C     subroutine sigmae - compute euler buckling stress
C
C.............................................................
C
      subroutine sigmae
      implicit real*8(a-h,o-z)
      common /geom/dia,t,xl,ende,area,gyr,alpha,xi,deltad,del0
      common /xmat/emod,sigy
      common /dmat/sigpd,sige
      common /dprop/theta,si,eta,aread,ed,rd,sd,deld,es,ddepth,xld,
     $          xid,xldent,xl1,xl2
```

```
      pi=4.0*datan(1.0d0)
      temp=2.0*pi*(xl1+xldent)/xl
      temp=((dsin(2.0d0*pi*xl1/xl) -dsin(temp))/2.0/pi )*(1 - xid/xi)
      xie=xi*((xl1+xl2+xid*xldent/xi)/xl - temp)
      sige=pi*pi*emod*xie/xl/xl/aread

      return
      end
C
C...........................................................
C
C    subroutine dentprop - compute section properties of dent section
C
C...........................................................
C
      subroutine dentprop
      implicit real*8(a-h,o-z)
      common /geom/dia,t,xl,ende,area,gyr,alpha,xi,deltad,del0
      common /xmat/emod,sigy
      common /dmat/sigpd,sige
      common /dprop/theta,si,eta,aread,ed,rd,sd,deld,es,ddepth,xld,
     $          xid,xldent,xl1,xl2
      pi=4.0*datan(1.0d0)
      temp=2.0*dsqrt(deld*(1.0-deld))
      theta=2.0*pi - 2.0*dasin(temp)
      si=pi-theta*0.5
      if(si.lt.1.0d-06) then
      eta=0.5*dia - 0.5*dia*dcos(si)
      else
      eta=0.5*dia*dsin(si)/si - 0.5*dia*dcos(si)
      endif
      aread=0.5*dia*t*theta
      ed=dia*dsin(theta*0.5d0)/theta
      temp=theta + dsin(theta)
      temp=temp - 8.0*dsin(0.5*theta)*dsin(0.5*theta)/theta
      temp2=1.0 - 2.0*deld + 2.0*ed/dia
      sd=dia*dia*t*temp*0.125/temp2
      rd=dsqrt(dia*dia*0.125d0*temp/theta)
      xid=dia*dia*dia*t*0.0625*temp
      xld=xl/rd - 0.2*pi*dsqrt(emod/sigy)
      return
      end
C...........................................................
C
C    subroutine sigpdd - compute dent plastification force
C
C...........................................................
C
      subroutine sigpdd
      implicit real*8(a-h,o-z)
      common /geom/dia,t,xl,ende,area,gyr,alpha,xi,deltad,del0
      common /xmat/emod,sigy
      common /dmat/sigpd,sige
      common /dprop/theta,si,eta,aread,ed,rd,sd,deld,es,ddepth,xld,
     $          xid,xldent,xl1,xl2
      ett=eta/t
      temp=4.0*ett*ett + 1.0
```

```
      sigpd=sigy*si*dia*t*(dsqrt(temp) - 2.0*ett)
C.... check limit for plastification force
      temp=0.5*dia-ddepth+ed
      xmax=sigy*si*dia*t*temp/(temp+eta)
      if(sigpd.gt.xmax) sigpd=xmax
C....
      return
      end
C.........................................................
C
C
C    subroutine eccen - compute dent section eccentricity
C
C.........................................................
C
      subroutine eccen
      implicit real*8(a-h,o-z)
      common /geom/dia,t,xl,ende,area,gyr,alpha,xi,deltad,del0
      common /xmat/emod,sigy
      common /dmat/sigpd,sige
       common /dprop/theta,si,eta,aread,ed,rd,sd,deld,es,ddepth,xld,
     $       xid,xldent,xl1,xl2
      es=eta+0.5*dia-ddepth+ed
      return
      end
C.........................................................
C
C
C    subroutine secdefl - compute second order deflections at dent
C
C.........................................................
C
      subroutine secdefl
      implicit real*8(a-h,o-z)
      common /geom/dia,t,xl,ende,area,gyr,alpha,xi,deltad,del0
      common /xmat/emod,sigy
      common /dmat/sigpd,sige
       common /dprop/theta,si,eta,aread,ed,rd,sd,deld,es,ddepth,xld,
     $       xid,xldent,xl1,xl2
      common /var/paxial
      pi=4.0*datan(1.0d0)
      temp=pi*(xl2+xldent*0.5)/xl
      cd=(xl/(2.0*xl1-xldent))*dsin(temp)
      xme=sigpd*(0.5*dia+ed+eta-ddepth)
      delb=xldent*xl1*(paxial*ed - xme)/emod/xid/(1.0+xl1/xl2)
      deltad=(delb+del0)*(1.0 + cd*sige*aread/(sige*aread - paxial))
      return
      end
```

Appendix B -
Specimen Dent Profiles

Specimen A1

Specimen A2

Specimen A3

Specimen B1

Specimen B2

Specimen B3

184

Specimen C1

Distance from Center of Dent, inch

Specimen C2

Distance from Center of Dent, inch

Specimen C3

Distance from Center of Dent, inch

Specimen C4

Distance from Center of Dent, inch
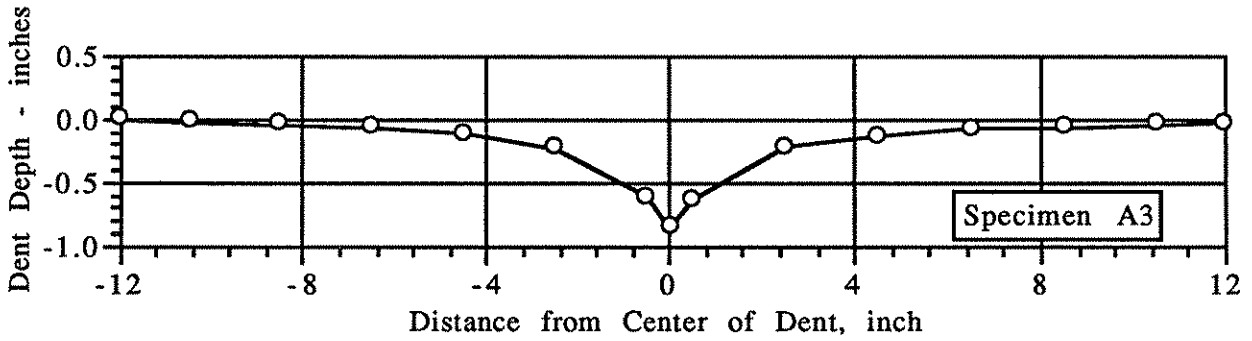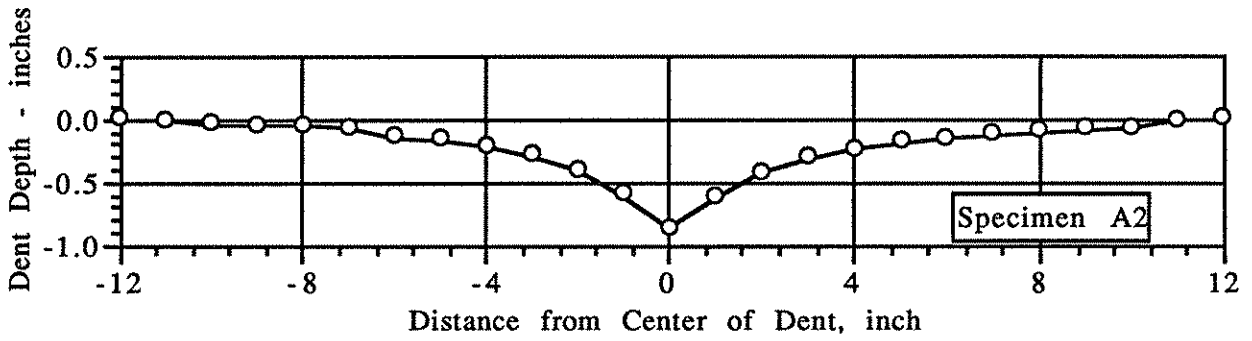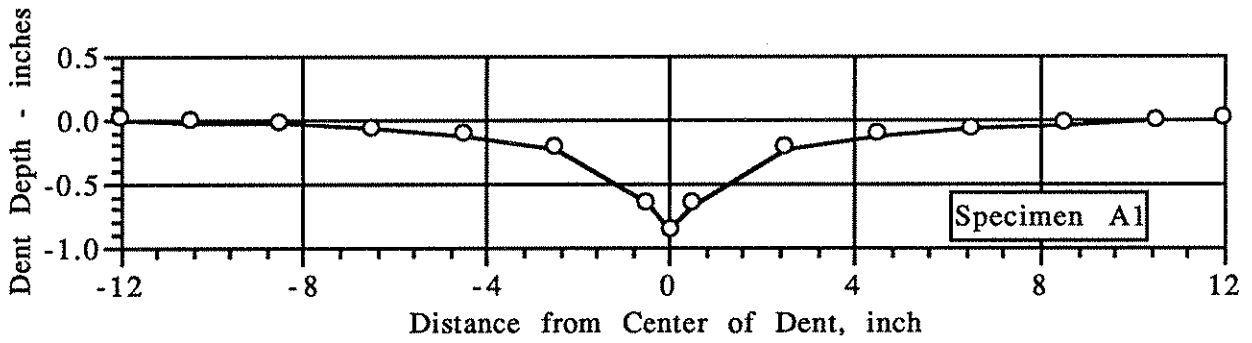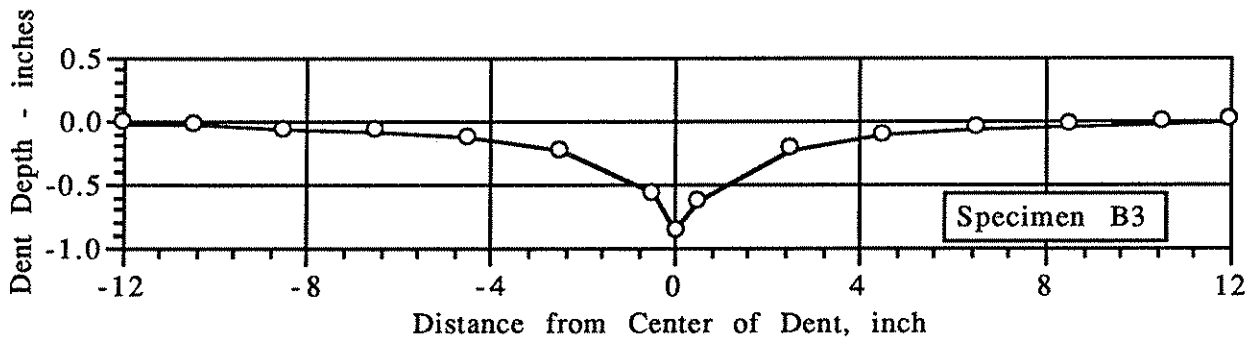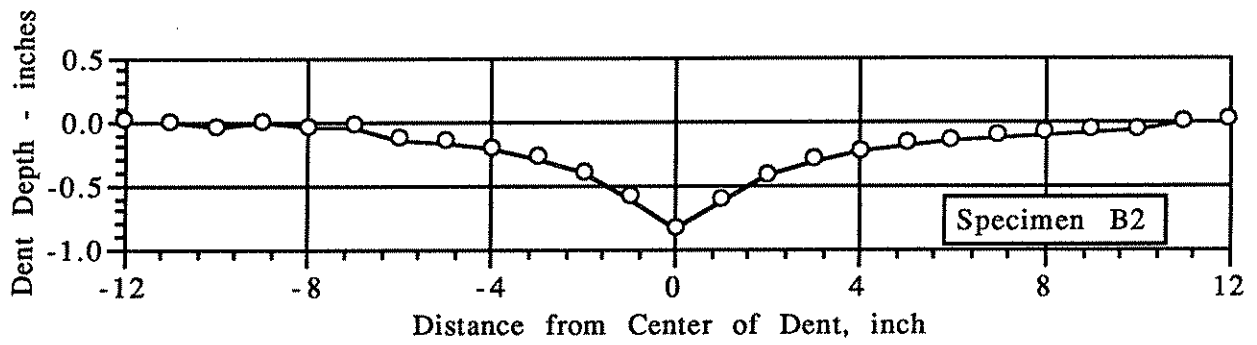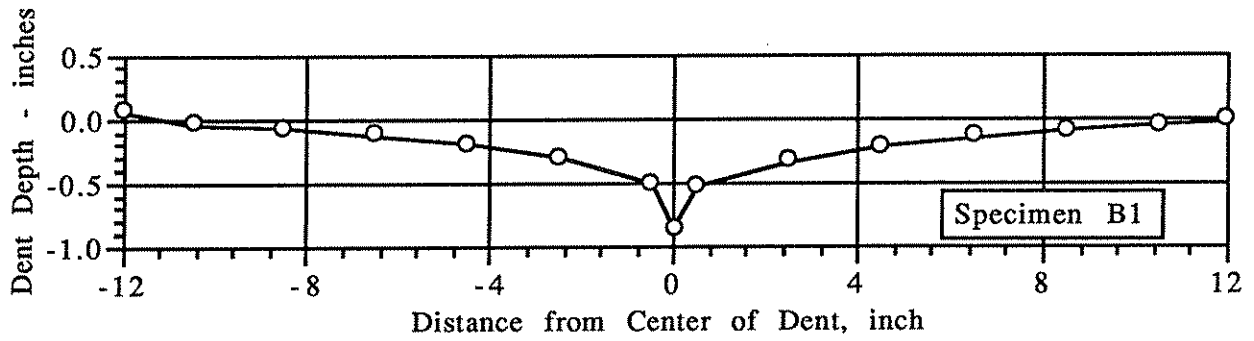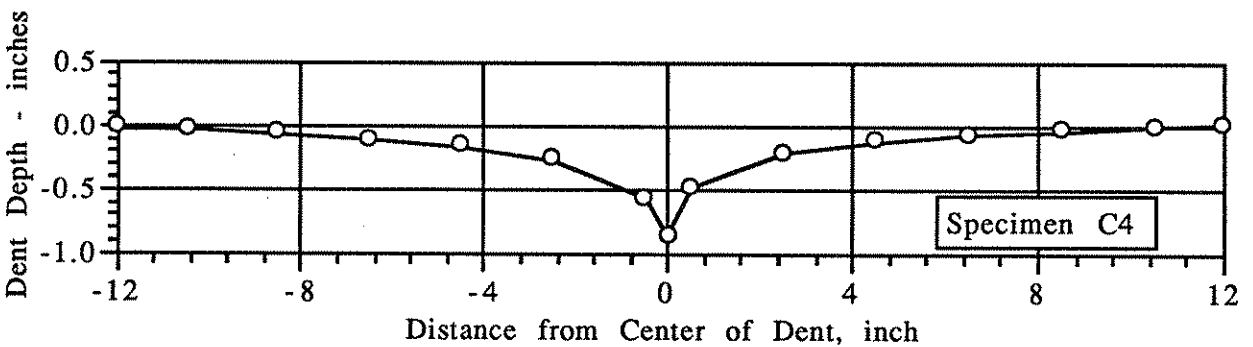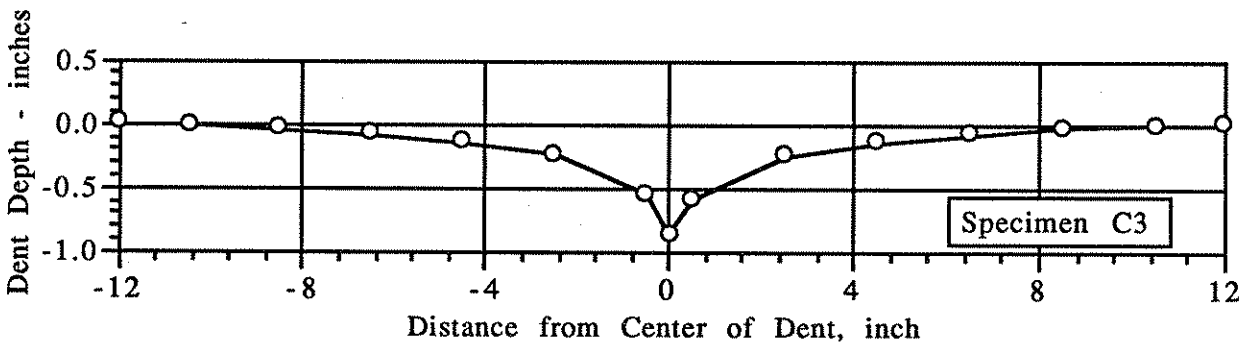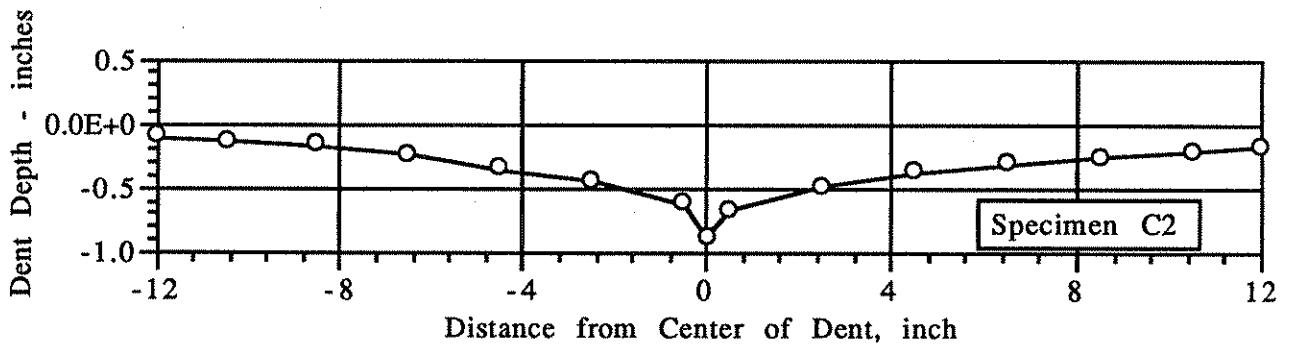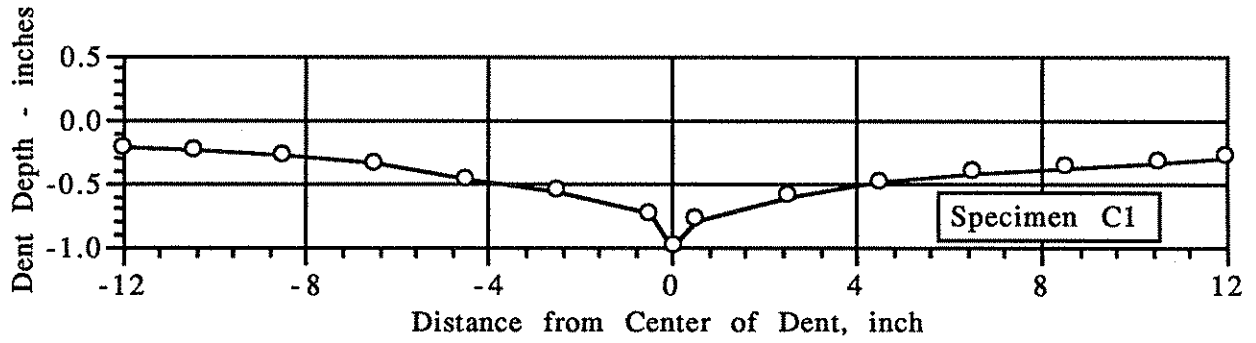
Appendix C -
Moment-Curvature Analysis of Internally
Grout Repaired Specimens

SPECIMEN A3 - Input data

Grout repaired specimen with D/t=34.5 w/ dent depth = 0.8625 in.
34.8 ksi steel ERW pipe
4375 psi unconfined grout, essentially elastic-plastic steel stress-strain. 6/4/92

IPLCEN = 0 IF PLASTIC CENTROID LOCATION IS UNKNOWN
      = 1 IF PLASTIC CENTROID LOCATION IS FED IN
YPLCEN IS THE COORD. OF THE P.C. (= 0 IF UNKNOWN)

IPLCEN   YPLCEN
  0 0.0000000E+00

INDIC =0 FOR BILINEAR STEEL
      =1 FOR "CUBIC" STEEL
      =2 FOR RAMB. OSGOOD STEEL (& = 3 FOR USER DEFINED)

INDIC   DEPTH = H
  1 0.8625000E+01

NC = # OF CONC. LAYERS
NS = # OF STEEL LAYERS

 NC NS
 19 20

     ***** STEEL PROPERTIES & DISTRIBUTION *****
     ****

IF1 = # OF 1ST. STEEL LAYER WHOSE STRESS-STRAIN HIST. IS SAVED
IF = 0: NO SAVING ----- IF1 =
  1

SIMILARLY, FOR 2ND. LAYER ---- IF2 =
  4

NGS =# OF STEEL LAYER GROUPS
NBIL=# OF STEEL TYPES
 NGS NBIL
 12   2

IAS = GROUP NUMBER
YS = COORDINATE
MATSTL = STEEL TYPE

LAYER IAS   YS MATSTL
  1   1 0.1250E+00   1
  2   2 0.4531E+00   1
  3   3 0.8594E+00   1
  4   4 0.7766E+01   1
  5   5 0.1266E+01   1
  6   5 0.7359E+01   1
  7   6 0.1672E+01   1
  8   6 0.6953E+01   1

```
 9    7 0.2078E+01      1
10    7 0.6547E+01      1
11    8 0.2484E+01      1
12    8 0.6141E+01      1
13    9 0.2891E+01      1
14    9 0.5734E+01      1
15   10 0.3297E+01      1
16   10 0.5328E+01      1
17   11 0.3703E+01      1
18   11 0.4922E+01      1
19   12 0.4109E+01      1
20   12 0.4516E+01      1
```

GROUP #	LAYERS IN GROUP	AREA
1	1	0.4852E+00
2	1	0.5791E+00
3	1	0.3637E+00
4	1	0.1388E+01
5	2	0.2975E+00
6	2	0.2624E+00
7	2	0.2405E+00
8	2	0.2260E+00
9	2	0.2161E+00
10	2	0.2095E+00
11	2	0.2054E+00
12	2	0.2034E+00

TYPE NUMBER
   1

INIT. SLOPE HARD. SLOPE YIELD STRESS YIELD STRAIN
0.29000E+05 0.30000E+03 0.34800E+02 0.12000E-02

      EH   EMAX   FMAX   ALPHA
0.146000E+01 0.110000E+01 0.60000E+02 0.00000E+00

TYPE NUMBER
   2

INIT. SLOPE HARD. SLOPE YIELD STRESS YIELD STRAIN
0.29000E+05 0.30000E+03 0.49000E+01 0.16897E-03

      EH   EMAX   FMAX   ALPHA
0.146000E+01 0.110000E+01 0.60000E+02 0.00000E+00

      ****** CONCRETE PROPERTIES & DISTRIBUTION *****
      ****

NGC = # OF CONC. LAYER GROUPS
NCON= # OF CONC. TYPES

 NGC NCON
  10   1

IAC = GROUP NUMBER
YC = COORDINATE
MATCON = CONC. TYPE

LAYER	IAC	YC	MATCON
1	1	0.4531E+00	1
2	2	0.8594E+00	1
3	2	0.7766E+01	1
4	3	0.1266E+01	1
5	3	0.7359E+01	1
6	4	0.1672E+01	1
7	4	0.6953E+01	1
8	5	0.2078E+01	1
9	5	0.6547E+01	1
10	6	0.2484E+01	1
11	6	0.6141E+01	1
12	7	0.2891E+01	1
13	7	0.5734E+01	1
14	8	0.3297E+01	1
15	8	0.5328E+01	1
16	9	0.3703E+01	1
17	9	0.4922E+01	1
18	10	0.4109E+01	1
19	10	0.4516E+01	1

GROUP #	LAYERS IN GROUP	AREA
1	1	0.9692E+00
2	2	0.1729E+01
3	2	0.2178E+01
4	2	0.2505E+01
5	2	0.2754E+01
6	2	0.2946E+01
7	2	0.3090E+01
8	2	0.3194E+01
9	2	0.3262E+01
10	2	0.3295E+01

ZS = SLOPE OF LINEAR DESCENDING PORTION (= -FC*Z)
EC DEFAULT = 2*FC/E0

TYPE NUMBER
 1

ZS	E20C	FR	ER	E0	FC
-0.521000E+02	0.500000E-01	-0.025000E+00	-0.104000E-04	0.200000E-02	0.437600E+01

E1	P85FC	EC	ECR	PTFC
0.800000E-02	0.372000E+01	0.240000E+04	0.100000E-00	0.218800E+01

Offshore Dented Tube Specimen A, P=0, No Fsp effect
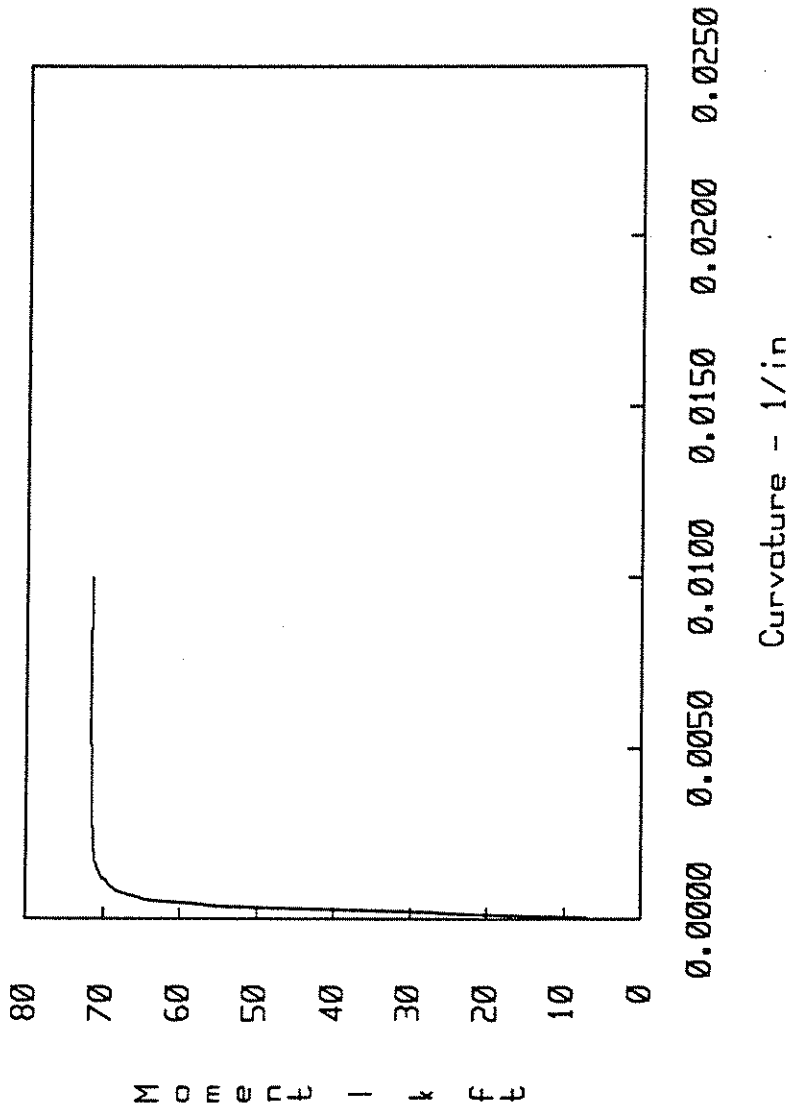
Offshore Dented Tube Specimen A, P=50, No Fsp effect
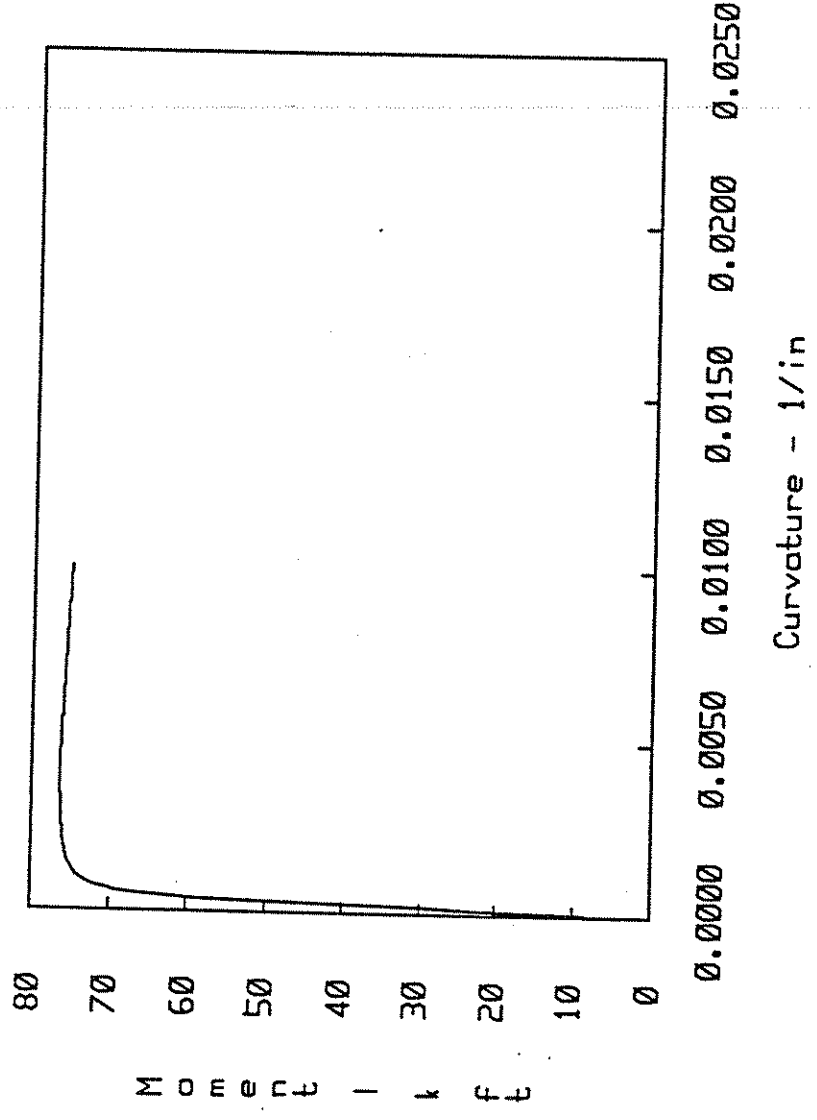
Offshore Dented Tube Specimen A, P=100, No Fsp effect
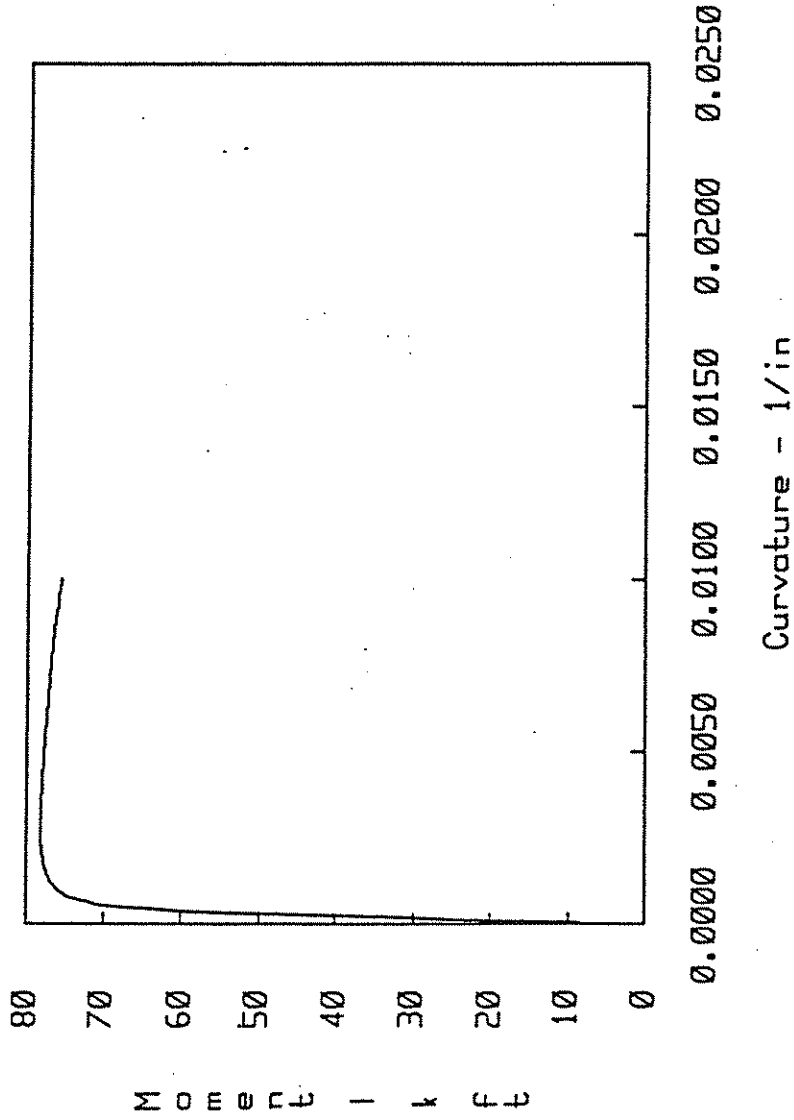
Offshore Dented Tube Specimen A, P=150, No Fsp effect

Moment - k ft

80
70
60
50
40
30
20
10
0

0.0000   0.0050   0.0100   0.0150   0.0200   0.0250

Curvature - 1/in
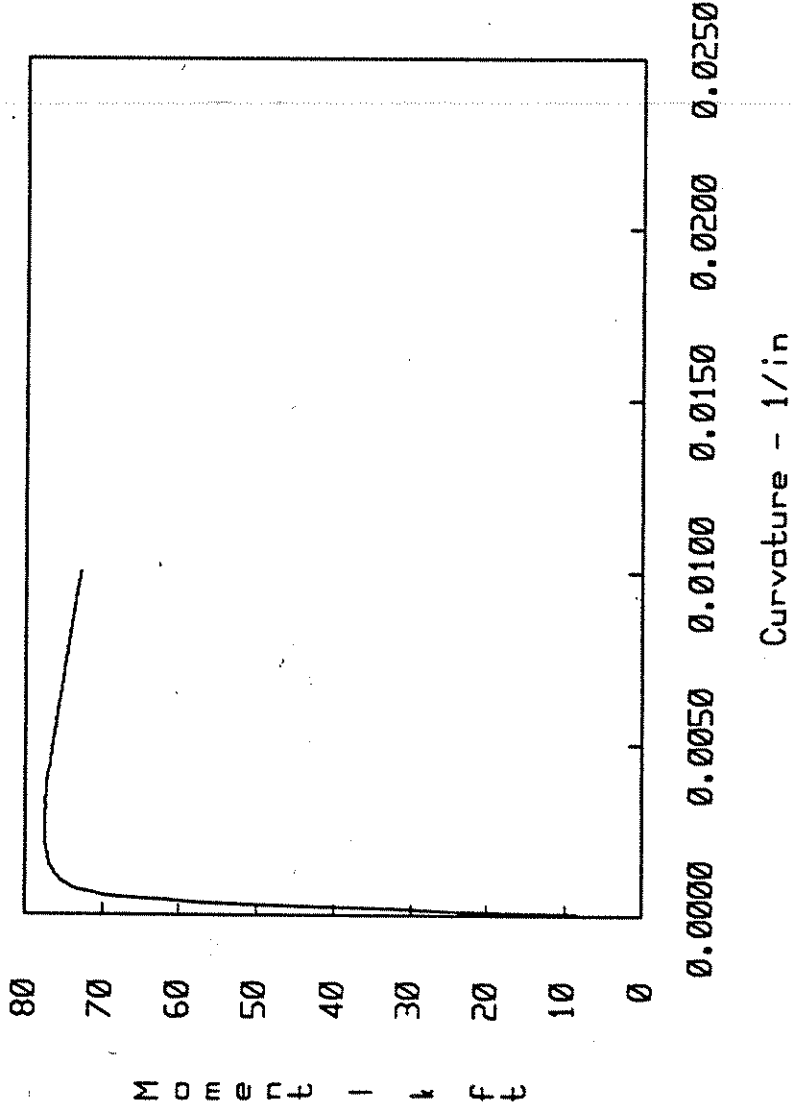
groucho 39%

Offshore Dented Tube Specimen A, P=200, No Fsp effect

Moment - k ft

Curvature - 1/in
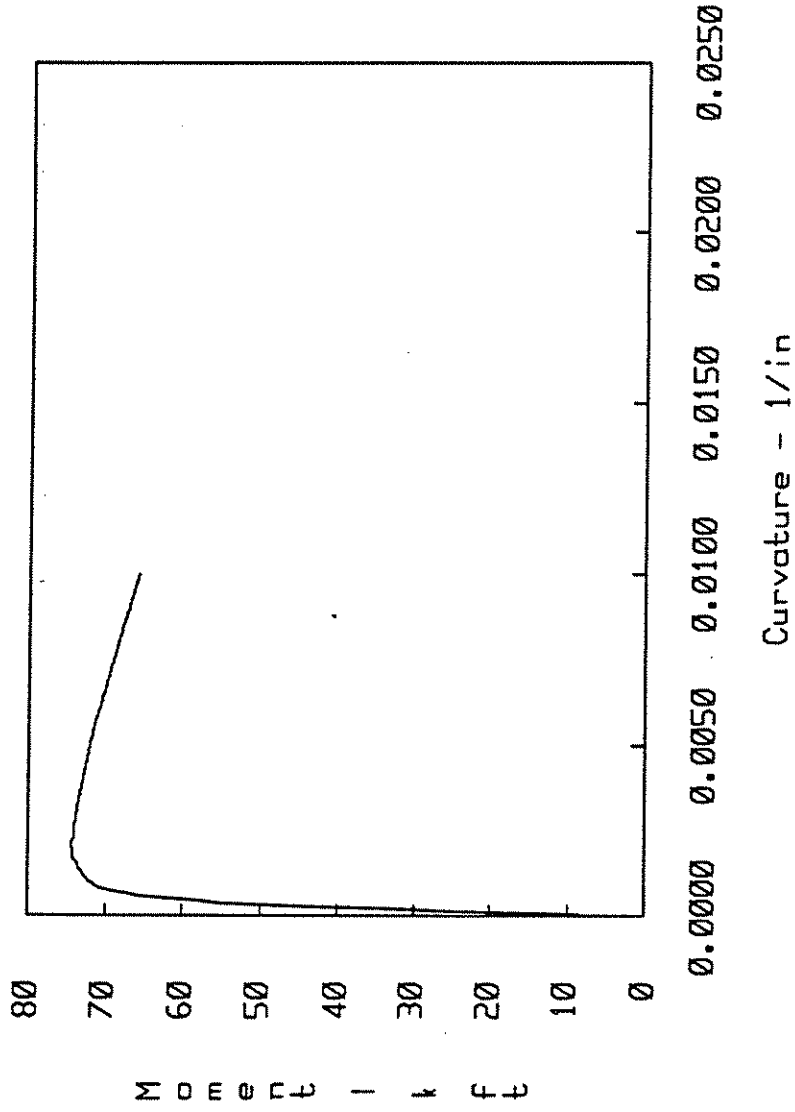
groucho 28%

Offshore Dented Tube Specimen A, P=250, No Fsp effect

groucho 41%

Offshore Dented Tube Specimen A, P=300, No Fsp effect

groucho 43%

Offshore Dented Tube Specimen A, P=350, No Fsp effect

Moment - k ft

Curvature - 1/in
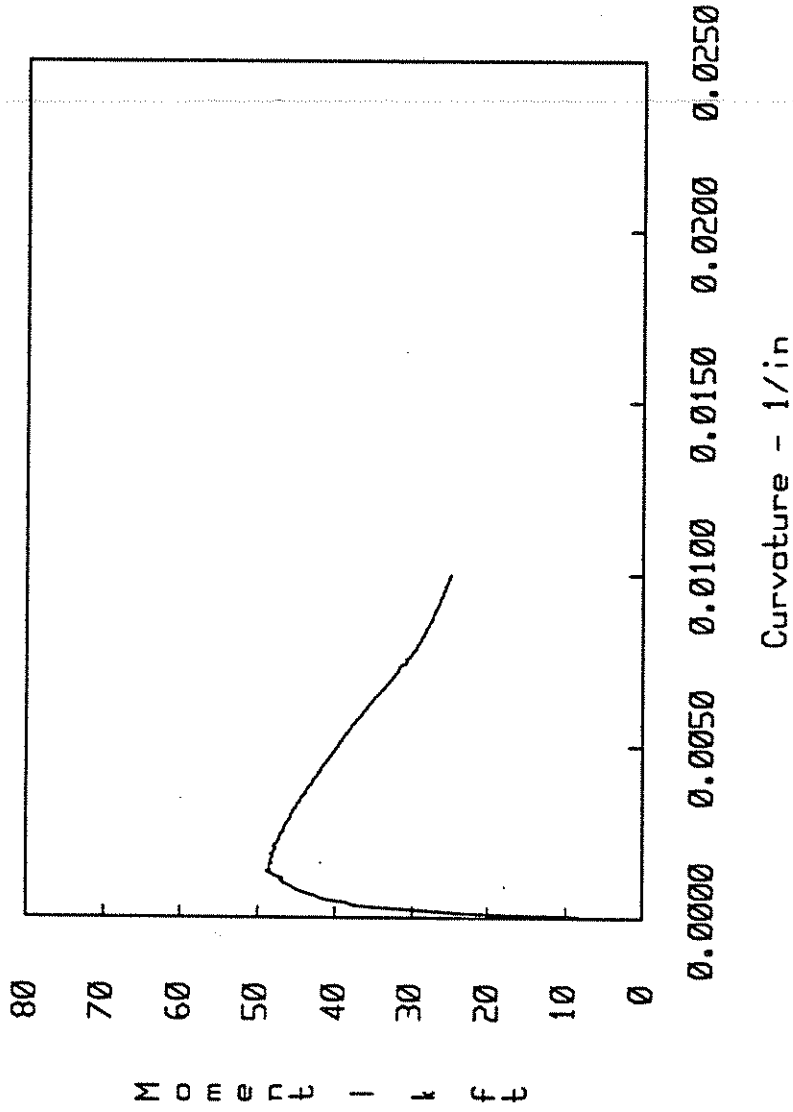
groucho 45%

Offshore Dented Tube Specimen A, P=400, No Fsp effect

Moment - k ft

80
70
60
50
40
30
20
10
0

0.0000 0.0050 0.0100 0.0150 0.0200 0.0250

Curvature - 1/in
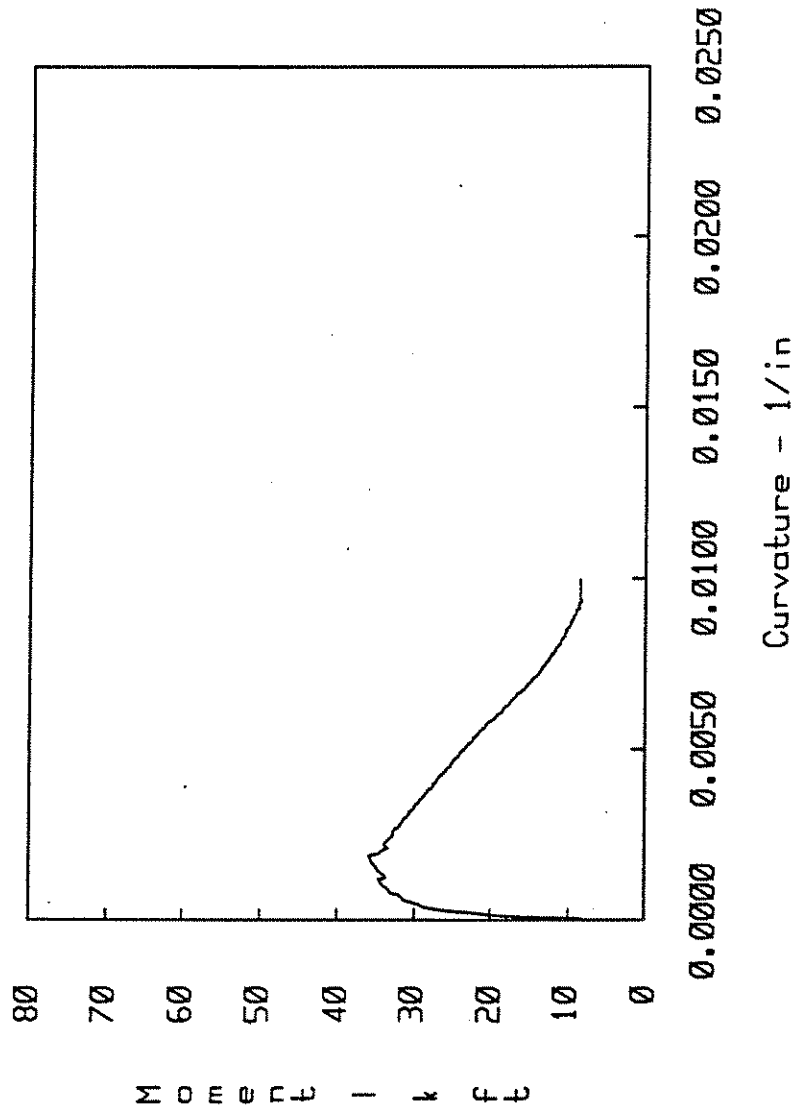
groucho 47%

Offshore Dented Tube Specimen A, P=450, No Fsp effect

Moment - kft

Curvature - 1/in

0.0000   0.0050   0.0100   0.0150   0.0200   0.0250

0   10   20   30   40   50   60   70   80
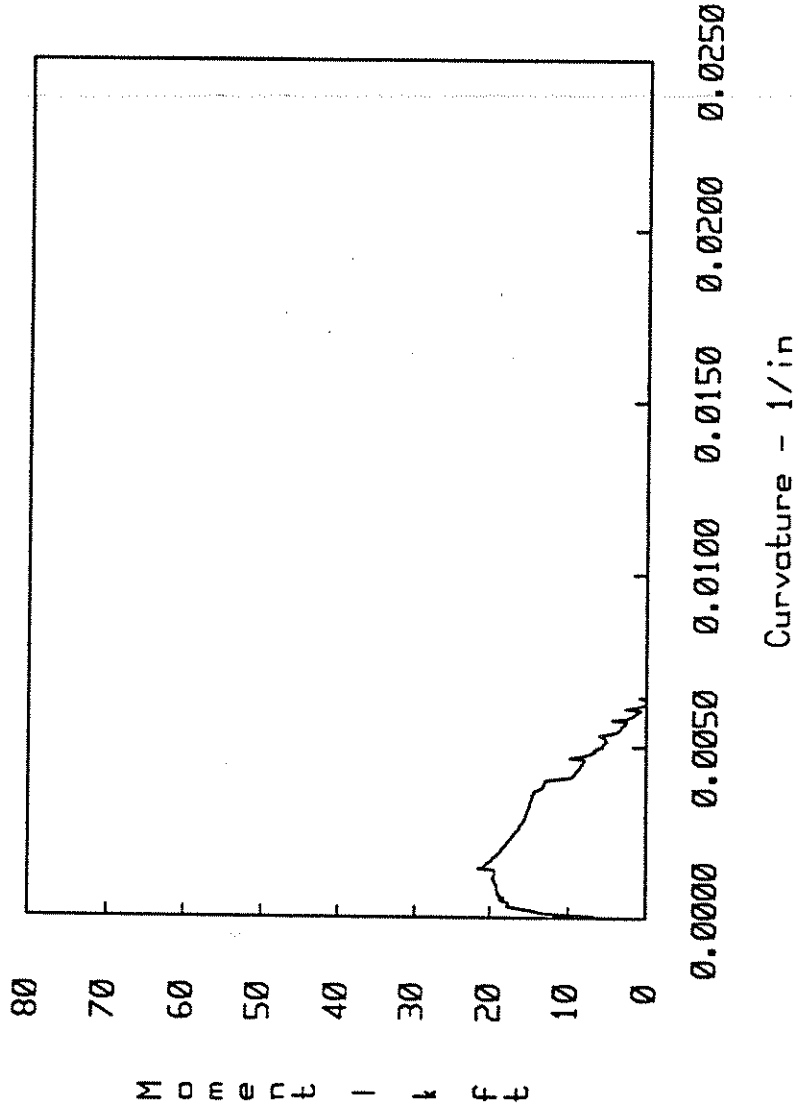
oroucho 49%

SPECIMEN B3 - Input data

Grout repaired specimen with D/t = 46 w/ dent depth = 0.8625 in.
33.4 ksi yield ERW steel pipe
3885 psi unconfined grout EPP steel behavior. 6/6/92

IPLCEN = 0 IF PLASTIC CENTROID LOCATION IS UNKNOWN
    = 1 IF PLASTIC CENTROID LOCATION IS FED IN
YPLCEN IS THE COORD. OF THE P.C. (= 0 IF UNKNOWN)

IPLCEN   YPLCEN
 0 0.0000000E+00

INDIC =0 FOR BILINEAR STEEL
    =1 FOR "CUBIC" STEEL
    =2 FOR RAMB. OSGOOD STEEL (& = 3 FOR USER DEFINED)

INDIC DEPTH = H
 1 0.8625000E+01

NC = # OF CONC. LAYERS
NS = # OF STEEL LAYERS

 NC NS
 18 20

    ***** STEEL PROPERTIES & DISTRIBUTION *****
    ****

IF1 = # OF 1ST. STEEL LAYER WHOSE STRESS-STRAIN HIST. IS SAVED
IF = 0: NO SAVING ------ IF1 =
  1

SIMILARLY, FOR 2ND. LAYER ---- IF2 =
  4

NGS =# OF STEEL LAYER GROUPS
NBIL=# OF STEEL TYPES
 NGS NBIL
 12   1

IAS = GROUP NUMBER
YS = COORDINATE
MATSTL = STEEL TYPE

LAYER	IAS	YS	MATSTL
1	1	0.9375E-01	1
2	2	0.3938E+00	1
3	3	0.8063E+00	1
4	4	0.7762E+01	1
5	5	0.1219E+01	1
6	5	0.7406E+01	1
7	6	0.1631E+01	1

8	6	0.6994E+01	1
9	7	0.2044E+01	1
10	7	0.6581E+01	1
11	8	0.2456E+01	1
12	8	0.6169E+01	1
13	9	0.2869E+01	1
14	9	0.5756E+01	1
15	10	0.3281E+01	1
16	10	0.5344E+01	1
17	11	0.3694E+01	1
18	11	0.4931E+01	1
19	12	0.4106E+01	1
20	12	0.4519E+01	1

GROUP #	LAYERS IN GROUP	AREA
1	1	0.3158E+00
2	1	0.4663E+00
3	1	0.2816E+00
4	1	0.1064E+01
5	2	0.2286E+00
6	2	0.2008E+00
7	2	0.1837E+00
8	2	0.1724E+00
9	2	0.1647E+00
10	2	0.1596E+00
11	2	0.1564E+00
12	2	0.1549E+00

TYPE NUMBER
   1

INIT. SLOPE	HARD. SLOPE	YIELD STRESS	YIELD STRAIN
0.29000E+05	0.30000E+03	0.33400E+02	0.11517E-02

EH	EMAX	FMAX	ALPHA
0.14600E+01	0.11000E+01	0.60000E+02	0.00000E+00

****** CONCRETE PROPERTIES & DISTRIBUTION *****
****

NGC = # OF CONC. LAYER GROUPS
NCON= # OF CONC. TYPES

NGC	NCON
10	1

IAC = GROUP NUMBER
YC = COORDINATE
MATCON = CONC. TYPE

LAYER	IAC	YC	MATCON
1	1	0.3938E+00	1
2	2	0.8063E+00	1
3	3	0.1219E+01	1
4	3	0.7406E+01	1
5	4	0.1631E+01	1
6	4	0.6994E+01	1

```
 7    5 0.2044E+01     1
 8    5 0.6581E+01     1
 9    6 0.2456E+01     1
10    6 0.6169E+01     1
11    7 0.2869E+01     1
12    7 0.5756E+01     1
13    8 0.3281E+01     1
14    8 0.5344E+01     1
15    9 0.3694E+01     1
16    9 0.4931E+01     1
17   10 0.4106E+01     1
18   10 0.4519E+01     1
```

GROUP #	LAYERS IN GROUP	AREA
1	1	0.9993E+00
2	1	0.1783E+01
3	2	0.2246E+01
4	2	0.2583E+01
5	2	0.2840E+01
6	2	0.3037E+01
7	2	0.3186E+01
8	2	0.3293E+01
9	2	0.3363E+01
10	2	0.3397E+01

ZS = SLOPE OF LINEAR DESCENDING PORTION (= -FC*Z)
EC DEFAULT = 2*FC/E0

TYPE NUMBER
  1

```
    ZS        E20C        FR        ER        E0        FC
-0.462500E+02 0.500000E-01-0.025000E+00-0.104000E-04 0.200000E-02 0.388500E+01

    E1       P85FC        EC        ECR       PTFC
0.800000E-02 0.330225E+01 0.240000E+04 0.100000E-00 0.194250E+01
```

202

Offshore Dented Tube Specimen B, P=0, No Fsp effect
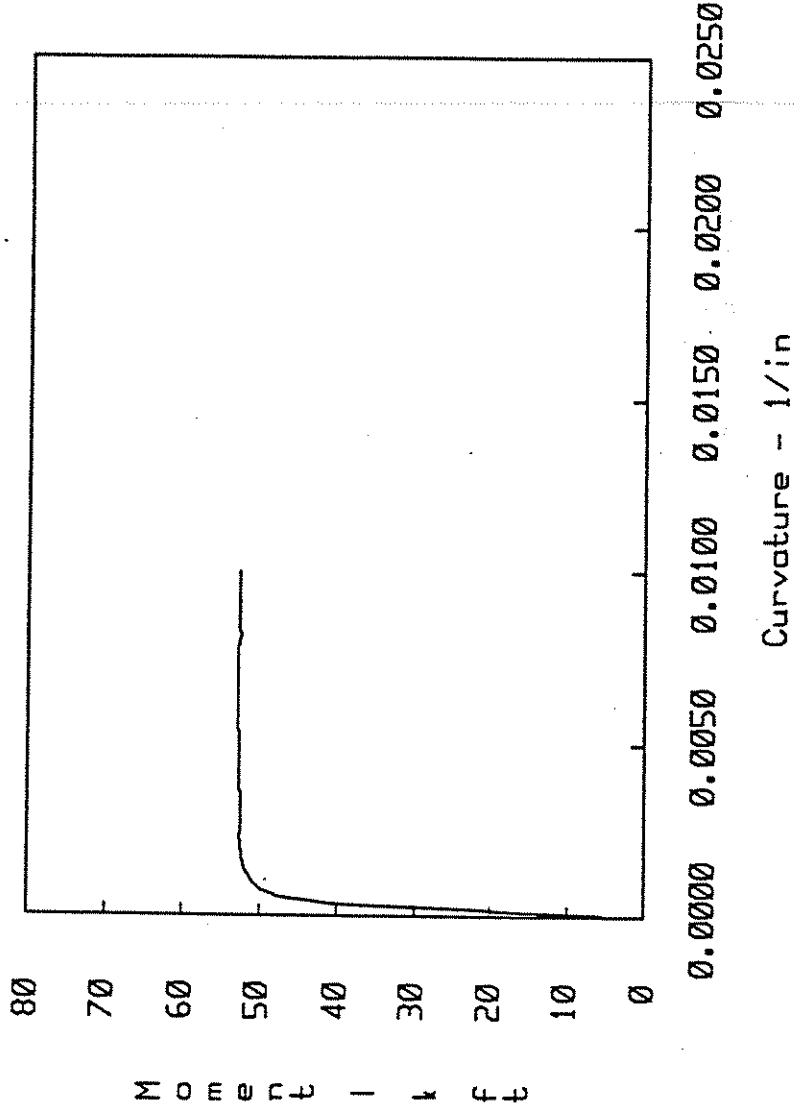
Offshore Dented Tube Specimen B, P=50, No Fsp effect

Curvature - 1/in

Moment - k ft
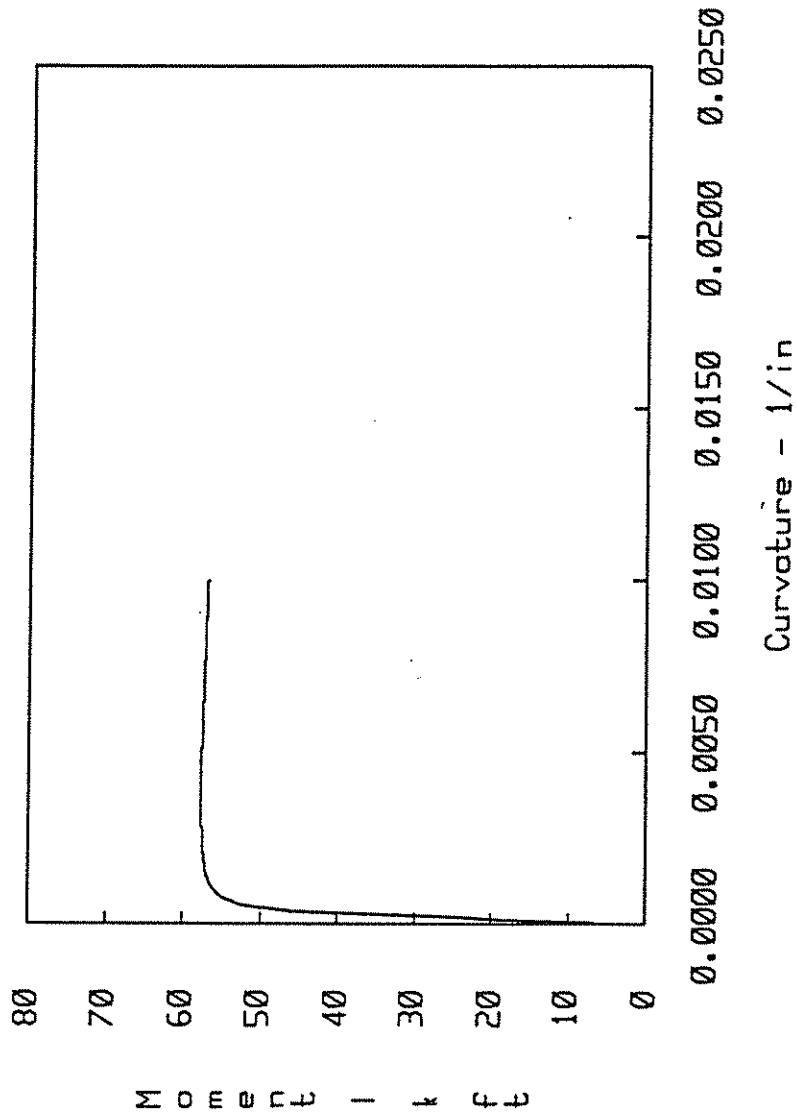
groucho 12%

Offshore Dented Tube Specimen B, P=100, No Fsp effect

Moment - k ft

80
70
60
50
40
30
20
10
0

0.0000 0.0050 0.0100 0.0150 0.0200 0.0250

Curvature - 1/in
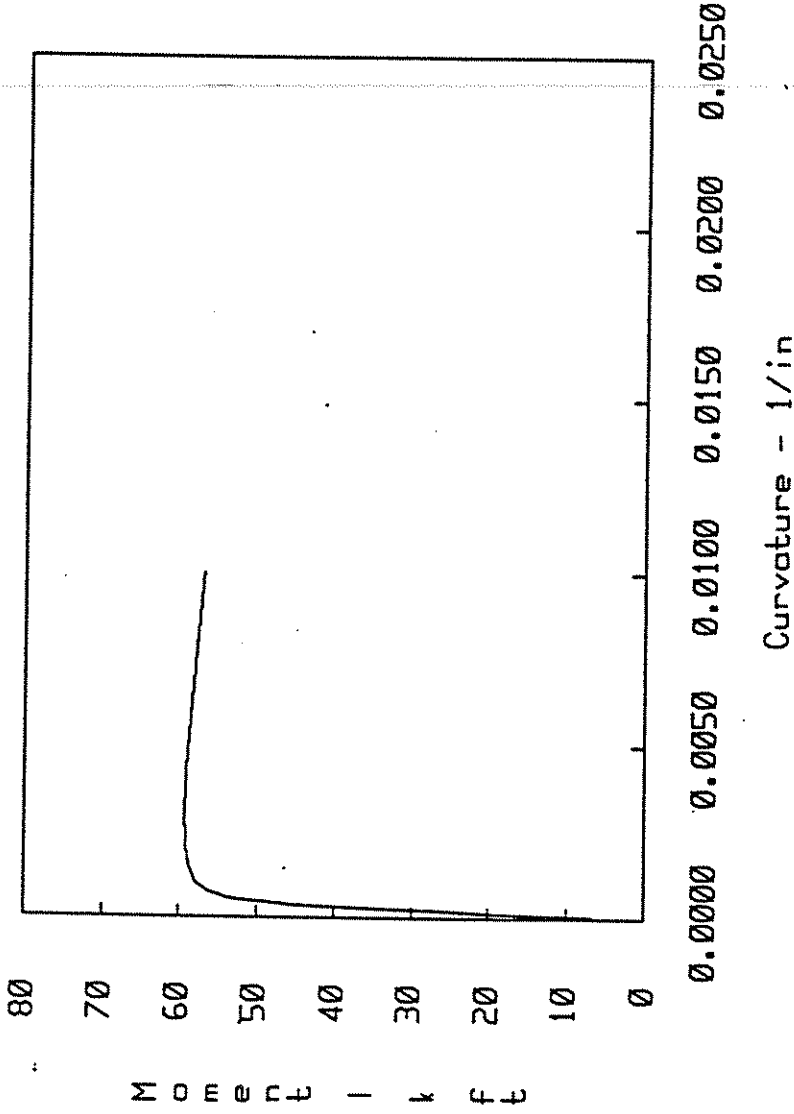
Offshore Dented Tube Specimen B, P=150, No Fsp effect

Curvature – 1/in

Moment – k ft

araucho 16%

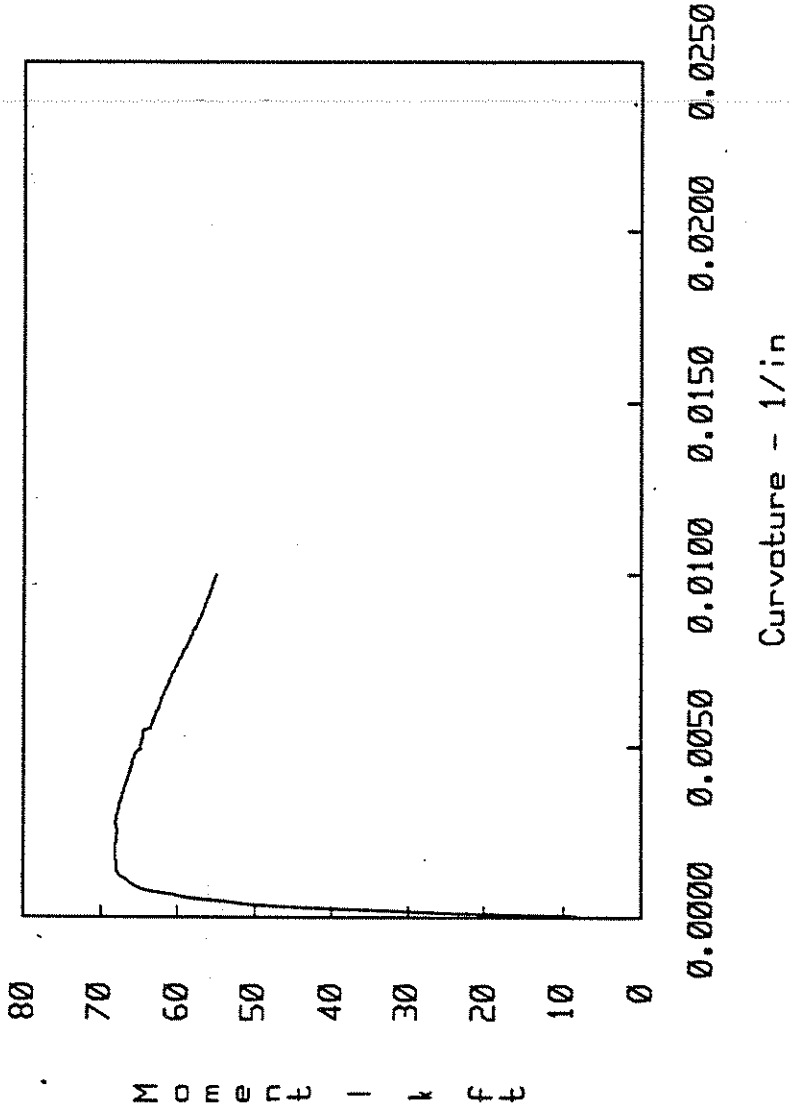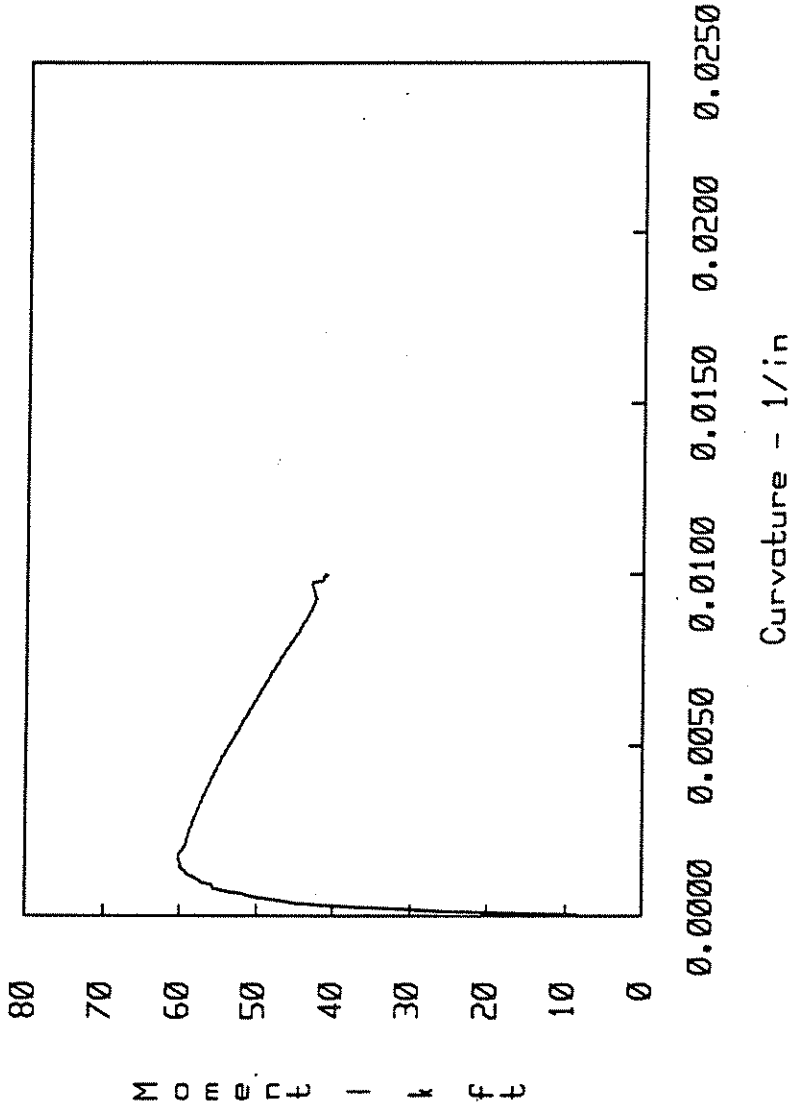Offshore Dented Tube Specimen B, P=200, No Fsp effect

groucho 18%

Offshore Dented Tube Specimen B, P=250, No Fsp effect

groucho 20%

Offshore Dented Tube Specimen B, P=300, No Fsp effect

Moment - k ft

Curvature - 1/in
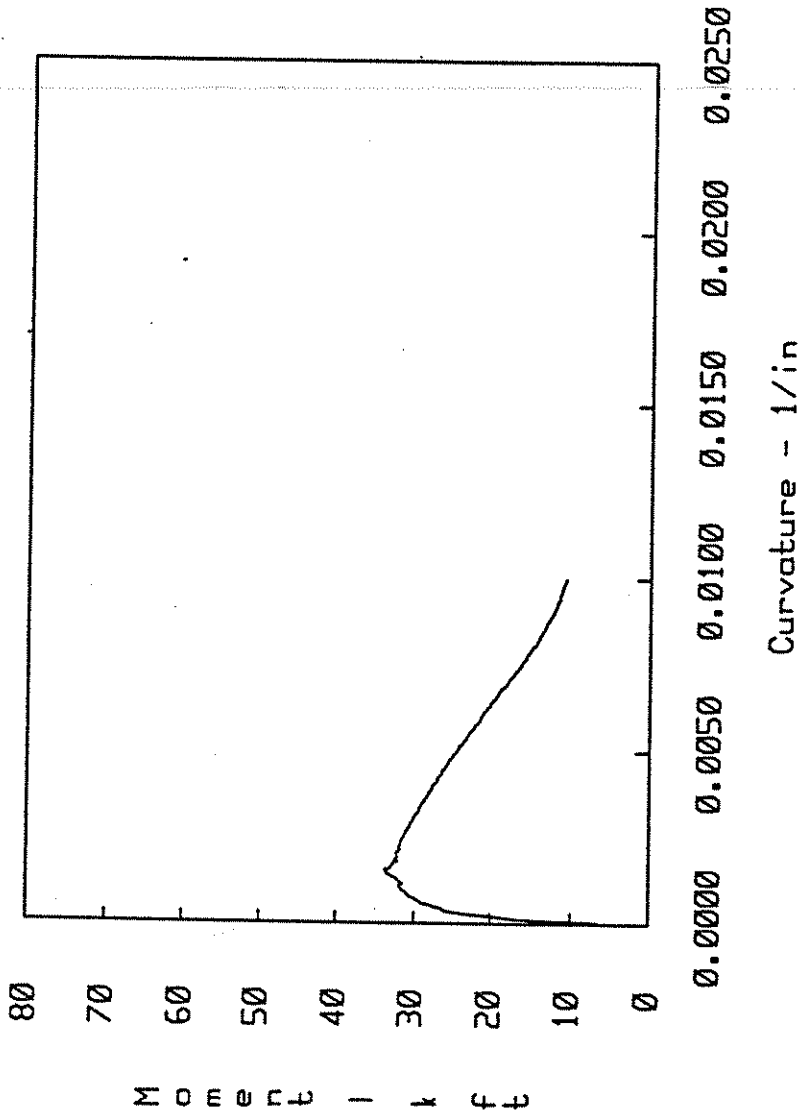
oroucho 22%

SPECIMEN C3 - INPUT DATA

Grout Repaired specimen with D/t=64 w/ dent depth =0.8625 in.
39.4 ksi steel ERW pipe
6894 psi unconfined grout, EPP steel behavior. 6/6/92

IPLCEN = 0 IF PLASTIC CENTROID LOCATION IS UNKNOWN
     = 1 IF PLASTIC CENTROID LOCATION IS FED IN
YPLCEN IS THE COORD. OF THE P.C. (= 0 IF UNKNOWN)

IPLCEN   YPLCEN
 0 0.0000000E+00

INDIC =0 FOR BILINEAR STEEL
    =1 FOR "CUBIC" STEEL
    =2 FOR RAMB. OSGOOD STEEL (& = 3 FOR USER DEFINED)

INDIC   DEPTH = H
 1 0.8625000E+01

NC = # OF CONC. LAYERS
NS = # OF STEEL LAYERS

 NC NS
 18 20

     ***** STEEL PROPERTIES & DISTRIBUTION *****
     ****

IF1 = # OF 1ST. STEEL LAYER WHOSE STRESS-STRAIN HIST. IS SAVED
IF = 0: NO SAVING ----- IF1 =
  1

SIMILARLY, FOR 2ND. LAYER ---- IF2 =
  4

NGS =# OF STEEL LAYER GROUPS
NBIL=# OF STEEL TYPES
 NGS NBIL
 12   1

IAS = GROUP NUMBER
YS = COORDINATE
MATSTL = STEEL TYPE

LAYER	IAS	YS	MATSTL
1	1	0.6750E-01	1
2	2	0.3439E+00	1
3	3	0.7616E+00	1
4	4	0.7695E+01	1
5	5	0.1179E+01	1
6	5	0.7446E+01	1
7	6	0.1597E+01	1

```
 8    6 0.7028E+01     1
 9    7 0.2015E+01     1
10    7 0.6610E+01     1
11    8 0.2433E+01     1
12    8 0.6192E+01     1
13    9 0.2850E+01     1
14    9 0.5775E+01     1
15   10 0.3268E+01     1
16   10 0.5357E+01     1
17   11 0.3686E+01     1
18   11 0.4939E+01     1
19   12 0.4104E+01     1
20   12 0.4521E+01     1
```

GROUP #	LAYERS IN GROUP	AREA
1	1	0.1933E+00
2	1	0.3597E+00
3	1	0.2084E+00
4	1	0.7493E+00
5	2	0.1679E+00
6	2	0.1471E+00
7	2	0.1343E+00
8	2	0.1259E+00
9	2	0.1202E+00
10	2	0.1164E+00
11	2	0.1141E+00
12	2	0.1130E+00

TYPE NUMBER
   1

INIT. SLOPE	HARD. SLOPE	YIELD STRESS	YIELD STRAIN
0.29000E+05	0.30000E+03	0.39400E+02	0.13586E-02

EH	EMAX	FMAX	ALPHA
0.46000E-01	0.10000E+00	0.60000E+02	0.00000E+00

****** CONCRETE PROPERTIES & DISTRIBUTION *****
****

NGC = # OF CONC. LAYER GROUPS
NCON= # OF CONC. TYPES

```
 NGC  NCON
 10    1
```

IAC = GROUP NUMBER
YC = COORDINATE
MATCON = CONC. TYPE

LAYER	IAC	YC	MATCON
1	1	0.3439E+00	1
2	2	0.7616E+00	1
3	3	0.1179E+01	1
4	3	0.7446E+01	1
5	4	0.1597E+01	1
6	4	0.7028E+01	1

```
 7    5 0.2015E+01      1
 8    5 0.6610E+01      1
 9    6 0.2433E+01      1
10     6 0.6192E+01     1
11     7 0.2850E+01     1
12     7 0.5775E+01     1
13     8 0.3268E+01     1
14     8 0.5357E+01     1
15     9 0.3686E+01     1
16     9 0.4939E+01     1
17    10 0.4104E+01      1
18    10 0.4521E+01      1
```

GROUP #	LAYERS IN GROUP	AREA
1	1	0.1025E+01
2	1	0.1828E+01
3	2	0.2304E+01
4	2	0.2649E+01
5	2	0.2912E+01
6	2	0.3115E+01
7	2	0.3268E+01
8	2	0.3378E+01
9	2	0.3449E+01
10	2	0.3484E+01

ZS = SLOPE OF LINEAR DESCENDING PORTION (= -FC*Z)
EC DEFAULT = 2*FC/E0

TYPE NUMBER
   1

```
    ZS      E20C       FR       ER       E0       FC
-0.521000E+02 0.500000E-01-0.250000E-01-0.104000E-04 0.200000E-02 0.689400E+01

    E1      P85FC       EC      ECR      PTFC
0.800000E-02 0.372000E+01 0.240000E+04 0.100000E+00 0.218800E+01
```

Offshore Dented Tube Specimen C, P=0, No Fsp effect
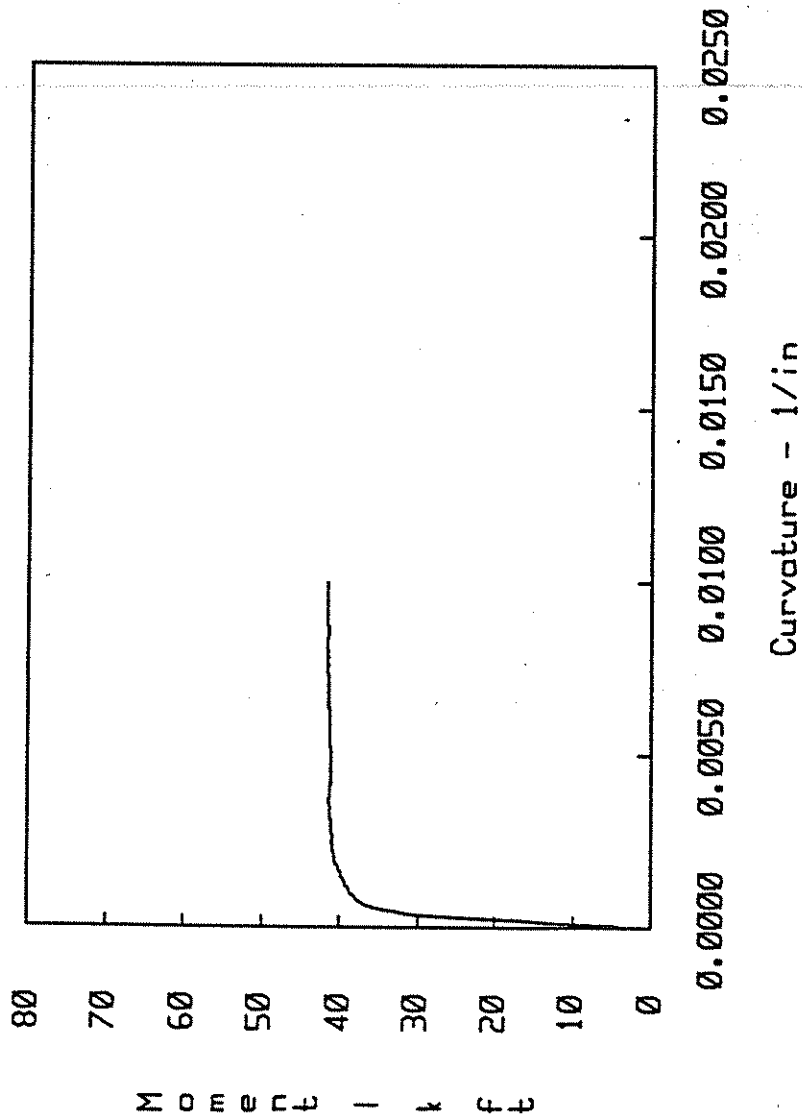
araucho 48%

Offshore Dented Tube Specimen C, P=50, No Fsp effect

Moment - k ft

80

70

60

50

40

30

20

10

0

0.0000 0.0050 0.0100 0.0150 0.0200 0.0250

Curvature - 1/in
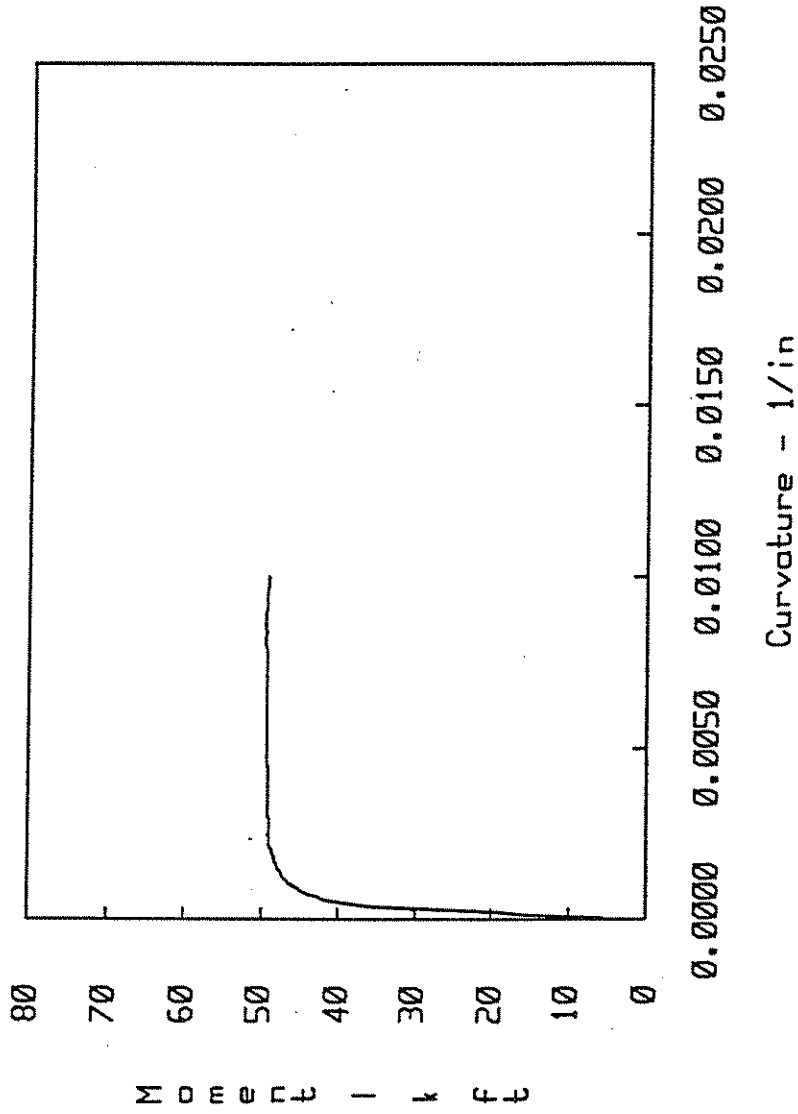
groucho 50%

Offshore Dented Tube Specimen C, P=100, No Fsp effect

Moment - k ft

80
70
60
50
40
30
20
10
0

0.0000 0.0050 0.0100 0.0150 0.0200 0.0250

Curvature - 1/in
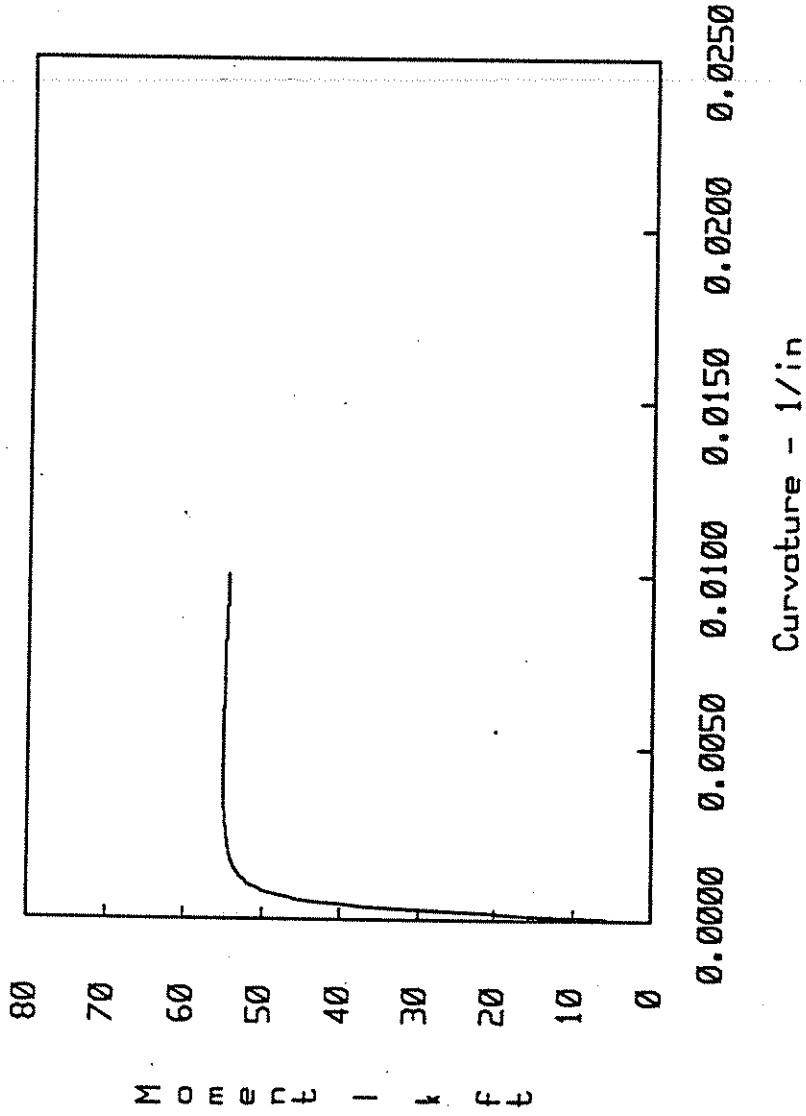
groucho 52%

Offshore Dented Tube Specimen C, P=150, No Fsp effect

Curvature - 1/in

Moment - k ft

groucho 54%

216
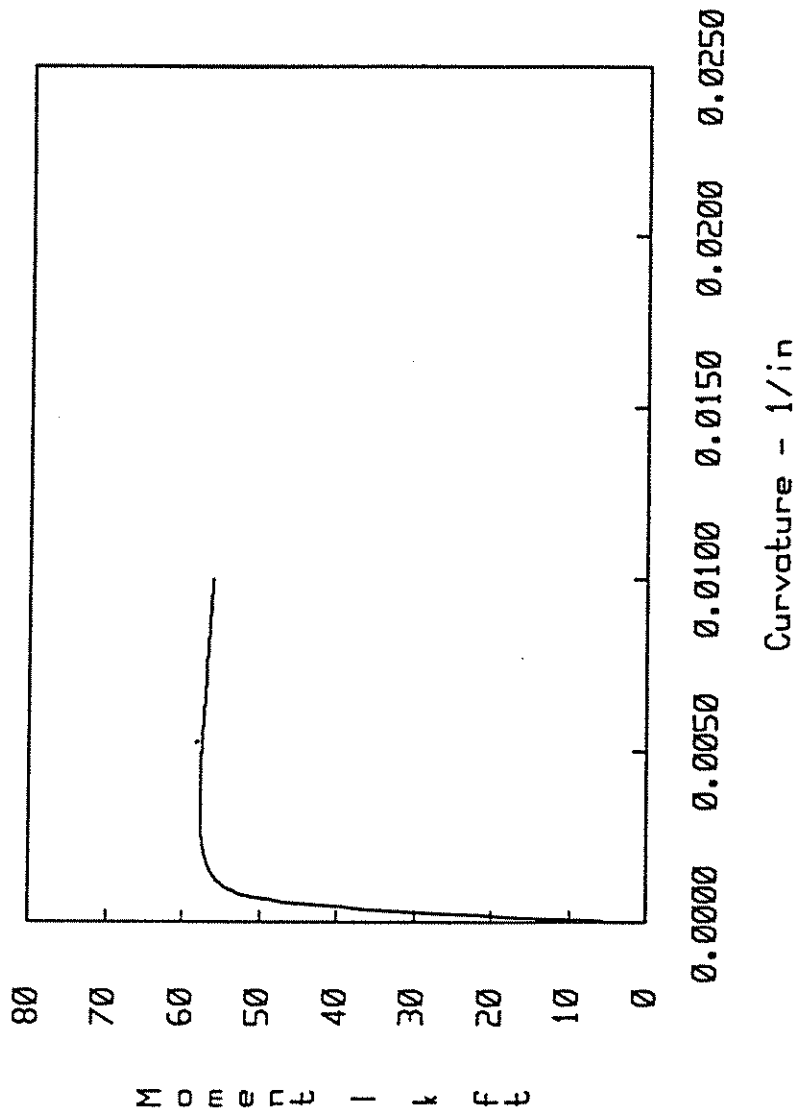
Offshore Dented Tube Specimen C, P=200, No Fsp effect
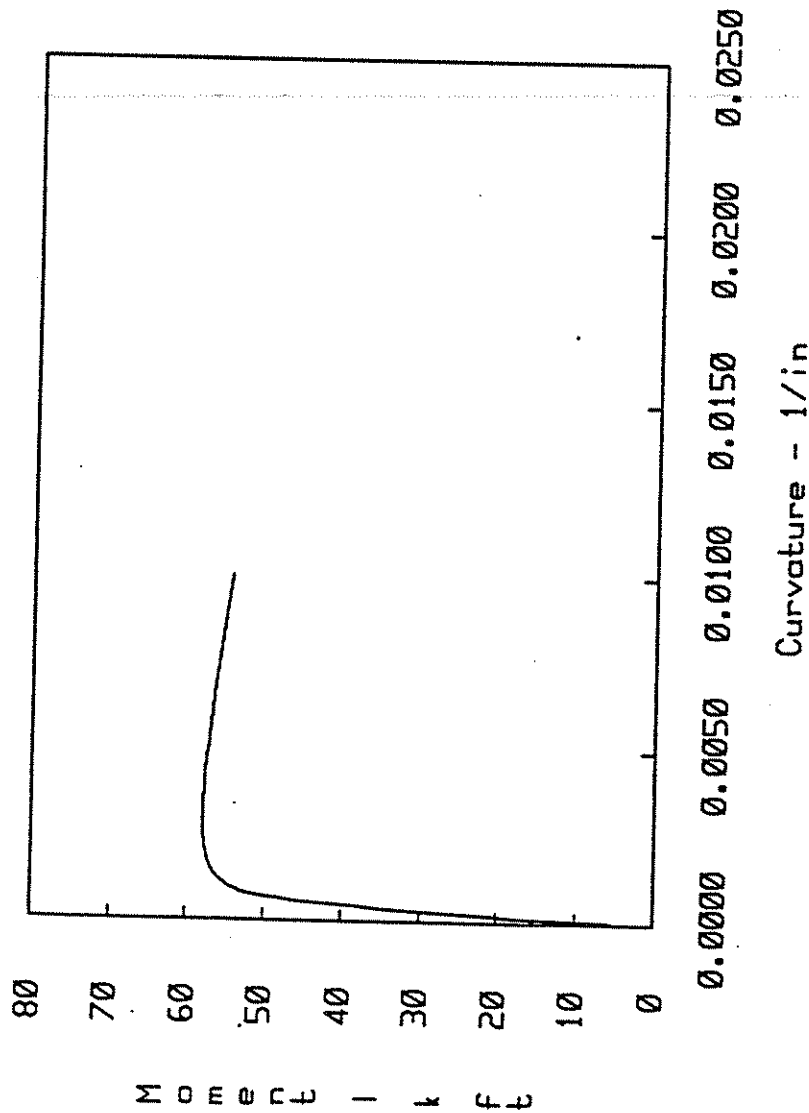
groucho 57%

Offshore Dented Tube Specimen C, P=250, No Fsp effect

Moment - k ft

80
70
60
50
40
30
20
10
0

0.0000   0.0050   0.0100   0.0150   0.0200   0.0250

Curvature - 1/in
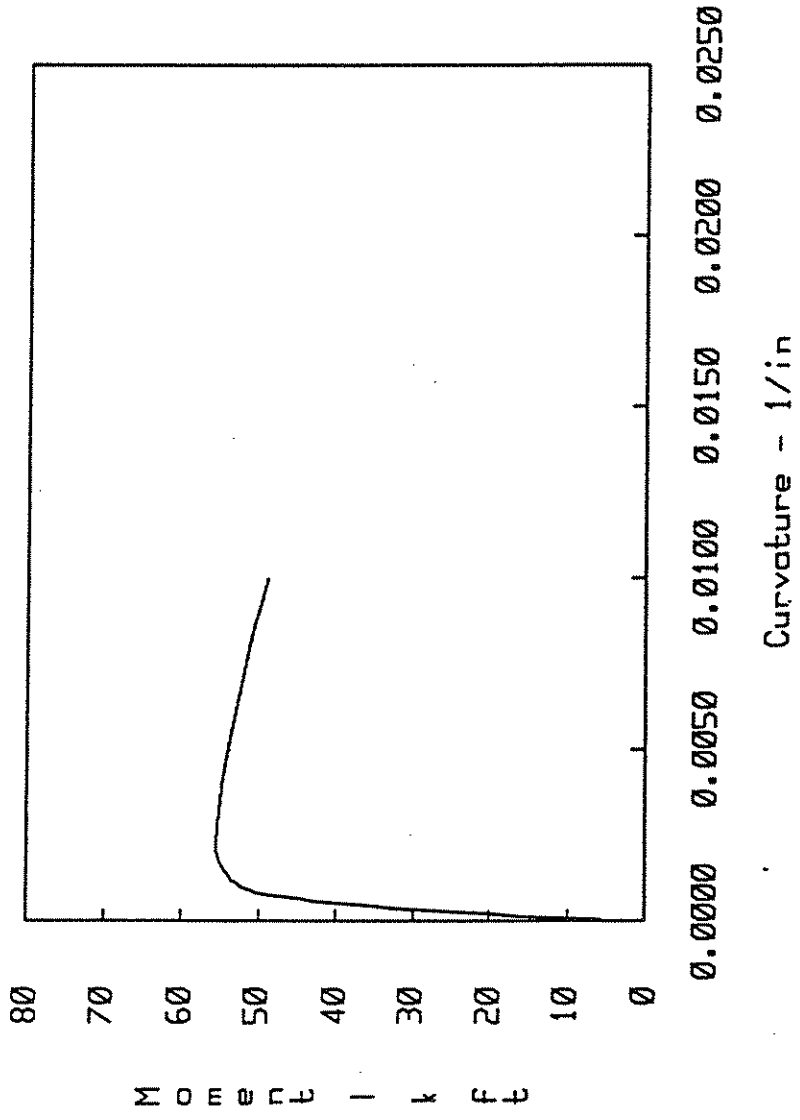
groucho 59%

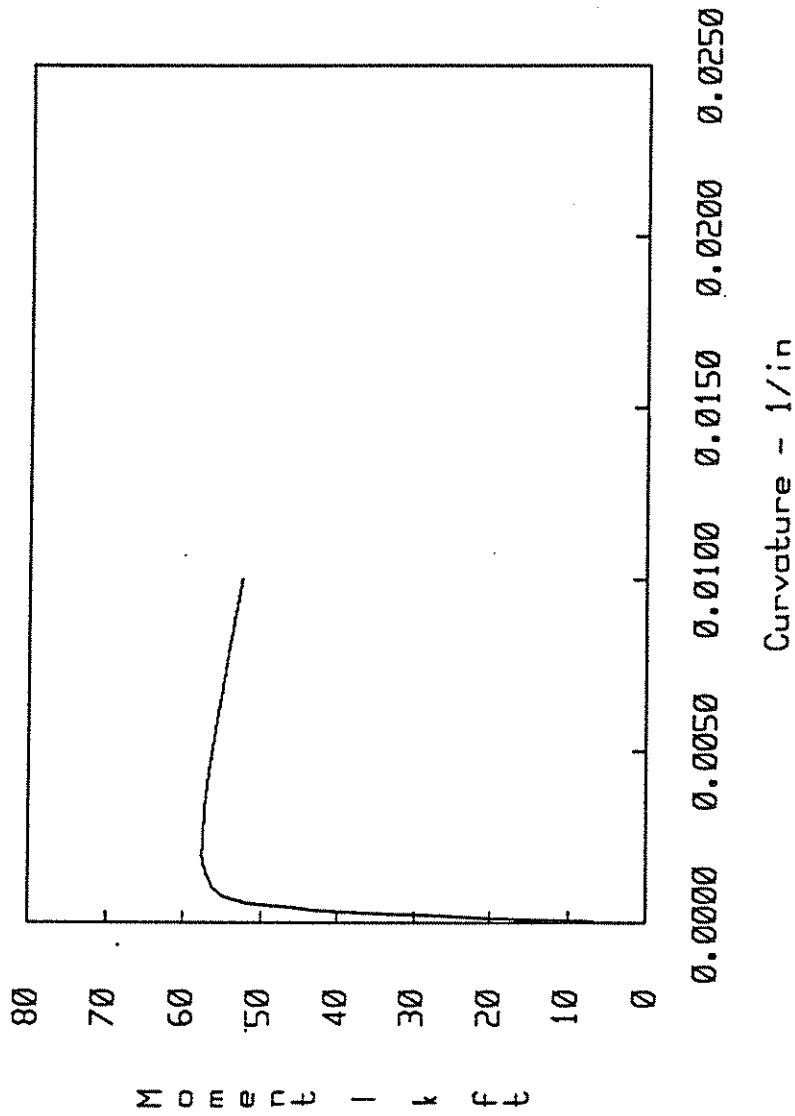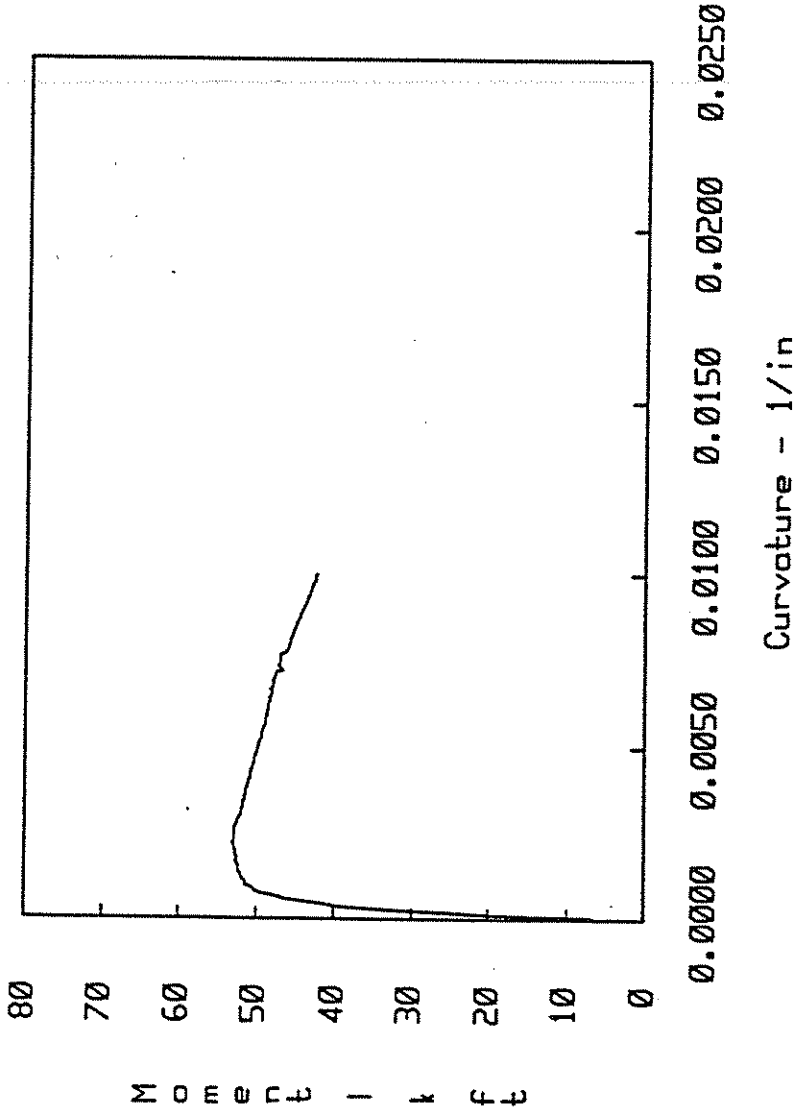Offshore Dented Tube Specimen C, P=300, No Fsp effect

Curvature - 1/in
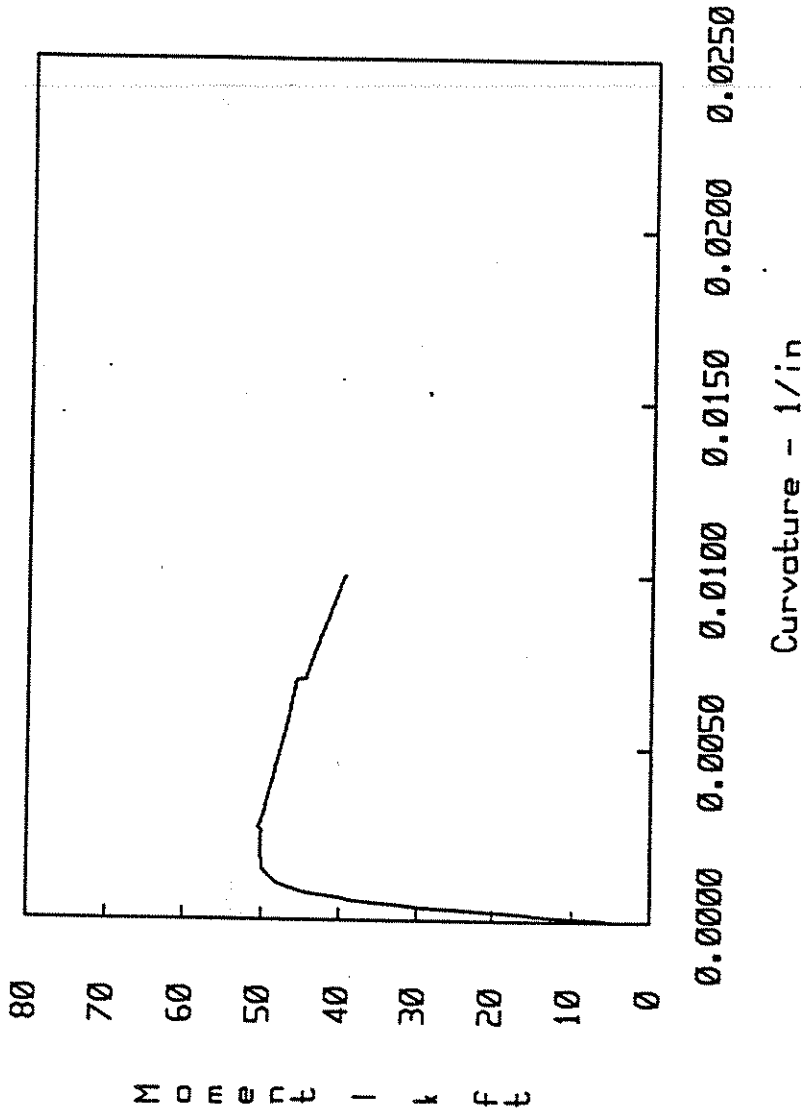
groucho 61%

Offshore Dented Tube Specimen C, P=350, No Fsp effect
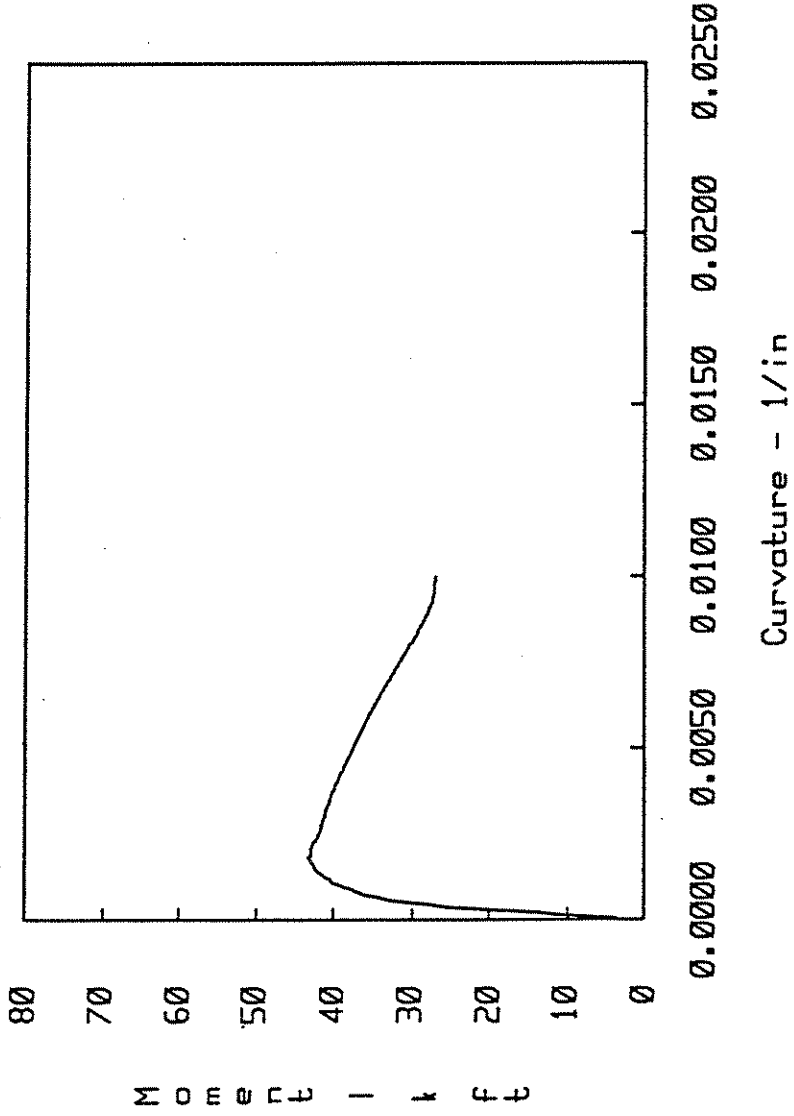
araucho 63%
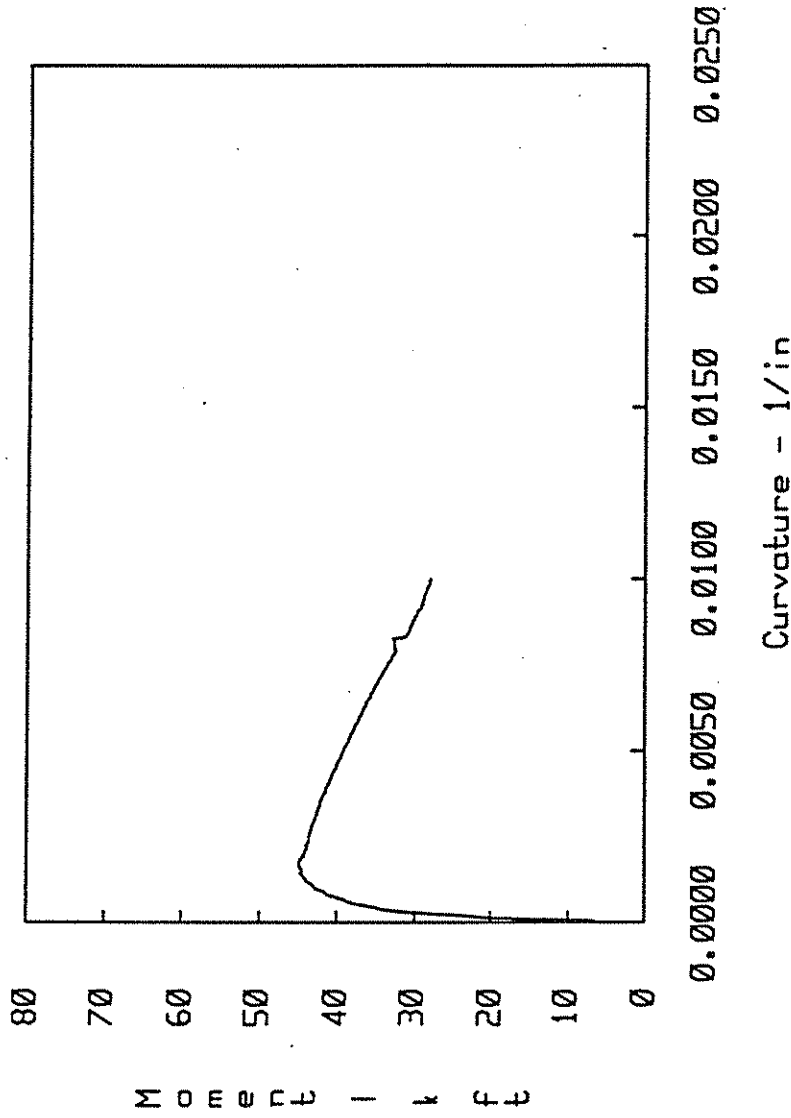
Offshore Dented Tube Specimen C, P=400, No Fsp effect

Moment - k-ft

Curvature - 1/in
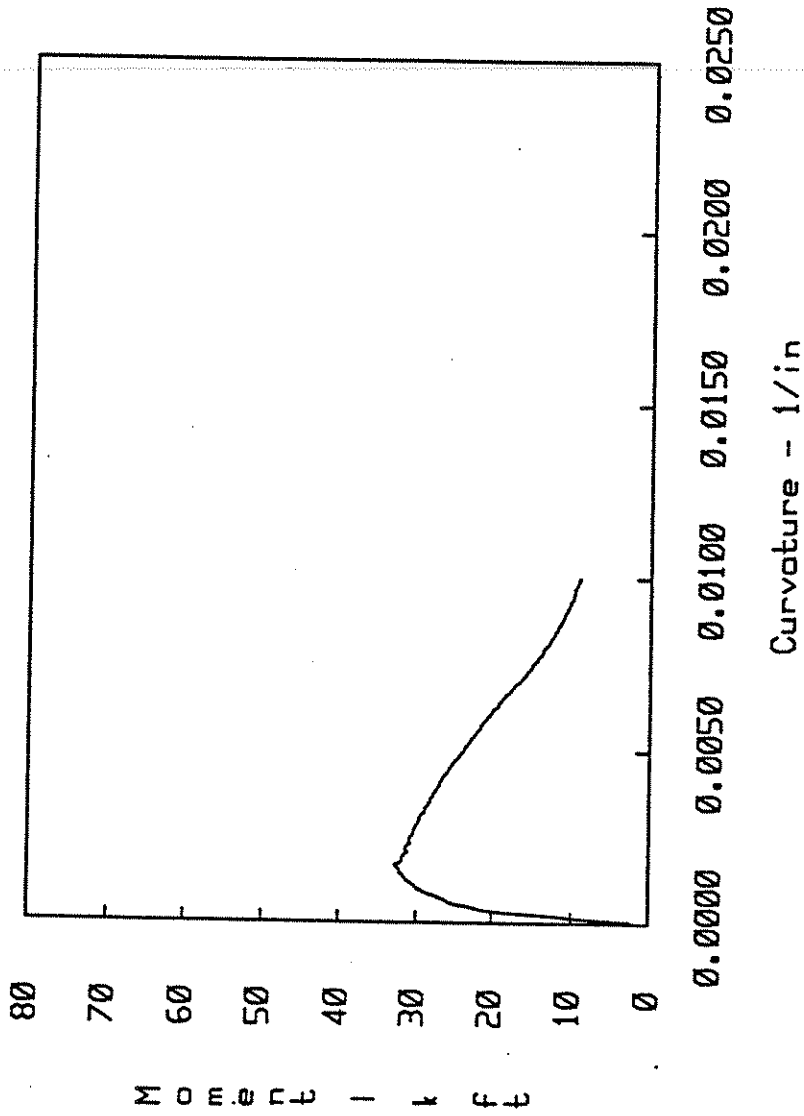
oraucho 65%

Appendix D -

Grouted Clamp Fabrication Drawings

Suggested Clamp Fabrication Sequence

1. Cut length of clamp (Carbon ERW Pipe with 42 ksi yield stress).
2. Cut slice along both sides of clamp, leaving a 2 inch length of material at each end uncut.
3. Tack weld small temporary plates across slice, spaced at 16 inches.
4. Weld stiffeners and plates of clamp (Part No. 1, 2, and 3), using a symmetric placement sequence to minimize distortion to clamp body due to welding.
5. Place one ring stiffener (Part No. 4) at each end of clamp.
6. Check fitup of clamp with member to be repaired, using a member of 8.625 in. outside diameter.
7. Cut clamp into two pieces, by removing remaining material along slices and temporary plates.
8. Place slice bearing plates (Part No. 5), using a symmetric placement sequence to minimize clamp distortion due to welding.
9. Recheck clamp fitup.

Exterior Clamp for Repair of Damaged Brace

Part No. 1

Part No. 2

Part No. 4

Part No. 5

Part No. 3

35.000

34.250

.750

16.306

8.500

4.425

E70 3/16

E70 3/16

.375

3.215

E70 3/16

E70 3/16

E70 3/16

E70 3/16

1.125

4.375 5.000

Grout inlet – to be sized

Grout outlet – to be sized

Centralizer studs, 1/2" bolt
4 each end
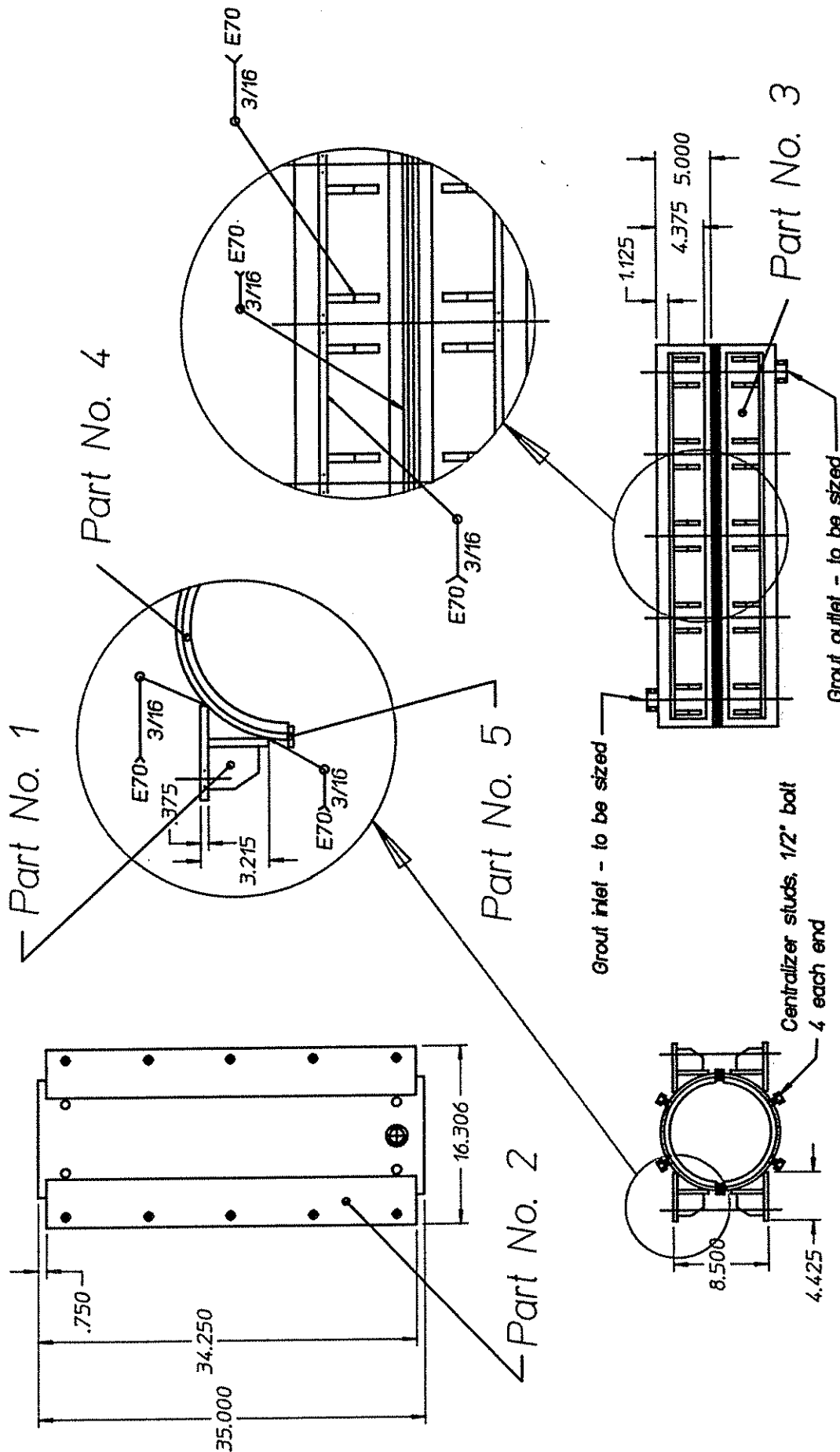
Note: All dimensions in inches

SCALE	DRAWN BY	APPROVED BY	BUDGET #	FILE NAME	Clamp_dsgn
	T. E. Gillum				
DATE	14 Jan 92	University of California, San Diego	REVISED	FAB #	DRAWING #

Fab. Part No. 1
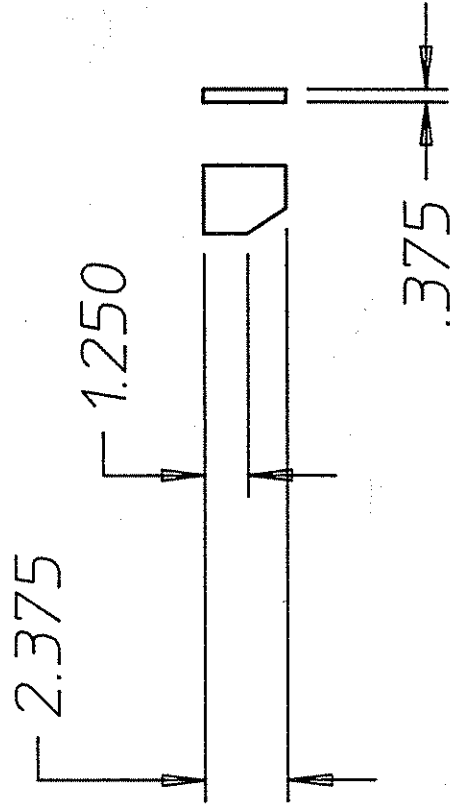
2.375

1.250

.375

Fab Part No. 2

Dimensions shown: 1.750, 9.250, 16.750, 24.250, 31.750, 33.500, .375, 3.431, 4.431

226

Fab. Part No. 3

2.840

33.500

.375

Fab. Part No. 4

R 5.068

40.0°

.500
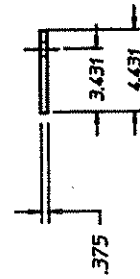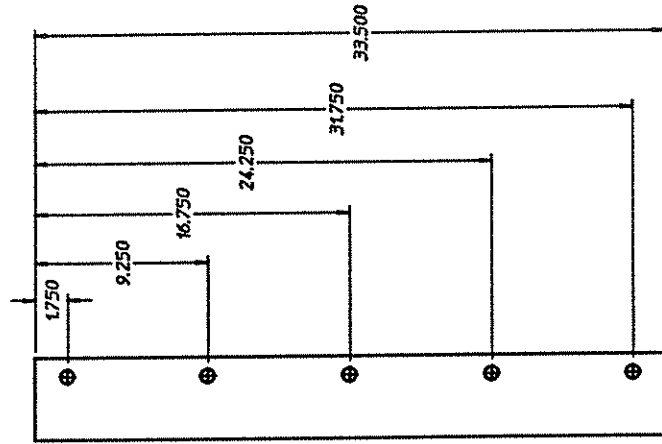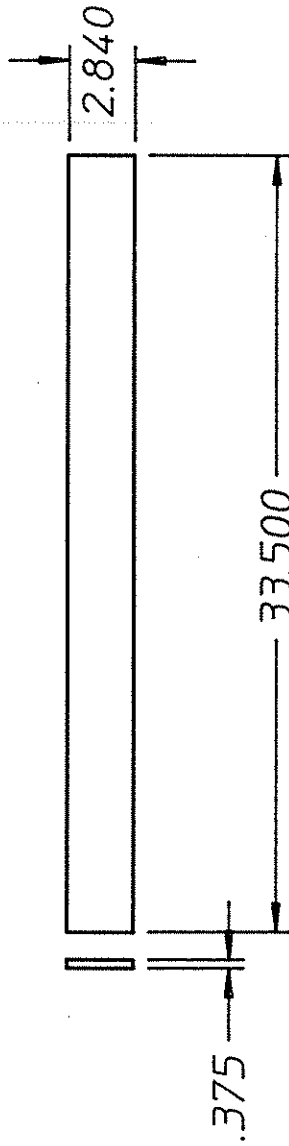
Note: Two Part 4's should have
3/16" Φ, which serve as ring
stiffeners. Other two Part 4's
should have 1/4" Φ.

DRAWN BY	APPROVED BY	BUDGET #	FILE NAME
SCALE			
DATE	REVISED	FAB #	DRAWING #

Fab. Part No. 5
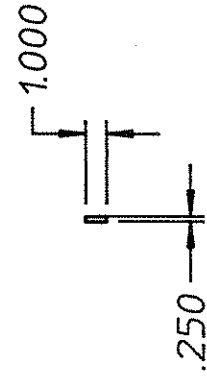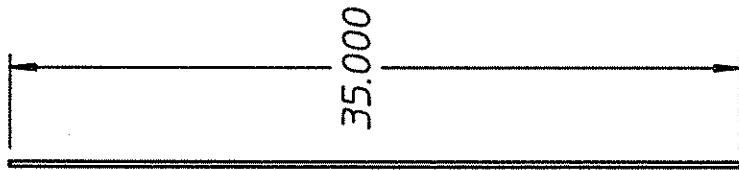
35.000

1.000

.250

Appendix E -

Experimental Test Frame Fabrication Drawings

- Spherical Ball and Socket Connection
- Specimen Load Collar

Part No.	Description
1	ball backplate
2	ball
3	socket ring

E70

3/4

DRAWN BY	APPROVED BY	BUDGET # 0287	FILE NAME
SCALE 5-2-91			
DATE	REVISED	FAB #	DRAWING #

3.00

4.00

3.688

1.323

.250

.344

1.50

MATERIAL: A36 STEEL, 2 REQUIRED

	BUDGET # 0287	FILE NAME ball
APPROVED BY		
REVISED	FAB #	DRAWING # part no. 2

SCALE	DRAWN BY
DATE 4-25-91	

2.000

.500

3.70" dia. inset

Holes to pass 1" dia. bolt

16.000

14.50 typ

12.688 typ

8.000

3.313 typ

.150 typ

2.50 typ

3.375 typ

8.063

12.75 typ

13.625 typ

16.000

MATERIAL: A36 STEEL. 2 REQUIRED

DRAWN BY	APPROVED BY	BUDGET # 0287	FILE NAME b-bplate-a
	REVISED	FAB #	DRAWING # part no. 1

SCALE

DATE 4-25-91

Part No.	Description
4	socket
5	socket backplate

E70 4 3/4

⊕ 4

⊕ 5
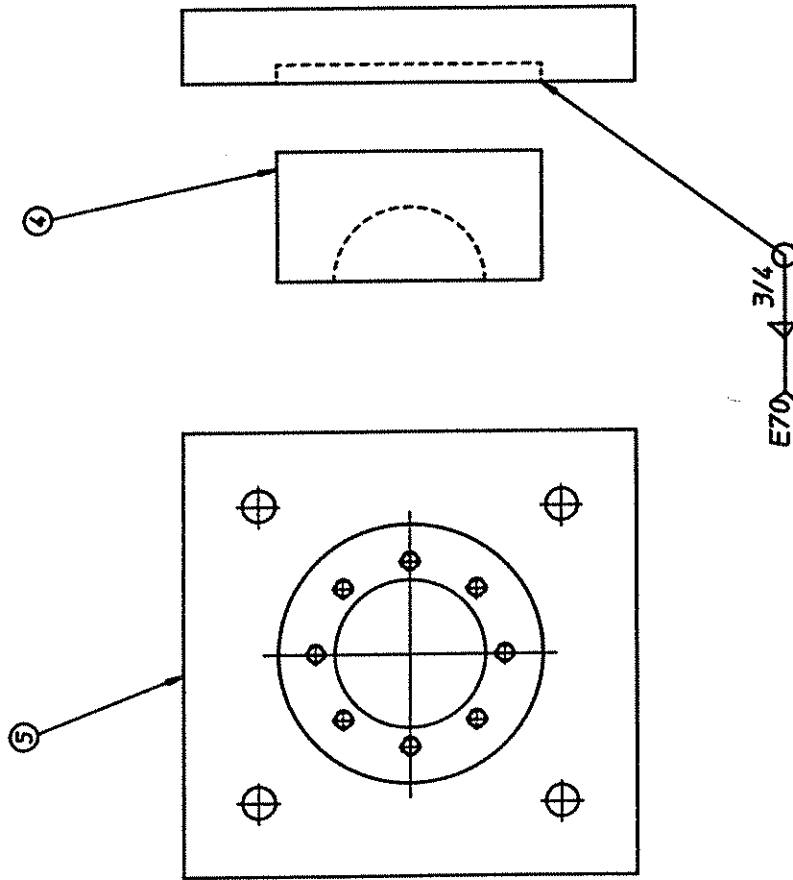
SCALE		DRAWN BY		APPROVED BY	BUDGET # 0287	FILE NAME
DATE 5-1-91				REVISED	FAB #	DRAWING #

234
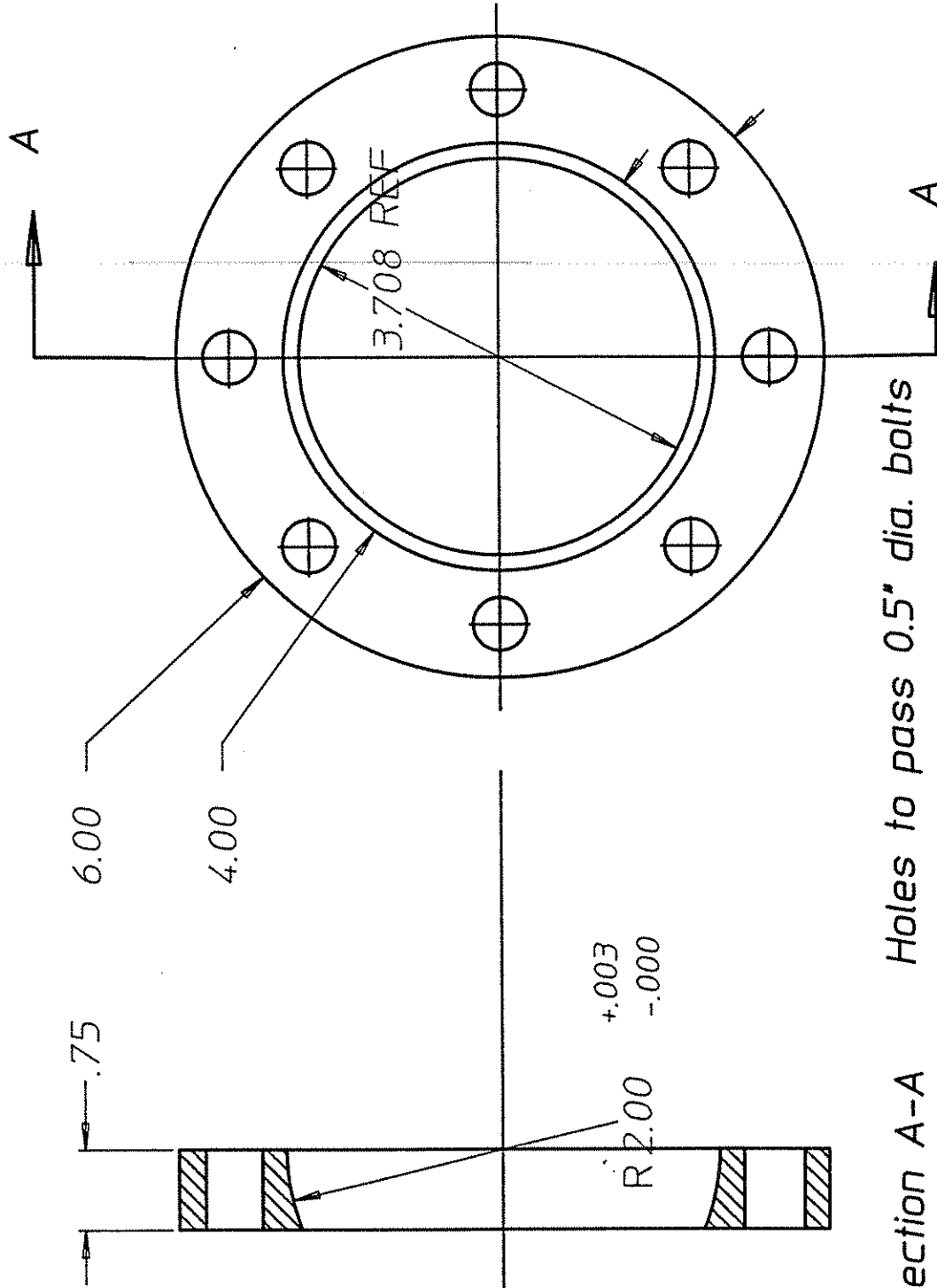
section A-A   Holes to pass 0.5" dia. bolts

3.708 REF

6.00

4.00

.75

R2.00 +.003 -.000

NOTE: 7.000 diam. to fit part no 5a

7.000

4.010

.500
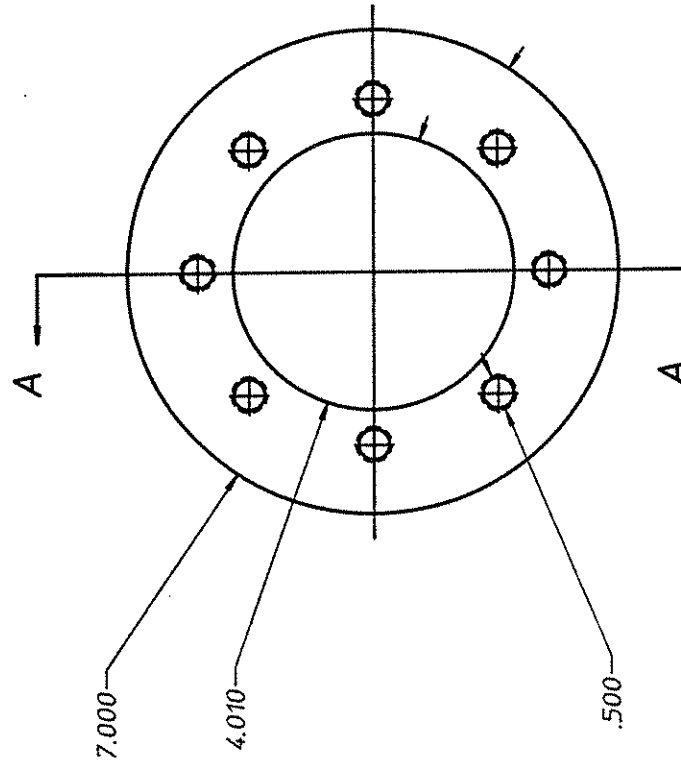
Holes for 0.5" dia. std. course thread bolts

A—A

3.500
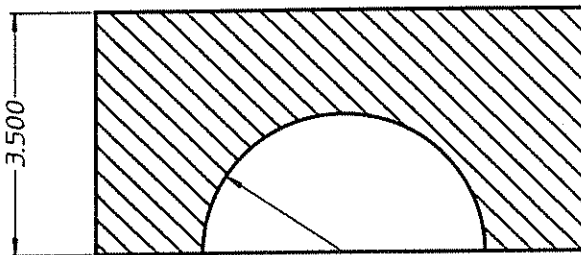
R 2.010 +.003 -.000

MATERIAL: A36 STEEL, 2 REQUIRED			
		BUDGET # 0287	FILE NAME socket
APPROVED BY			DRAWING # part no. 4
		FAB #	
REVISED			
DRAWN BY			
SCALE			
DATE 4-25-91			

236

NOTE: 7.01 diam. to fit part no. 4

12.000

9.75 typ

6.000

2.25 typ

2.25 typ

6.000

9.75 typ

12.000

7.01" dia. inset

Holes to pass 7/8"dia. bolts

2.000

.500

Part No.   Description

6   specimen attachment backplate
7   specimen sleeve
8   stiffener
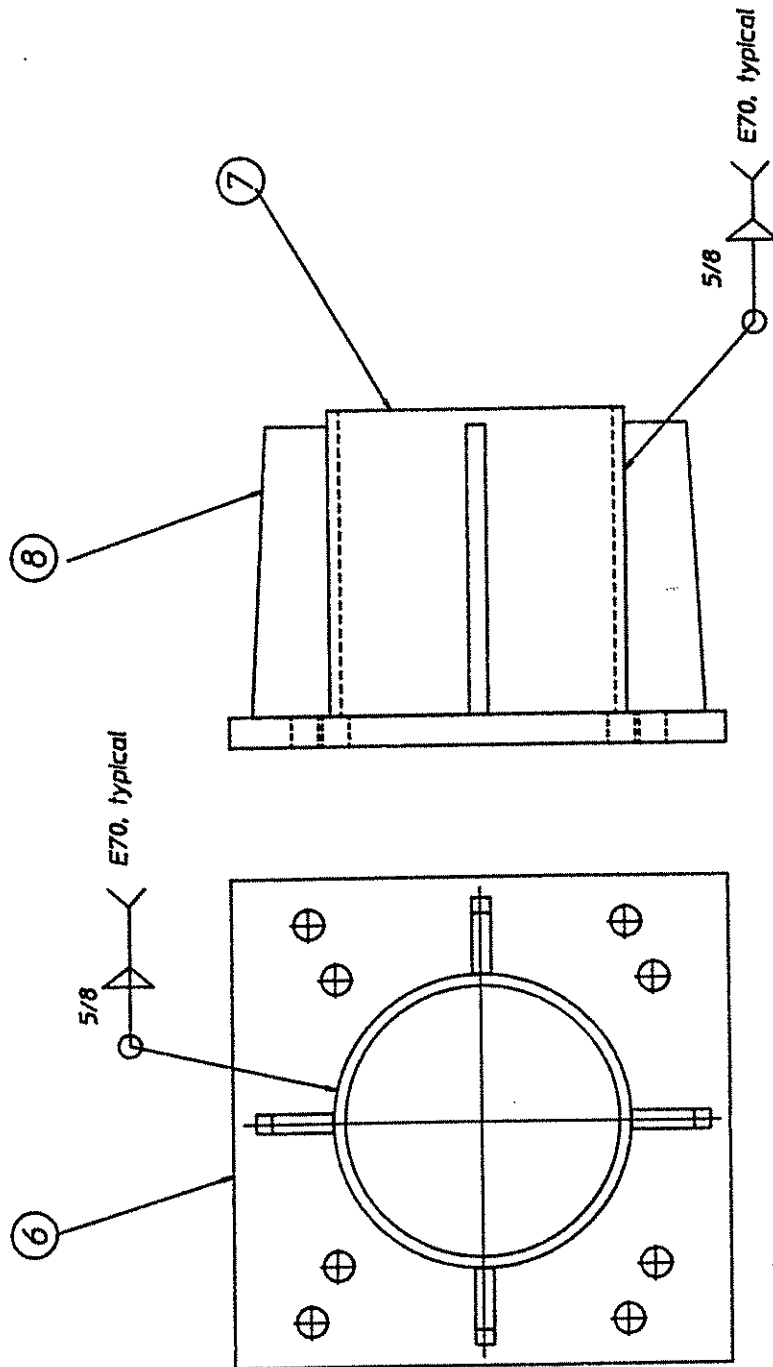
E70, typical

5/8

E70, typical

5/8

10.00

9.625 O.D.

8.875 I.D.
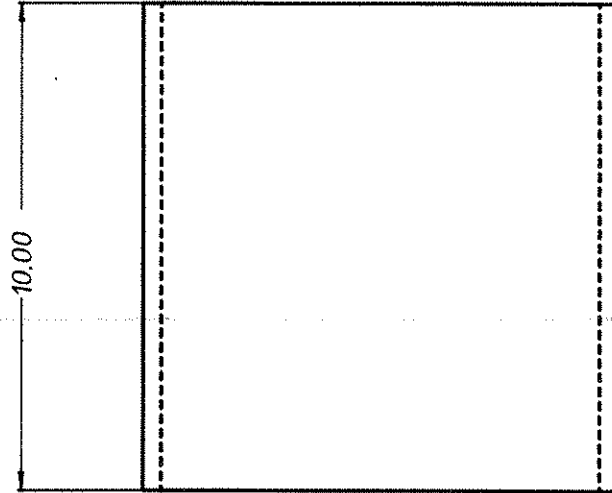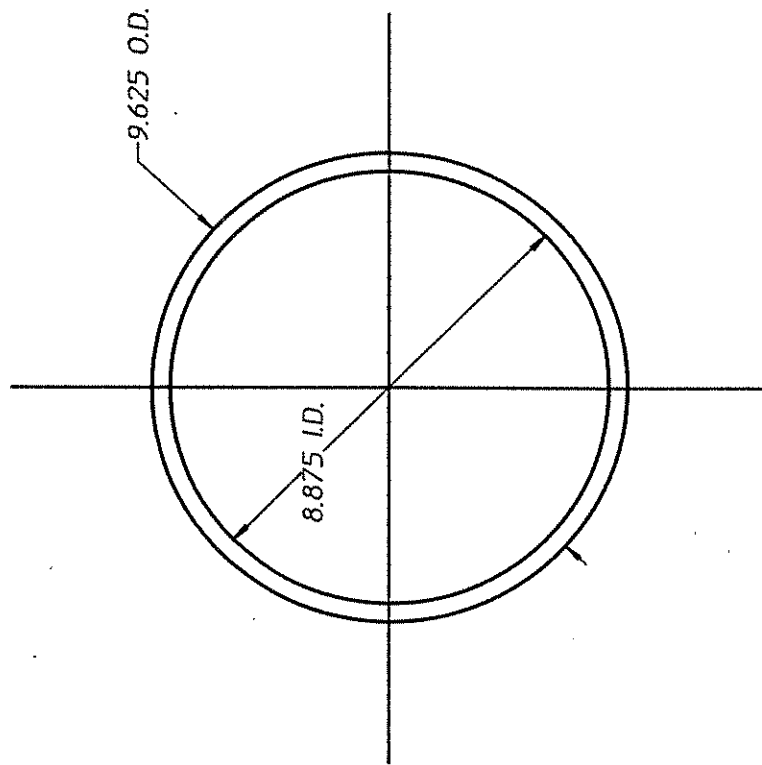
MATERIAL: A36 STEEL, 2 REQUIRED

APPROVED BY	DRAWN BY	BUDGET # 0287	FILE NAME attach
REVISED		FAB #	DRAWING # part no. 7
SCALE	DATE 4-25-91		

2.00

9.50

.625

2.50

MATERIAL: A36 STEEL, 8 REQUIRED

FILE NAME	*stiff*
BUDGET # 0287	
DRAWING # *part no. 8*	
APPROVED BY	
FAB #	
REVISED	
DRAWN BY	
SCALE 4-25-91	
DATE	

1.00

16.00
14.50 typ
12.688 typ
3.313 typ
1.50 typ
2.50 typ
3.375 typ
12.75 typ
13.625 typ
16.00
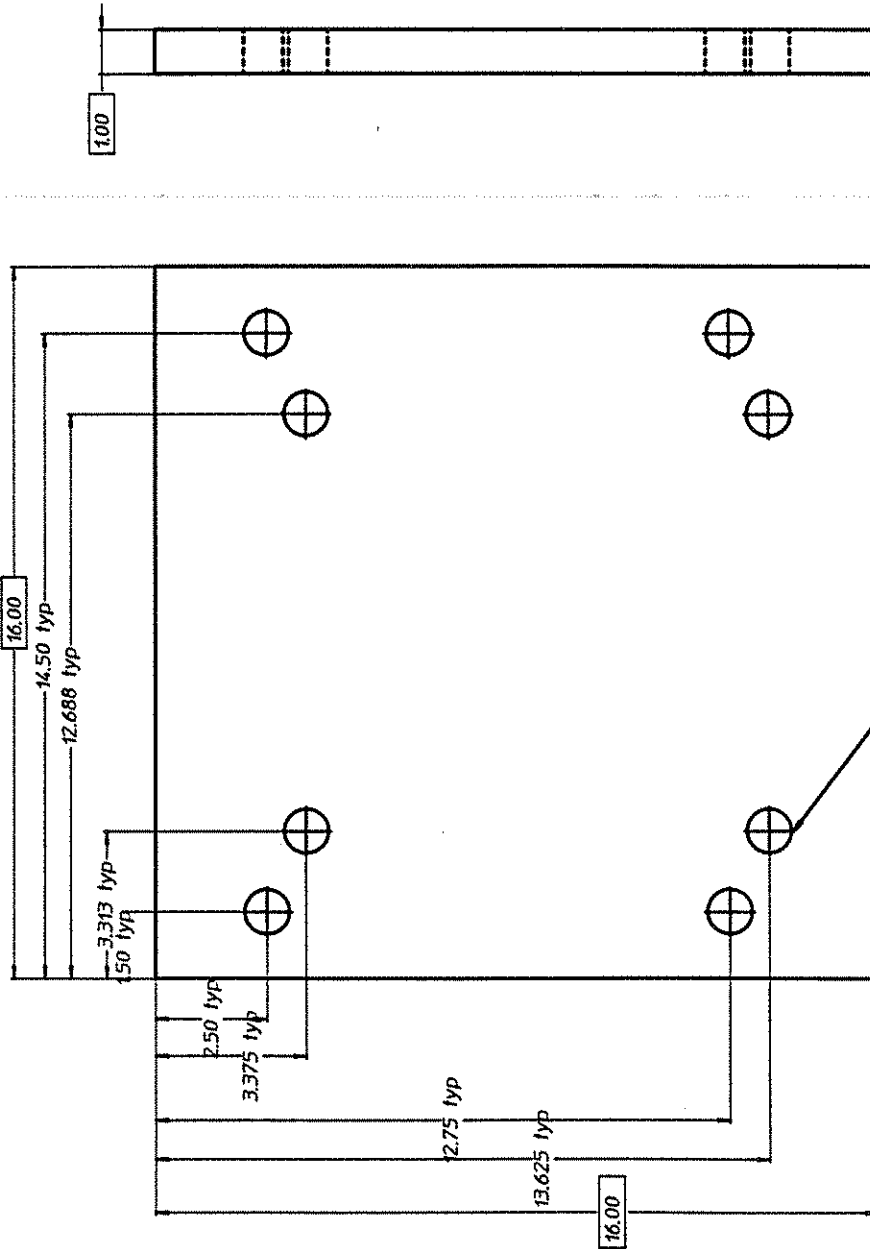
Holes to pass 1" bolt

MATERIAL: A36 STEEL, 2 REQUIRED

| SCALE | DRAWN BY | APPROVED BY | BUDGET # 0237 | FILE NAME b-bplate-b |
| DATE 4-25-91 | | REVISED | FAB # | DRAWING # part no. 6 |

Appendix F -
DATACQ User's Manual

Overall System Setup For Manual and Triggered Scanning:

```
              ╭──────────╮
             (  DATACQ    )
              ╰──────────╯
                   │
        ┌──────────────────────┐
        │   Enter Input File    │
        │  Containing Channel   │
        │     Information       │
        └──────────────────────┘
                   │
        ┌──────────────────────┐
        │    Take a Shunt       │
        │ Calibration and Store │
        │       to Disk         │
        └──────────────────────┘
                   │
        ┌──────────────────────┐
        │   Take a Zero Scan    │
        │   and Store to Disk   │
        └──────────────────────┘
                   │
        ┌──────────────────────┐
        │  Select Manual Scan   │
        ├──────────────────────┤
        │  Select File to Store │
        │   Data on Hard Disk   │
        │                       │
        │   Define Displayed    │
        │    Channels and       │
        │      Triggers.        │
        ├──────────────────────┤
        │  Take Manual Scans.   │
        └──────────────────────┘
                   │
              ╭──────────╮
             ( Reduce Data )
             ( DATARED     )
              ╰──────────╯
                   │
        ┌──────────────────────┐
        │  Data is Now Stored   │
        │ in Seperate Files for │
        │     Each Channel      │
        └──────────────────────┘
```
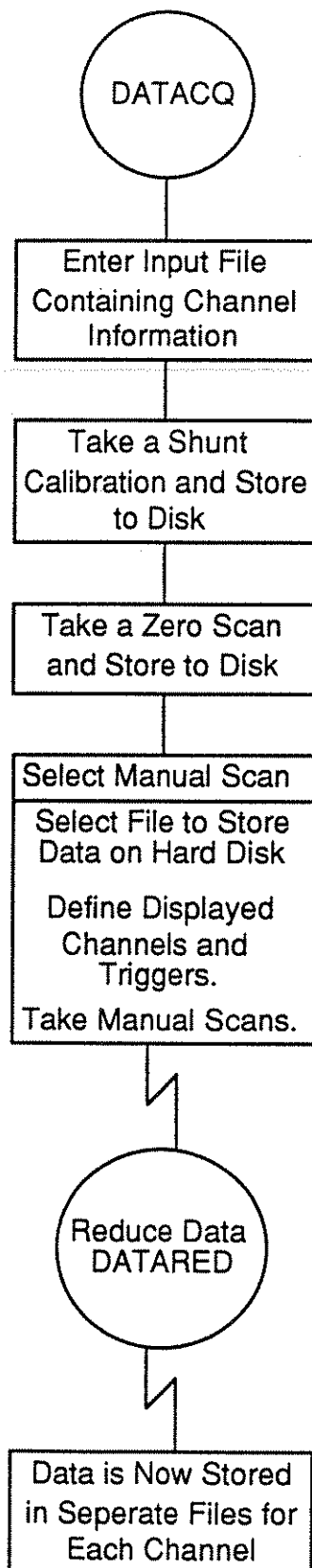
1. Introduction:

DATACQ is a data acquisition system written in C for IBM PC and PC compatible systems using National Instruments data acquisition boards. The system provides the capability of scanning up to 128 channels using triggers while also allowing the user to initiate manual scans. The software is pseudo real-time, acquisition is stopped only during input to questions, during normal acquisition: triggering, manual scanning, and real time display occur at the same time. Data is stored to the hard disk of a PC and the only limitation for the number of scans is dictated by available space.

It should be noted that this program no longer provides the taking of a number of samples over a period of time, this was used explicitly for the shake table and has not been implemented in DATACQ.

The following syntax will be used throughout this manual:

bold	Signifies that this is a required user action or input.
[...]	Describes where input should occur.
italics	Represent possible user values (string means any character string).
{ ... }	Signifies that this is not required.

2. Setting up the System for Manual Scanning:

2.1   Creating A Channel Definition File:

Create an input file for DATACQ using a text editor in the following format. If more lines are necessary to describe a channel configuration, place a "\" at the end of the line.

for strain gauges:

define/cha=[*0 .. 28*]**/ident=**[*string*]**/type=qb_strain/units=**[*string*]**/\
xfactor=**[*float*]**/gage_factor=**[*float*]**/gain=**[*float*]**/xfactor=**[*float*]**/\
x2factor=**[*float*]

for other transducers (i.e. linear pots, and inclinometers):

define/cha=[*0 .. 28*]**/ident=**[*string*]**/type=qb_strain/units=**[*string*]**/\

Examples from file 'GRANT.IN':

define/cha=0/ident=off_t_t/type=qb_strain/units=mstr/\
gage_factor=2.14/gain=200/xfactor=1.0e6/excitation=2.0/shunt=1000
...
define/cha=58/ident=incl_off/type=incline/units=deg/xfactor=16.6666
...

define/cha=60/ident=csn_v_s/type=lvdt/units=inch/xfactor=0.9474

2.2   Loading DATACQ, at the DOS prompt, type:

C:\> **datacq**

The screen will clear and the following message will appear:

Open of input file failed
Please type in filename for input: **grant.in**

As shown above, type in a filename (i.e. 'grant.in') which contains the channel definition files. The following will appear:

```
Open of input file failed
Please type in filename for input: grant.in
Input file open
Close of input file successful

A program to scan analog input channels and write the data to a disk file.
55 channels are defined, 64 channels will be scanned.

    DATACQ Updated by Paul Mihalic for
    Manual and Triggered Scanning
    Version 2.0  10/1/92


Do you wish to change programmable gains? y or n:
```

Press: **N** to select not to change programmable gains.

Notice that even though only 55 channels were read in, that 64 channels are scanned. This is a result of the National instrument boards which can only read in data in increments of 32, 64 or 128 channels.

2.3   Changing Programmable Gain:

The programmable gain is a global value for all gauges referring to a standard gain of 1,2,4 or 8 set at the voltage source and transducer cabinet (default is 1). This value can be changed later from the Main Menu option 1.

3. The Main Menu of DATACQ - Initialization of System.

Now the Main Menu for the system appears:

```
What action do you want to take?

Change programmable gains          : 1
Shunt calibration                  : 2
Take a zero scan                   : 3
Write zero bias data to file       : 4
Read zero bias data from file                : 5
Write shunt data to file           : 6
Read shunt data from file          : 7
Monitor up to 6 selected channels  : 8
Take a manual set of data          : 9
Quit                               : 0

    Enter number:
```

3.1   Performing a Zero Scan:

The first step is to take a zero scan and write this file to disk.
Press 3 at the menu prompt:

Enter number: **3**

**************** ZERO SCAN COMPLETE ******************
    Do you wish to write out zero bias data? y or n:

Press: **Y** to save this data to disk. You will now return to the main menu

3.2   Shunt Calibration:

At this point one can skip ahead to the next section and verify gauges by using the
real-time channel display. If you are ready to begin testing, the next step is to
perform a shunt calibration.
Press 2 at the menu prompt:

Enter number: **3**

******** PERFORMING SHUNT CALIBRATION *************
Make sure that shunts are turned OFF then hit a key:
Make sure that shunts are turned ON then hit a key:

Press 6 to store shunt data to disk:

Enter number: 6

*********** WRITING SHUNT DATA TO FILE ***************
Input the file to which shunt data is to be written: shunt.out

4. Manual and Triggered Scanning with DATACQ.

Press 9 on the Main Menu.

Enter number: 9

The screen will clear and the following questions may be asked:

No zero scan has been taken, do you wish to continue? y or n: y
No shunt calibration has been performed, do you wish to continue? y or n: y

If the above questions do not appear, this means a zero scan and shunt calibration have been performed. If the questions do appear, you can continue regardless by answering 'y' to both and the next question will appear. Otherwise you will be taken back to the main menu. Refer to zero scan and shunt calibration for help.

Input the file to store manual data in: **test.out**

Enter the name of a file to store the data for this experiment in. Note, that if this file exists, its information will be overwritten. This file will be used by DATARED to create separate channel files.

4.1   Screen Areas for Manual Scanning

```
┌─────────────────────────────────────────┐
│ MONITORED CHANNELS:                       │
│                                           │        **Displayed Channels Area**
│                                           │   ◄────  Updating Realtime
│                                           │
│                                           │
│                                           │
├─────────────────────────────────────────┤
│ Press 'C' to change displayed channels.   │
│ Press 'T' to set triggered channel.       │
│ Press 'P' to to toggle printer on(default) and off.  ◄────  **Help Area**
│ Press 'S' to change display rate of channels.            Command List
│ Press 'Q' to quit.                        │
│ Press any other key to take sample.       │
├─────────────────────────────────────────┤
│                                           │        **Response Area**
│                                      ◄────    Where User Will See Questions
│                                           │   In Response to Commands
└─────────────────────────────────────────┘
```
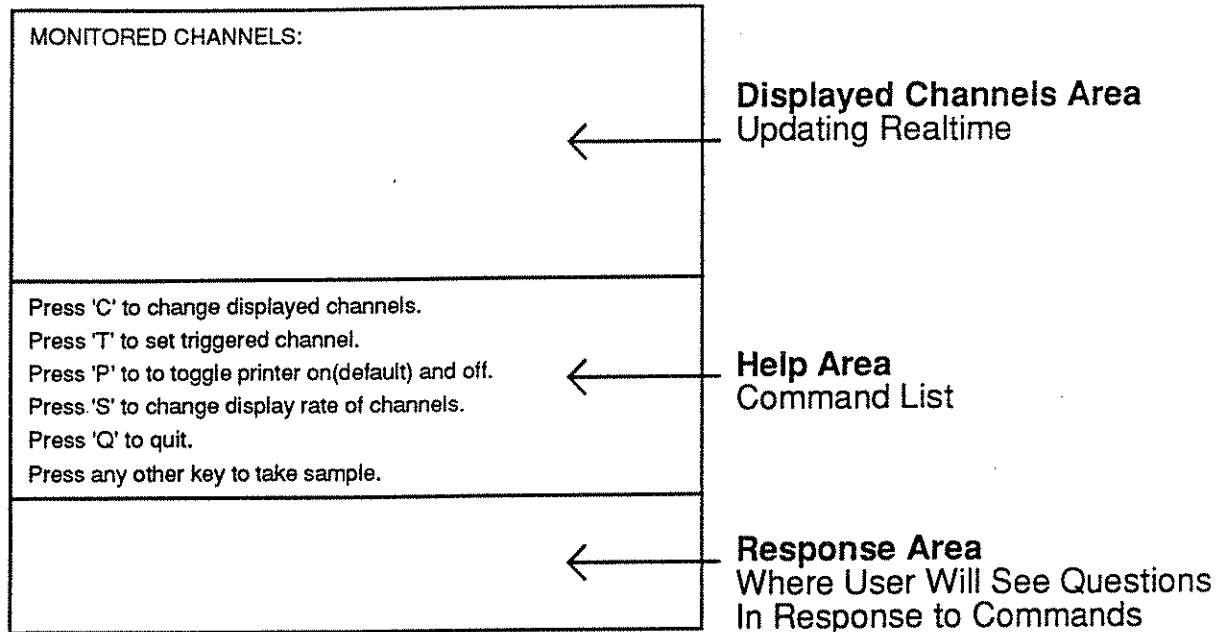
4.2   Setting Up Displayed Channels:

Press 'C,' and in the response area this request will appear:

> Enter the number of channels to display max is 10 (0 Display OFF):5
> Input the 1 channel:2
> Input the 2 channel:5
> Input the 3 channel:36
> Input the 4 channel:44
> Input the 5 channel:51

The sample dialogs above would cause channels 2, 5, 36, 44, 51 to appear in the displayed channels area. Note after each channel input this area is cleared and a next channel is asked for. Here is how the displayed channels area might look:

off_t_b =	0	mstr
off_l_s =	0	mstr
off_v_1 =	0	inch
on_s_t =	0	inch
csn_ov_t =	0	inch

Notice the system can be used as a visual monitoring program if necessary, by not selecting any triggered channels. Displayed channels can be modified at any time. To turn off displayed channels press 'C' and respond with a '0' to the prompt:

> Enter the number of channels to display max is 10 (0 Display OFF):0

You will notice a trailing cursor and values where the zero's appear will be changing either quickly or slowly.

4.3   Changing the Refresh Rate of Displayed Channels:

You can modify how fast the displayed channels area is updated by pressing 'S':

Enter the timing value: **20**

The default value is 40 at startup. By increasing this number a longer period of time will elapse before the screen is updated. Here we have changed it to 20. Now the screen will update twice as fast. This value signifies how many scans have been performed triggering, or no scans. For example, if triggering is enabled, the system has scanned the triggers 20 times before refreshing the display. During no triggering, the system will simply loop on unsolicited keyboard input 20 times. This is useful for computers that will be slower or faster than the current machine.

4.4   Setting Triggered Channels:

The entry for triggered channels is similar to displayed channels, press 'T':

Enter the number of channels to trigger on max is 10 (0 Trig OFF):**2**
Enter the 1 channel to trigger on:**2**
Enter the delta necessary to take a sample on this channel:**.2**
Enter the 2 channel to trigger on:**36**
Enter the delta necessary to take a sample on this channel:**.1**

With triggering you must enter a delta, this delta is an absolute value its units are the same as what is displayed on the screen in displayed channels. For example, we have selected 2 channels to trigger on (from the displayed channels above):

off_t_b   with a change of .2 mstr
off_v_1   with a change of .1 inch

When a trigger hits, that is the value for a channel has changed by delta, the following will be displayed in the response area: (i.e., change .2 to .4 for channel 2)

Scan 1 taken TRIGGED for channel off_t_b = .4 mstr

Note that this will notify you of which of the triggers set has hit and with what new value. The number following the word 'scan' tells you how many combined manual and triggered scans have been performed. Just as with displayed channels. triggers can be changed at any time during scanning. Also note that when triggering is

enabled, manual scans can still be performed and will automatically update triggers.
To turn off triggering press 'T' and respond with a '0' to the prompt:

Enter the number of channels to trigger on max is 10 (0 Trig OFF):0

****** WARNING ******
If you set the delta too small, and the value is fluctuating very rapidly, you may take hundreds if not thousands of scans.
TURN OFF TRIGGERING IMMEDIATELY

4.5   Taking a Manual Scan:

By pressing any key other than the commands listed (Note it is best to select a key i.e. Space-Bar or ENTER key) you can take a manual scan. The following will appear in the response area of the screen.   The number following the word scan notifies you of how many manual and triggered scans combined have been taken.

Scan 1 taken MANUAL

4.6   Turning the Printer Off and On:

To toggle the printer off and on press 'P.' Either of the following will be displayed in the response area: (The printer is on by default.)

PRINTER ON
PRINTER OFF

4.7   To Leave Manual and Triggered Scanning:

Press 'Q' and the data file will be saved. You will now be returned to the Main Menu.

(This page intentionally blank)

（空白处）

Appendix G -
Preliminary Nonlinear Finite Element Analysis

Preliminary nonlinear finite element analyses of steel tubular braces with dent damage and of various diameter to thickness (D/t) ratio were conducted using ABAQUS [32,33,34], a commercial nonlinear finite element program, to assess the applicability of the method in predicting the behavior of the non-repaired, damaged specimens.

Symmetry enabled a quarter section of the specimen to be modelled. The model was developed using quadrilateral shell elements. Care was taken to model the dented section of the tube with a refined mesh of elements in order to accurately analyze the nonlinear deformation. A four node, reduced integration, doubly curved shell element with hourglass control was selected for the preliminary analyses. The element was used for its numerical stability. Multi-point constraints (constraint equations) were incorporated into the model to impose the proper boundary conditions at the ends of the specimen, simulating the frictionless ball and socket connection.

The analysis involved three steps:

STEP 1 - Dent damage was imposed through contact with a predefined rigid surface, which had a prescribed movement into the deformable finite element model's mesh. Interface elements aligned the deformable mesh with the rigid surface.

STEP 2 - The dented section was unloaded by retracting the rigid surface through a prescribed movement. In steps 1 and 2 the tube was uniformly supported along the midspan to prevent global bending, which closely simulated experimental conditions. Furthermore, in both steps 1 and 2 the Newton-Raphson solution scheme was used. The depth of the dent was checked, to see if it complied with that of the specimen. Because of elastic rebound causing the dent depth to decrease under unloading, steps 1 and 2 were often repeated until the dent depth after unloading matched that of the specimen.

STEP 3 - The end of the tube was pinned through multi-point constraint conditions, and the midspan support was removed. An axial compressive force was applied at the dented section face through a prescribed displacement. The modified Riks method was utilized to analyze the nonlinear buckling behavior and trace out the load-shortening curve.

The solution scheme performed well when the mesh of the model was composed of a 4 node quadrilateral shell element. Results for the axial load-shortening response of Specimen A2 are shown in Figure G.1. Overall, reasonably good agreement exists between the finite element analysis and the experimental results. The deformed geometry of the finite element model during the several steps in the analysis is presented in Figures G.2 through G.4. The input file for this analysis, in addition to that for Specimens B2 and C2 are included in Appendix G, and follow Figure G.4. When a 9 node shell element was implemented for the same analysis, convergence problems were encountered.

Further improvement in the finite element results can be obtained by refining the mesh, particularly near the dented region. This would result in a better agreement in peak axial load between the analysis and experimental results. Also, the stress-strain curve presented in Figure 2.2 should be used in in place of the assumed elastic-perfectly plastic characterization adopted for the analysis presented herein.
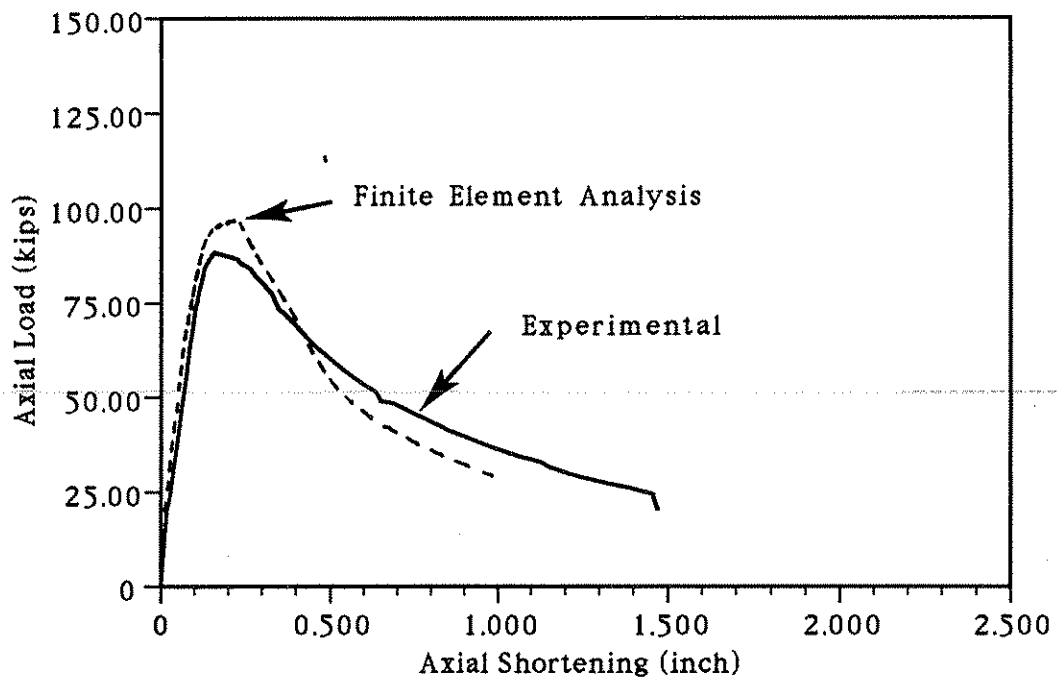
Figure G.1 Comparison of Experimental and Finite Element Analysis of Axial Load-Shortening Relationship, Specimen A2
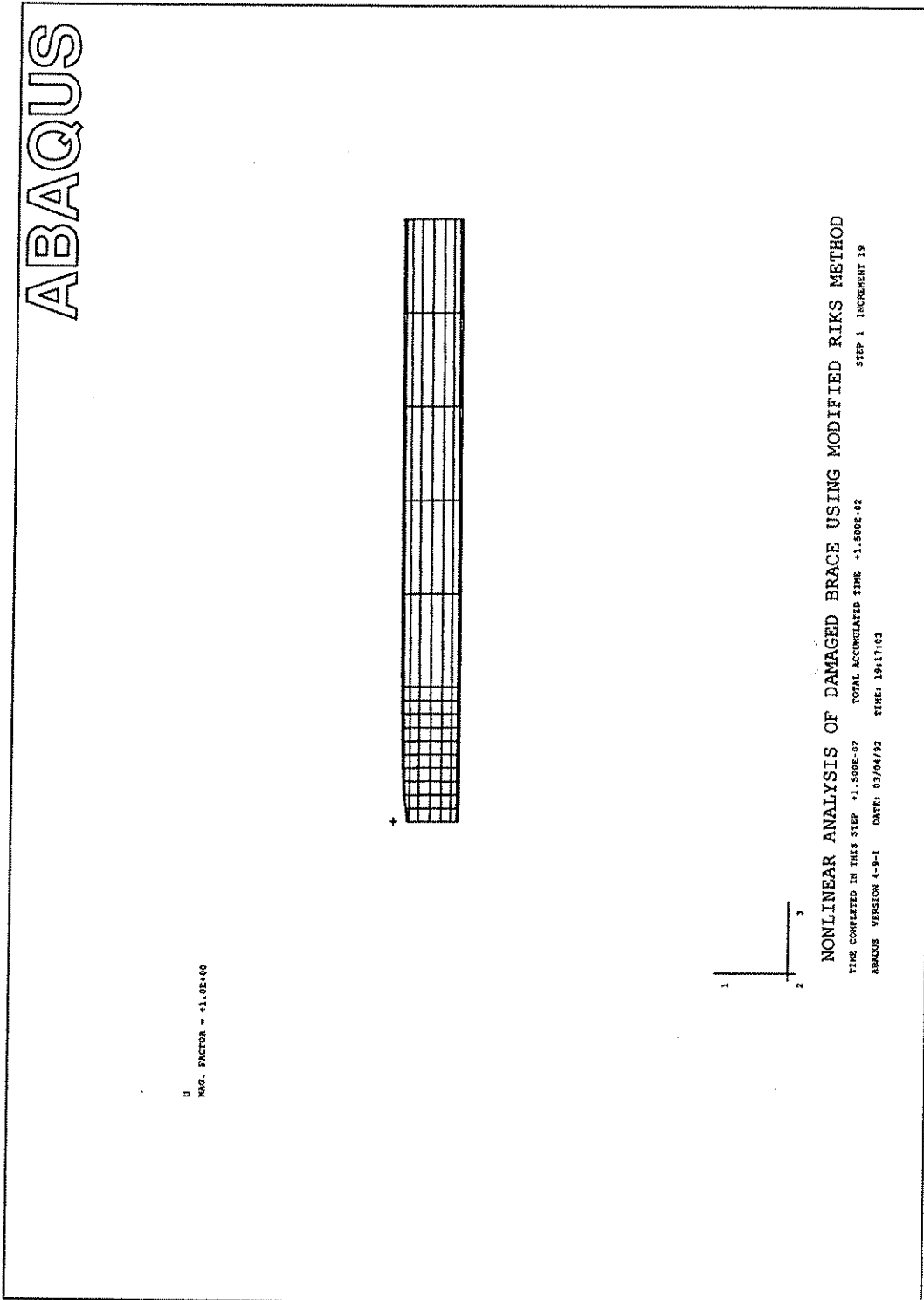
Figure G.2 Deformed Mesh in Step 1 Immediately After Denting.
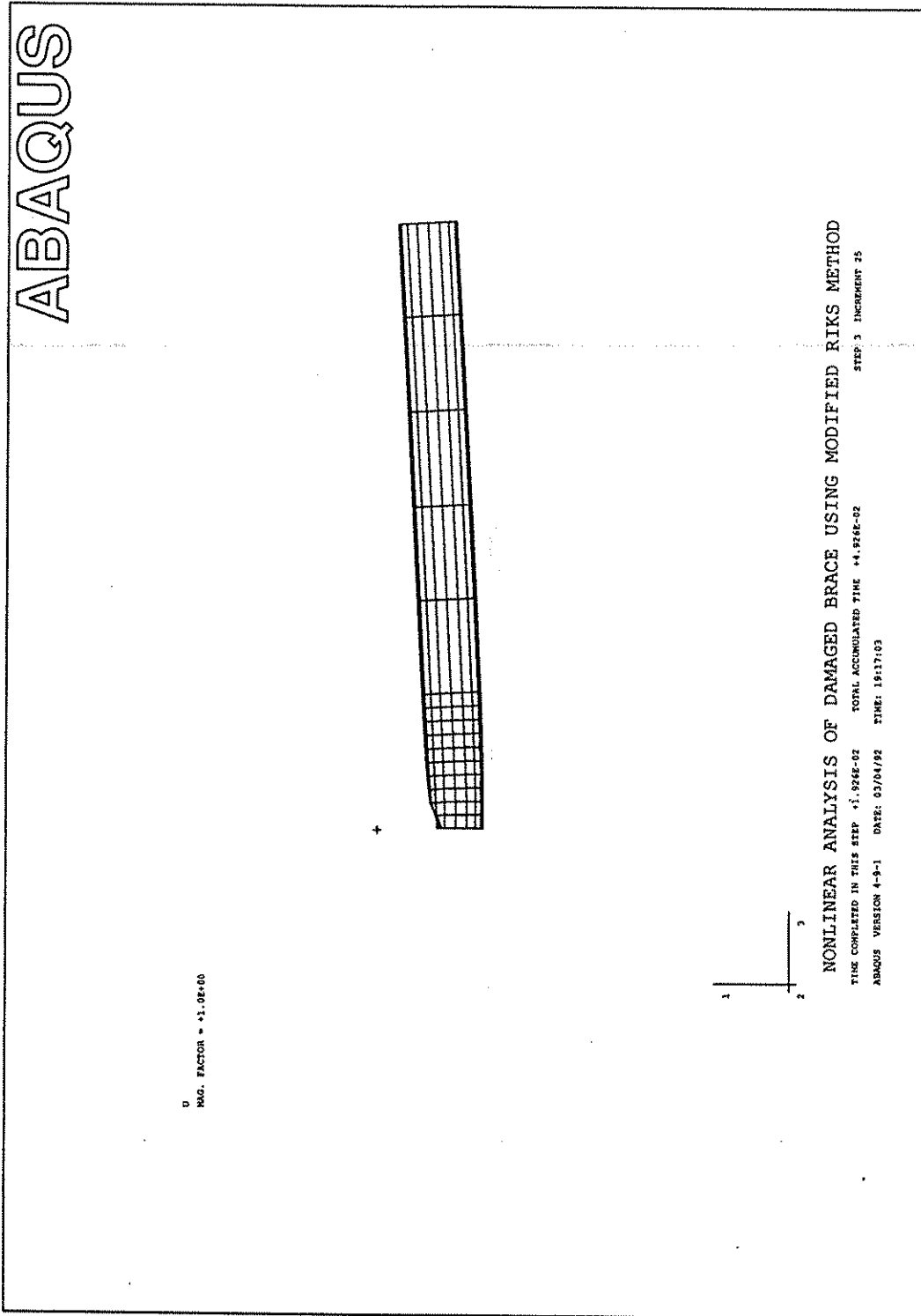
Figure G.3 Deformed Mesh in Step 3, Near Peak Axial Load.
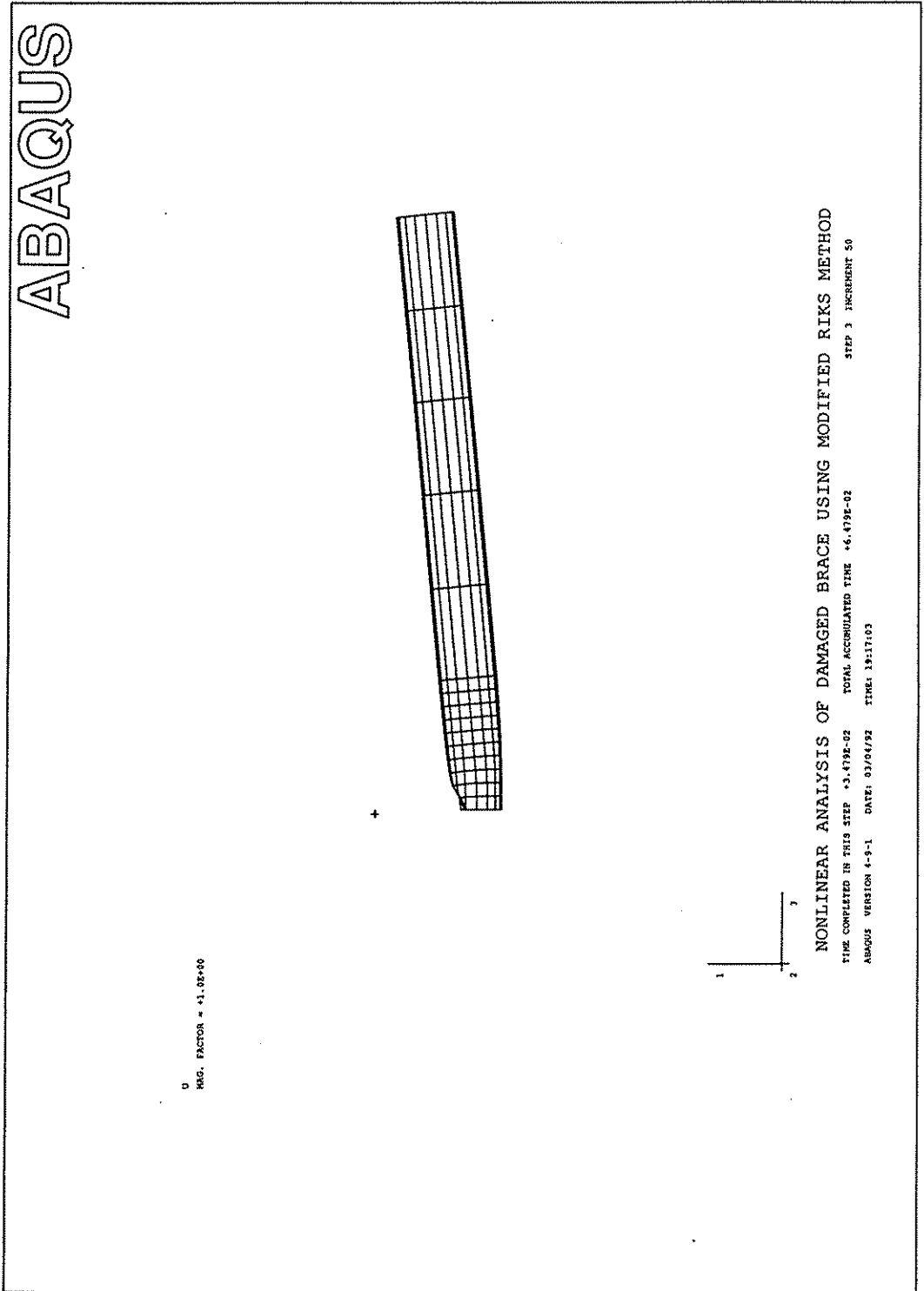
Figure G.4 Deformed Mesh in Step 3, At Deformation Beyond Peak Load.

SPECIMEN A2 - Input file, 4 node shell element.

```
*HEADING
 NONLINEAR ANALYSIS OF DAMAGED BRACE USING MODIFIED RIKS METHOD
*NODE,NSET=ALLN
1,-4.3125,0.,0.
5,0.,4.3125,0.
9,4.3125,0.,0.
91,-4.3125,0.,20.
95,0.,4.3125,20.
99,4.3125,0.,20.
136,-4.3125,0.,89.4
140,0.,4.3125,89.4
144,4.3125,0.,89.4
*NGEN,LINE=C,NSET=LOADB
1,5,1, ,0.,0.,0.
5,9,1, ,0.,0.,0.
*NGEN,LINE=C,NSET=BND3
136,140,1, ,0.,0.,89.4
140,144,1, ,0.,0.,89.4
*NGEN,LINE=C,NSET=BNDMID
91,95,1, ,0.,0.,20.
95,99,1, ,0.,0.,20.
*NGEN,NSET=BND1
1,91,9
91,136,9
*NGEN,NSET=BND2
9,99,9
99,144,9
*NGEN,NSET=REST
2,92,9
92,137,9
3,93,9
93,138,9
4,94,9
94,139,9
5,95,9
95,140,9
6,96,9
96,141,9
7,97,9
97,142,9
8,98,9
98,143,9
*NODE,NSET=N1000
1000,0.,0.,89.4
*NODE,NSET=N9999
9999,6.3125,0.,0.
*NSET,NSET=LDB1
1,9
*NSET,NSET=LDB2
2,3,4,5,6,7,8
*NSET,NSET=BND1A,GENERATE
1,127,9
*NSET,NSET=BND2A,GENERATE
```

```
9,135,9
*NSET,NSET=SUP
1,2,3,10,11,12,19,20,21,28,29,30,37,38,39,46,47,48,55,56,57
64,65,66,73,74,75,82,83,84,91,92,93
*NSET,NSET=ALLN
LOADB,BND1,BND2,BND3,REST
*ELEMENT,TYPE=S4R,ELSET=BRACE
1,1,10,11,2
*ELGEN,ELSET=BRACE
1,8,1,1,15,9,8
*ELSET,ELSET=CENT,GENERATE
8,120,8
1,8
*ELEMENT,TYPE=IRS12,ELSET=INTER
200,9,9999
201,8,9999
202,7,9999
203,6,9999
*RIGID SURFACE,ELSET=INTER,TYPE=SEGMENT
START,4.32,0.,0.
LINE,4.32,4.,0.
*MPC
7,136,1000
7,137,1000
7,138,1000
7,139,1000
7,140,1000
7,141,1000
7,142,1000
7,143,1000
7,144,1000
*ELSET,ELSET=ELPRT
CENT
INTER
*SHELL SECTION,ELSET=BRACE,MATERIAL=ERW
0.25,3
*MATERIAL,NAME=ERW
*ELASTIC
29797.,0.3
*PLASTIC
41.,0.
44.,0.0001
46.,0.0004
47.,0.0007
48.,0.0022
49.,0.0027
*INTERFACE,ELSET=INTER
*FRICTION
1.E12,1.E12
*BOUNDARY
BND1A,YSYMM
BND2A,YSYMM
LOADB,ZSYMM
SUP,1,2
SUP,4
SUP,6
N9999,2,6
```

```
*RESTART,WRITE,FREQ=20
*PLOT
*VIEWPOINT,DEFINITION=MODEL AXIS ROTATION
180.,90.,270.
*STEP,INC=50,NLGEOM,SUBMAX,CYCLE=8,MONOTONIC
 DENTING OF TUBE AT MIDSPAN TO PRESCRIBED 10%D DEPTH
*STATIC,PTOL=10.
20.E-5,15.E-3,,1.E-3
*BOUNDARY
9999,1,,-.9923
*PLOT,FREQ=25
*VIEWPOINT,DEFINITION=MODEL AXIS ROTATION
180.,90.,270.
*DISPLACED
U,1.,1
*END STEP
*STEP,INC=50,NLGEOM,SUBMAX,CYCLE=8,MONOTONIC
 RELEASING OF PRESCRIBED DEPTH TO UNLOAD DENT REGION
*STATIC,PTOL=10.
20.E-5,15.E-3,,1.E-3
*BOUNDARY
9999,1,,1.
*PLOT,FREQ=25
*VIEWPOINT,DEFINITION=MODEL AXIS ROTATION
180.,90.,270.
*DISPLACED
U,1.,1
*END STEP
*STEP,INC=50,NLGEOM,SUBMAX,CYCLE=8
 RIKS STEP ANALYSIS OF AXIAL LOADING
*STATIC,PTOL=20.,MTOL=20.,RIKS
20.E-5,15.E-3,,1.E-3
*BOUNDARY,OP=NEW
BND1A,YSYMM
BND2A,YSYMM
N9999,2,6
LOADB,ZSYMM
LOADB,3,,2.
N1000,1,4
N1000,6
*PLOT,FREQ=25
*VIEWPOINT,DEFINITION=MODEL AXIS ROTATION
180.,90.,270.
*DISPLACED
U,1.,1
*END STEP
```

```
*HEADING
 NONLINEAR ANALYSIS OF DAMAGED BRACE USING MODIFIED RIKS METHOD
*PREPRINT,ECHO=NO,HISTORY=NO,MODEL=NO
*NODE,NSET=N1000
1000,0.,0.,89.4
*NODE,NSET=N9999
9999,6.3125,0.,0.
*NODE,NSET=ALLN
1,-4.3125,0.,0.
17,0.,4.3125,0.
49,4.3125,0.,0.
1177,-4.3125,0.,10.5
1193,0.,4.3125,10.5
1225,4.3125,0.,10.5
1226,-4.3125,0.,11.375
1242,0.,4.3125,11.375
1258,4.3125,0.,11.375
1589,-4.3125,0.,21.
1605,0.,4.3125,21.
1621,4.3125,0.,21.
1787,-4.3125,0.,89.4
1803,0.,4.3125,89.4
1819,4.3125,0.,89.4
*NGEN,LINE=C,NSET=LOADB1
1,17,1, ,0.,0.,0.
*NGEN,LINE=C,NSET=LOADB2
17,49,1, ,0.,0.,0.
*NGEN,LINE=C,NSET=MIDB11
1177,1193,1, ,0.,0.,10.5
*NGEN,LINE=C,NSET=MIDB12
1193,1225,1, ,0.,0.,10.5
*NGEN,LINE=C,NSET=MIDB2
1226,1242,1, ,0.,0.,11.375
1242,1258,1, ,0.,0.,11.375
*NGEN,LINE=C,NSET=MIDB3
1589,1605,1, ,0.,0.,21.
1605,1621,1, ,0.,0.,21.
*NGEN,LINE=C,NSET=BND3
1787,1803,1, ,0.,0.,89.4
1803,1819,1, ,0.,0.,89.4
*NFILL,NSET=NUNDER
LOADB1,MIDB11,12,98
*NFILL,NSET=NDENT
LOADB2,MIDB12,24,49
*NFILL,NSET=NMID
MIDB2,MIDB3,11,33
*NFILL,NSET=NEND
MIDB3,BND3,6,33
*NSET,NSET=BND1,GENERATE
1,1177,98
1226,1754,33
*NSET,NSET=BND2,GENERATE
49,1225,49
```

```
1225,1786,33
*NSET,NSET=SUP,GENERATE
1,1177,98
2,1178,98
3,1179,98
4,1180,98
5,1181,98
1226,1589,33
1227,1590,33
1228,1591,33
1229,1592,33
1230,1593,33
*NSET,NSET=LOADB
LOADB1,LOADB2
*VIEWPOINT
1,1,1
*DRAW
*ELEMENT,TYPE=S9R5,ELSET=DENT
1,17,115,117,19,66,116,68,18,67
*ELGEN,ELSET=DENT
1,16,2,1,12,98,16
*ELEMENT,TYPE=S9R5,ELSET=UNDER
193,1,197,199,3,99,198,101,2,100
*ELGEN,ELSET=UNDER
193,8,2,1,6,196,8
*ELEMENT,TYPE=S9R5,ELSET=MID11
241,1177,1259,1261,1179,1226,1260,1228,1178,1227
*ELGEN,ELSET=MID11
241,8,2,1
*ELEMENT,TYPE=S9R5,ELSET=MID12
249,1193,1275,1277,1197,1242,1276,1244,1195,1243
250,1197,1277,1279,1201,1244,1278,1246,1199,1245
251,1201,1279,1281,1205,1246,1280,1248,1203,1247
252,1205,1281,1283,1209,1248,1282,1250,1207,1249
253,1209,1283,1285,1213,1250,1284,1252,1211,1251
254,1213,1285,1287,1217,1252,1286,1254,1215,1253
255,1217,1287,1289,1221,1254,1288,1256,1219,1255
256,1221,1289,1291,1225,1256,1290,1258,1223,1257
*ELEMENT,TYPE=S9R5,ELSET=END1
257,1259,1325,1327,1261,1292,1326,1294,1260,1293
*ELGEN,ELSET=END1
257,16,2,1,5,66,16
*ELEMENT,TYPE=S9R5,ELSET=END2
337,1589,1655,1657,1591,1622,1656,1624,1590,1623
*ELGEN,ELSET=END2
337,16,2,1,3,66,16
*ELSET,ELSET=BRACE
DENT,UNDER,MID11,MID12,END1,END2
*ELEMENT,TYPE=IRS12,ELSET=INTER
400,17,9999
401,18,9999
402,19,9999
403,20,9999
404,21,9999
405,22,9999
406,23,9999
407,24,9999
```

```
408,25,9999
409,26,9999
410,27,9999
411,28,9999
412,29,9999
413,30,9999
414,31,9999
415,32,9999
416,33,9999
417,34,9999
418,35,9999
419,36,9999
420,37,9999
421,38,9999
422,39,9999
423,40,9999
424,41,9999
425,42,9999
426,43,9999
427,44,9999
428,45,9999
429,46,9999
430,47,9999
431,48,9999
432,49,9999
*DRAW
*RIGID SURFACE,ELSET=INTER,TYPE=SEGMENT
START,4.32,0.,0.
LINE,4.32,4.,0.
*MPC
7,BND3,1000
*MPC
1,66,17,115
1,164,115,213
1,262,213,311
1,360,311,409
1,458,409,507
1,556,507,605
1,654,605,703
1,752,703,801
1,850,801,899
1,948,899,997
1,1046,997,1095
1,1144,1095,1193
1,1194,1193,1195
1,1196,1195,1197
1,1198,1197,1199
1,1200,1199,1201
1,1202,1201,1203
1,1204,1203,1205
1,1206,1205,1207
1,1208,1207,1209
1,1210,1209,1211
1,1212,1211,1213
1,1214,1213,1215
1,1216,1215,1217
1,1218,1217,1219
```

```
1,1220,1219,1221
1,1222,1221,1223
1,1224,1223,1225
*SHELL SECTION,ELSET=BRACE,MATERIAL=ERW
0.25,9
*MATERIAL,NAME=ERW
*ELASTIC
29797.,0.3
*PLASTIC
41.,0.
44.,0.0001
46.,0.0004
47.,0.0007
48.,0.0022
49.,0.0027
*INTERFACE,ELSET=INTER
*FRICTION
1.E12,1.E12
*BOUNDARY
BND1,YSYMM
BND2,YSYMM
N1000,YSYMM
LOADB1,ZSYMM
LOADB2,ZSYMM
SUP,1,2
SUP,4
SUP,6
N9999,2,6
*PLOT
*VIEWPOINT
1,1,1
*STEP,INC=50,NLGEOM,SUBMAX,CYCLE=8,MONOTONIC
 INDENTATION OF TUBE AT MIDSPAN TO A PRESCRIBED DEPTH
*STATIC,PTOL=10.
0.05,1.,,.001
*BOUNDARY
N9999,1,,-.9900
*NODE PRINT,NSET=LOADB,TOTALS=YES
RF
*NODE PRINT,NSET=N1000,TOTALS=YES
U
*PLOT,FREQ=10
*VIEWPOINT
1,1,1
*DISPLACED
U,1.,1
*END STEP
*STEP,INC=50,NLGEOM,SUBMAX,CYCLE=8,MONOTONIC
 RELEASING OF RIGID SURFACE TO ALLOW REBOUND OF MATERIAL
*STATIC,PTOL=10.
.05,1.,,.001
*BOUNDARY
N9999,1,,5.
*PLOT,FREQ=10
*VIEWPOINT
1,1,1
*DISPLACED
```

```
U,1.,1
*END STEP
*STEP,INC=50,NLGEOM,SUBMAX,CYCLE=8
 MODIFIED RIKS ANALYLSIS OF AXIAL LOADING
*STATIC,PTOL=20.,MTOL=20.,RIKS
.05,1.,,.001
*BOUNDARY,OP=NEW
BND1,YSYMM
BND2,YSYMM
N9999,2,6
LOADB1,ZSYMM
LOADB2,ZSYMM
N1000,1,2
N1000,4
N1000,6
N1000,3,,-2.
*PLOT,FREQ=5
*VIEWPOINT
1,1,1
*DISPLACED
U,1.,1
*END STEP
```

SPECIMEN B2 - Input file. 4 node shell element.

```
*HEADING
 NONLINEAR ANALYSIS OF DAMAGED BRACE USING MODIFIED RIKS METHOD
*NODE,NSET=ALLN
1,-4.3125,0.,0.
5,0.,4.3125,0.
9,4.3125,0.,0.
91,-4.3125,0.,20.
95,0.,4.3125,20.
99,4.3125,0.,20.
136,-4.3125,0.,89.4
140,0.,4.3125,89.4
144,4.3125,0.,89.4
*NGEN,LINE=C,NSET=LOADB
1,5,1, ,0.,0.,0.
5,9,1, ,0.,0.,0.
*NGEN,LINE=C,NSET=BND3
136,140,1, ,0.,0.,89.4
140,144,1, ,0.,0.,89.4
*NGEN,LINE=C,NSET=BNDMID
91,95,1, ,0.,0.,20.
95,99,1, ,0.,0.,20.
*NGEN,NSET=BND1
1,91,9
91,136,9
*NGEN,NSET=BND2
9,99,9
99,144,9
*NGEN,NSET=REST
2,92,9
92,137,9
3,93,9
93,138,9
4,94,9
94,139,9
5,95,9
95,140,9
6,96,9
96,141,9
7,97,9
97,142,9
8,98,9
98,143,9
*NODE,NSET=N1000
1000,0.,0.,89.4
*NODE,NSET=N9999
9999,6.3125,0.,0.
*NSET,NSET=LDB1
1,9
*NSET,NSET=LDB2
2,3,4,5,6,7,8
*NSET,NSET=BND1A,GENERATE
1,127,9
*NSET,NSET=BND2A,GENERATE
```

```
9,135,9
*NSET,NSET=SUP
1,2,3,10,11,12,19,20,21,28,29,30,37,38,39,46,47,48,55,56,57
64,65,66,73,74,75,82,83,84,91,92,93
*NSET,NSET=ALLN
LOADB,BND1,BND2,BND3,REST
*ELEMENT,TYPE=S4R,ELSET=BRACE
1,1,10,11,2
*ELGEN,ELSET=BRACE
1,8,1,1,15,9,8
*ELSET,ELSET=CENT,GENERATE
8,120,8
1,8
*ELEMENT,TYPE=IRS12,ELSET=INTER
200,9,9999
201,8,9999
202,7,9999
203,6,9999
*RIGID SURFACE,ELSET=INTER,TYPE=SEGMENT
START,4.32,0.,0.
LINE,4.32,4.,0.
*MPC
7,136,1000
7,137,1000
7,138,1000
7,139,1000
7,140,1000
7,141,1000
7,142,1000
7,143,1000
7,144,1000
*ELSET,ELSET=ELPRT
CENT
INTER
*SHELL SECTION,ELSET=BRACE,MATERIAL=ERW
0.188,3
*MATERIAL,NAME=ERW
*ELASTIC
29797.,0.3
*PLASTIC
41.,0.
44.,0.0001
46.,0.0004
47.,0.0007
48.,0.0022
49.,0.0027
*INTERFACE,ELSET=INTER
*FRICTION
1.E12,1.E12
*BOUNDARY
BND1A,YSYMM
BND2A,YSYMM
LOADB,ZSYMM
SUP,1,2
SUP,4
SUP,6
N9999,2,6
```

```
*RESTART,WRITE,FREQ=20
*PLOT
*VIEWPOINT,DEFINITION=MODEL AXIS ROTATION
180.,90.,270.
*STEP,INC=50,NLGEOM,SUBMAX,CYCLE=8,MONOTONIC
 DENTING OF TUBE AT MIDSPAN TO PRESCRIBED 10%D DEPTH
*STATIC,PTOL=10.
20.E-5,15.E-3,,1.E-3
*BOUNDARY
9999,1,,-.9923
*PLOT,FREQ=25
*VIEWPOINT,DEFINITION=MODEL AXIS ROTATION
180.,90.,270.
*DISPLACED
U,1.,1
*END STEP
*STEP,INC=50,NLGEOM,SUBMAX,CYCLE=8,MONOTONIC
 RELEASING OF PRESCRIBED DEPTH TO UNLOAD DENT REGION
*STATIC,PTOL=10.
20.E-5,15.E-3,,1.E-3
*BOUNDARY
9999,1,,1.
*PLOT,FREQ=25
*VIEWPOINT,DEFINITION=MODEL AXIS ROTATION
180.,90.,270.
*DISPLACED
U,1.,1
*END STEP
*STEP,INC=50,NLGEOM,SUBMAX,CYCLE=8
 RIKS STEP ANALYSIS OF AXIAL LOADING
*STATIC,PTOL=20.,MTOL=20.,RIKS
20.E-5,15.E-3,,1.E-3
*BOUNDARY,OP=NEW
BND1A,YSYMM
BND2A,YSYMM
N9999,2,6
LOADB,ZSYMM
LOADB,3,,2.
N1000,1,4
N1000,6
*PLOT,FREQ=25
*VIEWPOINT,DEFINITION=MODEL AXIS ROTATION
180.,90.,270.
*DISPLACED
U,1.,1
*END STEP
```

SPECIMEN C2 - Input file, 4 node shell element.

```
*HEADING
 NONLINEAR ANALYSIS OF DAMAGED BRACE USING MODIFIED RIKS METHOD
*NODE,NSET=ALLN
1,-4.3125,0.,0.
5,0.,4.3125,0.
9,4.3125,0.,0.
91,-4.3125,0.,20.
95,0.,4.3125,20.
99,4.3125,0.,20.
136,-4.3125,0.,89.4
140,0.,4.3125,89.4
144,4.3125,0.,89.4
*NGEN,LINE=C,NSET=LOADB
1,5,1, ,0.,0.,0.
5,9,1, ,0.,0.,0.
*NGEN,LINE=C,NSET=BND3
136,140,1, ,0.,0.,89.4
140,144,1, ,0.,0.,89.4
*NGEN,LINE=C,NSET=BNDMID
91,95,1, ,0.,0.,20.
95,99,1, ,0.,0.,20.
*NGEN,NSET=BND1
1,91,9
91,136,9
*NGEN,NSET=BND2
9,99,9
99,144,9
*NGEN,NSET=REST
2,92,9
92,137,9
3,93,9
93,138,9
4,94,9
94,139,9
5,95,9
95,140,9
6,96,9
96,141,9
7,97,9
97,142,9
8,98,9
98,143,9
*NODE,NSET=N1000
1000,0.,0.,89.4
*NODE,NSET=N9999
9999,6.3125,0.,0.
*NSET,NSET=LDB1
1,9
*NSET,NSET=LDB2
2,3,4,5,6,7,8
*NSET,NSET=BND1A,GENERATE
1,127,9
*NSET,NSET=BND2A,GENERATE
```

```
9,135,9
*NSET,NSET=SUP
1,2,3,10,11,12,19,20,21,28,29,30,37,38,39,46,47,48,55,56,57
64,65,66,73,74,75,82,83,84,91,92,93
*NSET,NSET=ALLN
LOADB,BND1,BND2,BND3,REST
*ELEMENT,TYPE=S4R,ELSET=BRACE
1,1,10,11,2
*ELGEN,ELSET=BRACE
1,8,1,1,15,9,8
*ELSET,ELSET=CENT,GENERATE
8,120,8
1,8
*ELEMENT,TYPE=IRS12,ELSET=INTER
200,9,9999
201,8,9999
202,7,9999
203,6,9999
*RIGID SURFACE,ELSET=INTER,TYPE=SEGMENT
START,4.32,0.,0.
LINE,4.32,4.,0.
*MPC
7,136,1000
7,137,1000
7,138,1000
7,139,1000
7,140,1000
7,141,1000
7,142,1000
7,143,1000
7,144,1000
*ELSET,ELSET=ELPRT
CENT
INTER
*SHELL SECTION,ELSET=BRACE,MATERIAL=ERW
0.135,3
*MATERIAL,NAME=ERW
*ELASTIC
29797.,0.3
*PLASTIC
41.,0.
44.,0.0001
46.,0.0004
47.,0.0007
48.,0.0022
49.,0.0027
*INTERFACE,ELSET=INTER
*FRICTION
1.E12,1.E12
*BOUNDARY
BND1A,YSYMM
BND2A,YSYMM
LOADB,ZSYMM
SUP,1,2
SUP,4
SUP,6
N9999,2,6
```

```
*RESTART,WRITE,FREQ=20
*PLOT
*VIEWPOINT,DEFINITION=MODEL AXIS ROTATION
180.,90.,270.
*STEP,INC=50,NLGEOM,SUBMAX,CYCLE=8,MONOTONIC
 DENTING OF TUBE AT MIDSPAN TO PRESCRIBED 10%D DEPTH
*STATIC,PTOL=10.
20.E-5,15.E-3,,1.E-3
*BOUNDARY
9999,1,,-1.1
*PLOT,FREQ=25
*VIEWPOINT,DEFINITION=MODEL AXIS ROTATION
180.,90.,270.
*DISPLACED
U,1.,1
*END STEP
*STEP,INC=50,NLGEOM,SUBMAX,CYCLE=8,MONOTONIC
 RELEASING OF PRESCRIBED DEPTH TO UNLOAD DENT REGION
*STATIC,PTOL=10.
20.E-5,15.E-3,,1.E-3
*BOUNDARY
9999,1,,1.
*PLOT,FREQ=25
*VIEWPOINT,DEFINITION=MODEL AXIS ROTATION
180.,90.,270.
*DISPLACED
U,1.,1
*END STEP
*STEP,INC=50,NLGEOM,SUBMAX,CYCLE=8
 RIKS STEP ANALYSIS OF AXIAL LOADING
*STATIC,PTOL=20.,MTOL=20.,RIKS
20.E-5,15.E-3,15.E-25,1.E-3
*BOUNDARY,OP=NEW
BND1A,YSYMM
BND2A,YSYMM
N9999,2,6
LOADB,ZSYMM
LOADB,3,,2.
N1000,1,4
N1000,6
*PLOT,FREQ=25
*VIEWPOINT,DEFINITION=MODEL AXIS ROTATION
180.,90.,270.
*DISPLACED
U,1.,1
*END STEP
```

270

(This page intentionally blank)

REFERENCES

1. California Sea Grant College, "California Sea Grant and the Coastal Ocean Environment," A Summary Report of the California Sea Grant College, 1992.

2. Ellinas, C.P., and Valsgard, S., "Collision and Damage of Offshore Structures: A State-of-the-Art," *Proceedings of the International Offshore Mechanics and Arctic Engineering Symposium*, Dallas, Texas, 1985.

3. American Institute for Steel Construction, "Specification for Structural Steel Buildings," 9th Edition, Chicago, Ill, 1989.

4. American Petroleum Institute, "Recommended Practice for Planning, Designing, and Constructing Fixed Offshore Platforms," RP2A, 18th Edition, 1989.

5. American Petroleum Institute, "Draft Recommended Practice for Planning, Designing and Constructing Fixed Offshore Platforms - Load and Resistance Factor Design," RP2A-LRFD, 1st Edition, 1989.

6. Sherman, D.R., "Tests of Circular Steel Tubes in Bending," *Journal of the Structural Division*, ASCE, Vol. 102, No. 11, November 1976.

7. Smith, C.S., Kirkwood, W., and Swan, J.W., "Buckling Strength and Post-Collapse Behavior of Tubular Bracing Members Including Damage Effects," *BOSS '79*, Imperial College, London, England, 1979.

8. Smith, C.S., Somerville, J.W., and Swan, J.W., "Residual Strength and Stiffness of Damaged Steel Bracing Members," *Proceedings of the Offshore Technology Conference*, OTC Paper 3981, Houston, Texas, 1981.

9. Taby, J., "Experiments with Damaged Tubulars," *NTNF Programme for Marine Structures*, SINTEF Report No. 6.07, Trondheim, October 1986.

10. Taby, J., "Residual Strength of Damaged Tubulars. Final Report," *NTNF Programme for Marine Structures*, SINTEF Report No. 6.10, Trondheim, October 1986.

11. Taby, J., "DENTA II - Users Manual (VAX - version 1.01)," Department of Marine Technology, The Norwegian Institute of Technology, The University of Trondheim, March 1988.

REFERENCES - CONTINUED

12. Yao, T., Taby, J. and Moan, T., "Ultimate Strength and Post-Ultimate Strength Behaviour of Damaged Tubular Members in Offshore Structures," *5th International Symposium on Offshore Mechanics and Arctic Engineering*, Tokyo, Japan, April, 1986.

13. Pacheco, L.A., and Durkin, S., " Denting and Collapse of Tubular Members - A Numerical and Experimental Study," *International Journal of Mechanical Sciences*, Vol. 30, No. 5, 1988.

14. Ueda, Y. and Rashed, S.M.H.," Behaviour of Damaged Tubular Structural Members," *4th International Symposium on Offshore Mechanics and Arctic Engineering*, Dallas, Texas, February 1985.

15. Padula, J.A. and Ostapenko, A., "Indentation Behavior of Tubular Members," Fritz Engineering Laboratory Report No. 508.8, June 1988.

16. Landet, E. and Lotsberg, I., "Laboratory Testing of Ultimate Capacity of Dented Tubular Members," *Journal of Structural Engineering*, ASCE, Vol. 118, No. 4, April 1992.

17. Parsanejad, S., "Experimental Strength and Post-Collapse Behavior of Grout Filled Damaged Tubular Members," *Proceedings of the Conference on Structural Faults and Repair*, University of London, July, 1987.

18. Tebbett, I.E., and Forsyth, P., "New Test Data on the Capacity of Cement-Filled Steel Tubulars," *Proceedings of the Offshore Technology Conference*, OTC Paper 5484, Houston, Texas, 1987.

19. Billington, C.J., Harwood, R.G., and Tebbett, I.E., "Grouted Repairs to Steel Offshore Structures," OTH 84 202, Offshore Technology Report, Wimpey Laboratories Limited, London, United Kingdom, 1984.

20. MacIntyre, J., and Birkemoe, P.C., "Damage of Steel Tubular Members in Offshore Structures: A Nonlinear Finite Element Analysis," Department of Civil Engineering, University of Toronto, 1991.

21. Duan, L., Chen, W.F., and Loh, J.T., "Analysis of Dented Tubular Members using Moment Curvature Approach," South Dakota School of Mines and Technology, Rapid City, South Dakota, to appear in ASCE Structures Journal, 1992.

REFERENCES - CONTINUED

22. Duan, L., Chen, W.F., and Loh, J.T., "Moment Curvature Relationships for Dented Tubular Sections," South Dakota School of Mines and Technology, Rapid City, South Dakota, to appear in ASCE Structures Journal, 1992.

23. Ellinas, C.P., "Ultimate Strength of Damaged Tubular Bracing Members," *Journal of Structural Engineering*, ASCE, Vol. 110, No. 2, February, 1984.

24. Jim T. Loh, Exxon Production Research Company, Houston, Texas, Technical Correspondence of March 18, 1992,

25. ASTM Special Technical Publication E8-91, "Test Method for Tensile Coupon Testing," American Society for Testing Materials, 1991.

26. Column Research Council, Technical Memorandum No. 3, "Stub-Column Test Procedure," 1974, (see Reference 29).

27. ASTM Special Technical Publication C109-87, "Test Method for Grout," American Society for Testing Materials, 1987.

28. Krahl, N.W. and Karsan, D.I., "Axial Strength of Grouted Pile-to-Sleeve Connections," *Journal of the Structural Division*, ASCE, Vol. 111, No.4, April 1985.

29. Galambos, T.V., Guide to Stability Design Criteria for Metal Structures, Fourth Edition, Wiley-Interscience Publication, New York, 1988.

30. Parsanejad, S., "Strength of Grout-Filled Damaged Tubular Members," *Journal of Structural Engineering*, ASCE, Vol. 113, No. 3, March 1987.

31. Taby, J., and Moan, T. "Theoretical and Experimental Study of the Behavior of Damaged Tubular Members in Offshore Structures," *Norwegian Maritime Research*, No.2, Trondheim, 1981.

32. ABAQUS Example Problems Manual (Version 4.8), Copyright 1989 Hibbitt, Karlsson and Sorensen, Inc., 100 Medway Street, Providence, Rhode Island, 02906.

33. ABAQUS Theory Manual (Version 4.8), Copyright 1989 Hibbitt, Karlsson and Sorensen, Inc., 100 Medway Street, Providence, Rhode Island, 02906.

34. ABAQUS User's Manual (Version 4.8), Copyright 1989 Hibbitt, Karlsson and Sorensen, Inc., 100 Medway Street, Providence, Rhode Island, 02906.

35. Boswell, L.F., and D'Mello, C.A., "Residual and Fatigue Strength of Grout-Filled Damaged Tubular Members," OTH 89 314, Offshore Technology Report, United Kingdom Department of Energy, 1990.

36. "Grout and Grouting for Construction and Repair of Offshore Structures - A Summary Report," OTH 88 289, Offshore Technology Report, United Kingdom Department of Energy, 1988.